1985

# Nonlinear polariton effects in naphthalene

Sylvia Hewitt Stevenson
*Iowa State University*

Stevenson, Sylvia Hewitt

NONLINEAR POLARITON EFFECTS IN NAPHTHALENE

*Iowa State University* PH.D. 1985

**PLEASE NOTE:**

In all cases this material has been filmed in the best possible way from the available copy. Problems encountered with this document have been identified here with a check mark __✓__.

1. Glossy photographs or pages _____
2. Colored illustrations, paper or print _____
3. Photographs with dark background _____
4. Illustrations are poor copy _____
5. Pages with black marks, not original copy _____
6. Print shows through as there is text on both sides of page _____
7. Indistinct, broken or small print on several pages ✓
8. Print exceeds margin requirements _____
9. Tightly bound copy with print lost in spine _____
10. Computer printout pages with indistinct print _____
11. Page(s) _____ lacking when material received, and not available from school or author.
12. Page(s) _____ seem to be missing in numbering only as text follows.
13. Two pages numbered _____. Text follows.
14. Curling and wrinkled pages _____
15. Dissertation contains pages with print at a slant, filmed as received _____
16. Other _____

_____

_____

# Nonlinear polariton effects in naphthalene

by

Sylvia Hewitt Stevenson

A Dissertation Submitted to the
Graduate Faculty in Partial Fulfillment of the
Requirement for the Degree of
DOCTOR OF PHILOSOPHY

Department: Chemistry
Major: Physical Chemistry

Approved:

Signature was redacted for privacy.

In Charge of Major Work

Signature was redacted for privacy.

For the Major Department

Signature was redacted for privacy.

For the Graduate College

Iowa State University
Ames, Iowa
1985

TABLE OF CONTENTS

# I. INTRODUCTION

Interest in the nonlinear optical behavior of organic compunds has grown enormously in the past few years (1-5). Optical nonlinearities both limit the usefulness of a material in linear applications, such as conventional waveguiding (providing, e.g., an upper limit to the intensity of the guided pulse), and make new applications like optical switching possible. Moreover, nonlinear spectroscopic techniques can yield information about molecular structure and dynamics not available through more traditional linear spectroscopies.

The study of molecular crystals using linear techniques has been actively pursued by many workers for quite some time (see, for example, the review articles by McClure (6,7) and by Wolf (8)). Solid state spectroscopic behavior at electronic frequencies is generally explained in terms of excitons, collective electronic excitations of the crystal. When the crystal approaches ideal chemical and physical purity, however, the exciton model breaks down and it is necessary to introduce the polariton, a particle with mixed exciton-photon character.

This dissertation is a study of nonlinear effects in naphthalene crystals at frequencies near half that of the lowest-lying exciton resonance. This chapter will present an historical overview of the theoretical and experimental background for this work. Later sections will describe both quantum mechanical (polariton) and semiclassical theoretical approaches to the question of the nonlinear behavior of molecular crystals, outline the experimental procedures used in this

study, and present the results obtained. These results will be discussed in the contexts of both the polariton and the semiclassical models of nonlinear effects.

## Nonlinear Optics

In conventional optics, it is assumed that the polarization induced in a material by an applied field is linearly proportional to that field. In fact, the linear term is only the first term in a series expansion in the field describing the induced polarization. Fields applied to a nonlinear medium interact through the nonlinear terms in the material polarization and may, for example, mix to produce output frequencies not present in the applied fields. These and other nonclassical optical phenomena which arise when the applied field is strong enough to make contributions from the nonlinear terms significant all come under the general heading of nonlinear optics.

Although nonlinear effects at radiofrequencies had been observed for some time, it was not until lasers became available to laboratory scientists that the power densities necessary for the observation of nonlinear effects at optical frequencies were attained. The first of these observations was made by Franken and coworkers (9), who used 6942 Å light from a ruby laser to observe frequency doubling (a 3471 Å signal) by quartz. Not long afterward, the first two-photon absorption was observed in $Eu^{++}$-doped $CaF_2$ by Kaiser and Garrett (10), also using a ruby laser. Interest in the field grew rapidly; the following year, Armstrong, Bloembergen, Ducuing and Pershan published a semiclassical description of nonlinear

behavior (11) utilizing a classical field model to describe the macroscopic effects and giving quantum mechanical expressions for the susceptibilities, the quantities which characterize the optical response of a medium. Over the past two decades, numerous articles (12-16) and books (17-21) reviewing the field of nonlinear optics have appeared; of these, the most thorough and lucid are those by Butcher (17) and Shen (14, 21).

Two-photon absorption (TPA), the simultaneous absorption of two photons to create an excited state, has been one of the most widely studied nonlinear effects in organic crystals. The phenomenon was first predicted by Göppert-Mayer, using second-order perturbation theory to obtain the transition rate in the dipole approximation (22). Because two-photon absorption cross sections are generally orders of magnitude lower than those of one-photon absorption, experimental observation of TPA requires the power densities available from lasers, and the effect was not seen until the work of Kaiser and Garrett. A great deal of theoretical work on TPA in solids was produced in short order (23-26), and the first spectroscopic measurement of TPA in neat organic solids was obtained by Hopfield et al. (27a) in 1963.

Although TPA was observed in a number of aromatic solid solutions and in crystalline anthracene as recently as 1963 by Peticolas et al. (28) and by Singh and Stoicheff (29), it was not until tunable dye lasers became available in the early 1970s that high-resolution, continuously scanned two-photon spectroscopic studies of aromatic molecular crystals became possible (30). Since that time, extensive work has been done on the TPA spectrum of naphthalene, both neat (31-33) and in solid solution (31a, 34),

as well as on benzene (35), phenanthrene (36, 37), and anthracene (38).

Second harmonic generation (SHG), or frequency-doubling, is the lowest-order nonlinear optical effect that is subject to a phase-matching condition. After the initial observation of SHG in quartz by Franken et al., the early 1960s saw considerable experimental and theoretical work on frequency-doubling and phase-matching, particularly in crystals (39-44). Observations of the oscillatory path-length dependence ("fringing") of SHG (40), the proposal and first demonstrations of phase-matching in anisotropic crystals via index-matching of the ordinary and extraordinary rays (39, 40), and the first report of sum frequency generation (45) were all published in the same issue of Physical Review Letters. Second harmonic generation was quickly recognized as a means of extending the wavelength range of available lasers (40), and consequently received a great deal of attention from optical experimentalists.

More recently, the spectroscopic aspects of SHG have begun to be considered. The effects of damping of the fundamental or harmonic wave on fringing behavior have been discussed by Rustagi et al. (46). Several workers (41, 47-50) have reported the observation of frequency-doubling in materials with inversion symmetry, a dipole-forbidden process. The behavior of the SHG signal near a resonance has been studied in anthracene (49), naphthalene (49, 50), and phenanthrene (37, 51). Measurements in several organic substances have been made for the purpose of correlating experimental observations of signal intensities with theoretical predictions based on quantum mechanical calculations of molecular orbitals and crystal-imposed symmetry restrictions (52-55).

In the past few years, the availability of higher-powered tunable lasers has made possible several new kinds of nonlinear optical measurements. Optical susceptibilities exhibit frequency dispersion which contains information about various microscopic or macroscopic motions (electronic, vibrational, stress-induced, etc.) of the medium. Consequently, techniques designed to map different aspects of the susceptibilities can complement many traditional spectroscopies. Common modern techniques for probing the optical behavior of organic compounds include third harmonic generation (56-59), electric field-induced SHG (60-62), wave-mixing (63, 64), and measurement of the Kerr and Pockels (AC and DC electro-optic) effects (65-68). Some of the most exciting recent work has been on the waveguiding properties of nonlinear materials (69, 70) and on optical bistability in nonlinear media (71, 72).

In gases, nonlinear phenomena may be understood as arising from the collective nonlinear properties of the gaseous molecules. In condensed phases, however, the effects of local perturbations on the molecules may be large. A currently active area of research aimed at understanding these effects is the relatively new field of nonlinear optical behavior at surfaces. These studies may be roughly divided into two categories: those aimed at understanding the observed substrate-dependent enhancements of nonlinear effects from monolayers of materials adsorbed onto metals, and those which study intensity-dependent changes in the surfaces themselves. In the first category, many of the experimental contributions have come from Shen and coworkers, who have observed SHG from centrosymmetric molecules adsorbed on a variety of surfaces (73). The effect of

varying the local field perturbation by roughening the substrate surface has been demonstrated by several workers (73d, 74, 75), and several theoretical interpretations have been published (76, 77). In the second category, the most spectacular example is that of LIPSS (Laser-Induced Periodic Surface Structure), in which a spontaneous rippling which is intensity- and pulse duration-dependent is observed on metallic or molten surfaces which are illuminated with laser light (78-81). Many of the current theories about this phenomenon involve nonlinear coupling to surface polaritons, vide infra.

## Excitons and the Exciton-Photon Interaction

The theory of collective excited states in weakly bound solids (molecular excitons) was first proposed in 1931 by J. Frenkel (82), but it was not until the late 1940s and 1950s that significant theoretical work in the field was done. Most of the modern theory of molecular excitons was developed by Davydov (83, 84), who applied the theory to aromatic crystals in order to explain sharp low-temperature structure in observed spectra. The details of the theory may be found in Davydov's book (84) and have been reviewed by numerous authors (6, 85-87).

In 1948, Davydov predicted a factor group splitting of transitions in crystals with more than one molecule per unit cell, a phenomenon that is now known as "Davydov splitting." This prediction, together with the prediction of transition shifts between molecular and molecular exciton spectra, provided a starting point for many experimentalists in the 1950s and 1960s (6-8). Extensive studies of the crystal spectra of aromatic

crystals, as model molecular crystals, were conducted. Benzene was, of course, the material of choice for theoretical calculations of Davydov splitting (89, 90), and some experimental work on benzene crystals was done (91, 92), notably by Broude; nevertheless, naphthalene (92-94) and anthracene (95-97), solids at room temperature, quickly became the prototypical aromatic crystals for spectroscopists. A thorough study of the vapor and crystal spectrum of phenanthrene was reported by Craig and Gordon (98).

Refinement of the theory of molecular exciton spectra in the 1970s was due largely to Philpott, who used dipole-dipole interactions to predict Davydov splittings and transition oscillator strengths (99). The results were somewhat unsatisfactory for naphthalene, and nondipolar interactions such as ion-pair states (100) and charge delocalization (101) were invoked by Silbey et al. and Greer et al. with some success. However, inclusion of higher-order multipoles in the dipole-dipole interaction calculations (101-103) has proven the most satisfactory solution.

The exciton model of one-photon absorption by molecular crystals treats the process perturbatively, using excitons as the unperturbed basis states and the photon-exciton interaction Hamiltonian as the perturbation. This is an appropriate treatment as long as the interaction is weak enough, and leads to the classical quantum mechanical absorption rate expression (the rate dependent on the transition oscillator strength) from which the familiar Beer's Law arises. However, under certain conditions it is necessary to refine the model by using mixed exciton-photon states as basis states. In a 1951 paper, Huang (104) pointed out that by describing the

lattice oscillations (phonons) in a crystal with classical equations of motion and subjecting them to Maxwell's equations, coupled solutions were produced which resembled the uncoupled solutions except near the crossing of the phonon and photon frequency-vs-wavevector dispersion curves. These same solutions were later obtained by Fano (105), using a quantum theory of interacting oscillators.

It was Hopfield (106, 107) who showed, by quantizing the photon field in an approach similar to Fano's, that the eigenstates of a system of any crystal states which could be represented as a "polarization field" and photons are particles which have both photon and excited state character. His general term for the uncoupled excited state was "polariton;" the contemporary meaning of that word is now the coupled particle itself. The origins of the various kinds of polaritons are indicated by compound terms like "phonon-polariton" or "exciton-polariton." (In this dissertation, the word "polariton" may generally be understood to mean "exciton-polariton.") Exciton-polaritons were also developed by Pekar (108), using approaches similar to Hopfield's and to Huang's. Agranovich (109) also used a second-quantization approach to calculate polariton dispersion and transition intensities. The theory of polaritons has recently been reviewed by Fishman (110) and by Johnson and Small (111).

Hopfield (106) recognized that one consequence of the polariton model of the interaction of crystals and light was that the absorption process must be viewed as consisting of two steps instead of one: exciton-photon interaction to form a polariton, followed by scattering of the polariton off a third body such as a defect, phonon or chemical impur-

ity. Without the scattering step, the polariton is re-emitted on the other side of the crystal as a photon of the same frequency and absorption has not occurred. Davydov (112) has shown that in the limit of strong exciton-photon coupling (the polariton limit), the absorption rate is governed by the polariton scattering frequency, while in the weak-coupling limit the classical exciton result (dependence on the coupling strength) is recovered. That is, it is the slow step of the two-step process which is rate-limiting.

This picture of the absorption process provides the basis for an experimental test of the polariton model: a transition with sufficiently high oscillator strength in a crystal of a very high degree of physical and chemical perfection should exhibit temperature dependence in the integrated intensity of its absorption profile. The signal should increase with the number of scatterers (phonons) until the scattering rate becomes high enough to reach the classical limit of temperature-independent intensity. This behavior has been demonstrated in CdS by Voigt (113), in $Cu_2O$ by Kreingol'd and Makarov (114), in anthracene by Ferguson (115), in GaSe by Bosacchi et al. (116), and in naphthalene at the 31475 $cm^{-1}$ (0,0) a-exciton resonance by Robinette and coworkers (117). The predictions of the polariton model were tested further by Robinette by comparing the results obtained from high-quality, strain-free crystals to those obtained from doped or intentionally strained (imperfect) crystals. In the latter cases, the classical limit was achieved much more quickly. The polariton model has also been used to explain directional dispersion in reflectance and emission spectra from cyanine dye crystals (118) and thin GaAs layers

(119). Surface exciton-polaritons (120) have been used to explain similar observations in attenuated total reflection (ATR) signals from ZnO (121, 122).

Near k=0, in the region of a photon dispersion curve, the polariton dispersion curves display considerable photon character. For much of the crystal Brillouin zone, however, polariton dispersion is largely exciton-like. Consequently, theoretical work on the behavior of excitons, for instance on exciton spatial dispersion effects (112c, 123-127), may apply to polaritons as well. In the past decade, a good deal of the work on interactions of excitons with other particles has centered on the exciton-phonon interaction (128, 129). Damping by phonons is responsible for exciton linewidths, and exciton-phonon coupling theory may be used to predict this and other temperature-dependent lineshape behavior (129a, 130, 131). Observations of asymmetric lineshapes (50b, 117c) have been interpreted according to the Urbach-Martienssen rule (117a), which has been derived from exciton-phonon coupling theory by Cho and Toyozawa (129a) and by Sumi (131). A more satisfactory explanation of the low-energy tailing asymmetry observed in one-photon spectra of the naphthalene (0,0) transition has been proposed (50b, 132), based on contributions to the overall lineshape from "hot and cold" phonons (analogous, e.g., to the hot-band transitions seen in molecular electronic spectra). Other contemporary work on the exciton-phonon interaction has included unification of the strong and weak coupling cases for Frenkel excitons (133), and generalization of the theory to obtain Frenkel (localized) and Wannier (delocalized) exciton-phonon coupling as limiting cases (134). Recent

theoretical treatments of the specific interactions of polaritons with phonons have dealt mainly with the effects of phonon damping on the polariton dispersion curves (135-138).

The primary dynamic aspect of exciton interactions is the phenomenon of energy transport in crystals. In situations involving relatively high concentrations of chemical impurities, the motion of the exciton is incoherent and "hopping" or percolation models apply (139). When the crystal is more nearly perfect, long-range interactions dominate and diffusion models of energy transport (140-143) are appropriate. Discussions of the theories of exciton energy transfer may be found in recent reviews on exciton dynamics (139b, 142-144). Measurements of singlet exciton diffusion in naphthalene crystals doped with varying concentrations of anthracene have been obtained by several workers (145-147). More recently, observations have been reported of the energy transfer behavior of singlet excitons in anthracene-doped naphthalene following nonlinear excitation of the exciton, with some interesting results (148, 149) which provide a contrast between the behavior of one- and two-photon-generated excitons (polaritons).

Particularly germane to the topic of energy transport mechanisms is the issue of the group velocities of the excitations. A polariton may be viewed as an exciton dressed to some extent with photon character, and can be expected to carry electronic excitation much more rapidly than an exciton. The group velocity question provides another test for the polariton model and will be treated later in this dissertation. Polariton group velocities have been measured directly by Duong et al. in CdSe (150) using

time-of-flight experiments, and recently in anthracene by Vidmont and coworkers (151).

## Nonlinear Interactions in the Polariton Model

As long ago as the early 1960s it was suggested by Ovander, and later by others (152-154), that polaritons rather than excitons were the appropriate basis states for nonlinear interactions in solids. A correct theoretical treatment should predict nonlinear optical behavior in a molecular solid, with the "local field effects" of the semiclassical model arising naturally by proper choice of the crystal Hamiltonian. The theory of two-photon nonlinear interactions of bulk polaritons was developed in the 1970s (155-160) and is reviewed in the article by Johnson and Small (111). More recently, nonlinear interactions of surface polaritons have been studied as well (161-164).

Second harmonic generation in the polariton model is a two-step process: formation of "fundamental" polaritons by coupling the incoming beam to the material, followed by a phase-matched "polariton fusion" step (156, 159) to produce the polariton at the doubled frequency. Two-photon absorption is viewed as arising from the same fundamental process, followed by scattering from an impurity, defect or phonon. Consequently, the TPA and SHG signals may be seen as two aspects of the same event, and the polariton fusion model predicts that there will be a well-defined branching ratio between the two which will be determined by the scattering rate for the doubled polariton in the solid, while the total intensity will be determined by the fusion rate. Temperature-dependent measure-

ments of SHG and TPA (or TPE) in molecular crystals may therefore provide another test for the polariton model. In addition, the phase-matching behavior of the polariton fusion rate may be studied by varying the orientation of the sample.

Because of the coherent nature of the fusion process, the nonlinear interactions of polaritons are especially useful for mapping of polariton dispersion curves. Early work along these lines was done by Hopfield and others using Raman scattering to determine dispersion curves for phonon-polaritons in ZnO (165, 166) and in GaP (167, 168). Dispersion of exciton-polaritons in CuCl has been observed by means of SHG (169) and crossed-beam TPA (169c, 170, 171), and more recently in CdS using resonant Brillouin scattering (172) and Raman scattering (173). Exciton-polariton dispersion in CdS has lately also been measured by the Rozhdestvenskii hook method, a linear technique which measures the frequency dispersion of the dielectric constant directly in an interferometer (174).

Polariton fusion was not observed in molecular crystals until 1977, when Hochstrasser and Meredith used SHG to map the dispersion curves of polaritons in anthracene and naphthalene (49). TPE was observed as well for naphthalene, and displayed some dispersive behavior, but did not exhibit the clear phase matching effects that the SHG signal did. Data on higher-quality crystals of naphthalene have since been reported by Stevenson and Small which demonstrate matched dispersion in both signals (50). These results will be discussed in this dissertation.

The possibility of correlations among the various kinds of nonlinear measurements has been recognized for quite some time. Pao and Rentzepis

(175) were among the first to consider the effects of second harmonic generation on observed two-photon absorption signals, and evidence of these effects has recently been seen in phenanthrene by Johnson and Small (37, 176). These observations have not been limited to solids; apparent competition for intensity between third harmonic generation and multi-photon ionization in xenon has been reported by Glownia and Sander (177) and discussed by Jackson and Wynne (178) in terms of destructive interference between coherent excitations.

The behavior of simultaneously generated second-harmonic generation and two photon excited emission signals near the frequency of the lowest (0,0) exciton resonance in naphthalene is the subject of this dissertation. The data which will be presented will demonstrate the complementary nature of the two signals with respect to dispersion, lineshapes and intensities. The effects of phase-matching and polariton group velocity on lineshapes at various points along the polariton dispersion curves will be discussed. Finally, the question of the applicability of the semiclassical and polariton models of nonlinear optical behavior will be addressed.

# II. THEORY

The semiclassical model of nonlinear interactions is a useful tool for understanding the optical behavior of materials at frequencies which are far from resonances. Less well defined is the extent of its applicability in cases where one or more electromagnetic fields are strongly coupled to the optical medium.

Linear (i.e., one-photon) absorption in molecular crystals is successfully treated as a strong-coupling situation, with a quantum mechanical model which uses mixed exciton-photon particles (polaritons) as the basis states. This model must be distinguished from the quantum mechanical treatment which uses excitons as basis states and treats the absorption interaction as arising from the perturbative (weakly coupled) presence of the photon field. The semiclassical model is a somewhat ambiguous mix of the two viewpoints; the field and medium are strongly coupled through the constitutive relations of classical optics, and the microscopic origins of the macroscopic susceptibilities which define these relations are derived using a quantum mechanical treatment based on weak coupling theory.

The polariton model views one-photon absorption (OPA) as a two-step process: first creation of the polariton through coupling of the field to the material, and then scattering of the polariton (127). The exciton model of absorption neglects the importance of the scattering step and treats absorption mainly as a function of coupling strength. The semiclassical model predicts qualitatively the same thing as the polariton model;

the coupling strength determines the propagation characteristics (e.g., refractive index) of the field in the medium, but attenuation must be accomplished through damping, which provides an imaginary part to the first-order susceptibility. The importance of the damping or scattering step even in weak transitions in solids has been established by Robinette and others (113-117).

Nonlinear interactions in solids may also be treated by the polariton model. Two-photon absorption (TPA), for instance, is viewed in much the same manner as OPA, but with an additional intermediate step: the phase-matched "fusion" (156, 159) of two polaritons to form a new polariton at the sum frequency. Second harmonic generation (SHG) and TPA are thus two aspects of the same process, with the fate of the fused polariton determining the signal to which it contributes. In the semiclassical model, however, nonlinear processes occur through higher-order susceptibilities. The out-of-phase actions of polarizations generated through complex susceptibilities are responsible for absorptions, and the constructive interferences of real polarizations lead to the growth of sum (or difference) - frequency fields.

This chapter will present the theory of the semiclassical and polariton models of nonlinear interactions. Expressions applicable to the cases of TPA and SHG will be developed. Later chapters will present data relevant to the issue of the nonlinear behavior of the (0,0) a-exciton polariton in naphthalene and will address the question of the applicability of the two models.

## Nonlinear Optics in the Semiclassical Model

The behavior of electromagnetic fields in a nonmagnetic medium is dictated by Maxwell's equations:

$$\nabla \times \underline{E} = -\frac{1}{c}\frac{\partial \underline{B}}{\partial t}$$

$$\nabla \times \underline{B} = \frac{1}{c}\frac{\partial \underline{E}}{\partial t} + \frac{4\pi}{c}\underline{J}$$

$$\nabla \cdot \underline{E} = 4\pi\rho$$

$$\nabla \cdot \underline{B} = 0 \qquad [1]$$

where c is the speed of light, $\rho$ is the charge density and $\underline{J}$, $\underline{E}$, and $\underline{B}$ (the current density, electric field vector, and magnetic field vector, respectively) are all understood to be functions of position, $\underline{r}$, and time, t. The current density $\underline{J}$ may be divided into time-independent and time-dependent parts:

$$\underline{J} = \underline{J}_{DC} + \frac{\partial \underline{P}}{\partial t} + c\nabla \times \underline{M} + \frac{\partial}{\partial t}(\nabla \cdot \underline{Q}) + \ldots\ , \qquad [2]$$

where $\underline{P}$ and $\underline{Q}$ are the electric dipole and electric quadrupole polarizations of the medium and $\underline{M}$ is the magnetization (magnetic dipole). The series is written $\underline{J} = \underline{J}_{DC} + \partial\underline{\mathbf{P}}/\partial t$, where $\underline{\mathbf{P}}$ is a general polarization. Substitution of [2] into [1] yields:

$$\nabla \times \underline{E} = -\frac{1}{c}\frac{\partial \underline{B}}{\partial t}$$

$$\nabla \times \underline{B} = \frac{1}{c}\frac{\partial}{\partial t}\left(\underline{E} + 4\pi\underline{\mathbf{P}}\right) + \frac{4\pi}{c}\underline{J}_{DC}$$

$$\nabla \cdot \left(\underline{E} + 4\pi\underline{\mathbf{P}}\right) = \nabla \cdot \underline{D} = 0$$

$$\nabla \cdot \underline{B} = 0 \qquad [3]$$

The polarization $\underline{\mathbf{P}}$ is some function of the applied field $\underline{E}$, and may be expressed as an expansion in $\underline{E}$:

$$\mathbf{P}(\underline{r},t) = \sum_n \int \underline{\chi}^{(n)}(\underline{r}-\underline{r}_1, t-t_1, \cdots \underline{r}-\underline{r}_n, t-t_n) : \underline{E}(\underline{r}_1,t_1)\cdots\underline{E}(\underline{r}_n,t_n) \times d\underline{r}_1 dt_1 \cdots d\underline{r}_n dt_n \qquad [4]$$

where the $n^{th}$ order susceptibilities, $\underline{\chi}^{(n)}$, are characteristics of the medium. (The implicit assumption that the series will converge is generally correct.) If $\underline{E}$ can be expressed as a sum of monochromatic plane waves, $\underline{E}(\underline{r},t) = \Sigma_i \underline{E}(\underline{k}_i, \omega)$ then the Fourier transform of $\underline{\mathbf{P}}(\underline{r},t)$ is, from equation [4]:

$$\mathbf{P}(\underline{k},\omega) = \sum_n \underline{\chi}^{(n)}(\underline{k}, \underline{k}_1, \cdots \underline{k}_n, \omega, \omega_1, \omega_n) : \underline{E}(\underline{k}_1, \omega_1)\cdots\underline{E}(\underline{k}_n, \omega_n) , \quad [5]$$

where $\Sigma_i \underline{k}_i = \underline{k}$ and $\Sigma_i \omega_i = \omega$.

In the electric dipole approximation, $\underline{J}$ is truncated after the first time-dependent term in [2] and the $\underline{\chi}^{(n)}$ do not exhibit spatial dispersion (are independent of $\underline{k}$). Thus, the electric dipole approximation is not useful for explaining phenomena like optical anisotropy in cubic crystals (126). It will be used here for the sake of simplicity; the conventional notation for an $n^{th}$ order optical susceptibility will be $\underline{\chi}^{(n)}(-\omega, \omega_1, \omega_2, \cdots \omega_n)$, where the $\omega_i$ are the frequencies of the fields which interact through $\underline{\chi}^{(n)}$ to produce a response at frequency $\omega$. An applied (absorbed) frequency is conventionally given a positive sign; a generated (emitted) frequency

is negative. In this notation, all frequencies in the argument must sum to zero.

The linear response of a system to an applied field $\underline{E}(\underline{k},\omega)$ at frequency $\omega$ is contained in the first term in equation [5], $\underline{\chi}^{(1)}(-\omega,\omega)\cdot\underline{E}(\underline{k},\omega)$. The remainder of the terms may be grouped together as $\underline{P}^{NL}$, the nonlinear polarization response at $\omega$. $\underline{\chi}^{(1)}(-\omega,\omega)$ is related to the familiar dielectric permittivity, $\underline{\epsilon}_\omega$, by the expression

$$\underline{\epsilon}_\omega = \underline{1} + 4\pi\underline{\chi}^{(1)}(-\omega,\omega) \quad . \qquad [6]$$

The first two of Maxwell's equations [3] may be combined to give directly the wave equation that governs optical wave propagation in a medium. Using the relation [6] and separating the linear and nonlinear polarizations:

$$\nabla\times\nabla\times\underline{E}_\omega - \frac{\omega^2}{c^2}\underline{\epsilon}_\omega\cdot\underline{E}_\omega = \frac{4\pi\omega^2}{c^2}\underline{P}^{NL}_\omega \quad , \qquad [7]$$

where the notation for the electric field $\underline{E}(\underline{k},\omega)$ and nonlinear polarization $\underline{P}^{NL}(\underline{k},\omega)$ vectors has been abbreviated $\underline{E}_\omega$ and $\underline{P}^{NL}_\omega$. Since $P^{NL}_\omega$ contains contributions from fields at frequencies other than $\omega$, equation [7] illustrates the manner in which $\underline{P}^{NL}_\omega$ couples these fields to the one at frequency $\omega$ and provides a mechanism for energy exchange between fields. The complete optical behavior of a system is expressed by a set of coupled equations of the form [7], one for each frequency present. Since the polarization produced by applied fields at frequencies $\omega_i=\omega_1,\omega_2,\cdots\omega_n$ oscillates at some $\omega=\sum_i\omega_i$ which may not be the same as any of the $\omega_i$, new

fields may also be created through the wave equation. These fields may in turn interact with the applied field to give rise to new nonlinear polarizations and new fields, and so on. The complete set of equations describing a given system is infinite, but may in general be truncated if all the $\underline{\chi}^{(n)}$ are small enough (a typical $\underline{\chi}^{(2)}$ is about $10^{-8}$ e.s.u.) so that a field created by the interaction between existing fields can be expected to be much weaker than any of its predecessors. Furthermore, $\underline{\chi}^{(n)}$ for a given material is usually orders of magnitude smaller than $\underline{\chi}^{(n-1)}$, so that higher-order effects are progressively weaker and may be ignored. If the experiment to be described is carried out in a frequency region which enhances any of the $\underline{\chi}^{(n)}$ through resonance interactions, vide infra, the results will be dominated by those terms and the problem may be reduced to relatively few equations.

Numerical evaluation of the intensities of the coupled fields requires knowledge of the values of the susceptibilities. The $\underline{\chi}^{(n)}$ depend on the microscopic structure of the medium and the values may, in principle, be predicted from quantum mechanical calculations. The expression for a given order of $\underline{\chi}$ may be derived from the appropriate order of perturbation calculation. Treatments involving straightforward use of time-dependent perturbation theory to obtain the first few orders of nonlinear polarization have been published by Armstrong et al. (11a) and Ducuing (12). Butcher (17), Shen (14b, 21) and others (15) have used a density-matrix formalism to derive general formulae for any order of susceptibility. Several authors (20, 21) have also demonstrated the utility of Feynman vector diagrams (179) in obtaining expressions for $\underline{\chi}^{(n)}$.

In the classical treatment of nonlinear optical behavior, the material with which the electromagnetic fields interact is approximated as a collection of forced, damped anharmonic oscillators and a perturbation calculation is used to obtain expressions for the susceptibilities (15, 19, 21). This is a helpful initial approach to the problem, as some useful intuitive ideas can result. The (one dimensional) polarization induced by an applied field E is P = -Nex, where

$$\frac{d^2x}{dt^2} + \Gamma\frac{dx}{dt} + \omega_o^2 x + ax^2 = \frac{-e}{m}E \quad , \qquad [8]$$

describes the motion of an oscillator in the system. Here $\omega_o$ is the natural frequency, $\Gamma$ the damping constant, and a the anharmonicity of the oscillator. If the field applied is a monochromatic plane wave, $E = E_o\,[e^{-i\omega t} + e^{i\omega t}]$ (neglecting spatial dependence for now), the solution for the case a = 0 (Lorentz oscillators) is

$$x^{(1)} = \frac{\frac{-e}{m}E_o}{\omega_o^2 - \omega^2 - i\omega\Gamma}\, e^{-i\omega t} + \text{c.c.} \qquad [9]$$

Thus, the first-order polarization is written:

$$P = \frac{Ne^2}{m}\sum_i \frac{F_i}{\omega_{io}^2 - \omega^2 - i\omega\Gamma_{io}}\, E \quad , \qquad [10]$$

summed over all the oscillator frequencies in the system, where each oscillator is weighted by a "strength" F; or

$$\epsilon_\omega = 1 + 4\pi\chi^{(1)}(-\omega,\omega) = 1 + \frac{4\pi N e^2}{m} \sum_i \frac{F_i}{\omega_{io}^2 - \omega^2 - i\omega\Gamma_{io}}$$

$$= \epsilon_0 + \frac{4\pi N e^2}{m} \frac{F}{\omega_o^2 - \omega^2 - i\omega\Gamma}$$

$$= \epsilon_0 + \frac{\omega_p^2 F}{\omega_o^2 - \omega^2 - i\omega\Gamma} \quad , \qquad [11]$$

where $\omega_p^2$ is the so-called "plasma frequency," and it is assumed that $\omega$ is near only one resonant frequency so that the constant and slowly-varying terms may be gathered into $\epsilon_0$. Equation [11] is the Lorentz expression for the dielectric constant.

If the anharmonicity is small, a second-order solution may be found by squaring the harmonic result and substituting it into the equation of motion. The solution is now (21):

$$\chi^{(2)} = \frac{-a\left(\frac{e}{m}\right)^2 E_o^2 e^{-2i\omega t}}{(\omega_o^2 - \omega^2 - i\omega\Gamma)^2 (\omega_o^2 - 4\omega^2 - 2i\omega\Gamma)}$$

$$- \frac{2a\left(\frac{e}{m}\right)^2 E_o^2}{\omega_o^2(\omega_o^2 - \omega^2 - i\omega\Gamma)} + \text{c.c.} \quad ; \qquad [12]$$

that is, in second order the polarization has acquired a component at $2\omega$ (second harmonic generation) and a D.C. component (optical rectification). The susceptibilities $\chi^{(2)}$ are obtained by making the obvious substitutions. It is now apparent that it is the anharmonicity in the system which leads

to nonlinear behavior; a set of perfectly harmonic oscillators which oscillate at different frequencies cannot couple.

The density matrix approach is probably the most generally useful means of obtaining quantum mechanical expressions for the nonlinear susceptibilities, particularly when there is damping in the system. Following the development by Shen (14b, 21), the density matrix operator $\underline{\rho}$ is defined by

$$\underline{\rho} = \overline{|\Psi\rangle\langle\Psi|} \quad , \qquad [13]$$

where $\Psi$ is the system wavefunction and the bar denotes ensemble averaging. If the eigenstates of the unperturbed system are the states $\{|n\rangle\}$, so that the state of the system may be written $|\Psi\rangle = \Sigma_n a_n|n\rangle$, the diagonal matrix element $\rho_{ii} = |a_i|^2$ gives the proportion of the population in state $|i\rangle$. A nonzero value of the off-diagonal matrix element $\rho_{ij}$ accordingly signifies coherent mixing of states $|i\rangle$ and $|j\rangle$. The expectation value for any operator $\underline{Q}$ representing a physical quantity (such as polarization) may be written as $Tr\{\underline{\rho}\underline{Q}\}$.

The time evolution of the density matrix is given by the Liouville equation, a form of the Schrödinger equation:

$$\frac{\partial \underline{\rho}}{\partial t} = \frac{-i}{\hbar}[\mathcal{H}, \underline{\rho}] = \frac{-i}{\hbar}[\mathcal{H}_0 + \mathcal{H}_{INT}, \underline{\rho}] + \left(\frac{\partial \underline{\rho}}{\partial t}\right)_{\mathcal{H}_r} \quad , \qquad [14]$$

where the Hamiltonian for the system is divided into that for the unperturbed system, $\mathcal{H}_0$, the interaction Hamiltonian $\mathcal{H}_{INT}$ describing the perturbation applied to the system, and a "relaxation Hamiltonian" $\mathcal{H}_r$ which

describes the perturbation in the system resulting from its environment, e.g., the "thermal bath." The time evolution of the density matrix due to this last term is written phenomenologically as $(\partial\rho_{ij}/\partial t) = (\Gamma_{ij}/2)\rho_{ij}$ and $\partial(\rho_{ii}-\rho_{ii}^{o})/\partial t = -(1/T_1)_i(\rho_{ii}-\rho_{ii}^{o})$, where $(1/\Gamma_{ij}) = 2(T_2)_{ij}$ and $T_1$ and $T_2$ are the transverse and longitudinal relaxation times, respectively.

Writing $\rho$ as a perturbation expansion and collecting terms of like order in equation [14] gives a general set of equations of the form (for the $n^{th}$-order solution):

$$\frac{\partial \underline{\rho}^{(n)}}{\partial t} = \frac{-i}{\hbar}[\mathcal{H}_0, \underline{\rho}^{(n)}] = \frac{-i}{\hbar}[\mathcal{H}_{INT}, \underline{\rho}^{(n)}] + \left(\frac{\partial \underline{\rho}^{(n)}}{\partial t}\right)_{\mathcal{H}_r} . \qquad [15]$$

For the case of an applied field in the electric dipole approximation, $\mathcal{H}_{INT} = e\underline{r}\cdot\underline{E}$ and the induced polarization $\underline{P} = -Ne\underline{r}$, where N is the volume density of oscillators (induced dipoles). Using equation [5] to define the suceptibilities, equation [15] leads to the general result (17):

$$\underline{\chi}^{(n)}(-\omega, \omega_1, \omega_2, \cdots \omega_n) =$$

$$\frac{N}{n!\hbar^n} S_T \sum_{i_j} \frac{\underline{Q}_{gi_1}\underline{Q}_{i_1 i_2}\underline{Q}_{i_2 i_3}\cdots\underline{Q}_{i_n g}}{(\Omega_{gi_1} - \omega_1 - \cdots - \omega_n - i\Gamma_{gi_1}/2)}$$

$$\times \frac{1}{(\Omega_{gi_2} - \omega_2 - \cdots - \omega_n - i\Gamma_{gi_2}/2)\cdots(\Omega_{gi_n} - \omega_n - i\Gamma_{gi_3}/2)} . \qquad [16]$$

Here $\underline{Q}_{ij}$ is the transition dipole matrix element between states $\langle i|$ and $|j\rangle$, $\Omega_{ij} = \omega_j - \omega_i$, and $S_T$ is a total symmetrizer indicating summation of all terms of the form in the argument of $S_T$, permuting all the n+1 frequency

arguments; essentially, permuting the order in which the fields are applied (generated). For example, in the case of SHG it is terms of the form $\underline{\chi}^{(2)}(-2\omega,\omega,\omega)$ through which energy is transferred from the fundamental to the frequency-doubled field, and terms of the form $\underline{\chi}^{(2)'}(-\omega,-\omega,2\omega)$ which represent the energy transfer back to the fundamental field. In a lossless medium, it is the equilibrium between these two exchange processes which determines the intensities of the two fields at a given point.

The first-order susceptibility, from equation [16], is written:

$$\underline{\chi}^{(1)}(-\omega,\omega) = \frac{N}{\hbar}\sum_{i}\frac{\underline{Q}_{gi}\underline{Q}_{ig}}{\Omega_{ig}-\omega-i\Gamma_{ig}/2} \quad . \qquad [17]$$

Near a resonance, this may be written as

$$\underline{\chi}^{(1)}(-\omega,\omega) = \underline{\chi}^{(1)}_{nr} + \left(\frac{N}{\hbar}\right)\frac{\underline{Q}_{gi}\underline{Q}_{ig}}{\Omega_{ig}-\omega-i\Gamma_{ig}/2} \quad . \qquad [18]$$

Then the expression for the dielectric permittivity is:

$$\epsilon = \epsilon_o + \left(\frac{4\pi N}{\hbar}\right)\frac{\underline{Q}_{gi}\underline{Q}_{ig}}{\Omega_{ig}-\omega-i\Gamma_{ig}/2}$$

$$= \epsilon_o + \frac{\omega_p^2 F_{ig}/\omega}{\Omega_{ig}-\omega-i\Gamma_{ig}/2} \quad , \qquad [19]$$

where $|\underline{Q}_{ij}|^2 = e^2\hbar F/m\omega$ has been used. This is equivalent to the Lorentz

expression [11] when $\omega$ is close to $\Omega_{ig}$, and substituting $\Gamma$ for $\Gamma/2$. (Recall that the sense of damping in the Lorentz oscillator model is simply the reciprocal of the relaxation time, which differs from the convention used above by a factor of two.)

Since the $\underline{\chi}^{(n)}$ contain products of n dipoles, they are $(n+1)^{th}$ rank tensors. The $i_0^{th}$ component of the nonlinear polarization, $P_{i_0}^{(n)}$, is given according to equation [5] by:

$$P_{i_o}^{(n)}(\omega) = \chi_{i_o i_1 \cdots i_n}^{(n)}(-\omega, \omega_1, \cdots \omega_n) E_{i_1}(\omega_1) \cdots E_{i_n}(\omega_n), \qquad [20]$$

where summation over the $i_j$ is understood. It has been shown by Butcher (17) that the $(\omega_j, i_j)$ pairs may be permuted without changing the value of $\underline{\chi}^{(n)}$; this is equivalent to the statement that the ordering of the fields which contribute to $\underline{P}_{\omega}^{(n)}$ is unimportant. A further permutation symmetry holds when the medium is lossless, so that the damping terms in [16] may be neglected; then $\underline{\chi}^{(n)}$ becomes invariant to permutation among any of the $i_j$. This simplification ($\underline{\chi}^{(2)}$, for example, collapses from 27 to 10 independent elements), first proposed by Kleinman (180), is widely used, although it is not strictly correct for most real situations.

In addition to permutation symmetry, the point group symmetry of the optical medium may reduce the number of independent elements in the $\underline{\chi}^{(n)}$ tensors, since the susceptibilities must be invariant under symmetry operations of the medium. Tabulations of the relations between tensor elements for $\underline{\chi}^{(2)}$ and for $\underline{\chi}^{(3)}$ for all the crystal classes and point symme-

tries may be found in numerous references (17, 21, 181). An example of the effect of structural symmetry on the values of the $\underline{\chi}^{(n)}$ components is that of a medium with inversion symmetry when n is an even number. Equation [20] can be used to demonstrate that in this case, in the electric dipole approximation $\chi^{(n)} = -\chi^{(n)}$ for every element; that is, $\underline{\chi}^{(n)}$ is identically zero. Processes such as SHG which occur via even-order susceptibilities are thus electric dipole forbidden in media with inversion symmetry.

The imposition of symmetry requirements is not the only effect condensed phases have on the values of nonlinear susceptibilities. The quantum-mechanical derivation of $\underline{\chi}^{(n)}$ treats it as a microscopic property (an $n^{th}$-order hyperpolarizability) multiplied by the number density of sites and subjected to symmetry restrictions. It is assumed in equation [16] that there is no interaction between molecules. Dipole-dipole interactions are introduced in this model by the inclusion of "local field factors" which modify the susceptibilities (60, 182, 183). A thorough discussion of the relationship between molecular hyperpolarizabilities and macroscopic susceptibilities in solids may be found in the review article by Chemla (16). For most purposes, the local field factors for molecular crystals are assumed to be close to 1; that is, the crystal is treated as an "oriented gas."

To illustrate the phenomenon of energy exchange between fields of different frequencies in a nonlinear medium, consider the case of an infinitely extended monochromatic plane wave propagating in the forward direction along $\underline{z}$ and primarily of transverse character. Then

$$\underline{E}_\omega = E_\omega e^{i(k_\omega z - \omega t)} \quad , \qquad [21]$$

where $E_\omega$ is the amplitude of the wave and $k_\omega$ is its associated wavevector amplitude. In this case, the nonlinear wave equation [7] may be written:

$$\frac{\partial^2}{\partial z^2}\underline{E}_\omega + \frac{\omega^2}{c^2}\epsilon_\omega \cdot \underline{E}_\omega = -\frac{4\pi\omega^2}{c^2}\underline{P}_\omega^{NL} \quad . \qquad [22]$$

This expression may be reduced to a first-order differential equation by invoking the approximation that $k(\partial E_\omega/\partial z) \gg (\partial^2 E_\omega/\partial z^2)$; in other words, that the amplitude of each interacting wave in the medium varies negligibly on the scale of a wavelength. This is referred to as the Slowly-Varying Amplitude (SVA) approximation. Then equation [22] becomes:

$$\frac{\partial}{\partial z}E_\omega = \frac{2\pi i\omega^2}{c^2 k_\omega}\underline{P}_\omega^{NL} e^{-i(k_\omega z - \omega t)} \quad , \qquad [23]$$

where the relation $\epsilon_\omega = c^2k^2/\omega^2$ has been used. This expression is valid for each field generated in the medium as well as for the applied fields. For the case of the field at $2\omega$ which is generated through the polarization

$$\underline{P}_{2\omega}^{NL} = \underline{\chi}^{(2)}\underline{E}_\omega\underline{E}_\omega = \underline{\chi}^{(2)}E_\omega^2 e^{i(2k_\omega z - 2\omega t)} \quad ,$$

$$\frac{\partial}{\partial z}E_{2\omega} = \frac{8\pi i\omega^2}{c^2 k_{2\omega}}\underline{\chi}^{(2)} e^{i\Delta k z} E_\omega^2 \quad , \qquad [24]$$

where $\Delta k = 2k_\omega - k_{2\omega}$. The quantity $\Delta k$ is the "phase mismatch" between $\underline{P}_{2\omega}$ and $\underline{E}_{2\omega}$ and arises because momentum need not be exactly conserved

in a medium of finite extent. Its effect may be understood by picturing the induced polarization as an array of dipoles coherently driven by $\underline{E}_\omega$ (separated in space by $2\pi/k_\omega$), each radiating a wave at $2\omega$ which propagates with pseudomomentum $k_{2\omega}$. If there is frequency dispersion in k, so that $k_{2\omega} \neq 2k_\omega$, the radiated waves will interfere destructively to some extent. The intensity of the second harmonic beam at z = L is found by integrating equation [24] from 0 to L and multiplying the modulus squared of the result by the factor $n_{2\omega}c/2\pi$:

$$I_{2\omega}(L) = \frac{n_{2\omega}c}{2\pi} |E_{2\omega}|^2(L)$$

$$= \frac{32\pi n_{2\omega}\omega^4}{c^3} \left| \frac{\underline{\chi}^{(2)}}{k_{2\omega}\Delta k} (e^{i\Delta kL} - 1) \right|^2 |E_\omega|^4 , \qquad [25]$$

where it has been assumed that the depletion in the fundamental beam is negligible. For the case where all quantities are real (i.e., a lossless medium),

$$I_{2\omega}(L) = \frac{8\pi n_{2\omega}L^2}{c\epsilon_{2\omega}} \operatorname{sinc}^2\left(\frac{\Delta kL}{2}\right) |\chi^{(2)}|^2 |E_\omega|^4 , \qquad [26]$$

where sinc(x) = sin(x)/x. Thus, in a transparent frequency region, the intensity of the generated second harmonic beam should be an oscillatory function with respect to path length or to phase mismatch.

The first experiment to demonstrate this behavior was performed in 1961 by Maker et al. (40). Varying the path length of a ruby laser through a plate of quartz by rotation of the plate, they observed the expected

$\sin^2(\Delta kL)$ dependence. The maxima in such a pattern are now called "Maker fringes," and the spacing between the fringes corresponds to the coherence length $L_c = \pi/\Delta k$ of the signal in the material. (Although formally only the pattern observed when varying the path length through a plane-parallel sample by rotation is a Maker fringe pattern, the term is often used to mean any oscillating signal observed by scanning $\Delta kL$, e.g., by transverse translation of a wedge-shaped sample.)

Interestingly, it was in the same paper that Maker et al. reported the first observation of index matching in anisotropic media. Since k may be written as $n\omega/c$, where n is the index of refraction and all quantities are assumed real, frequency dispersion in k corresponds to frequency dispersion in n. Matching of the indices of refraction of the input and signal beams is then equivalent to phase matching in a lossless medium. Using polarized input, in an anisotropic crystal with normal indicial dispersion an extraordinary doubled beam is generated by an ordinary fundamental with high conversion efficiency when $n_e(2\omega) = n_o(\omega)$. (This is now called Type I index matching.) Maker et al. were able to observe this phenomenon in a crystal of potassium dihydrogen phosphate (KDP). Using an unfocused ruby laser and a 1.5 mm thick sample, they achieved a 300-fold increase in the SHG signal upon proper (i.e., index-matching) orientation of the crystal.

From equation [23] it is apparent that an imaginary (out of phase) component in the nonlinear polarization at $\omega$, $\underline{P}^{NL}_{\omega}$, leads to depletion of the field at $\omega$. The nonlinear susceptibilities responsible for generation and maintenance of $\underline{P}^{NL}_{\omega}$ are all those of significant magnitude whose first argument is $-\omega$. In the case of a system where two fields, an applied

field at $\omega$ and a generated one at $2\omega$, dominate (equation [16] illustrates how this might be possible when $2\omega$ is near a resonance), there are two nonlinear source terms for $\underline{P}_{\omega}^{NL}$: $3\chi^{(3)}(-\omega,-\omega,\omega,\omega)\underline{E}_{\omega}|E_{\omega}|^2$ and $2\chi^{(2)'}(-\omega,-\omega,2\omega)\underline{E}_{2\omega}\underline{E}_{\omega}^{*}$, where the numerical coefficients arise from permutation symmetry:

$$\underline{P}_{\omega}^{NL} = 3\chi^{(3)} E_{\omega} |E_{\omega}|^2 e^{i(k_{\omega}z - \omega t)} + 2\chi^{(2)'} E_{2\omega} E_{\omega}^{*} e^{i[(k_{2\omega} - k_{\omega})z - \omega t]} \quad , \quad [27]$$

where the susceptibilities have been approximated as scalars for this purpose. It is assumed that the frequency $\omega$ is not near a resonance, so that the linear suceptibility $\underline{\chi}^{(1)}(-\omega,\omega)$ does not contribute via one-photon absorption (OPA) to the depletion of the fundamental wave. Combining equation [27] with [23] and [25] gives the position-dependent amplitude $E_{\omega}$:

$$\frac{\partial E_{\omega}}{\partial z} = \frac{2\pi i \omega^2}{c^2 k_{\omega}} \left\{ 3\chi^{(3)} + \frac{16\pi\omega^2 \chi^{(2)}\chi^{(2)'}}{c^2 k_{2\omega} \Delta k} [1 - e^{-i\Delta k z}] \right\} E_{\omega} |E_{\omega}|^2, \quad [28]$$

or

$$\frac{\partial}{\partial z}(|E_{\omega}|^2) = \frac{-4\pi\omega^2}{c^2 k_{\omega}} \operatorname{Im}\left\{ 3\chi^{(3)} + \frac{16\pi\omega^2 \chi^{(2)}\chi^{(2)'}}{c^2 k_{2\omega} \Delta k} [1 - e^{-i\Delta k z}] \right\} |E_{\omega}|^4. \quad [29]$$

This may be used as before to obtain the fundamental beam amplitude and hence the intensity at position L:

$$|E_\omega|^2(L) = |E_\omega|^2(0) - \frac{4\pi\omega^2 L}{c^2 k_\omega} \mathrm{Im}\left\{3\chi^{(3)} + \frac{16\pi\omega^2 \chi^{(2)}\chi^{(2)'}}{c^2 k_{2\omega}\Delta k} \times \left[1 + \frac{1}{i\Delta k L}(e^{-i\Delta k L} - 1)\right]\right\} |E_\omega|^4(L) \quad . \qquad [30]$$

The explicit formulae for the nonlinear susceptibilities in the above expression are, from equation [16]:

$$\chi^{(2)}(-2\omega,\omega,\omega) = \chi^{(2)}_{nr} + \left(\frac{N}{2\hbar}\right) \frac{\underline{Q}_{oi}\underline{Q}_{io}}{(\omega_{io} - 2\omega - i\Gamma_{io}/2)} \quad , \qquad [31a]$$

$$\chi^{(2)'}(-\omega,-\omega,2\omega) = \chi^{(2)'}_{nr} + \left(\frac{N}{2\hbar}\right) \frac{\underline{Q}_{oi}\underline{Q}_{io}}{(\omega_{io} - 2\omega - i\Gamma_{io}/2)} \quad , \qquad [31b]$$

and

$$\chi^{(3)}(-\omega,-\omega,\omega,\omega) = \chi^{(3)}_{nr} + \left(\frac{N}{6\hbar}\right) \frac{\underline{Q}_{oi}\underline{Q}_{io}}{(\omega_{io} - 2\omega - i\Gamma_{io}/2)} \quad , \qquad [31c]$$

where

$$\underline{Q}_{io} = \sum_j \frac{\underline{Q}_{ij}\underline{Q}_{jo}}{(\omega_{jo} - \omega - i\Gamma_{jo}/2)}$$

is the two-photon transition polarizability between states $|o\rangle$ and $\langle i|$ and the terms in equation [16] from states other than the resonance state $|i\rangle$

have been grouped into a slowly varying nonresonant term in each of the above expressions. From equations [31] it can be seen that all the susceptibilities in [30] are enhanced by the resonance at state $|i\rangle$. The dipole-forbidden nature of second-order processes in a medium with inversion symmetry is illustrated again by the fact that $\underline{\omega}_{i0}$ and $\underline{\Omega}_{i0}$ cannot both be nonzero in such a case.

Previous accounts of two-photon absorption (TPA) in the semiclassical model have treated it as arising primarily through the imaginary part of the third-order susceptibility $\chi^{(3)}$ (18, 20, 37, 184), and have interpreted this as implying independent mechanisms for SHG, which arises through $\chi^{(2)}$, and TPA (20, 37, 50c). However, consideration of expressions [30] and [31] leads to two conclusions: (1) that under the phase matched conditions necessary to enhance SHG there is a significant contribution from the $\chi^{(2)}\chi^{(2)'}$ term in equation [30]; and (2) that susceptibilities of different order are not as a rule independently valued (for example, examination of the expressions for $\chi^{(2)}$ and $\chi^{(3)}$ shows that in general they depend on the same quantities). Meredith (185, 186) has done theoretical and experimental work on the effects of lower-order terms on higher-order processes, a phenomenon he has termed "cascading." Following his work (185), the observed signal from a two-photon excited emission (TPE) experiment in which TPA is measured by collecting the incoherent emission from the excited state $|i\rangle$ should be proportional to the difference between the total energy removed from the fundamental beam and that contributed to the second harmonic:

$$I_{TPE} \approx \frac{c\, n_{2\omega}}{2\pi} \{ |E_{\omega}|^2(0) - |E_{\omega}|^2(L) - |E_{2\omega}|^2(L) \}, \quad [32]$$

where the proportionality factor is determined by the quantum yield for the emission and by the details of the experiment, and the results from equations [25] and [30] are used. Thus, even though TPA is not a phase-matched process via $X^{(3)}$, under the phase matching conditions for SHG the TPE signal becomes a linear combination of three terms which may interfere constructively or destructively to produce changes in the intensity, lineshape, and position of the signal. The $X^{(3)}$ term may be expected to dominate the signal in situations where phase matching in $X^{(2)}$ does not occur at frequencies near resonance. When phase matching does occur near resonance, the $X^{(2)}$ terms in the TPE intensity expression are resonantly enhanced and are relatively more important.

The above approach can easily be extended to explain the disruption of resonantly enhanced three-photon ionization signals when third-harmonic generation becomes important. This phenomenon was observed recently by Glownia and Sander (177) and interpreted by Wynne (178b), using an argument which depended on zero-valued first-order susceptibilities (an approximation valid only for low-pressure gases). The general treatment in Meredith's 1981 paper (185) may be used to obtain Wynne's result as a special case.

Results [25] and [30] are appropriate for transverse plane waves of infinite extent, coupling with material resonances through electric dipole interactions. In situations where the fields cannot be described as infinite plane waves, the theoretical treatment is more complicated. The

propagation characteristics of a beam in a nonlinear medium are altered when there is transverse variation in intensity, as the effective dielectric constant for the beam center differs from that experienced by the wings. Ward and New (187) have done an extensive mathematical treatment of the propagation of Gaussian beams, and the results have been adapted by Meredith et al. (57a, 182) into a useful algorithm for analyzing the results of higher-order nonlinear measurements with near-Gaussian ($TEM_{00}$) laser beams.

If the electric field is longitudinal, the solution to the wave equation [7] is:

$$E_\omega = \frac{-4\pi}{\epsilon_\omega} P_\omega e^{i\Delta k z} \quad , \qquad [33]$$

where $\Delta k = k_P - k_E$, the difference between the wavevectors of the polarization and electric fields. Longitudinal components of the field consequently alter the distribution of intensities among fields. A discussion of longitudinal nonlinear behavior may be found in the book by Shen (21). The interactions which occur through the magnetic dipoles and electric quadrupoles have been discussed by Adler (188) and result in seven additional terms contributing to the field. None of these terms is sensitive to inversion symmetry. The polarization due to their contributions is found to be $\pi/2$ out of phase with that due to the electric dipole term. The theory of multipole moments and multipolar polarizabilities has recently been reviewed by Applequist (189). The spatial dispersions of the nonlinear susceptibilities have been considered by Flytzanis (190), who obtained

multipolar expressions in his results as a consequence.

## Polaritons in the Semiclassical Model

The stationary states of an unperturbed molecular crystal are the pseudolocalized collective excitations called Frenkel (or molecular) excitons. The theory of molecular excitons has been extensively reviewed (for example, see references 6, 84-86, 111, and 117a). In general they are successfully treated as collections of interacting dipoles.

The semiclassical model treats all optical interactions in nonmagnetic media as arising from Maxwell's equations [3]. The material properties are incorporated in the second and third expressions, which contain the dielectric permittivity tensor $\underline{\underline{\epsilon}}$ (or, equivalently, the polarization field vector $\underline{P}$). Combining the first two of equations [3] leads to the material wave equation:

$$\nabla \times \nabla \times \underline{E} = \frac{-1}{c^2} \frac{\partial^2}{\partial t^2} \underline{D} \quad , \qquad [34]$$

equivalent to equation [7] when the nonlinear polarization is neglected. If the field quantities are expressed as forward-moving infinite plane waves, $F = F_0 e^{i(k \cdot r - \omega t)}$, where $\underline{F} = \underline{E}$ or $\underline{D}$, then equation [34] becomes:

$$k^2 \underline{E} - (\underline{k} \cdot \underline{E})\underline{k} = \frac{\omega^2}{c^2} \underline{D} \quad . \qquad [35]$$

In the coordinate system where $\underline{k}$ is parallel to $z$, this expression gives the three simultaneous equations:

$$k^2 E_x = \frac{\omega^2}{c^2} D_x \qquad [36a]$$

$$k^2 E_y = \frac{\omega^2}{c^2} D_y \qquad [36b]$$

$$0 = \frac{\omega^2}{c^2} D_z \qquad [36c]$$

The last expression may be divided into two cases: either $\underline{D}$ is identically zero, or it is not, in which case it must be transverse to $\underline{k}$. In the first instance, it follows from [36a] and [36b] that if $\underline{D}$ is zero then $\underline{E}$ must be wholly longitudinal for a nontrivial result. Then, according to the material relation

$$\underline{D} = \underline{\epsilon} \cdot \underline{E} = \underline{E} + 4\pi \underline{P} \quad , \qquad [37]$$

it follows that $|\underline{\epsilon}| = 0$. The solutions where $|\underline{\epsilon}| = 0$ are called longitudinal solutions since when $\underline{E}$ is longitudinal and $\underline{D}$ is zero the polarization in the material relation [37] must be longitudinal.

In the case where $\underline{D}$ is transverse, equations [36a] and [36b] may be written as:

$$\underline{E}^{\perp} = \frac{\omega^2}{k^2 c^2} \underline{D} \quad , \qquad [38]$$

where $\underline{E}^{\perp}$ is the transverse part of $\underline{E}$, and [37] may be written as:

$$\underline{E}^{\perp} = (\underline{\epsilon}^{-1})^{\perp} \cdot \underline{D} \quad , \qquad [39]$$

where $(\underline{\epsilon}^{-1})^{\perp}$ is the 2x2 x-y submatrix of the inverted dielectric tensor. Here also there are two cases: either $\underline{E}^{\perp} = 0$ or $\underline{E}^{\perp} \neq 0$. Since $\underline{D} \neq 0$, for the

first case to obtain it must be assumed that the speed of light c is infinite; in other words, that there is no retardation in electromagnetic interactions. The solution is then $|(\underline{\epsilon}^{-1})^t| = 0$. This is the transverse solution; since $\underline{D}$ is transverse and $\underline{E}$ is not, $\underline{P}$ must have transverse character. (There is also an apparent unretarded solution to [36] with longitudinal $\underline{D}$, but this solution would violate the third of Maxwell's equations [3] and so will not be considered.)

If $\underline{E}^t \neq 0$, retardation must be taken into account (c must be finite, from equation [38]) and it is more convenient to cast equation [35] in a coordinate system where $\underline{k}$ is not necessarily parallel to a Cartesian axis,but where the dielectric tensor is diagonalized. Then [35] may be written as three equations for the $E_j$, uncoupled (unless there is a symmetry condition):

$$k^2 E_j - (\underline{k}\cdot\underline{E})k_j = \frac{\omega^2}{c^2}\epsilon_{jj}E_j \qquad [40]$$

Combination of these three equations gives an expression which is a dispersion relation for k and $\omega$:

$$\frac{\omega^2}{c^2} = \frac{k_x^2}{\frac{c^2k^2}{\omega^2} - \epsilon_{xx}} + \frac{k_y^2}{\frac{c^2k^2}{\omega^2} - \epsilon_{yy}} + \frac{k_z^2}{\frac{c^2k^2}{\omega^2} - \epsilon_{zz}} \qquad [41]$$

This is Fresnel's equation in classical optics. If the propagation direction is in a given plane, for instance the xz plane at an angle $\varnothing$ from the z axis, then:

$$\frac{\omega^2}{c^2} = \frac{k^2 \sin^2\phi}{\frac{c^2k^2}{\omega^2} - \epsilon_{xx}} + \frac{k^2 \cos^2\phi}{\frac{c^2k^2}{\omega^2} - \epsilon_{yy}} \quad , \qquad [42]$$

or

$$\frac{c^2k^2}{\omega^2} = \epsilon \quad , \qquad [43]$$

where

$$\epsilon = \frac{\epsilon_{xx}\epsilon_{zz}}{\epsilon_{xx}\sin^2\phi + \epsilon_{zz}\cos^2\phi} \quad . \qquad [44]$$

If the $\epsilon$ values in equations [41]-[43] are not functions of frequency, then these equations give the dispersion relation for photons. Near a resonance, however, the functional form for $\epsilon$ is in the dipole approximation that which was derived from the density matrix formalism, equation [19]. If the transition dipole orientation is known accurately, in principle $\underline{\underline{\epsilon}}$ can be diagonalized and the form [41] or [42] used. In practice, it is usually more reasonable to compute $\epsilon_o$ from an expression like [44], using the known values from the diagonalized nonresonant $\underline{\underline{\epsilon}}_o$ tensor, and then use the isotropic form [43] of the dispersion expression:

$$\frac{c^2k^2}{\omega^2} = \epsilon_o + \frac{\omega_p^2 F}{\omega_o^2 - \omega^2} \quad , \qquad [45]$$

where the undamped Lorentz form for the permittivity has been used. Note that in the limit of very large c, the unretarded transverse solution of

$\epsilon^{-1} = 0$ is recovered; this solution is $\omega = \omega_o$ and is the (transverse) exciton frequency. In the limit where k is large, the same solution is obtained. Thus, it is only in the region of the Brillouin zone near k=0 that the coupling effects are important.

Equation [45] may be written as a biquadratic equation in $\omega$:

$$\omega^4 - \omega^2\left[\frac{c^2k^2}{\epsilon_o} + \omega_o^2 + \frac{\omega_p^2 F}{\epsilon_o}\right] + \frac{\omega_o^2 c^2 k^2}{\epsilon_o} = 0. \quad [46]$$

There are two solutions for $\omega > 0$; they are plotted in Figure 1 along with the longitudinal solution $\omega_L = (\omega_o + \omega_p^2 F/\epsilon_o)^{1/2}$ for the region near k=0. The longitudinal solution is independent of retardation as it does not couple with the field. The transverse exciton frequency is shown as a straight line at $\omega_o$ in this approach, since the expression for $\epsilon$ was derived in the dipole approximation without inclusion of the higher-order terms which would have led to spatial dispersion. The effect of spatial dispersion on polariton dispersion curves has been discussed by Hopfield and Thomas (123). It is expected to be unimportant at optical frequencies, where the wavelength of light is much greater than the lattice constant of a molecular crystal (111).

The limit of the upper branch of the polariton dispersion curve as k approaches zero is the longitudinal frequency $\omega_L$. Similarly, the high-k limit of the lower branch is the transverse exciton frequency $\omega_o$). For frequencies in the region $\omega_o < \omega < \omega_L$, in the zero-damping limit there are no allowed polariton states and all incident photons are reflected. This

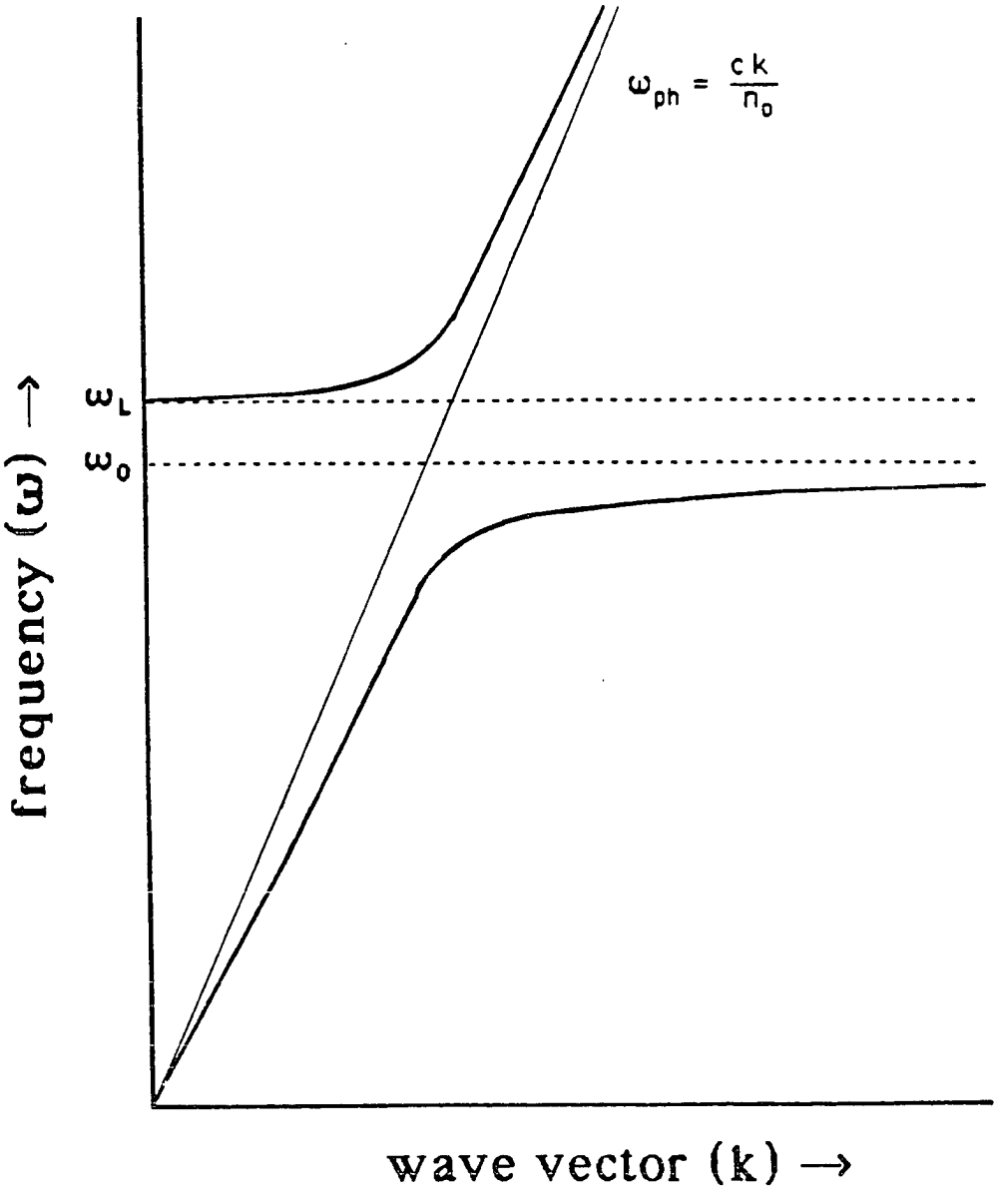


Figure 1. Typical polariton dispersion curve, shown with the longitudinal, $\omega_L$, and transverse, $\omega_T$ (shown here with no spatial dispersion) excitons (dashed lines), and the photon dispersion ("light line")

region is called the stopgap, and its width ($\omega_L - \omega_o$) is approximately proportional to the oscillator strength of the exciton transition.

The photon dispersion is shown in Figure 1 as an asymptotic "light line." A photon entering the crystal does not exhibit this sort of dispersion behavior, but instead excites a coupled mode at the same frequency on the polariton dispersion curve. (Conservation of momentum, k, is not required in a finite medium.) Near the resonance frequency of the transverse exciton, a polariton which is very exciton-like will be created, while at frequencies far from resonance photon-like polaritons will form. In the case of second harmonic generation near a resonance frequency, when the polaritons associated with the fundamental beam are far from resonance they are photon-like and the associated dispersion relation is $\omega^2 = c^2k^2/\epsilon_\omega$, a straight line (if dispersion in n is weak) with slope $c/n_\omega$. Where this line crosses the polariton dispersion curve at $2\omega$, the phase velocities $\omega/k$ are equal and phase matching occurs. Consequently, it is possible to map a polariton dispersion curve by varying $\epsilon$ of the fundamental beam, e.g., by varying the sample orientation.

## Polaritons in the Second Quantization Approach

The second quantization formalism is the method by which creation and annihilation operators for the states which diagonalize a Hamiltonian may be found when the Hamiltonian is expressed in terms of creation and annihilation operators for a set of basis states which is not diagonalizing. The goal of the procedure is to derive the relationships between the "old" operators and the "new" ones. Second quantization was the method

employed by Hopfield (106) in his initial general paper on polaritons. The procedure for exciton-polaritons in molecular crystals was worked out by Agranovich (109) and has recently been reviewed in detail by Johnson and Small (111). The major results of the second quantization approach to the coupling of photons and molecular excitons will be outlined in this section.

In the polariton problem, the exciton field and photon field are modeled as quantum mechanical harmonic oscillators:

$$\mathcal{H}_{EX} = \sum_{\underline{k}\mu} E_{\underline{k}\mu} B^{\dagger}_{\underline{k}\mu} B_{\underline{k}\mu} \qquad [47a]$$

and

$$\mathcal{H}_{PH} = \sum_{\underline{q}j} \frac{\hbar q c}{n} a^{\dagger}_{\underline{q}j} a_{\underline{q}j} \quad , \qquad [47b]$$

where the constant terms have been omitted. The operators $a^{\dagger}_{\underline{q}j}$ and $a_{\underline{q}j}$ are the Bose creation and annihilation operators for photons of wavevector $\underline{q}$ and polarization j transverse to $\underline{q}$. The operators $B^{\dagger}_{\underline{k}\mu}$ and $B_{\underline{k}\mu}$ are the creation and annihilation operators for delocalized excitons of wavevector $\underline{k}$ on branch $\mu$, and approximately obey Bose commutation rules (152b) as long as the volume density of excitations remains low (the Heitler-London approximation of one excited site only will be made throughout):

$$[a_{\underline{q}j}, a^{\dagger}_{\underline{q}'j'}] = \delta_{qq'}\delta_{jj'} \; ; \quad [B_{\underline{k}\mu}, B^{\dagger}_{\underline{k}'\mu'}] = \delta_{kk'}\delta_{\mu\mu'} \quad . \qquad [48]$$

The Hamiltonian for the complete system is:

$$\mathcal{H} = \mathcal{H}_{EX} + \mathcal{H}_{PH} + \mathcal{H}_{INT},$$

where $\mathcal{H}_{INT}$ is the interaction Hamiltonian which couples the excitons and

the photons. The form of the solution sought is:

$$\mathcal{H} = \sum_{k\rho} E_{k\rho} a^{\dagger}_{k\rho} a_{k\rho} \quad , \qquad [49]$$

where $a^{\dagger}_{k\rho}$ and $a_{k\rho}$ are the creation and annihilation operators for a system of uncoupled harmonic oscillators of wavevector k and branch ρ. The interaction Hamiltonian in the Coulomb gauge ($\nabla \cdot \underline{A} = 0$) is (84, 111):

$$\mathcal{H}_{INT} = \frac{-e}{2mc} \sum_{n\alpha} [\underline{A}(\underline{r}_{n\alpha}) \cdot \underline{P}_{n\alpha} + \underline{P}_{n\alpha} \cdot \underline{A}(\underline{r}_{n\alpha})]$$

$$+ \frac{e^2 S}{2mc^2} \sum_{n\alpha} \underline{A}^2(\underline{r}_{n\alpha}) \quad , \qquad [50]$$

where the vector potential $\underline{A}$ is in the long-wave approximation (negligible variation over the interaction distance; that is, over one unit cell) evaluated at the position $r_{n\alpha}$ of the $\alpha^{th}$ molecule in the $n^{th}$ unit cell. Here S is the number of electrons per molecule and $\underline{P}$ is the momentum operator.

The operators in equation [50] may be expressed in terms of the operators of equation [47]. To simplify the problem it is assumed that the quantization volumes for the excitons and for the photons are the same and equal to V. The vector potential $\underline{A}$ is written as (106):

$$\underline{A}(\underline{r}) = \left(\frac{hc}{nqV}\right)^{1/2} \sum_{gj} \hat{e}_j (a_{gj} e^{iq \cdot r} + a^{\dagger}_{gj} e^{-iq \cdot r}) \quad , \qquad [51]$$

where $\hat{e}_j$ is the unit polarization vector for the $j^{th}$ polarization and n is the real refractive index of the medium. The second term in the interaction Hamiltonian [50] can then be written as:

$$\mathcal{H}^{(2)}_{INT} = \sum_{qj} \frac{\hbar\omega_p^2}{4qcn} \left(a_{qj}a_{-qj} + a_{qj}a^{\dagger}_{qj} + a^{\dagger}_{qj}a_{qj} + a^{\dagger}_{qj}a^{\dagger}_{-qj}\right) \quad , \qquad [52]$$

where $\omega_p^2 = 4\pi Ne^2/m$ is the square of the plasma frequency, and N is the number of electrons per unit cell.

The field operator analogous to $\underline{A}$ in equation [51] which contains the exciton operators is the polarization density operator. The momentum operator, $\underline{P}$, may be written in second quantization form by using the quantized form of the position operator $\underline{R}$:

$$\underline{R}_{\pm}(\underline{k}) = \sum_{jna} \hat{e}_j \cdot \underline{r}_{na} = \sum_{na} \sum_{ff'} e^{\pm i\underline{k}\cdot\underline{r}} \underline{Q}^{ff'}_{aj} \left(b^{\dagger}_{naf} b_{naf'}\right) \quad , \qquad [53]$$

where the $\underline{Q}^{ff'}_{aj}$ are the transition dipole moments for the molecular f'->f transition. The operators $b^{\dagger}_{naf}$ and $b_{naf'}$ are the Pauli creation and annihilation operators for molecular states |f> and |f'>, from which the $B_{k\mu}$ of equation [47a] are themselves obtained through a second quantization procedure. Using |f'> = |o>, localized exciton operators which are approximate Bose operators, <u>vide supra</u>, may be constructed from the Pauli operators:

$$B_{na} = b^{\dagger}_{nao} b_{naf} \qquad \text{and} \qquad B^{\dagger}_{na} = b^{\dagger}_{naf} b_{nao} \, . \qquad [54]$$

The transformation to the delocalized operators $B_{k\mu}$ is accomplished by requiring that they obey the Hamiltonian commutation relations for Bose operators,

$$[B_{k\mu}, \mathcal{H}] = E_{k\mu} B_{k\mu} \qquad \text{and} \qquad [B^{\dagger}_{k\mu}, \mathcal{H}] = -E_{k\mu} B^{\dagger}_{k\mu} \, , \qquad [55]$$

and expressing the Hamiltonian in terms of the localized operators $B_{n\alpha}$. The result is of the form:

$$\underline{B}_{n\alpha} = N^{-1/2} \sum_{\underline{k}\mu} [\, \underline{B}_{\underline{k}\mu} u_{\alpha\mu}(\underline{k})\, e^{i\underline{k}\cdot\underline{r}} + \underline{B}'^{\dagger}_{\underline{k}\mu} v^{*}_{\alpha\mu}(-\underline{k})\, e^{-i\underline{k}\cdot\underline{r}} \,] \quad , \qquad [56]$$

where the transformation coefficients u and v are the so-called Tyablikov coefficients. A complete description of the second quantization procedure for excitons including the exact forms of the Tyablikov coefficients may be found in the references by Agranovich (109) and by Johnson and Small (111). Using [56], it is then possible to write the position operator $\underline{R}_{\pm}$ in terms of the delocalized exciton operators $B_{k\mu}$ and $B'^{\dagger}_{k\mu}$.

At this point it is convenient to define a momentum operator $\underline{J}_{\pm}$ which is a sum of one-particle momentum operators in the same way that $\underline{R}_{\pm}$ is a sum of one-particle position operators:

$$\underline{J}_{\pm}(\underline{k}) = \sum_{jn\alpha} (\hat{e}_j \cdot \underline{P}_{n\alpha})\, e^{\pm i\underline{k}\cdot\underline{r}_{n\alpha}} \quad . \qquad [57]$$

Then the position-momentum commutation relation may be expressed as:

$$[\underline{R}_{\pm}(\underline{k}), \mathcal{H}_{EX}] = \frac{i\hbar}{m} \underline{J}_{\pm}(\underline{k}) \quad . \qquad [58]$$

Using equation [51] and the definition [57], the first term in $\mathcal{H}_{INT}$ (equation [50]) is written in the form:

$$\mathcal{H}^{(1)}_{INT} = -\sum_{qj} \frac{e}{m} \left[\frac{\hbar}{qVcn}\right]^{-1/2} [\underline{J}_{+}(\underline{q})\, a_{qj} + \underline{J}_{-}(\underline{q})\, a'^{\dagger}_{qj}] \quad , \qquad [59]$$

where the $\underline{J}_{\pm}$ may be expressed in terms of the $B_{k\mu}$ by using the relation [58] and the second-quantized form of $\underline{R}_{\pm}$. The resulting Hamiltonian for

the exciton-photon system, using the expressions [47], [52], and [59] with the second-quantized forms of the $\underline{J}_{\pm}$, is (111):

$$\mathcal{H} = \sum_{\underline{k}\mu} E_{\underline{k}\mu} B^{\dagger}_{\underline{k}\mu} B_{\underline{k}\mu} + \sum_{\underline{q}j} \frac{\hbar q c}{n} a^{\dagger}_{\underline{q}j} a_{\underline{q}j} + \sum_{\underline{q}j\mu} \{ \underline{I}(j,-\underline{q},\mu) a_{\underline{q}j} B_{-\underline{q}\mu}$$

$$+ \underline{I}(j,\underline{q},\mu) a^{\dagger}_{\underline{q}j} B_{\underline{q}\mu} + \underline{I}^{*}(j,\underline{q},\mu) a_{\underline{q}j} B^{\dagger}_{\underline{q}\mu} + \underline{I}^{*}(j,-\underline{q},\mu) a^{\dagger}_{\underline{q}j} B^{\dagger}_{-\underline{q}\mu} \}$$

$$+ \sum_{j} \frac{\hbar \omega_{\underline{p}}^{2}}{4qcn} (a_{\underline{q}j} a_{-\underline{q}j} + a_{\underline{q}j} a^{\dagger}_{\underline{q}j} + a^{\dagger}_{\underline{q}j} a_{\underline{q}j} + a^{\dagger}_{\underline{q}j} a^{\dagger}_{-\underline{q}j}) \quad , \qquad [60]$$

where $\underline{I}(j,\underline{q},\mu)$ is a weighted sum over sites $\alpha$ of transition dipoles $\underline{g}^{fo}_{\alpha j}$ between states $|o\rangle$ and $\langle f|$ at polarization j:

$$\underline{I}(j,\underline{q},\mu) = ie\left[\frac{2\pi}{qvcnh}\right]^{1/2} \sum_{\alpha} \underline{g}^{fo}_{\alpha j} [u_{\alpha\mu}(\underline{q}) + v_{\alpha\mu}(\underline{q})] E_{\underline{q}\mu} \qquad [61]$$

and v is the unit cell volume.

The Hamiltonian in [60] is expressed in terms of the creation and annihilation operators of the coupled oscillators (the excitons and photons). The remaining problem is to find the coefficients analogous to the u and v Tyablikov coefficients of the exciton second quantization, which transform equation [60] to the form [49] of a Hamiltonian of uncoupled oscillators:

$$a_{\underline{q}j} = \sum_{\rho} [u_{\rho j}(q) \alpha_{\rho\underline{q}} + v^{*}_{\rho j}(-q) \alpha^{\dagger}_{\rho-\underline{q}}]$$

$$B_{\underline{k}\mu} = \sum_{\rho} [u_{\rho\mu}(k) \alpha_{\rho\underline{k}} + v^{*}_{\rho\mu}(-k) \alpha^{\dagger}_{\rho-\underline{k}}]$$

(plus the two conjugate equations). [62]

The Tyablikov method is again used: the commutators of the Hamiltonian from equation [60] with the delocalized exciton and photon creation and annihilation operators are found, and equation [62] is used to express the commutators in terms of the polariton operators. The polariton creation and annihilation operators are then required to obey the appropriate Hamiltonian commutation relations:

$$[\alpha_{\rho\underline{k}}, \mathcal{H}] = E_{\rho\underline{k}}\alpha_{\rho\underline{k}} \quad \text{and} \quad [\alpha'_{\rho\underline{k}}, \mathcal{H}] = -E\,\alpha'_{\rho\underline{k}} \; . \qquad [63]$$

The resulting expressions for the new Tyablikov coefficents are quite complicated and will not be reproduced here. The exact solutions may be found in the review by Johnson and Small (111).

If the commutation relation [63] is treated like an eigenvalue problem, the energies $E_{\rho k}$ may be extracted. For the case where only one exciton level is important, the result is (106, 109, 111):

$$E_{\rho j\underline{k}} = \frac{\hbar^2 k^2 c^2}{n^2} + \frac{(2-j)\,\omega_p^2}{n^2}\,\frac{E_{\rho j\underline{k}}}{E^2_{\rho j\underline{k}} - E^2_{\mu\underline{k}}}\,F_\mu \sin^2\varnothing \; , \qquad [64]$$

where the polarization j=2 is not coupled with the exciton and $\varnothing$ is the angle between $\underline{k}$ and $\underline{Q}$.

The solutions to [64] are identical in form to those obtained in the semiclassical treatment, equation [46]. This result is unsurprising, as both approaches model the interaction as the coupling of harmonic oscillators. However, a distinction may be drawn when damping is introduced. Damping arises in the polariton model when the term $c^2k^2/\omega^2$ (the dielectric constant) is complex. The two limiting cases for this condition are

when k is complex and $\omega$ is real (the spatially inhomogeneous, temporally homogeneous solution) and when $\omega$ is complex and k real (spatially homogeneous, temporally inhomogeneous solution ). The difference between the two cases is not a trivial one. Damping alters the form of the polariton dispersion curves somewhat, and spatially damped polariton dispersion curves are quite dissimilar to temporally damped curves. Temporal damping has the effect of "flattening" the curves a bit while retaining their essential character, while spatial damping unmistakedly alters the shapes of the curves (e.g., removing the stop gap). This has been shown explicitly by Merten and Borstel (137) and may be understood intuitively by considering that the quantity which relates the spatial and temporal position of a polariton, the group velocity $\partial\omega/\partial k$, is not a constant along the dispersion curves. Most authors (37, 117a, 137) have considered the temporal damping case to be the more correct description of polariton damping in a two-photon study such as Raman spectroscopy (with phonon-polaritons) or second harmonic generation, where the polariton is formed in the bulk of the crystal. Evidence for this point of view will be presented in Chapter IV of this dissertation. The spatially inhomogeneous model may be the more correct description for one-photon polariton effects (117d), where the polaritons are formed at the front surface of the crystal and the assumption of an infinite crystal is less appropriate. In either case, it is the damping of the polariton which determines the intensity and shape of the resulting signal.

In the semiclassical model, the damping term in the dielectric constant arises as described in the previous section. The meaning of the

damping term $\Gamma_{ig}$ in equation [19] is "the damping of the state whose resonant frequency is $\omega_{ig}$;" that is, it is the temporal damping of the uncoupled exciton. In the polariton model, in the second (scattering) step of the two-step absorption process it is the excitonic character of the polariton which is responsible for its damping, but it is the polariton state which is damped. This is a distinction which may have important experimental consequences. The inverse of the Tyablikov transformation [62] gives the four polariton creation and annihilation operators in terms of the $a_{qj}$'s and the $B_{k\mu}$'s, e.g.:

$$\alpha^{\dagger}_{\underline{k}} = r^{*}_{\underline{q}}\, a^{\dagger}_{\underline{q}} + r^{*}_{\underline{k}}\, B^{\dagger}_{\underline{k}} + s_{-\underline{q}}\, a_{-\underline{q}} + s_{-\underline{k}}\, B_{-\underline{k}} \qquad [65]$$

The r and s coefficients are related to the u and v coefficients of equation [62] by the Bose commutation rules for the $a_{qj}$, the $B_{k\mu}$, and the $\alpha_{k\rho}$ operators. For example, the coefficient $r_{\underline{k}}$ is (107c):

$$r_{\underline{k}} = \frac{i\left[\dfrac{\omega_p^2 F}{4\epsilon_0\omega_0^2}\right]^{1/2}(1+\omega/\omega_0)}{(\omega/\omega_0)^{1/2}\left[(1+\omega^2/\omega_0^2)^2 + \dfrac{\omega_p^2 F}{\epsilon_0\omega_0^2}\right]^{1/2}} \qquad [66]$$

Hopfield (107c) has pointed out that for an appreciable part of the polariton dispersion curve the approximation $r_{\underline{q}} \approx s_{\underline{q}} \approx s_{-\underline{k}} \approx 0$; $|r_{\underline{k}}| \approx 1$ is a good one. Values for $|r_{\underline{k}}|$ appropriate for the case of the 31475 $cm^{-1}$ a-exciton polariton in naphthalene are shown in Figure 2. The figure illustrates that there is quite a large frequency range, about 15 $cm^{-1}$, over which the polariton may be said to be chiefly excitonlike ($|r_{\underline{k}}| > .95$) while exhibiting

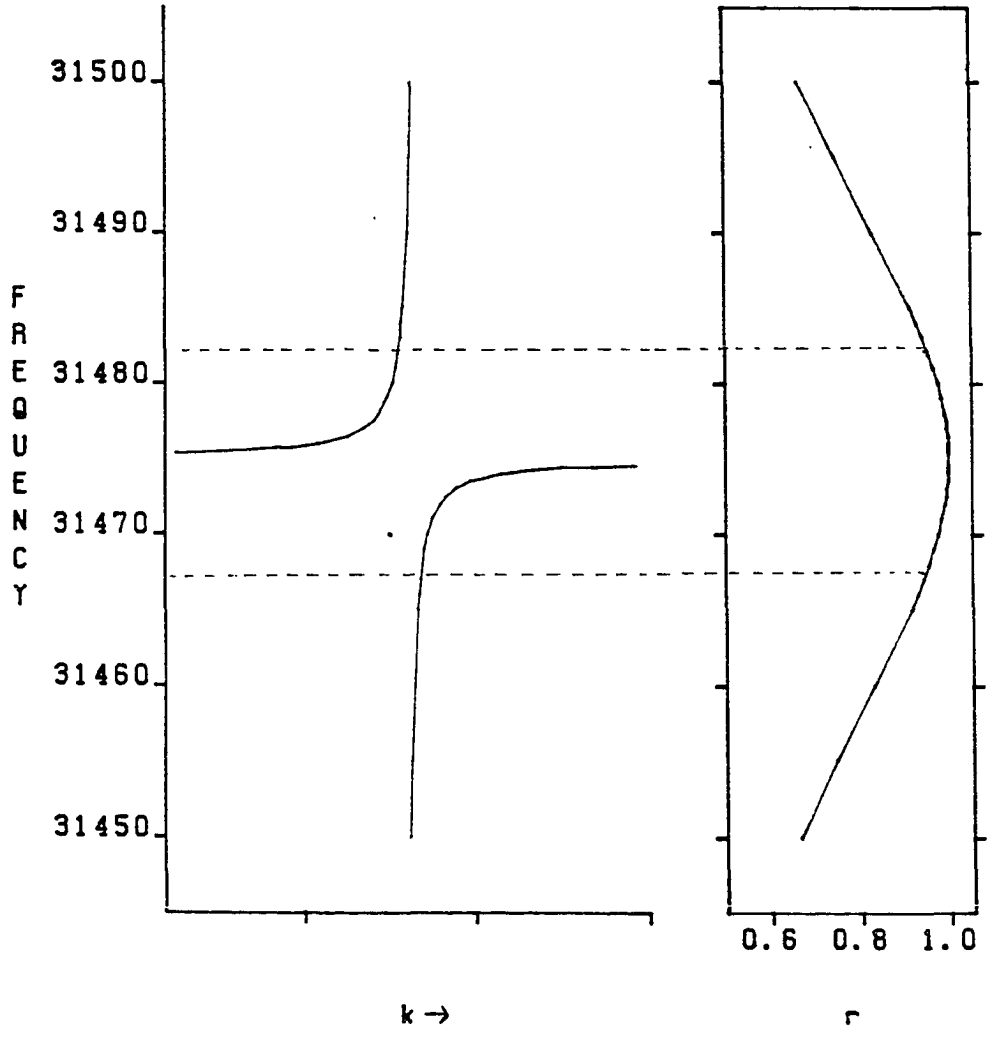


Figure 2. At right, the coefficient $|r_k|$ of the exciton creation operator in the expression [65] for the creation operator of the a-exciton polariton in naphthalene. At left, a typical naphthalene a-exciton polariton dispersion curve. The dashed lines delimit the frequency region where $|r_k| > 0.97$

considerable photon character in its dispersion behavior.

## Nonlinear Behavior in the Polariton Model

In the classical treatment of coupled oscillators described in an earlier section, nonlinear effects were introduced by allowing the oscillators to become anharmonic and the solution was obtained by treating the anharmonicity as a perturbation. Similarly, nonlinear optical effects in the polariton model are obtained by expanding $\mathfrak{H}_{EX}$ and $\mathfrak{H}_{INT}$ beyond the quadratic terms given in expressions [47a], [52], and [59]. The total crystal Hamiltonian is obtained in terms of the photon and exciton creation and annihilation operators, as in the linear case; they are then replaced by the polariton basis states of the linear crystal Hamiltonian by means of the Tyablikov transformation. This method of expressing the nonlinear crystal Hamiltonian has been described by Ovander (152) and by Johnson and Small (111). This section will outline the treatment and will present the results which are applicable to two-photon resonance-enhanced SHG and TPA.

Following the notation of Johnson and Small, the exciton and interaction Hamiltonians may each be written as a sum of third order and lower order terms:

$$\mathfrak{H}_{EX} = \mathfrak{H}_{EX}^{(0)} + \mathfrak{H}_{EX}^{(2)} + \mathfrak{H}_{EX}^{(3)} \qquad [67a]$$

$$\mathfrak{H}_{INT} = \mathfrak{H}_{INT}^{I(2)} + \mathfrak{H}_{INT}^{II(2)} + \mathfrak{H}_{INT}^{I(3)} + \mathfrak{H}_{INT}^{II(3)} \quad , \qquad [67b]$$

where $\mathfrak{H}_{INT}$ has further been subdivided into terms associated with the $\underline{A}\cdot\underline{P}$ term (I) and terms associated with the $\underline{A}^2$ term (II). The third order term

in $\mathcal{H}'_{INT}$ is obtained in the same manner as was used to find the lower order part. The definition of the position operator $\underline{R}_{\pm}$ is again generalized from equation [53] using the Heitler-London approximation, but the sum over molecular states $|f'\rangle$ is retained to allow for the participation of intermediate states in higher order processes. The resulting expression is:

$$\underline{R}_{\pm}(\underline{q}) = 2\sum_{n\alpha}\sum_{ff'} e^{\pm i\underline{q}\cdot\underline{r}}\, \underline{Q}^{ff'}_{\alpha j}\, B^{\dagger}_{n\alpha f}\, B_{n\alpha f'} \qquad [68]$$

The momentum operator $\underline{J}_{\pm}$ is again defined by the commutator of the exciton Hamiltonian with the position operator, using the form [68] for $\underline{R}_{\pm}$:

$$[\,\underline{R}_{\pm}(\underline{q})\,,\ \mathcal{H}^{(0)}_{EX} + \mathcal{H}^{(2)}_{EX}\,] = \frac{i\hbar}{m}\,\underline{J}_{\pm}(\underline{q}) \qquad [69]$$

and equation [59] is used to find the expression for $\mathcal{H}'_{INT}$. In the Heitler-London approximation, the third order term is (37):

$$\mathcal{H}'^{(3)}_{INT} = \sum_{\underline{k}}\sum_{\underline{q}j\mu_1\mu_2}\sum -i\left[\frac{2\pi e^2}{Nvqcn\hbar}\right]^{1/2}\sum_{ff'\alpha} \underline{Q}^{ff'}_{\alpha j}\,[\,a_{\underline{q}j}\,B^{\dagger}_{\underline{k}\mu_1}B_{(\underline{k}-\underline{q})\mu_2}$$

$$\times\,(E_{\underline{k}\mu_1} - E_{(\underline{k}-\underline{q})\mu_2}) + a^{\dagger}_{\underline{q}j}\,B^{\dagger}_{\underline{k}\mu_1}B_{(\underline{k}+\underline{q})\mu_2}$$

$$\times\,(E_{\underline{k}\mu_1} - E_{(\underline{k}+\underline{q})\mu_2}) \qquad [70]$$

The polariton Tyablikov transformation [62] is then used to express $\mathcal{H}'^{(3)}_{INT}$ in terms of polariton creation and annihilation operators. Each of the two terms in equation [70] leads to eight terms in the new expression, each containing a product of three of the polariton operators and three

Tyablikov coefficients. Similar expressions are derived for the third order contributions to the Hamiltonian from $\mathcal{H}_{EX}$ and $\mathcal{H}^{II}_{INT}$, but it has been shown that the contributions from these terms may generally be neglected in treating SHG and TPA (37, 111). Terms in $\mathcal{H}_{EX}$ may become important if there is a resonance near the fundamental frequency. (The local field effects of the semiclassical model arise from dipole-dipole interactions contained in $\mathcal{H}_{EX}$.)

The terms in the third order Hamiltonian which are important to SHG are those which describe the annihilation of two polaritons and the creation of a third. This process has been called "polariton fusion" by Fröhlich (159). The rate of fusion may be extracted from these terms using the Fermi golden rule:

$$W^{\mu 0}(\underline{k}) = \frac{2\pi}{\hbar}\Big|\sum_{\rho_1\rho_2\rho_3}\sum_{\underline{k}_1\underline{k}_2}\langle n_{3(\underline{k}_1+\underline{k}_2)}+1;\, n_{2,\underline{k}_2}-1;\, n_{1,\underline{k}_1}-1|$$

$$\times \underline{R}(\underline{k}_1,\underline{k}_2;\rho_1\rho_2\rho_3)\, a_{1\underline{k}_1} a_{2\underline{k}_2} a^{\dagger}_{3\underline{k}_1+\underline{k}_2}$$

$$\times |n_{3(\underline{k}_1+\underline{k}_2)};n_{2,\underline{k}_2};n_{1,\underline{k}_1}\rangle\Big|^2 \delta[E_{1,\underline{k}_1}+E_{2,\underline{k}_2}-E_{3(\underline{k}_1+\underline{k}_2)}]\,. \quad [71]$$

In the case where the created polariton is at an exciton resonance frequency, the polariton fusion matrix element is (111):

$$\underline{R}(\underline{k}_1,\underline{k}_2;\rho_1\rho_2\rho_3) = -\left[\frac{2\pi e^2\hbar}{Nvcm^2}\right]\frac{1}{k_1k_2n_1n_2}|u_{\rho_1 j\underline{k}_1}||u_{\rho_2 j\underline{k}_2}|$$

$$\times\sum_{\mu}\left[\frac{\langle \underline{k}_1+\underline{k}_2,\mu_f|J_+(\underline{k}_1)|\mu,\underline{k}_2\rangle\langle \underline{k}_2,\mu|J_+(\underline{k}_2)|0\rangle}{E_{\mu\underline{k}_2}-\hbar\omega_2}+I(1,2)\right]. \quad [72]$$

As in the previous section, the assumption made throughout this treatment is that the crystal may be approximated as infinite, so that pseudomomentum may be treated as a good quantum number. If the finite extent of the crystal is admitted, the sum over n in the localized representation of the position operator, equation [68], must be retained and the fusion rate is multiplied by the factor:

$$\left|\sum_{n} e^{i\Delta\underline{k}\cdot r}\right|^2 \quad \text{or} \quad \frac{N}{L}\left|\int_0^L e^{i\Delta\underline{k}x}\,dx\right|^2 , \qquad [73]$$

where $\Delta\underline{K} = \underline{k}_1 + \underline{k}_2 - \underline{k}$. The fusion rate is consequently maximized when $\Delta\underline{k} = 0$, and polariton fusion is a phase matched process in accordance with the predictions of classical field theory.

It has been suggested (37, 111) that the polariton fusion process provides the natural extension to two-photon absorption processes of Hopfield's model of the one-photon absorption process. The similarity between the fusion rate expression and the classically derived SHG intensity expression [25] is immediately apparent. If the SHG signal results from polariton fusion, scattering of the fused polaritons must be observed as TPA. (This process corresponds to the phase matched term in the classically derived expression, [30]. To obtain the second quantization expression corresponding to the non-phase matched $X^{(3)}$ term, it is necessary to extend the treatment of this section to include fourth order terms in the crystal Hamiltonian.) Thus, phase matched two-photon absorption is viewed as a three-step process: formation at the crystal surface of the photon-like polaritons at the fundamental frequency, followed by polariton

fusion in the bulk of the crystal, followed by scattering of the fused polariton from a chemical impurity or a physical defect such as a phonon. In this model, SHG and TPA or TPE signals should appear to compete for intensity as the number of fourth-body scatterers is varied.

The subject of this dissertation is an experimental study of the simultaneous second harmonic generation and two-photon emission signals observed from "perfect" naphthalene crystals near the lowest frequency zero-phonon exciton. Temperature studies were conducted in order to test the predictions of the polariton fusion model. Signal intensity and broadening behavior were examined. Finally, the effect of the phase matching condition on the appearance of a signal in a frequency region of rapidly changing phase velocity (the "elbow" and "knee" regions of the polariton dispersion curves) was explored.

# III. EXPERIMENTAL PROCEDURES

The results of several temperature studies of simultaneous second harmonic generation (SHG) and two-photon excited emission (TPE) in naphthalene crystals at various angles of incidence are presented in Chapter IV. The experiment involved purification, growth and strain-free mounting of naphthalene crystals, control of the sample temperature, optimization of a laser-based optical system, computer-controlled data acquisition, and data processing.

## Sample Preparation and Mounting

The crystals used in the experiment were sublimation flakes of very pure naphthalene. A few crystals were doped lightly ($10^{-5}$ - $10^{-4}$ mole per mole naphthalene) with anthracene.

The naphthalene used was from Aldrich Chemical, with a nominal purity of 98%. Purification was accomplished by fusion with sodium or potassium metal to remove ß-methylnaphthalene (117a, 191, 192), refluxing the mixture for 30 minutes under a nitrogen atmosphere of about 50 mm Hg at 100°C. The naphthalene was transferred by decanting the clear liquid and then subliming as much as possible from the residue to a zone-refining tube, still under nitrogen. In this way the greater part of the metal salt remained in the reaction vessel. The remainder of the salt and other impurities were then removed by zone-refining, 110 passes at 4 cm/hour with a melt zone of about 0.5 cm, under 100 mm Hg of nitrogen. The center third of the tube material was used for the experiment, and the

rest was discarded. The concentration of imputities in the material used was estimated to be better than 1 ppm (117a).

The most satisfactory method for growth of thin, high-quality flakes with large surface area is illustrated in Figure 3. About five grams of crushed naphthalene was placed in the bottom of a sublimation apparatus outfitted with a modified top on which the glass cold finger had been replaced with a copper rod terminating in an inverted conical bell, also of copper. The lower lip of the bell was about 2 cm from the upper suface of the naphthalene. The apparatus was immersed to the level of the lower edge of the bell in an oil bath kept at 78-80 °C. A short length of heating tape was wrapped around the sublimator to warm the walls in the vicinity of the bell. Previous work on naphthalene crystal growth by sublimation (117a) has demonstrated the importance of the magnitude of the temperature gradient established between growth surface and evaporation surface in obtaining high-quality flakes. Equally critical are the concentration gradient over the same region and the rate of mass flow past the crystal growth surface. All these conditions seemed to be optimized in the system described so long as the stopcock of the sublimator was left open. Attempts to grow samples in closed systems invariably resulted in unsatisfactory needle-like crystals and "frost."

Naphthalene flakes doped with anthracene were grown in the same apparatus with the oil bath at 82-84 °C. The anthracene and naphthalene were crushed together and placed in the bottom of the apparatus. Because the doped crystals tended to be very thin and cellophane-like, it was necessary to insert a piece of pierced filter paper between the solid and

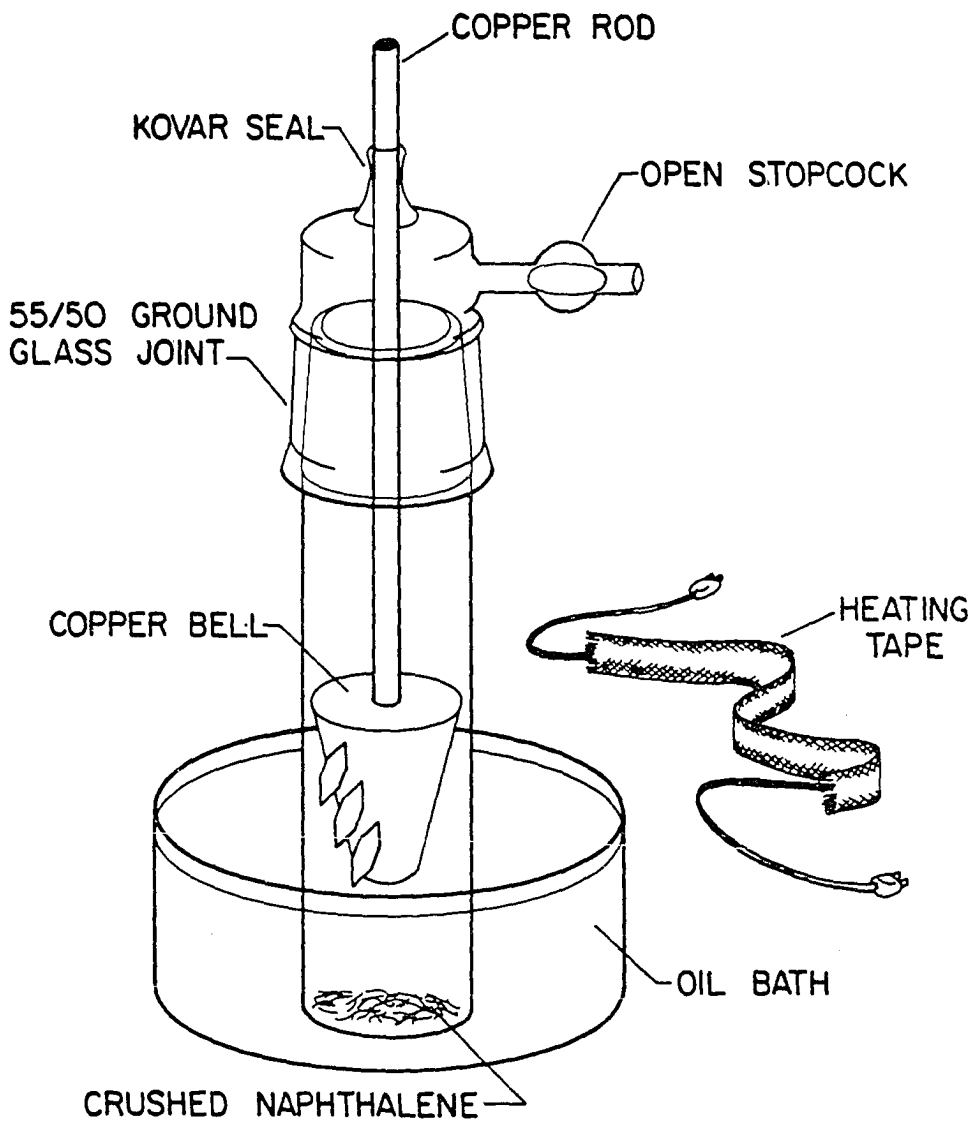


Figure 3. Crystal growth apparatus

the bell to prevent crystals formed at the surface from floating up and attaching themselves to previously formed crystals. All crystals formed on the bell were preserved and later dissolved to obtain an average anthracene concentration approximating that of the sample used in the experiment. Examination of the material obtained from different regions of the bell showed no difference in anthracene concentration.

To retard vaporization degradation of the naphthalene crystal surfaces, the samples were mounted and aligned in a refrigerated room kept at about 35 °F. The crystals were touched only with waxed weighing paper and Teflon-coated utensils, as contact with utensils of other materials generally resulted in complete or partial adhesion to the utensils, with consequent strain.

Alignment of the sample was accomplished coniscopically, using a Leitz Ortholux-Pol polarizing microscope. Naphthalene produces ab sublimation flakes, and the optic plane is (010) (193); the a-axis (and therefore the b-axis) could be located by the dark brush produced by convergent light under crossed polarizers (see Appendix A). Crystals were aligned in the sample holder so that the b-axis would be parallel to the sample rod; rotation of the sample rod would then be equivalent to rotating the crystal about b.

Sample thicknesses less than 19 μm could be measured with the Leitz Tilting Compensator M (see Appendix A). One very thick sample was measured using a Poland micrometer and found to be 55±3 μm thick. The thicknesses of crystals in the 20-35 μm range were estimated from the appearance of the samples under crossed polarizers.

The sample holder is shown in Figure 4. The design was intended to allow accessibility of the crystal to incoming beams at diverse angles, maximize the fluorescence signal (viewed normal to the incoming beam, vide infra), minimize strain on the sample, and provide for an accurate and reproducible sample temperature measurement. The strain-free mounting technique was similar to that used in reference 117a.

The base of the holder was a flat piece of copper with a slot cut into one side, extending most of the way across the plate, and with a divot cut out of the other side at the same position. A small hole was drilled into the plate near the divot. A black paper mask was cemented to the plate and a smaller slot cut out of the mask. To the paper was fastened another mask, made of laboratory tissue paper (Kimwipes) and glued only at the corners. The slot in the tissue mask was cut large enough so that a view from the other side of the sample holder revealed only black paper. (This precaution was taken so that emission from the tissue edge excited by emergent SHG would not augment the TPE signal from the naphthalene crystal.) Another tissue-and-paper mask was prepared and affixed to the sample holder via a pressure tape "hinge" so that the two tissue layers faced one another. Layers of paper pressure tape were built up on the first mask above and below the slot. A crystal was mounted by placing it on the sample holder over the slot, rotating it until the a-axis brush lined up with the slot (horizontally, in the lab frame), closing the second mask over the crystal, and taping the whole thing shut with pressure tape strips wrapped around the sample holder at the positions of the interior tape layers. As long as the pressure tape layers were thicker than the crystal,

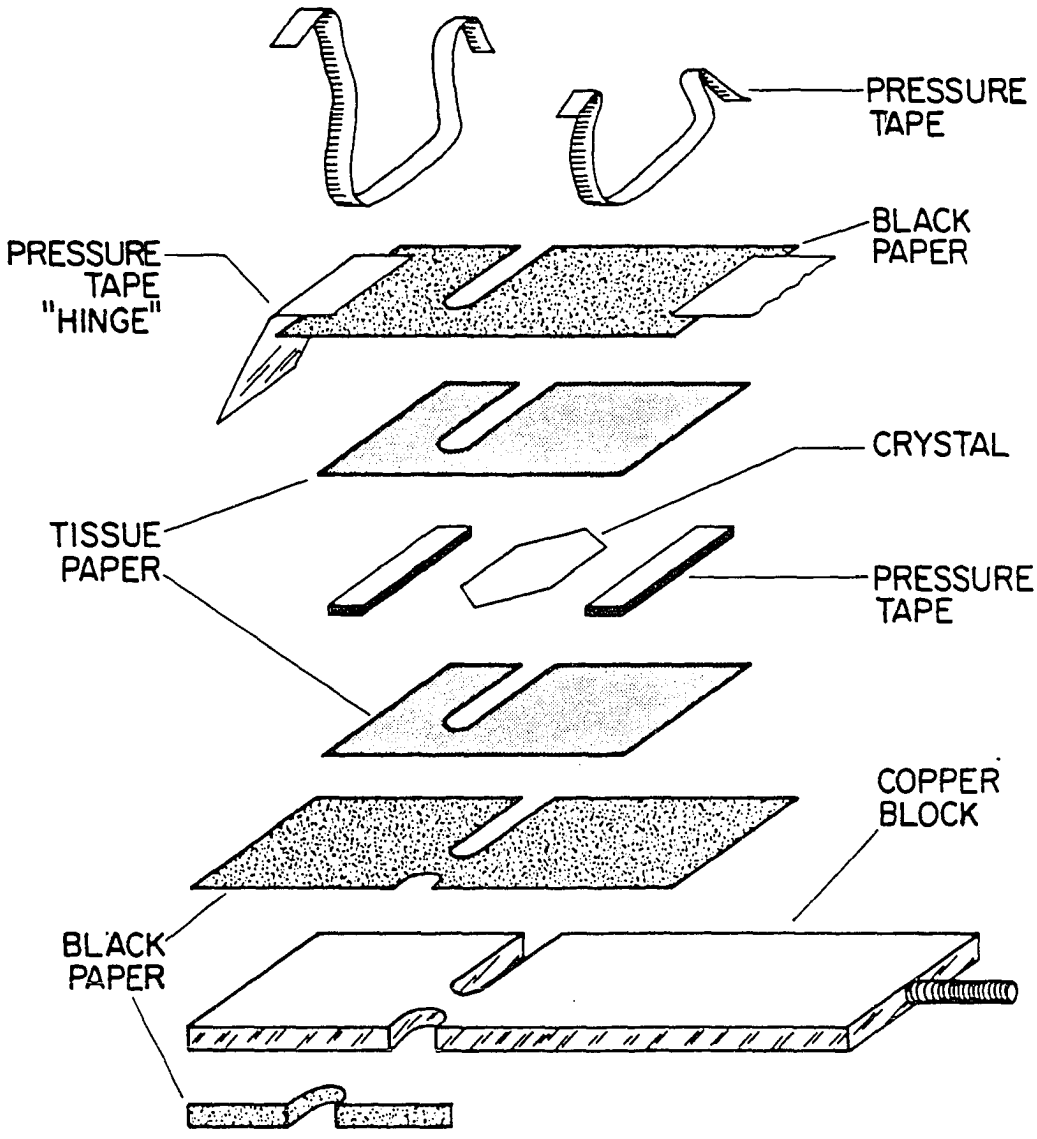


Figure 4. Strain-free sample holder

the holder could be securely fastened without putting strain on the sample. The crystal was then held in position by the fibers protruding from the relatively rough surfaces of the Kimwipe masks.

The mounted crystal was placed in a closed jar containing crushed naphthalene and allowed to come nearly to room temperature to prevent moisture from condensing on the surface of the sample while the holder was being transferred to the cryostat used in the experiment. A thread through the small drilled hole in the copper plate allowed for reproducible positioning of a temperature-sensing diode (Lakeshore Cryotronics DT-500K) in the divot next to the sample slot. The divot was lined with paper to give the diode thermal contact with the sample holder similar to that experienced by the sample.

The sample temperature was read from the diode by measuring the voltage necessary to balance a 10 microampere current across the diode; this was accomplished with a Lakeshore Cryotronics DTC-500 Cryogenic Temperature Controller (used only to monitor and not to control the temperature). The cryostat used, a Janis 8DT "Supervaritemp" stainless steel optical Dewar, allowed control of the sample temperature above 4.2 K by varying the rate at which liquid helium or cold helium gas throttled from a reservoir into the sample chamber. Temperatures from 1.3 to 6 or 7 degrees Kelvin could be reached and maintained by pumping with a Stokes pump on liquid helium in the sample chamber and varying both the throttling rate and the pumping speed. The best temperature control, even below 4.2K, was achieved by keeping the level of the liquid helium below the sample. A resistive heater, also provided with the cryostat, was not

used. The temperature stability of the sample during a scan was generally about ± 0.1 K at the higher temperatures used (15-25 K), and better at lower temperatures, especially while pumping over the sample chamber.

## Lasers and Optics

The light source used in the experiments was a Hänsch-type oscillator/amplifier dye laser (194, 195), National Research Group PTL-2000, pumped by an NRG 0.7-5-200 pulsed nitrogen laser (196). The output of the nitrogen laser at 20 Hz was 4-6 mJ per pulse, with a 5 nanosecond pulse duration. The dye solution used in the laser to get output at 6352 Å was Rhodamine-640 in ethanol, $5 \times 10^{-3}$M, with potassium hydroxide added to shift the gain curve to higher frequencies. The optimum ratio was determined to be about 0.75 moles KOH per mole R640. Typical output from the dye laser was about 50 µJ per pulse.

The laser wavelength could be scanned by means of a stepping motor driving a set of gears which rotated the grating of the dye laser, 0.0017 Å/step in ninth order. The full-width at half-maximum (FWHM) of the dye laser output was about 0.4 $cm^{-1}$. For high-resolution experiments, a 5 mm etalon with a total finesse of $F_T \approx 35$ was placed external to the oscillator cavity and before the amplifier, theoretically narrowing the output at 6352 Å to 0.03 $cm^{-1}$. Examination of the beam profile with a Burleigh TL-15-14 Fabry-Perot interferometer showed the FWHM to be 0.03-0.04 $cm^{-1}$. Tuning of the laser with the etalon in place was accomplished by pressuring the etalon and grating chambers with nitrogen gas at a fixed grating orientation. Over a pressure range of 0 to 2 atomospheres (abso-

lute), the tuning range was about 3 Å, more than sufficient for most measurements in this experiment. The pressure was monitored by a Wallace-Tiernan needle gauge and by a National Semiconductor pressure transducer with a linear output of 0-5 volts over the 0-2 atm range. The scanning rate was set with the needle valve through which the nitrogen was bled into the system; a high supply pressure (40 psig) ensured a near-constant scanning rate throughout the pressure range.

Wavelength calibration of the laser output and monitoring of the beam profile were accomplished using a Jobin-Yvon HR1500 single-pass 1.5 meter high-resolution scanning monochromator equipped with a CIV 301 controller and an EMI 9659 QB photomultiplier tube. The theoretical resolving power of the instrument was 260,000; generally it was measured at about 250,000. The spectrometer was calibrated by using several of the lines from a neon penlamp (Oriel). Absolute calibration of spectra obtained from pressure-tuned scans of the laser was reproducible to within 1 $cm^{-1}$; relative calibration was much better. The grating-tuned scans were somewhat more accurate in absolute calibration.

The configuration of the optics used in the experiment is shown in Figure 5. The laser output, vertically polarized by means of a Glan-Thompson prism placed before the amplifier, was collimated and passed through an iris diaphragm, a glass wedge beam splitter, another Glan-Thompson polarizer, and then lightly focused onto the sample with a 50 cm lens. Second harmonic generation (SHG) was detected collinearly with an Amperex 56DVP photomultipier tube in a fast-response base (type "B," Products for Research), filtered by a Schott UG-11 filter and a Corion

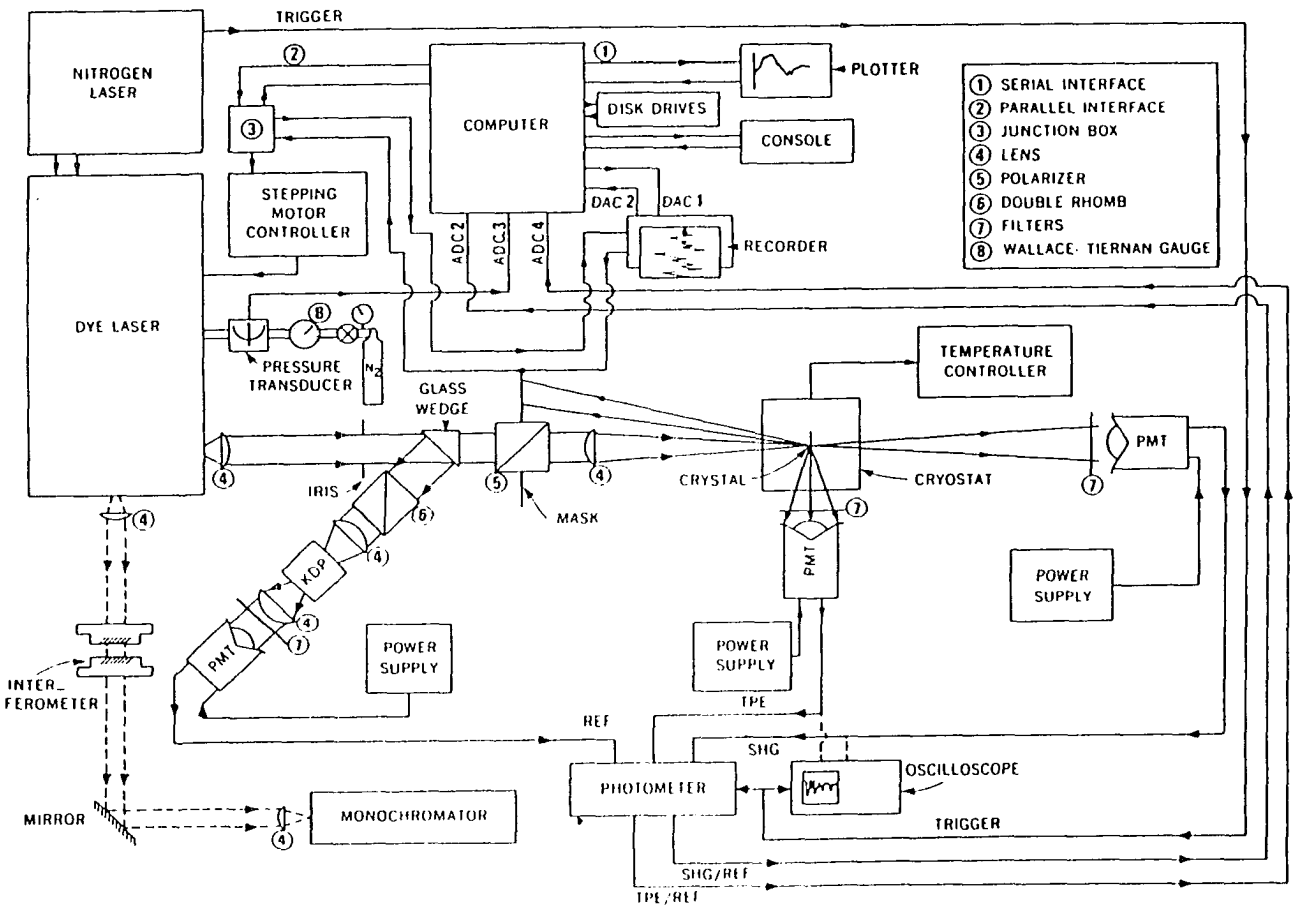


Figure 5. Experimental configuration for normalized variable temperature measurement of second harmonic generation and two-photon excited emission

3200 Å interference filter. The probability of accidental detection of the incoherent two-photon emission signal (TPE) in collinear geometry was minimized by positioning the SHG photomultiplier tube about 50 cm from the sample. The detector output was also monitored occasionally with a fast oscilloscope (Tektronix 475A). No signal with a duration longer than that of the laser pulse was observed. Since the fluorescence lifetime of the exciton studied in this experiment is on the order of 100 ns, discrimination was judged to be satisfactory. Emission was detected normal to the incident beam and as close as possible to the sample by an Amperex XP2232B photomultiplier tube, also in a PFR "B" base, filtered by a Schott UG-11 filter with transmission between 3000 and 3800 Å. Periodic monitoring of this signal with the oscilloscope showed no evidence of contributions from scattered SHG.

The portion of the beam split off by the wedge passed through a double Fresnel rhomb (to rotate the polarization) and was focused by a 10 cm lens onto a lasermetrics KDP frequency-doubling crystal on a Gimbal mount. (The purpose of rotating the polarization was to align the finer of the two tilting adjustments of the Gimbal mount with the critical alignment direction of the reference KDP crystal.) The frequency-doubled light was detected by an RCA 1P28 photomultiplier tube filtered by a Schott UG-11 filter and a Molectron TF interference filter. The output of the doubling crystal was intense enough to cause fluorescence visible to the eye from a white card. Random noise for this signal was minimal and fluctuations in intensity were mainly due to fluctuations in the laser beam intensity. For this reason and because the doubled beam had the same

power dependence as the nonlinear signals under investigation, it was used as a normalizing reference beam.

Because the sample was mounted with the crystalline b-axis vertical, variation of the direction of k in the ac plane was accomplished by rotation of the sample rod. The exact normal incidence position (k along c') was determined by retroreflection of the incident beam. Other angles of incidence could be read from the top of the sample rod. Angles less than about 10° in either direction could be cross-checked by reflection of the beam off the crystal face onto a large cardboard mask affixed to the polarizer mount (see Figure 3). Agreement was generally to within half a degree.

## Data Acquisition and Control

The second harmonic generation, two-photon excited emission, and reference signals were collected by a Lambda-Physik LF300 laser photometer with a 50 microsecond gate, triggered by a pulse from the nitrogen laser which preceded the laser pulse by about 25 ns. The photometer normalized the two signals to the reference and a 10-pulse averaged result was available at two output channels.

Experimental control/monitoring and data acquisition and storage was implemented by one of two programs run on a Digital Equipment Corporation LSI-11/03 computer: program PTUNE for pressure-tuned laser scans, and program GTUNE for grating-stepped scans. Listings of both programs may be found in Appendix B. Normalized SHG and TPE data from the photometer was read by an ADAC multichannel analog-to-digital

converter and stored along with temperature and scan position information. The temperature voltage reading could be entered through the console keyboard at any time during the scan; it was not read directly by the computer. The scan position information stored was either the total number of grating steps moved since program initiation (for GTUNE) or the voltage from the pressure transducer read via the A-to-D converter (for PTUNE). During pressure scans, the pressure transducer was read by the computer and the reading used to determine when to collect a data point; during grating scans, the computer stepped the grating at a selected rate using a KW11P programmable real-time clock (MDB Electronics) and an MDB MLSI-DRV11C parallel line interface to send pulses to a controller built for the stepping motor by Ames Laboratory Instrumentation Services. Data collection was then synchronized to the stepping of the grating, typically one point for four steps (.01 Å).

Because the performance of the pressure transducer was found to vary with ambient conditions, particularly with barometric pressure, PTUNE contained an option to calibrate the transducer against the Wallace-Teirnan gauge. The transducer was generally calibrated in this manner about twice a day during an experiment. These data were stored along with the scan data. All information was saved on floppy disks for later processing and the signals were scaled and output through the ADAC digital-to-analog converters to a two-pen stripchart recorder (Heath SR206). A digital Butterworth filter (197) could be impemented optionally, but was found to be an unsatisfactory method of noise reduction.

## Data Processing

Conversion of pressure transducer voltage (or grating position) -vs.- intensity data to wavelength -vs.- intensity information was effected by a file-processing program (FPPROG, Appendix B). The processed file, smoothed by discrete-window smoothing and optional ensemble smoothing, could then be output to the chart recorder. Alternatively, the file could be drawn on a Houston Instruments DMP4 x-y plotter. The optional smooth for the plotter output was a moving window with optional spike elimination.

Integrated peak intensities were measured by tracing or photocopying the output from one of the above two program sequences, cutting the peaks out, and weighing them on a Mettler analytical balance. The major source of error in this method was in determination of the baseline for signals that were often rather noisy. This was a more serious problem for the higher-temperature peaks, which were lower and broader than those from lower-temperature scans and thus suffered both from a lower signal-to-noise ratio and from increased relative importance of the baseline to the integrated area. For this reason, the high-temperature data (anything above about 13 K) for each run were analyzed several times, occasionally by more than one person (198), and the averaged results were used for analysis. Typical deviations for high temperature integrated intensities were on the order of 5 %. Low temperature intensity uncertainties were on the order of .5%.

# IV. RESULTS AND DISCUSSION

The experiment described in this dissertation is a study of the two-photon excited emission (TPE) and second harmonic generation (SHG) signals associated with the ac-polarized zero-phonon exciton at 31475 $cm^{-1}$ in naphthalene. This state is the lower of the two factor group components which arise from the lowest excited singlet state in the naphthalene molecule. The molecular state is polarized along the long axis of the molecule and has $B_{2u}$ symmetry in the molecular $D_{2h}$ point group; the transition to this state occurs in naphthalene vapor at 32030 $cm^{-1}$ (31b, 199). The naphthalene crystal is monoclinic and belongs to crystal class 2m, isomorphic with $C_{2h}$, with two molecules per unit cell (93, 200). The higher in energy of the two resulting k=0 factor group components is $A_u$ and is polarized along the crystalline b axis (the twofold screw axis); the other is $B_u$ and polarized perpendicular to b. The factor group splitting is about 150 $cm^{-1}$ (93, 117a).

One-photon absorption studies of the ac-polarized (0,0) exciton ($B_u$) using very thin, very pure strain-free ab naphthalene flakes and a-polarized light by Robinette et al. (117) have clearly demonstrated strong coupling of the exciton to the photon field. The purpose of the investigation described here was to use nonlinear spectroscopies to probe polariton behavior in naphthalene and to establish the importance of polariton states in the dynamical behavior of molecular crystals. In the nonlinear experiments, the primary event in the polariton fusion model is the phase

matched fusion in naphthalene of two b-polarized polaritons at a frequency of about 15737 $cm^{-1}$ to form a single polariton, polarized in the ac plane and containing a substantial amount of exciton character from the 31475 $cm^{-1}$ lowest electronic material resonance. These "blue" polaritons, propagating undisturbed through the crystal, are observed as SHG; those which scatter from impurity centers, defects, phonons, etc., produce the TPE signal.

The two-photon absorption spectrum of the naphthalene molecule in solid solution and of the pure naphthalene crystal has been well-documented by several workers (31, 33, 34). Although a two-photon transition to an ungerade state is dipole-forbidden, a weak $^1B_{2u}$ (0,0) absorption is generally observed. A combination electric dipole-magnetic dipole or electric dipole-electric quadrupole mechanism would be symmetry-allowed:

$$\langle f|\underline{M}|i\rangle\langle i|\underline{g}|o\rangle = \langle B_u|A_g|i\rangle\langle i|B_u|A_g\rangle$$

$$\text{or} \qquad = \langle B_u|B_g|i\rangle\langle i|A_u|A_g\rangle ,$$

considering the lower Davydov component only, where $\{E_x, E_y\} \in B_u$; $\{E_z\} \in A_u$; $\{R_z, E_{xy}\} \in A_g$; and $\{R_x, R_y, E_{yz}, E_{xz}\} \in B_g$. Theoretical work by Hochstrasser et al. (201) predicts the magnetic dipole effect for $\pi$-electron systems such as naphthalene to be substantially larger than the electric quadrupole effect. The dominant magnetic component in $\pi$ systems is expected to be the one along the axis normal to the molecular plane (31b), a result which may be obtained intuitively if the $\pi$-electrons are pictured

as a current loop. Given these predictions, a much stonger TPE signal is expected when the incident light is linearly polarized along z (crystal b) than when it is polarized in the xy (ac) plane. Recalling that the fusion rate expression (or, alternatively, the semiclassical expression for $\chi^{(2)}$) contains the two-photon absorption matrix element as well as a one-photon fluorescence matrix element describing the output polarization, one would expect the SHG signal arising from a z-polarized incident fundamental beam to be substantially stronger than that produced by an incident beam polarized perpendicular to z. In the one instance in this study when a sample was mounted so that the incident light was polarized along a, such was observed to be the case: no two-photon emission was seen, and a very weak SHG signal was observed. Since for naphthalene the 31475 $cm^{-1}$ exciton has been demonstrated to be strongly one-photon coupled to the field and polariton fusion is a weakly allowed process, an approach which treats nonlinear optical behavior as a consequence of a perturbation on a strongly coupled exciton-photon system (as outlined in Chapter II) is appropriate.

The directional dispersion, temperature behavior, and profile shapes of TPE and SHG signals were studied in this investigation for several pure naphthalene samples and one crystal doped with anthracene. This chapter presents and discusses some of the data obtained.

## Dispersion Curve Fitting

Because the "red" polaritons are far enough removed from any resonance to be essentially photon-like, phase matching occurs in the limit of

zero damping at the frequency and value of k where the b-polarized photon dispersion line $\omega = ck/n_b$ crosses the polariton dispersion curve, given in the Lorentz model by

$$\omega^4 - \omega^2 \left\{ \frac{c^2 k^2}{n_o^2} + \omega_o^2 + \frac{\omega_p^2 F}{n_o^2} \right\} + \frac{\omega_o^2 c^2 k^2}{n_o^2} = 0 , \qquad [74]$$

where $\omega_o$ is the frequency of the transverse exciton interacting with the photon field, F is the oscillator strength of the transition, $\omega_p$ is the plasma frequency of the material, and the relation $\epsilon_o = n_o^2$ has been used. The value for the background refractive index $n_o$, which determines the slope of the asymptotic "light line" shown in Figure 1, is selected by the sense of $\underline{k}$. That is, the direction of beam incidence in the ac plane of the crystal, varied by rotation of the sample about its b-axis, determines the dispersion of the fused polariton and therefore the phase-matching frequency. This situation is illustrated in Figure 6, which shows ac-polarized polariton dispersion curves for several values of the incident photon angle with respect to the crystal c' axis. The values of the physical parameters of equation [74] used in computing the curves were obtained experimentally, vide infra. The dispersion of the "red" polaritons, produced by the incident 15737 $cm^{-1}$ beam and polarized along b, is not affected by rotation of the crystal about b.

Directional dispersion of the kind described above was observed in these experiments for both the SHG and the TPE signals, and is illustrated in Figure 7 for the SHG profiles obtained from one "perfect" pure strain-free (PSF) naphthalene crystal, about 27 μm thick. The sample tempera-

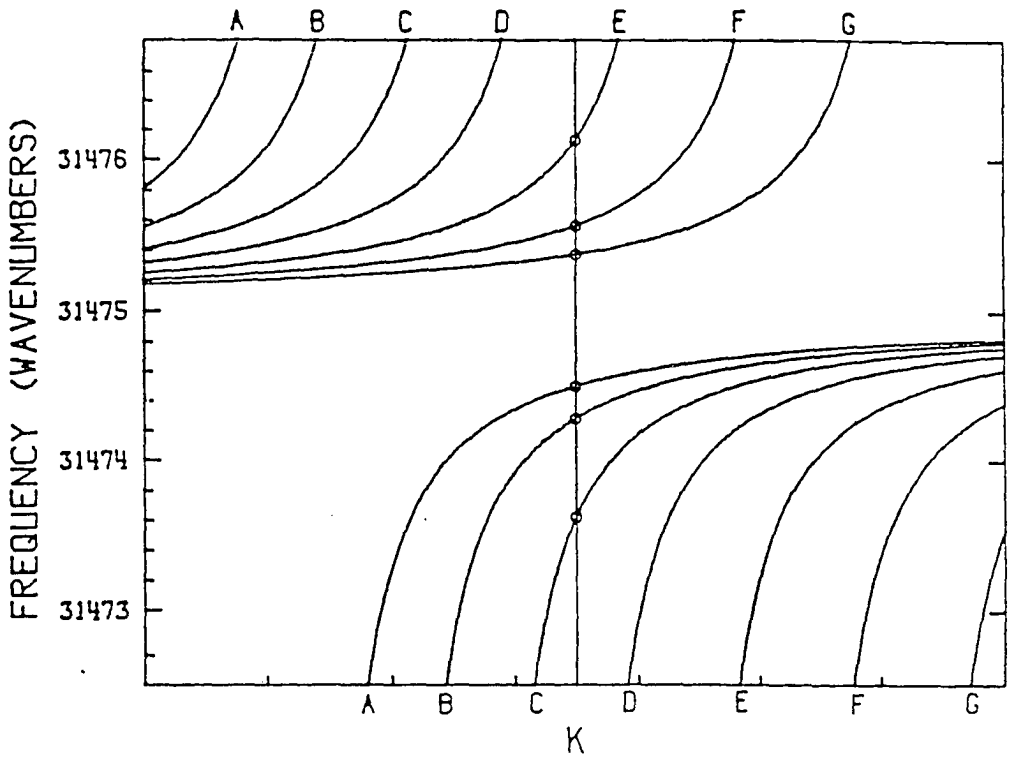


Figure 6. Calculated dispersion curves for the ac-polarized polariton in naphthalene making an external angle of : A) 15°, B) 10°, C) 5°, D) 0°, E) -5°, F) -10°, and G) -15° with the crystal c'-axis. Dispersion of the b-polarized polariton appears as a straight photon-like line. The phase matched frequency at each orientation is circled

ture was 7 K for all profiles shown in the figure. The angle of incidence to which the figure caption refers describes the angle the incident laser beam makes with the crystal c' axis, external to the crystal. A few observations may be made immediately:

1. Mapping onto the upper (lower) branch of the ac-polariton dispersion curve occurs at negative (positive) angles;
2. The crossover from one dispersion curve branch to the other occurs at or near 0° (normal) incidence;
3. On a given branch, the phase matching frequency increases with increasing incident angle; and
4. The profiles broaden and become more asymmetric as the incident angle approaches 0° from either direction; the side of the peak nearer the transverse exciton frequency is the steeper side.

Angles of incidence closer to normal than those illustrated in Figure 7 produce multiple SHG maxima, with a broad asymmetric contribution from each of the polariton branches and several smaller sharper peaks between the two. For some samples, the maximum of the TPE signal at these orientations is offset in frequency by a small amount from that of the SHG signal. The shapes of the TPE and SHG profiles will be more thoroughly discussed in a later section.

Directional dispersion of second harmonic generation similar to that described here has also been observed in naphthalene by Hochstrasser and Meredith (49). The major differences between the results of that study and those reported here are that the crossover point (observation #2, above) was observed by Hochstrasser and Meredith to lie between -5° and

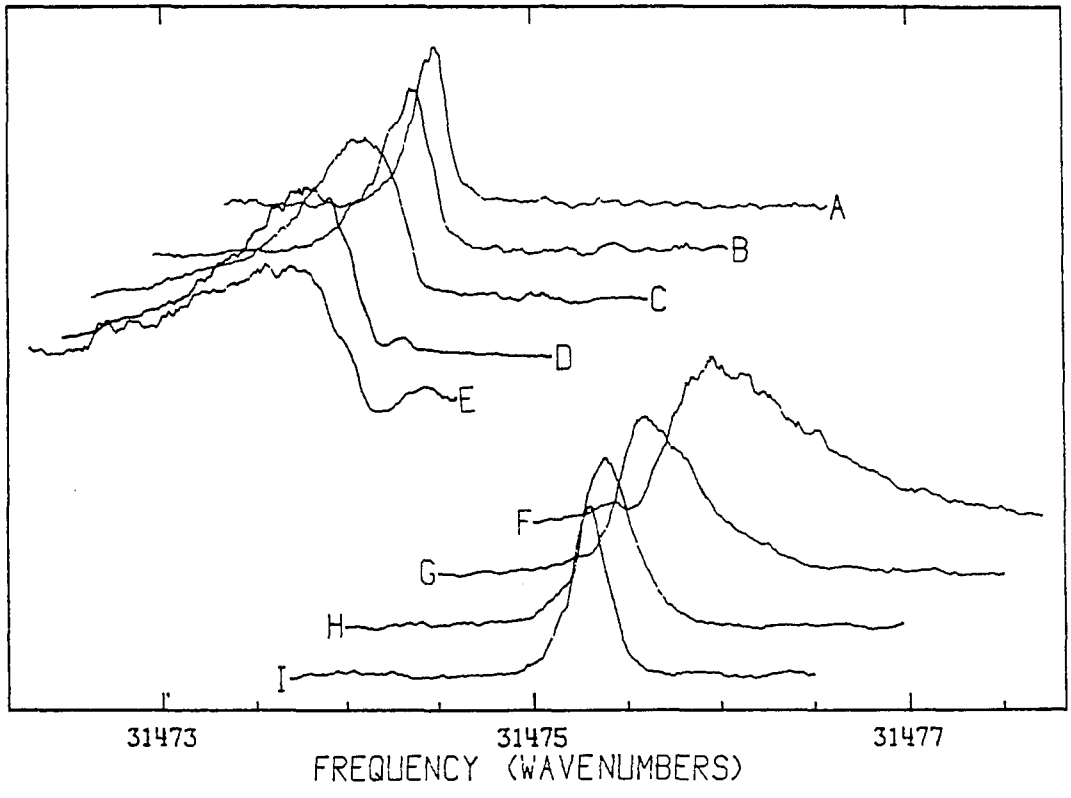


Figure 7. Directional dispersion of ac-polarized second harmonic generation in naphthalene. Experimental profiles are shown for incident angles: A) 17.5°, B) 12.5°, C) 7.5°, D) 5°, E) 2.5°, F) -5°, G) -7.5°, H) -12.5°, and I) -17.5° with respect to the crystal c'-axis

-10° incidence and that the TPE signal observed in the same experiment displayed little or no directional dispersion. A shift in crossover point to -4° was observed in one crystal out of the twelve used in this study; later examination of that crystal revealed evidence of strain and surface damage. Such imperfections distort a phase-matched signal by effectively providing multiple input angles and several consequent possible phase matching conditions which may be satisfied at slightly different frequencies. It seems likely that the same explanation applies to the differences between the results reported here and those reported by Hochstrasser and Meredith. The sample used in their study was cut from a melt-grown crystal and is not likely to have been free of strain and surface imperfections. This opinion is further borne out by the appearance of their experimental SHG profile, shown in reference (49b).

Meredith (185) has interpreted the dispersive behavior of both SHG and TPE according to the semiclassical approach discussed in Chapter II. Using expressions similar to those obtained from equations [25], [30], and [32] in Chapter II, which are:

$$I_{SHG}(L) = \frac{32\pi n_{2\omega}\omega^4}{c^3}\left|\frac{\underline{\chi}^{(2)}}{k_{2\omega}\Delta k}\left(e^{i\Delta kL} - 1\right)\right|^2 |E_\omega|^4, \qquad [75]$$

and

$$I_{TPE} = \frac{2n_{2\omega}\omega^2 L}{c^2 k_\omega} \mathrm{Im}\left\{3\chi^{(3)} + \frac{16\pi\omega^2 \chi^{(2)}\chi^{(2)'}}{c^2 k_{2\omega}\Delta k}\right.$$

$$\left. \times \left[1 + \frac{1}{i\Delta k L}(e^{-i\Delta k L} - 1)\right]\right\} |E_\omega|^4 - I_{SHG}(L), \qquad [76]$$

for the SHG and TPE rates, respectively, he showed that when the crystal is several absorption lengths thick a maximum will appear in each signal when $\mathrm{Re}(\Delta\epsilon) = 0$, where $\Delta\epsilon$ is the difference between the dielectric permittivities of the free and bound waves in the medium. This is approximately the same as the phase matching criterion $\Delta k = 0$ and predicts directional dispersion behavior similiar to that predicted by the polariton fusion model.

The results of low-temperature studies of peak signal frequency as a function of crystal orientation may be fit to the undamped polariton dispersion expression [74] to obtain values for the exciton oscillator strength, resonant frequency, and crystal refractive indices $n_{a^*}$ and $n_{c^*}$ (see Appendix A) near resonance. The fitting procedure is described below. The results are shown in Figure 8 for a 30 μm PSF naphthalene flake.

To fit the observed dispersion data to the predictions of the polariton model, equation [74] may be rewritten specifically for the phase-matched frequency $\omega_{pm}$ by making the substitution

$$k = \frac{n_b \omega_{pm}}{c}, \qquad [77]$$

where $n_b$ is the index of refraction of the ordinary (b-polarized) ray at

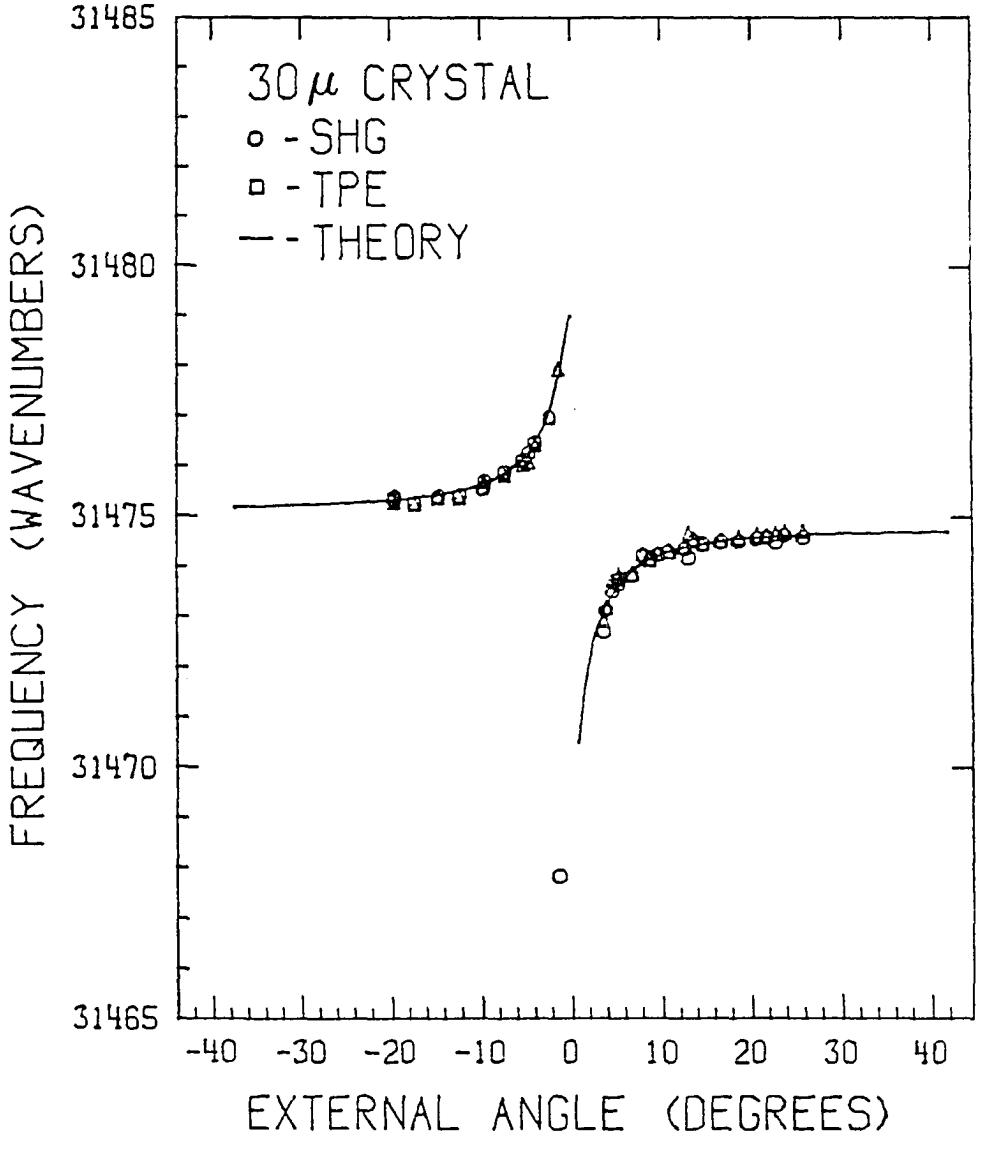


Figure 8. Directional dispersion of the extraordinary polariton in a 30 μm PSF naphthalene crystal. Experimental data shown is from both TPE and SHG signals. The solid curves are computed from expressions [78] and [80] using $n_b = 1.7115$, $n_{a^*} = 1.64$, $n_{c^*} = 2.36$, and $\omega_p^2 F = 5750\ cm^{-2}$ (see text)

$\omega_{red}$. The result is an expression relating the phase-matching frequency $\omega_{pm}$ to the background refractive index $n_0$ at $\omega_{blue}$ at incident angle $\Theta_{EXT}$:

$$\omega_{pm}^2 = \omega_o^2 + \frac{\omega_p^2 F}{n_o^2 - n_b^2} \quad , \qquad [78]$$

where $\omega_o$ is the frequency of the transverse exciton to which the blue photons are coupled.

The value of $n_0$ is dependent on the angle $\varnothing$ between the polariton wavevector $\underline{k}$ and the crystal $\underline{c}^*$ axis. To relate the measured value of $\Theta_{EXT}$ to $\varnothing$, it is first necessary to make an assumption about the orientation of the optical indicatrix (see Appendix A) for naphthalene near 31475 $cm^{-1}$. McClure and Schnepp (93) have reported the $\underline{a}^*$-$\underline{c}^*$ axial dispersion in naphthalene to be less than 2° in the $\underline{ac}$ plane over the wavelength range 3341Å - 5790 Å. In the higher frequency region where naphthalene is not transparent, however, it would not be surprising to observe somewhat greater axial dispersion. No information about the optical indicatrix for naphthalene near resonant ultraviolet frequencies has been reported. For purposes of fitting the data to equation [78], therefore, it was first assumed that the orientation of the ellipsoid with respect to the crystal axes was unchanged from 5461Å to 3176Å; that is, it was assumed that the crystal $\underline{c}'$ axis makes an angle of 23°25' with optical $\underline{c}^*$. This assumption was later checked experimentally and found to be good to within 0.5°.

The angle made by the wavefront normal of the incident photons with $\underline{c}'$ may be found by using Snell's law and the value $n_b = 1.7115$ (from data in references 193 and 202; see Appendix A). The same angle is formed by

the crystal a axis and the dielectric displacement vector D of the incident photons. The observation that $\omega_{pm}$ increases as $\theta$ increases, using for $\theta$ the sign convention of Figures 7 and 8, implies by equation [78] that $n_0$ decreases with increasing $\theta$. D is therefore moving toward optical $a^*$, the minor axis of the indicial ellipsoid, as $\theta$ is increased. Thus, $\varnothing$ may be computed from $\theta_{EXT}$ by

$$\varnothing = \partial - \sin^{-1}\left\{\frac{\sin\theta_{EXT}}{n_b}\right\} \qquad [79]$$

where $\partial = 23°25'$. Following the procedure outlined in Chapter II and making use of equation [44], the quantity $n_0$ may be replaced in equation [78] by a function of $\varnothing$:

$$n_o = \left\{\frac{n_{a^*}^2 n_{c^*}^2}{n_{a^*}^2\cos^2\varnothing + n_{c^*}^2\sin^2\varnothing}\right\}^{1/2}, \qquad [80]$$

where $n_{a^*}$ and $n_{c^*}$ are the lengths of the minor and major axes, respectively, of the optical indicatrix for naphthalene at 31475 $cm^{-1}$, the values of which must be found from the fit. Because the "crossover point" must occur when the b-polarized red polaritons fail to intersect the ac-polariton dispersion curves; that is, when $n_0 = n_b$, there is a relationship between $n_{a^*}$ and $n_{c^*}$ dictated by the value of $\theta_{EXT}$ at branch crossover. Using $\theta_{EXT} = 0°$ or $\varnothing = \partial$ results in:

$$n_{a^*}^2 = \frac{n_{c^*}^2 n_b^2 \cos^2\partial}{n_{c^*}^2 - n_b^2\sin^2\partial} \qquad [81]$$

There remain two quantities to determine in the phase-matched

directional dispersion expression. The resonant frequency $\omega_o$ of the transverse a-exciton must be found from the fit, as the absolute wavelength calibration for these measurements cannot be assumed perfect. The plasma frequency, $\omega_p$, is computed from the expression

$$\omega_p^2 = \frac{4\pi e^2 N}{m_e} ,$$

where N is the volume density of absorbers, e the electron charge, and $m_e$ the electron mass. To obtain the value of N, unit cell dimensions for naphthalene at 77 K reported by Cruickshank and Robertson (203) may be used, assuming negligible thermal deformation occurs between 5 K and 77 K: a = 8.235 Å, b = 6.003 Å, c = 8.658 Å, and ß = 122°55'. The value of $\omega_p^2$ is then $2.50 \times 10^8$ $cm^{-2}$.

The oscillator strength F has been determined in a-polarized one-photon absorption (OPA) studies to be $2.3 \times 10^{-5}$. The effective oscillator strength should vary as $\cos^2\alpha$, where $\alpha$ is the angle the molecular transition dipole makes with the polarization vector of the photon. The quantity $\omega_p^2 F$ should therefore depend on the sense of $\underline{k}$ and should vary with $\Theta_{EXT}$. The value of $\alpha$ could be computed from $\varnothing$ by assuming that the transition dipole remains oriented along the long axis of the molecule in the crystal. Unfortunately, this is not a satisfactory assumption; polarization ratios of the $^1B_{2u}$ factor group components in OPA have demonstrated (93) that a simple "oriented gas" picture is not a good one for the lowest singlet excited state of naphthalene crystals. It might be possible to extract the variation in F with incident angle by fitting the experimentally obtained

dispersion curve to equation [78] piecewise, allowing the value of F to behave as a parameter. Within the limits of experimental error, however, it turns out that the entire experimental curve may be fit using as a constant the value measured for F in OPA experiments using polarization along a (normal incidence), the middle of the range of polarization orientations in this experiment. The result of fitting data from three PSF samples (27, 30, and 55 μm thick) was a value for $n_{c*}$ at 31475 $cm^{-1}$ of 2.36 and a consequent (through expression [81]) value for $n_{a*}$ of 1.64. The directional frequency dispersion computed from equation [74] using these values is shown as a solid line in Figure 8. The theoretical curve fits the data quite well.

Further calculations including the effects of damping on directional dispersion, as well as observation of the behavior of thinner samples, show that for thin crystals the intensity maximum of the nonlinear signal is shifted toward $\omega_0$ at near-normal angles of incidence. These calculations will be discussed more fully later; for now it suffices to note that the data used to obtain working values for $n_{a*}$ and $n_{c*}$ were from fairly thick crystals. Furthermore, the data affecting most strongly the fitted result are those at high values of $|\theta_{EXT}|$; that is, those deviating least from $\omega_{pm}$ even in thinner crystals.

The values of $n_{a*}$ and $n_{c*}$ derived from the directional dispersion data and the value of $\omega_p^2 F$ obtained from OPA measurements are used in all computations to follow.

Temperature Behavior of SHG and TPE Signals

For each crystal that was studied, several angles of orientation were chosen. At each angle, the temperature-dependent behavior of the SHG and TPE signals was observed. Data of this type have not been published previously for any system. This section will describe the results of these experiments.

Data from a typical temperature study, with $\theta_{EXT}$ held constant at 10° with respect to the $\underline{c}'$ axis of a 27 μm PSF naphthalene crystal, are shown in Figure 9. The significant results, to be discussed in turn, are:

1. The low-temperature full widths at half-maximum (FWHM's) of the signals appear constant at a "residual" width, and further broadening in both signals commences at about 9 K;
2. Both TPE and SHG profiles appear asymmetric at low temperatures, with a steeper slope on the high-frequency side; at higher temperatures, the TPE signal approaches a symmetric Lorentzian shape;
3. The integrated intensities of the two signals display opposite trends with temperature: the TPE integrated intensity is small at low temperatures and grows to a constant high-temperature value, while that of the SHG profile diminishes from its low-temperature value, all but disappearing by 15 K; and
4. The onset of broadening occurs at a much higher temperature than does the onset of the intensity progressions, indicating that the residual FWHM is not a result of homogeneous broadening.

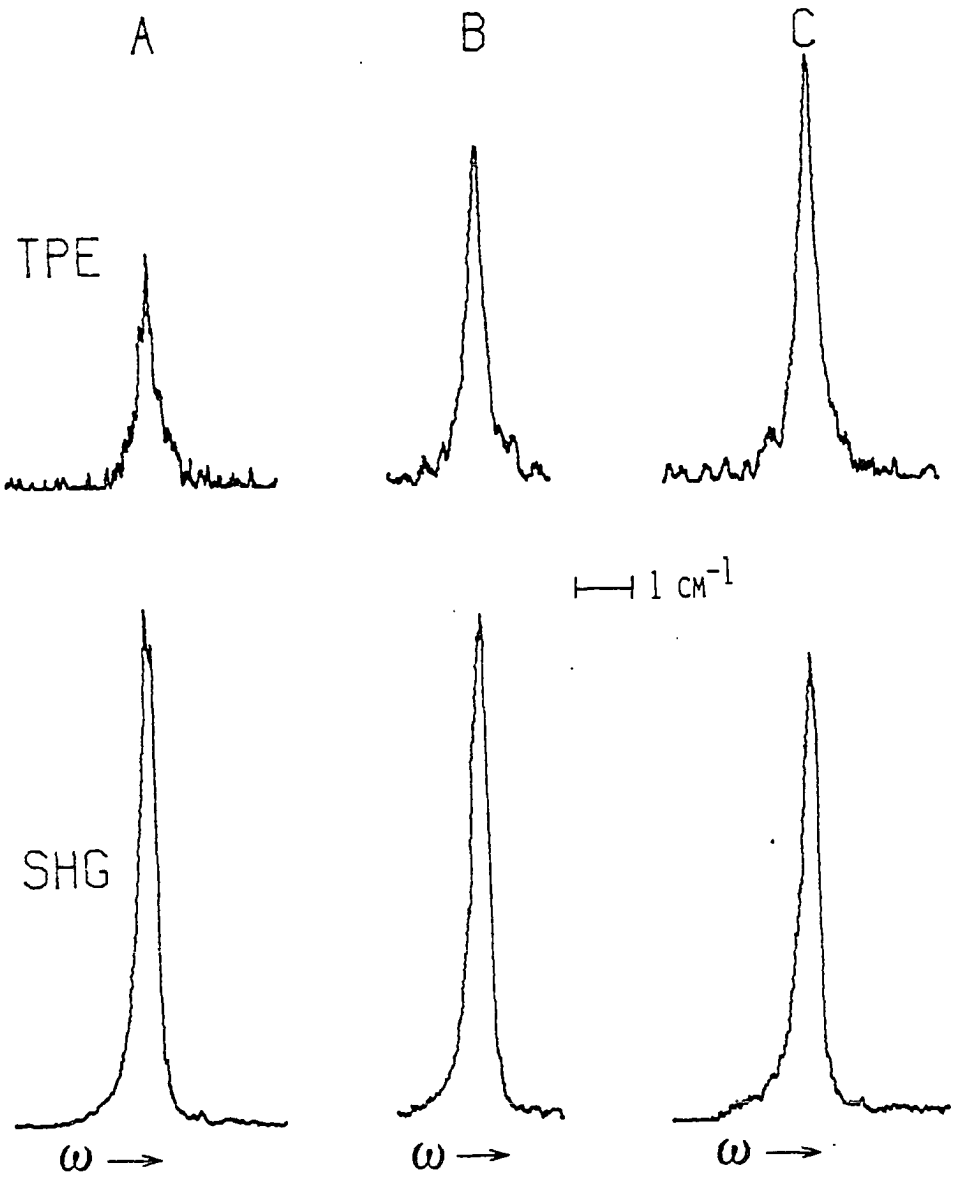


Figure 9. Two-photon excited emission (TPE, top) and second harmonic generation (SHG, bottom) data from a 27 μm PSF naphthalene crystal at an incident angle 10° from normal and temperatures of: A) 1.8, B) 4.5, C) 5.6, D) 7.0, E) 8.1, F) 9.5, G) 10.2, H) 11.8, I) 12.5, and J) 14.7 degrees Kelvin. The intensity scale for each signal remains the same throughout the figure

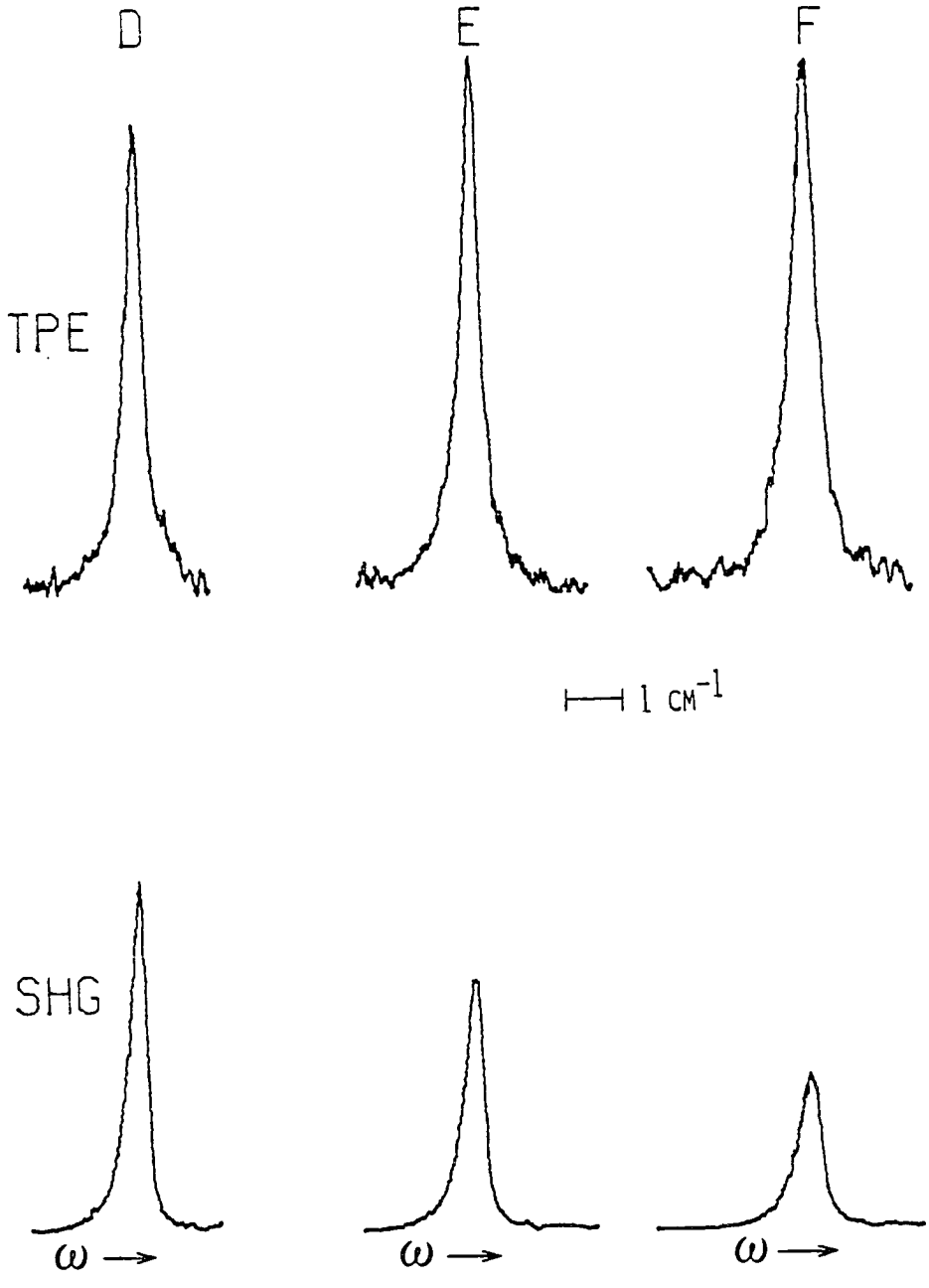


Figure 9. (continued)

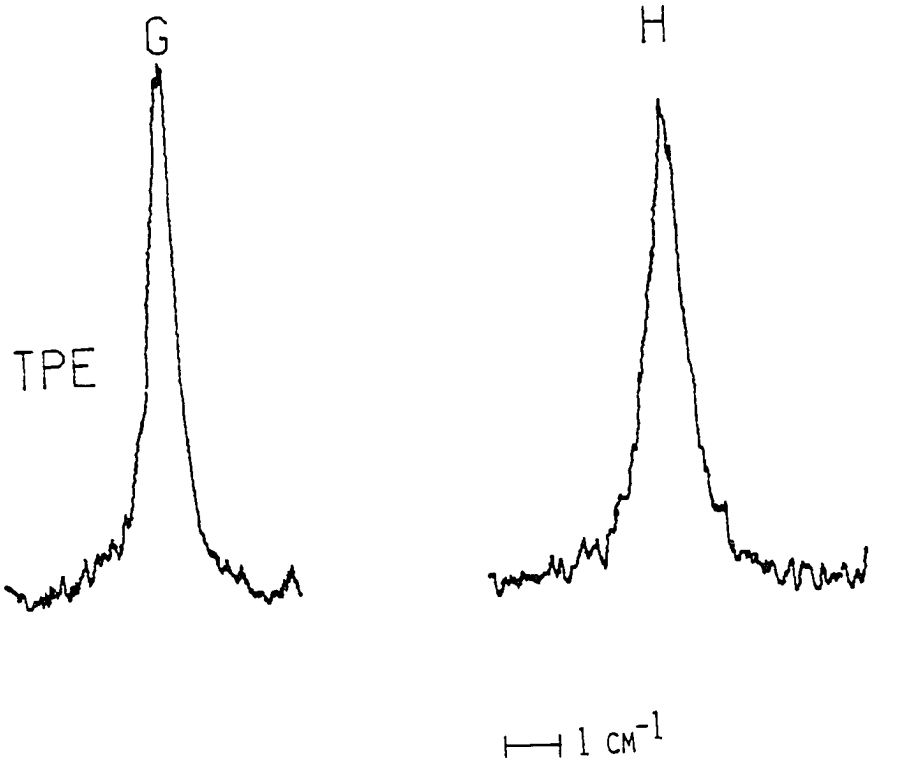


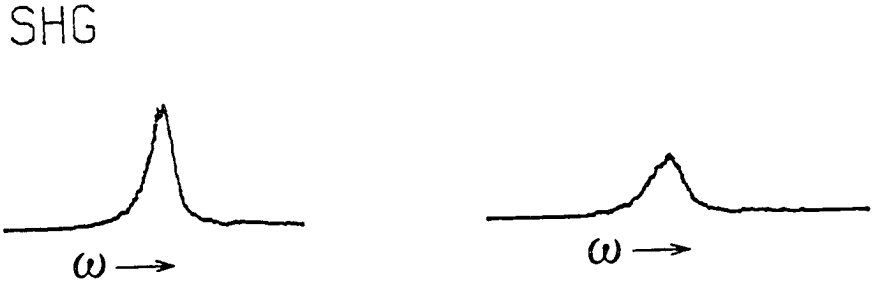


Figure 9. (continued)

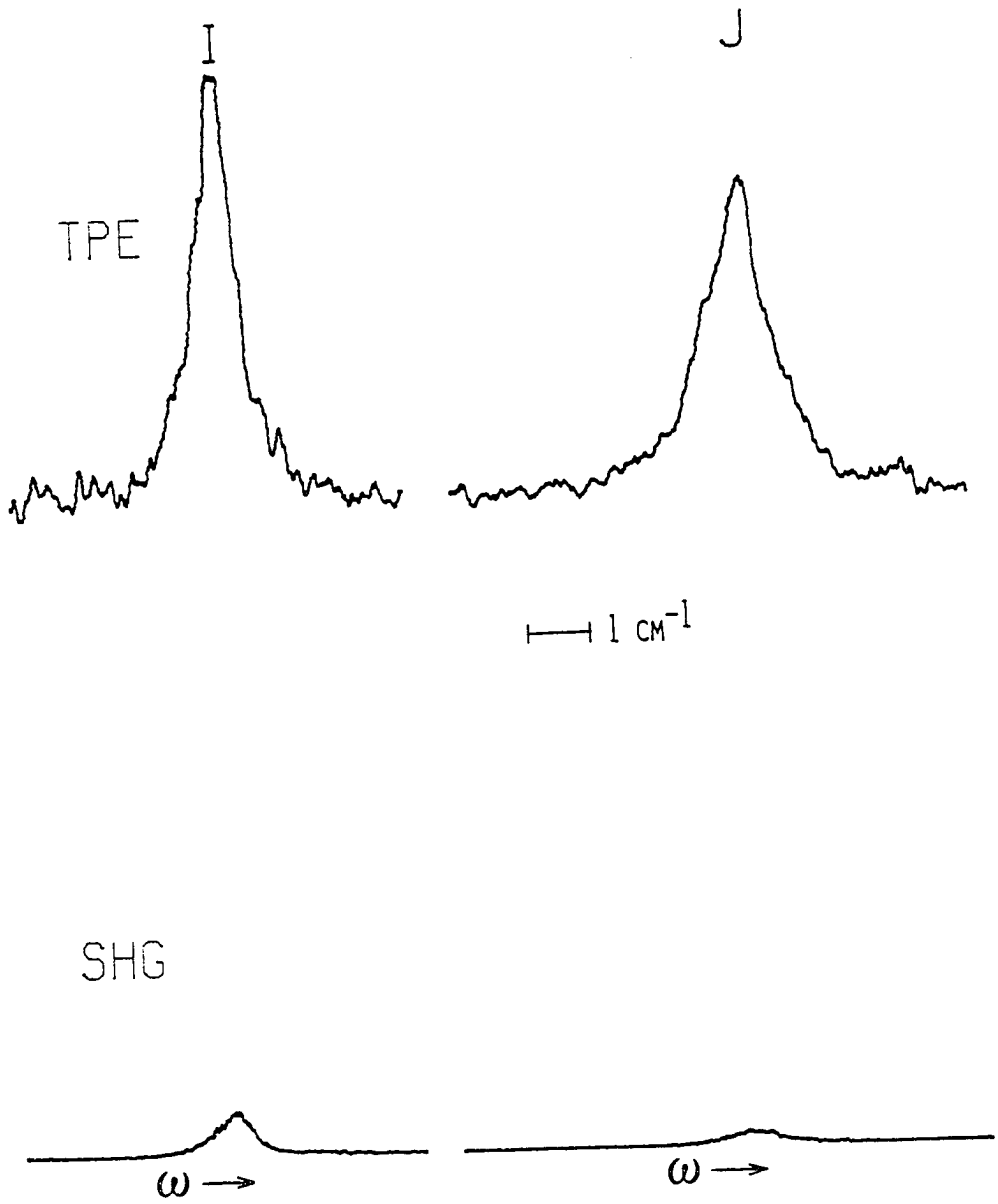


Figure 9. (continued)

Temperature-broadening of nonlinear signals

Temperature-broadening data for several PSF naphthalene crystals are shown in Figures 10-14. Data for several values of $\theta_{EXT}$ are plotted for each crystal, offset by the amount of the low-temperature residual width. Because the SHG signal is generally weak or nonexistent at temperatures above 9 or 10 K, the broadening behavior of the TPE signal over the whole temperature range is easier to obtain and is what is plotted in the figures. The SHG data collected showed the same linewidth behavior as did the TPE data, but with much worse scatter at high temperatures, where the SHG signal is weak. Occasionally the low-temperature residual FWHM of the SHG profile was a little less than that of the TPE profile, vide infra, but the broadening remained the same.

Although the residual FWHM is different for different values of $\theta_{EXT}$ for a given crystal, the broadening of the profiles as a function of temperature appears to be the same for all the orientations studied and for all PSF samples studied. It should also be noted that the nature of the experiment is such that each crystal is subjected to several thermal cycles during data collection. No perceptible changes in linewidth were observed as a function of age or thermal history over the course of a run, typically about two weeks and a dozen or more temperature cycles.

In the approximation that the polariton scatters primarily upwards through interaction with a phonon of effective frequency $\Omega$, the linewidth is expected to broaden with increasing temperature in proportion to the thermal occupation number of a phonon of frequency $\Omega$:

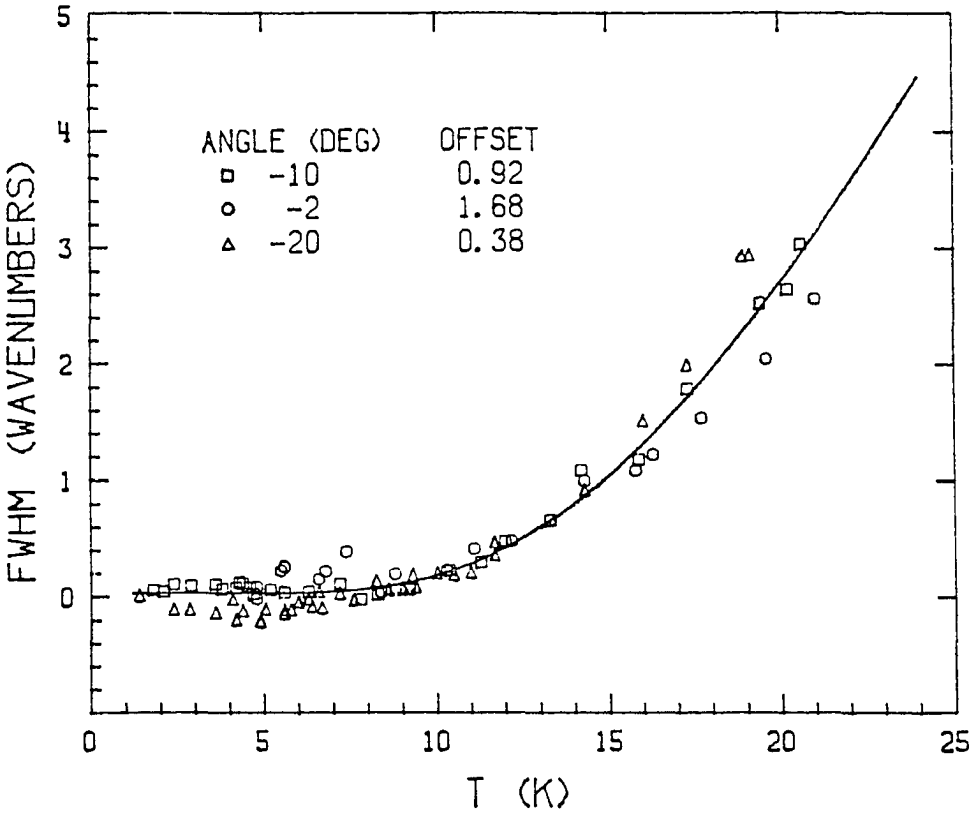


Figure 10. Temperature-broadening data for a 12.5 μm PSF naphthalene crystal at three angles of incidence with respect to c'. Data are offset at each angle by the residual low-temperature width observed for that orientation. The solid curve is obtained from expression [82], using an effective phonon frequency of $\Omega = 39\ cm^{-1}$ and preexponential value $C = 43\ cm^{-1}$

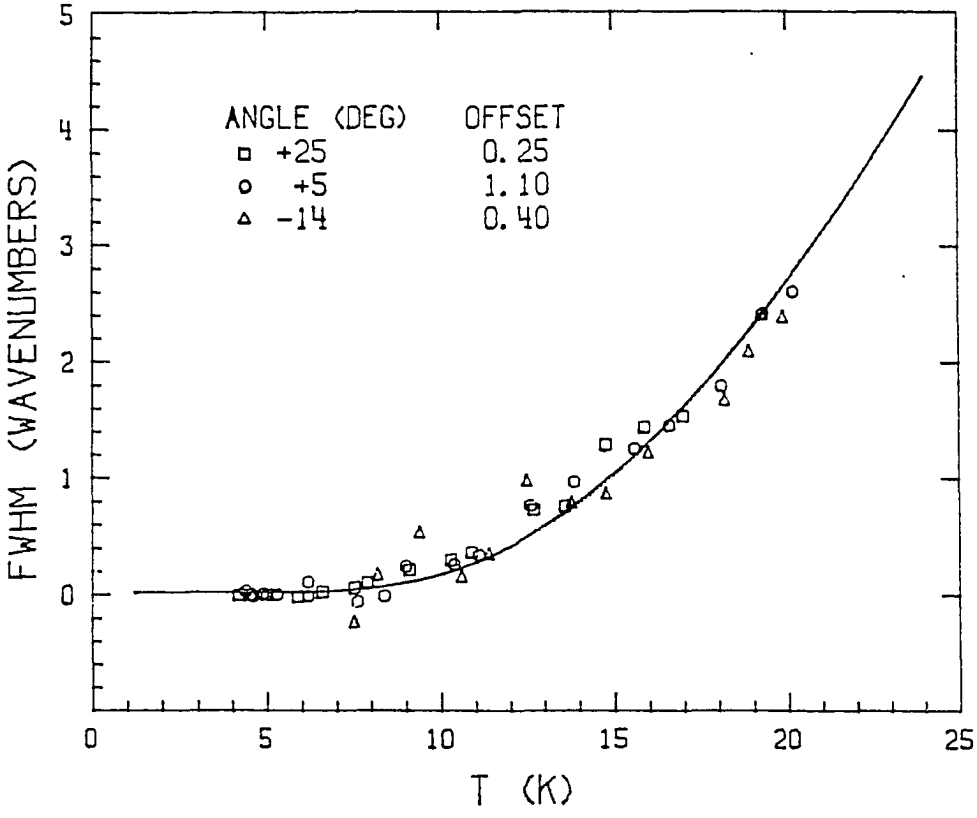


Figure 11. Temperature-broadening data for a 23 μm PSF naphthalene crystal at three angles of incidence with respect to c'. Data are offset at each angle by the residual low-temperature width observed for that orientation. The solid curve is obtained from expression [82], using an effective phonon frequency of $\Omega = 39\ cm^{-1}$ and preexponential value $C = 43\ cm^{-1}$

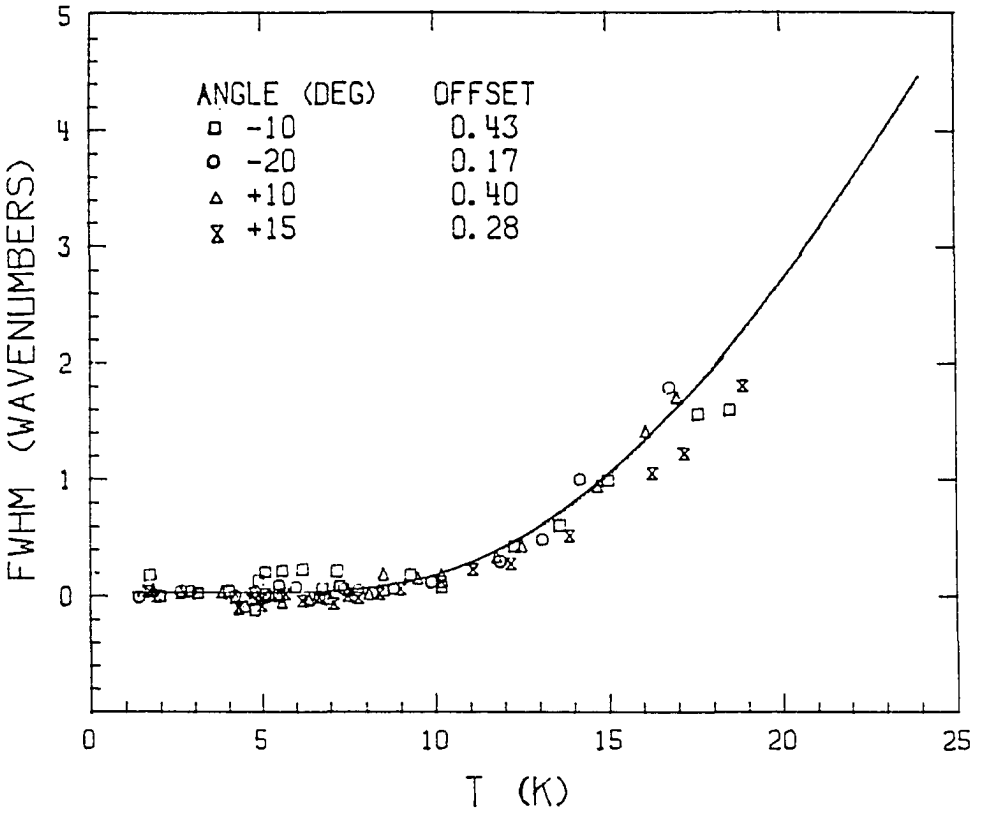


Figure 12. Temperature-broadening data for a 27 μm PSF naphthalene crystal at four angles of incidence with respect to $\underline{c}'$. Data are offset at each angle by the residual low-temperature width observed for that orientation. The solid curve is obtained from expression [82], using an effective phonon frequency of $\Omega = 39\ cm^{-1}$ and preexponential value $C = 43\ cm^{-1}$

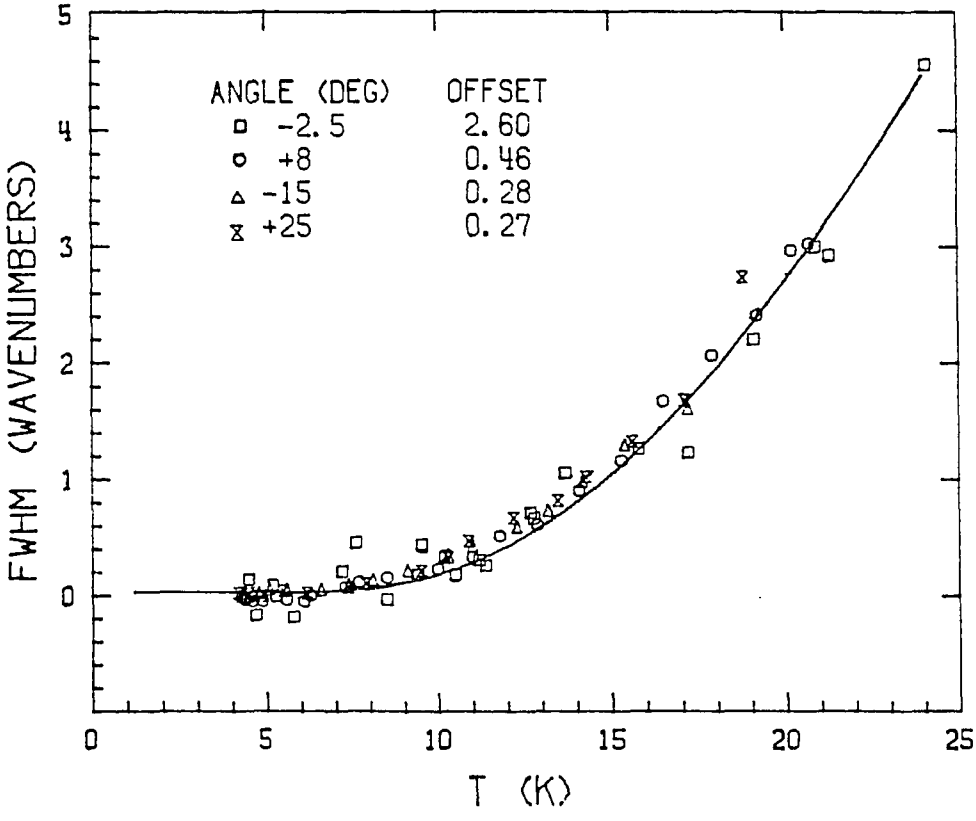


Figure 13. Temperature-broadening data for a 30 μm PSF naphthalene crystal at four angles of incidence with repsect to $\underline{c}'$. Data are offset at each angle by the residual low-temperature width observed for that orientation. The solid curve is obtained from expression [82], using an effective phonon frequency of $\Omega = 39\ cm^{-1}$ and preexponential value $C = 43\ cm^{-1}$

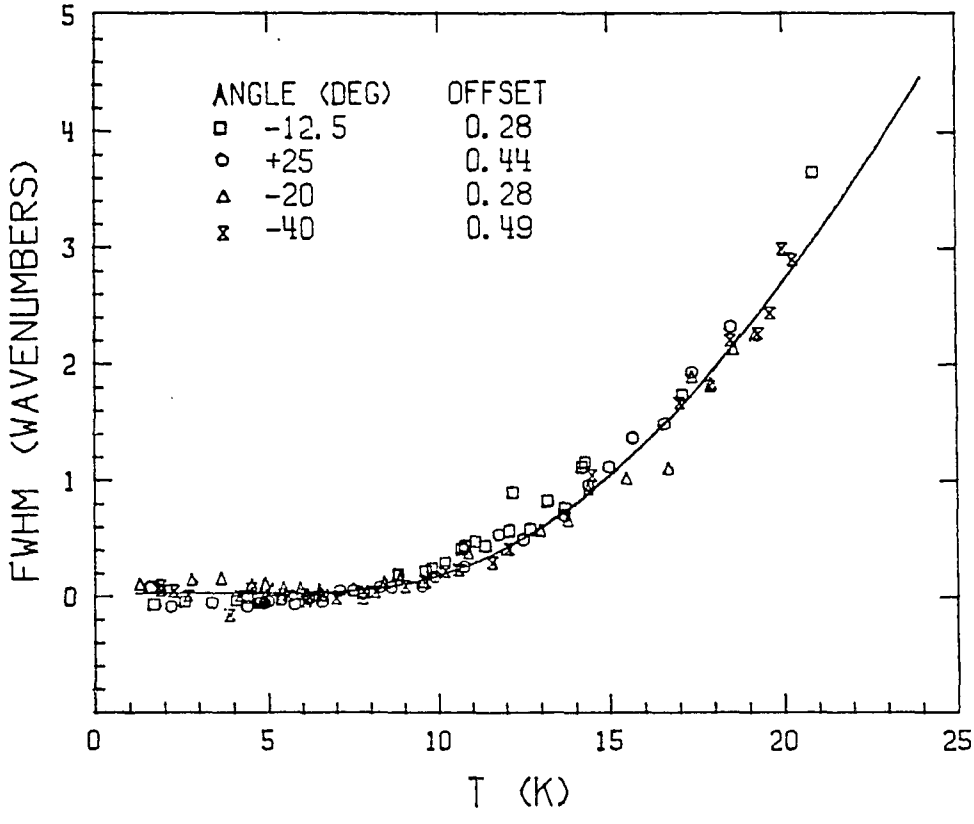


Figure 14. Temperature-broadening data for a 55 μm PSF naphthalene crystal at four angles of incidence with respect to c'. Data are offset at each angle by the residual low-temperature width observed for that orientation. The solid curve is obtained from expression [82], using an effective phonon frequency of $\Omega = 39\ cm^{-1}$ and preexponential value $C = 43\ cm^{-1}$

$$\Gamma = C\langle n \rangle = C\left\{ e^{(\Omega/kT)} - 1 \right\}^{-1} \quad , \qquad [82]$$

where k= Boltzmann's constant and T is the temperature in degrees Kelvin. Data in this study are successfully fit to expression [82] using an effective phonon frequency $\Omega$ = 39 $cm^{-1}$, a low optical phonon frequency, and a value for the preexponential factor C of 43 $cm^{-1}$. The function [82] is shown as the solid line in Figures 10-14.

Data from OPA studies of PSF naphthalene flakes (117) also fit an effective one-phonon annihilation scattering mechanism well. There is, however, one important difference: the active phonon appears to be one which is much lower in frequency, about 12 $cm^{-1}$ (an acoustic phonon frequency). Figure 15 shows OPA broadening data from reference (117a) for two crystals, each about 5 µm thick. For comparison, TPE data from this study for several crystals of from 12.5 to 55 µm are shown. The nonlinear profiles broaden much more slowly with temperature than do those of the OPA experiment. The OPA broadening behavior illustrated in Figure 15 is also exhibited by the thicker naphthalene crystals studied by Robinette (117), and is consistent with one-photon excited emission measurements made in work done preliminary to this study, using the same laser and much the same experimental configuration as that described in Chapter III.

One important difference between the one-photon polaritons of the OPA experiment and the two-photon polaritons of the SHG/TPE experiment is in the value of |k| for the prepared polariton; that is, the region of the dispersion curve accessible to the experiment. In the one-photon experiment, polariton formation from incident photons occurs at the front

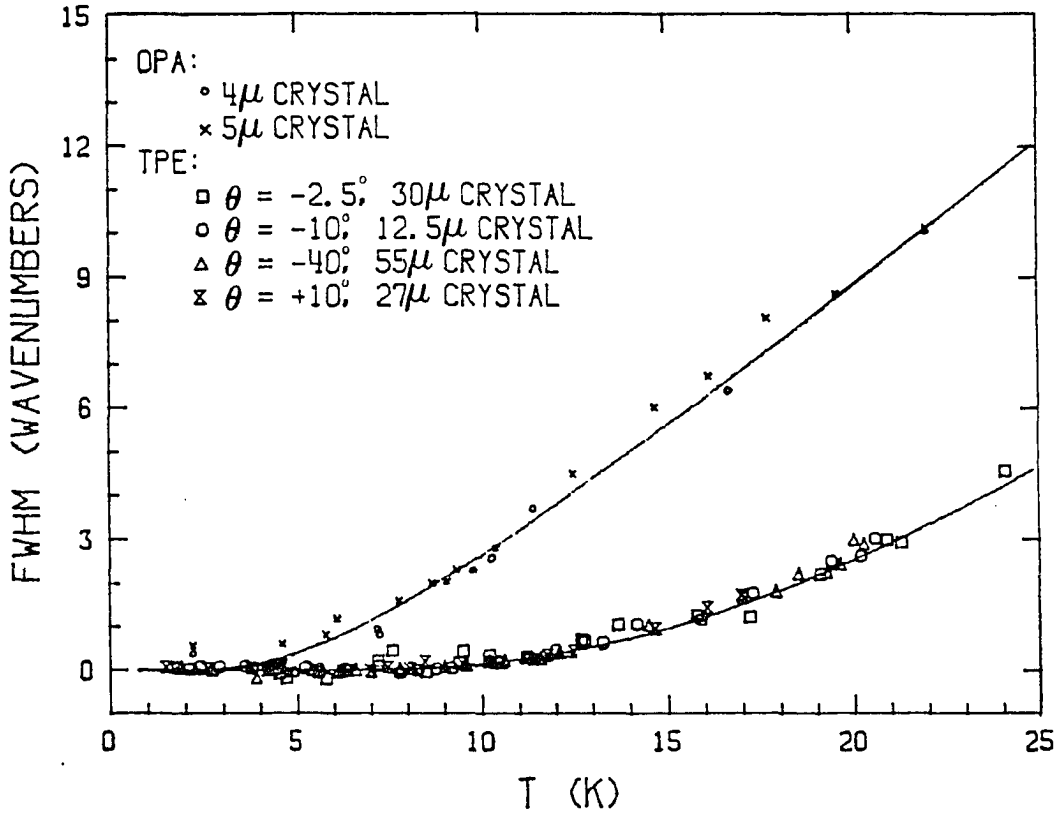


Figure 15. Temperature-broadening data for TPE (large symbols) and one-photon absorption (small symbols) profiles from PSF naphthalene crystals of various thicknesses. The solid curves are thermal occupation numbers calculated from equation [82] for 12 $cm^{-1}$ (upper curve) and 39 $cm^{-1}$ (lower curve) phonons

surface of the crystal, where k is not a good quantum number and therefore need not be conserved in the process. Conservation of energy dictates that a photon at the resonant exciton frequency $\omega_o$ form a polariton at the same frequency, well into the exciton-like part of the polariton dispersion curve. Although the entire frequency range is scanned in the OPA experiment, the profile shape and temperature broadening are dominated by these exciton-like polaritons. The polaritons which result from the nonlinear fusion process, on the other hand, are formed in the bulk of the crystal, where momentum is approximately conserved, and they are therefore subject to a phase matching requirement. For a particular direction of $\underline{k}$, only polaritons with a well defined range of |k| values are prepared, and polariton behavior at the "knee" and "elbow" regions of the dispersion curve may be probed by controlling the sense of $\underline{k}$ experimentally. The fundamental difference between the coherently generated polaritons formed in the nonlinear experiment and those which govern the results of the linear experiment lies in their proximity on the polariton dispersion curve to the photon light line; that is, in the amount of photon character which clothes the excitation.

A physical quantity which varies with position on any dispersion curve which is not a straight line is the group velocity of the associated particle, $\partial\omega/\partial k$. The expression for the group velocity of a polariton may be calculated from the dispersion relation, equation [74]:

$$v_g = \frac{c\left[n_0^2 + \omega_p^2 F/(\omega_o^2 - \omega^2)\right]^{1/2}}{n_0^2 + \omega_p^2 F \omega_o^2/(\omega_o^2 - \omega^2)^2} \quad , \qquad [83]$$

where the values of the parameters have been given above and $n_0$ may be computed from $\theta_{EXT}$ and the values for $n_{a*}$ and $n_{c*}$, derived from the dispersion curve fit. The computed group velocities of the polaritons generated in this experiment ranged from $6 \times 10^5$ to $5 \times 10^8$ cm-s$^{-1}$. The group velocity of the a-exciton at $\omega_0$ is on the order of $10^3$ cm-s$^{-1}$ (117c).

The period of a 12 cm$^{-1}$ acoustic phonon lattice distortion (the approximate frequency of the phonon which dominates the broadening behavior of the OPA signal) is 2.8 picoseconds (ps). This is fast on the time scale of exciton motion; the exciton propagates from one unit cell to the next in about 100 ps, and lattice distortion may occur in a unit cell before the exciton has left the site. The exciton and the distortion may be spatially correlated, leading to stong coupling and allowing for the activity of acoustic modes. The nonlinearly generated polaritons, however, propagate from unit cell to unit cell in 0.2 ps or less, fast on the time scale of an acoustic lattice distortion. Coupling between the exciton and the lattice distortion is weakened and exciton-optical ($k \approx 0$) phonon interactions dominate. Thus, it is the difference in polariton velocities in different regions of the Brillouin zone which results in the difference in temperature broadening in the OPA and TPE profiles in naphthalene, and the linewidth behavior of the two signals is evidence of the unique nature of coherently generated polaritons.

Modification of the temperature dependence of the polariton line shape by crossing from a "slow" polariton regime to a "fast" one may be thought of as analogous to the motional narrowing observed in NMR signals (204). The implication is that by mixing a small amount of photon charac-

ter into an electronic excitation, one not only achieves a considerable increase in the propagation velocity but improves the coherence length as well by weakening the scattering mechanism.

It is necessary at this point to consider just how much excitonic character remains in the polaritons generated in this experiment. As Hopfield (107c) pointed out, the exciton occupation number remains close to unity even for polaritons quite close to the light line. From equation [65] of Chapter II, the polariton creation operator may be written as

$$\alpha_{\underline{k}}^{\dagger} = r_{\underline{q}}^{*} a_{\underline{q}}^{\dagger} + r_{\underline{k}}^{*} B_{\underline{k}}^{\dagger} + s_{-\underline{q}} a_{-\underline{q}} + s_{-\underline{k}} B_{-\underline{k}} \quad , \qquad [84]$$

where $a_q^{\dagger}$ and $a_q$ are photon creation and annihilation operators, respectively, and $B_k^{\dagger}$ and $B_k$ are creation and annihilation operators for the exciton. The coefficient $r_k^*$ is given by equation [66]:

$$r_{\underline{k}} = \frac{i\left[\frac{\omega_p^2 F}{4\epsilon_0 \omega_0^2}\right]^{1/2} (1 + \omega/\omega_0)}{(\omega/\omega_0)^{1/2}\left[(1 + \omega^2/\omega_0^2)^2 + \frac{\omega_p^2 F}{\epsilon_0 \omega_0^2}\right]^{1/2}} \quad . \qquad [85]$$

For $|\omega - \omega_0| \leq 6\ cm^{-1}$ (corresponding to $|\theta_{EXT}| \geq 0.8°$) the value of $|r_k|$ is $\geq 0.97$ (see Figure 2). All polaritons created in this experiment may therefore be considered chiefly exciton-like, distinguished mainly by the amount of photon character with which they are clothed. The propagation velocity and coherence properties of the excitation are strongly dependent on the choice of $\underline{k}$, while the essential character of the excitation is not.

For example, at 10 K the coherence length, which is dominated by damping at nonzero temperatures and may be expressed as $\pi v_g/\gamma$, is on the order of 10 μm for a polariton with group velocity of $10^7$ cm-$s^{-1}$; for excitons at the same temperature the coherence length is about $10^{-5}$ μm.

A further comment should be made regarding the nature of the OPA experiments cited (117). These measurements were conducted using a broadband source and a high resolution monochromator. The monochromator was scanned and the signal collected as transmission data. It has already been emphasized that the observed temperature-dependent behavior was overwhelmingly that of an exciton-like polariton. That is not to say, however, that polaritons near the knee and elbow regions cannot be created in a one-photon experiment. The value of k, not a conservative quantity at the crystal surface, is determined by the value of the incident frequency, which must be conserved. In this regard it is worth noting that the one-photon photoexcitation (OPE) studies which were the preliminary work for the nonlinear experiment always produced a profile with a narrow "hole" at a frequency near that of the peak maximum (see Figure 16). The estimated value for the oscillator strength of the naphthalene a-exciton was at the time of the OPE study about an order of magnitude low and consequently the width of the polariton stop gap , $\omega_L - \omega_o \approx \omega_p^2 F/2\epsilon_o\omega_o$ , was thought to be on the order of $10^{-3}$ $cm^{-1}$, too narrow to be observed with a source of 0.04 $cm^{-1}$ bandwidth (the FWHM for the etalon-narrowed doubled output of the NRG dye laser). The intensity dip was therefore assumed to be an experimental artifact. Correction of the value for F to $2.3 \times 10^{-5}$ leads to a computed stop gap width of 0.03 $cm^{-1}$, which should

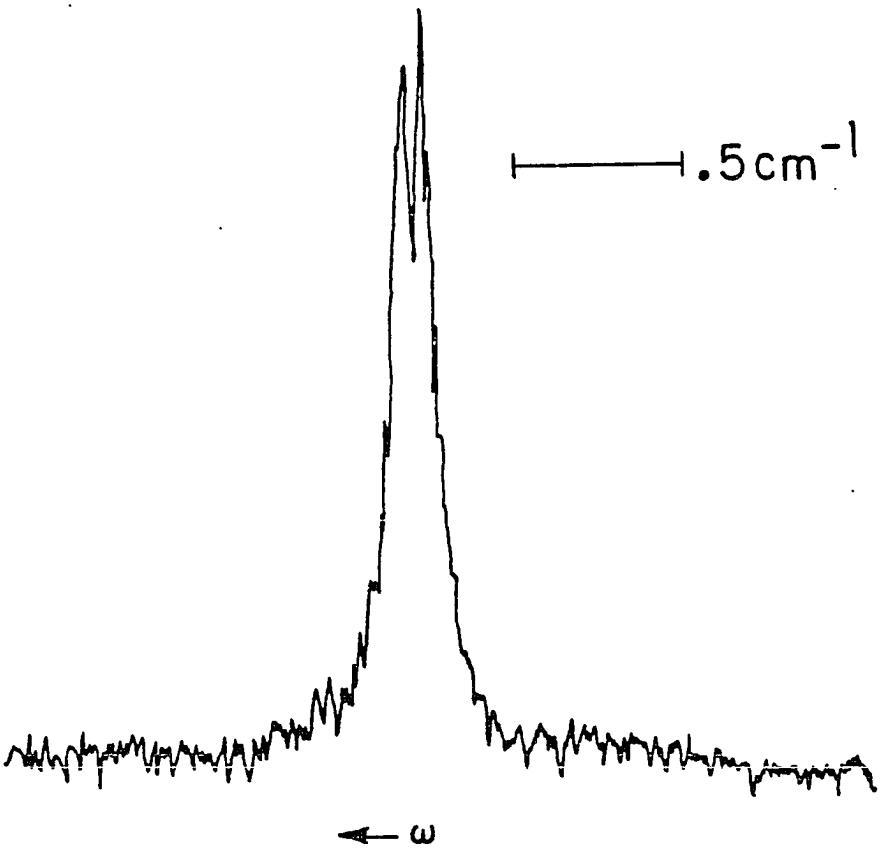


Figure 16. One-photon fluorescence excitation profile of the a-exciton of naphthalene, at T≈ 5 K, obtained using a narrow-line source

be observable via OPE and may explain the dip, illustrating the process of mapping out the polariton dispersion curve by varying $\omega$ in a one-photon experiment. (The stop gap would not be observable in a transmission experiment like that of Robinette et al. (117), since the transmission signal is equal to 1 - A - R, where A and R are the absorption and reflection probabilities. This situation is discussed in reference (117a). The OPE experiment is a direct measurement of A only.) Thus, once the dispersion behavior is well understood from nonlinear studies, it should be possible to investigate polariton group velocities in the time domain with one-photon experiments, using a narrow line source. Such experiments would have the advantage of access to all parts of a single dispersion curve (cf. Figure 6), but would have to be carried out at very low temperatures in order to avoid domination of all parts of the signal profile by the excitons produced at $\omega_o$.

Temperature-dependent intensities of nonlinear signals

Prediction of the temperature behavior of the total intensities of TPE and SHG is accomplished by integrating the intensity expressions over frequency for values of $\gamma(T)$ computed from the appropriate form of equation [82]. $\gamma$ is taken to be equal to the sum of $\gamma(T)$ plus a small temperature-independent part, $\gamma_o$. The usual treatment of two-photon processes (184) which neglects the effect of $X^{(2)}$ on the TPE intensity fails to predict dispersion in the TPE signal and will not be considered here.

In the semiclassical model, the damping is included in the suscepti-

bility expressions and corresponds to the damping of the material oscillations. The value for $\gamma(T)$ is therefore the experimentally determined (117) exciton damping, obtained by setting $\Omega = 12\ cm^{-1}$ and $C = 13\ cm^{-1}$ in equation [82]. Using the susceptibility expressions given in Chapter II as equations [18] and [31]:

$$\chi^{(1)}(-\omega,\omega) = \chi^{(1)}_{nr} + \left(\frac{N}{\hbar}\right)\frac{\underline{Q}_{gi}\underline{Q}_{ig}}{\omega_o - \omega - i\Gamma/2}$$

$$\chi^{(2)}(-2\omega,\omega,\omega) = \chi^{(2)}_{nr} + \left(\frac{N}{2\hbar}\right)\frac{\underline{Q}_{oi}\underline{a}_{io}}{\omega_o - 2\omega - i\Gamma/2}$$

$$\chi^{(2)'}(-\omega,-\omega,2\omega) = \chi^{(2)'}_{nr} + \left(\frac{N}{2\hbar}\right)\frac{\underline{a}_{oi}\underline{Q}_{io}}{\omega_o - 2\omega - i\Gamma/2}$$

$$\chi^{(3)}(-\omega,-\omega,\omega,\omega) = \chi^{(3)}_{nr} + \left(\frac{N}{6\hbar}\right)\frac{\underline{a}_{oi}\underline{a}_{io}}{\omega_o - 2\omega - i\Gamma/2} \qquad [86]$$

where N is the number density of oscillators, $\underline{Q}$ is the one photon transition dipole matrix element, assumed real and related to the transition oscillator strength by

$$|Q|^2 = F\hbar e^2/2m_e\omega \quad ,$$

$\underline{a}$ is the two-photon transition polarizability:

$$a_{io} = \left(\frac{2}{\hbar}\right)\sum_j \frac{\underline{Q}_{ij}\underline{Q}_{jo}}{\omega_{jo} - \omega - i\Gamma_{jo}/2} \qquad [87]$$

and $\omega_o$ is the transverse exciton frequency, numerical integration of the semiclassical intensity expressions [75] and [76] at various temperatures

predicts simple competitive behavior between TPE and SHG if the nonresonant part of $\chi^{(2)}$ is set equal to zero. Meredith (205) has suggested a value for naphthalene of $10^{-9}$ e.s.u. for $|\chi_{nr}^{(2)}|$. The magnitude of $\chi_{nr}^{(2)}$ will be discussed further in a later section.

The complete polariton fusion rate expression given in Chapter II contains the phase matching term:

$$R \approx \frac{1}{L^2}\left|\int_0^L e^{i\Delta kx}\, dx\right|^2 , \qquad [88]$$

where L is the crystal thickness and $\Delta k$ is the phase mismatch between the fundamental and doubled polaritons. The temperature behavior of the nonlinear signals is contained in this term, as the fusion rate in an infinite crystal is expected to be independent of temperature (50c, 152b). Damping in the polariton model (discussed in Chapter II) is viewed as temporal damping, where the frequency is assumed complex and its imaginary part is equal to $\gamma/2$. Inclusion of damping in the phase matching expression [88] gives:

$$R \approx \frac{1}{L^2}\left|\int_0^L e^{i\Delta kx}\, e^{-\gamma t/2}\, dx\right|^2 \qquad [89]$$

or

$$R \approx \frac{1}{L^2}\left|\int_0^L e^{i(\Delta k + i\gamma/2v_g)x}\, dx\right|^2 , \qquad [90]$$

where t has been written as a function of x for purposes of integration:

$t = x/v_g$, where $v_g$ is the polariton group velocity $\partial\omega/\partial k$. Doing the integration in [90] gives the phase matching term in the rate expression for damped polariton fusion:

$$R \approx \frac{1 + e^{-\gamma L/v_g} - 2e^{-\gamma L/2v_g}\cos\{\Delta kL\}}{\{\Delta kL\}^2 + \gamma^2 L^2/4v_g^2} \quad , \qquad [91]$$

$\Delta k$ may be written as a function of $\omega - \omega_{pm}$, where $\omega_{pm}$ is the phase matched ($\Delta k = 0$) frequency, by expanding k as a function of $\omega$ about the phase matching point. Truncation after the first-order term yields

$$k - k_{pm} \equiv \Delta k = \frac{(\omega - \omega_{pm})}{v_g} \quad , \qquad [92]$$

where $v_g$ is understood to be evaluated at $\omega_{pm}$. This gives the fusion rate expression the following form:

$$R \approx \frac{1 + e^{-\gamma L/v_g} - 2e^{-\gamma L/2v_g}\cos\{\omega' L/v_g\}}{\{\omega' L/v_g\}^2 + \gamma^2 L^2/4v_g^2} \quad , \qquad [93]$$

where $\omega' = \omega - \omega_{pm}$. Integration of equation [93] over all $\omega$ gives the integrated SHG intensity at the exit face of the crystal:

$$I_{SHG} \approx \frac{2\pi v_g^2}{\gamma L^2}\left[1 - e^{-\gamma L/v_g}\right] \quad . \qquad [94]$$

In the limit of zero damping ($\gamma = 0$) this reduces to $I_{SHG}^{2D} = 2\pi v_g/L$. Two-photon absorption, to which TPE is proportional, is viewed as scattering of the doubled polariton; the TPE intensity is accordingly proportional to the

difference between $I_{SHG}^{ZD}$ at zero damping and $I_{SHG}$:

$$I_{TPE} \approx \frac{2\pi v_g}{L} - \frac{2\pi v_g^2}{\gamma L^2}\left[1 - e^{-\gamma L/v_g}\right] \quad . \qquad [95]$$

Normalizing to the zero-damping intensity gives simple expressions for the signal intensities as functions of $\gamma$:

$$I_{SHG} = \frac{v_g}{\gamma L}\left[1 - e^{-\gamma L/v_g}\right]$$

$$I_{TPE} = 1 - \frac{v_g}{\gamma L}\left[1 - e^{-\gamma L/v_g}\right] = 1 - I_{SHG} \quad . \qquad [96]$$

Truncating the expansion in k after the second term (the approximation made in equation [92]) is equivalent to assuming the profiles to be perfectly symmetric about $\omega_{pm}$, true only in the limit of high $|\Theta_{EXT}|$. Exact evaluation of $\Delta k$ as a function of $\omega$ using the polariton dispersion relation [74] gives the expression:

$$\Delta k = \frac{\omega}{c}\left[n_o\left\{1 - \frac{\omega_p^2 F}{n_o^2(\omega_o^2 - \omega^2)}\right\}^{1/2} - n_b\right] \quad , \qquad [97]$$

Numerical integration of equation [97] over frequency yields exactly the same relative branching behavior as equations [96]. Since many profiles are decidedly asymmetric, it is evident that the major effect of inclusion of asymmetry (further terms in the expansion [92]) on expression [93] is the addition of an odd part which does not affect the integrated result.

Interestingly, the intensity expressions [96] may also be obtained in

a simpler way, neglecting the coherent nature of the nonlinear process. One assumes that the fusion rate is constant over the length of the crystal, and that polaritons formed at a distance z from the exit face of the crystal decays as $\exp(-\gamma z/v_g)$. The assumption is also made here as in all calculations in this chapter that the path length through the crystal (effective crystal thickness) does not change appreciably over the range of values employed for $|\Theta_{EXT}|$. The final normalized SHG intensity is the average $\langle \exp(-\gamma z/v_g) \rangle_z$ over all values of z:

$$I_{SHG} = \frac{1}{L} \int_0^L e^{-\gamma z/v_g} \, dz \quad .$$

Equations [96] result. Neglect of coherence is equivalent to assuming very short coherence lengths, again the high-$\Theta_{EXT}$ limit found to be sufficient in the previous derivation of [96].

Figure 17 shows the results of the temperature-dependent intensity calculations based on the semiclassical and polariton fusion models for a 30 μm crystal at $\Theta_{EXT} = 10°$ (a typical value). The intensities of the TPE signals are constant at low temperatures where scattering is dominated by $\gamma_o$, the temperature-independent part of $\gamma$. The two models predict similar behavior: the temperature-dependent branching changes rapidly over an intermediate temperature range and then reaches a plateau at higher temperatures, where the SHG intensity approaches zero. The semiclassical calculations were done using a value of 0 for $\chi_{nr}^{(2)}$, vide infra; the justification for the choice is at this point only that it results in the prediction of the simply competitive intensity behavior observed experimentally.

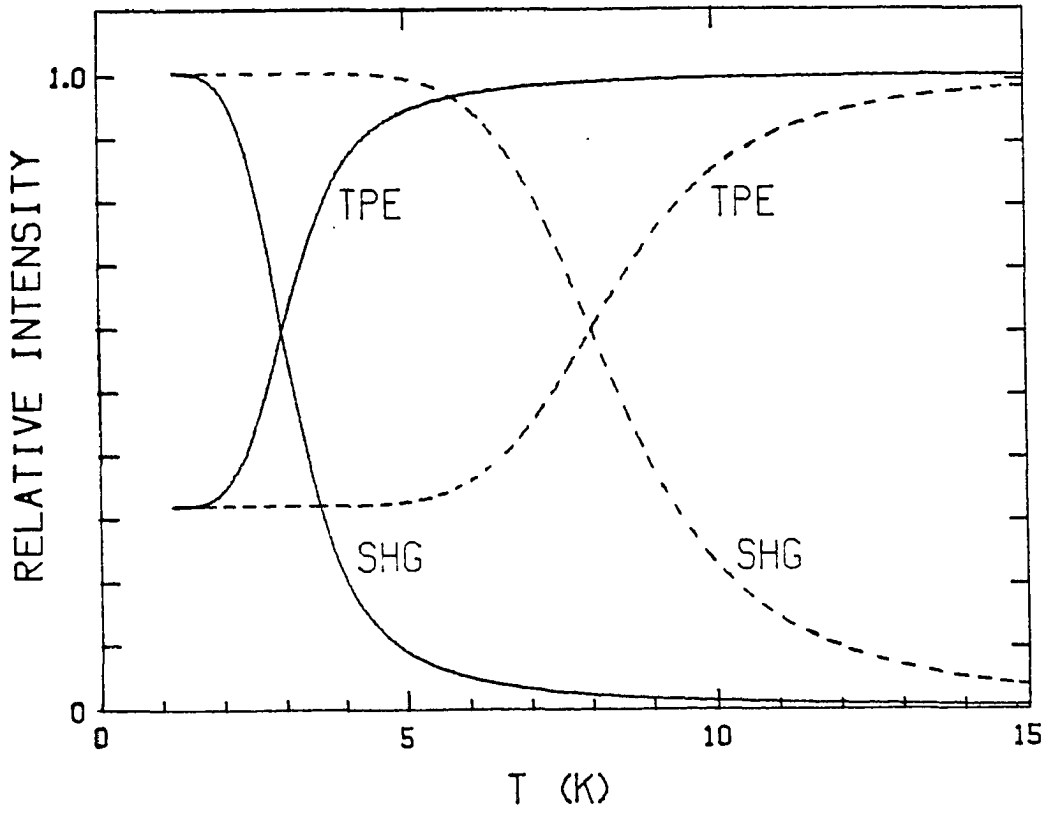


Figure 17. Calculated nonlinear signal intensities as a function of temperature for a 30 μm naphthalene crystal with the fundamental beam incident on an ab slab at 10° with respect to c'. The solid curves are obtained from integration of the semiclassical rate expressions [75] and [76], using values of $\chi_{nr}^{(2)} = 0$, $\omega_p^2 F = 5750\ cm^{-2}$, $\alpha = 1.4 \times 10^{-25}$ e.s.u., $\omega_o = 31475\ cm^{-1}$, $\gamma_o = 4 \times 10^9\ s^{-1}$, $\Omega_{eff} = 12\ cm^{-1}$ (exciton damping), and $2\pi N/h = 2.64 \times 10^{48}\ cm^{-3}\text{-}erg^{-1}\text{-}s^{-1}$ (see text). The dashed curves are obtained from the polariton fusion rate expressions, [96], or the semiclassical expressions using $\Omega_{eff} = 39\ cm^{-1}$ (polariton damping)

The predictions of the two models differ chiefly in the temperature range over which the greater part of the intensity changes occur. The semiclassical model predicts the growth of the TPE signal to be essentially complete at a far lower temperature than does the fusion model. Interestingly, substitution of the polariton damping constant from the nonlinear broadening data into the semiclassical expression in place of the exciton damping constant results in the same relative intensity predictions as those of the polariton fusion model. It is difficult to explain the use of the new damping constant from the classical viewpoint. The coupling of field and material oscillations is in this picture effected through the susceptibilities, which are material parameters and should not contain terms pertinent to the coupled states. The damping constant in the susceptibility expression [86] refers to the damping of the resonance at $\omega_o$. The equivalence of the two approaches, allowing the assumption of 39 $cm^{-1}$ damping to be made phenomenologically in the semiclassical case, is not obvious from the formalisms and deserves further investigation.

Temperature-dependent intensity data for several values of $v_g$ ($\Theta_{EXT}$) were collected for several PSF naphthalene crystals of thicknesses ranging from 12.5 to 55 μm. The value of $\gamma_o$, the temperature-independent residual damping constant, was treated as a parameter and the value which best fit the greater part of the data collected was used in computing theoretical I-vs.-T curves for comparison with data. Although a case can be made for allowing $\gamma_o$ to vary slightly from crystal to crystal, for example as strain induced by handling the sample might vary with

sample thickness, chemical purity and surface quality might vary, etc., a value of $\gamma_o = 4 \times 10^9\ s^{-1}$ was found to be satisfactory for all PSF crystals studied. It was not possible to fit the temperature behavior with the semiclassical approach using the exciton damping constant values; predictions of the polariton fusion model equations [96] (or the semiclassical model with polariton damping) were in most cases successful in accounting for the data.

The effect of holding L constant and varying $v_g$ are illustrated in Figure 18 for a 55 μm sample at four values of $\theta_{EXT}$. The values of $v_g$ for which temperature data were obtained from this crystal ranged from $6 \times 10^5$ to $5 \times 10^8$ cm-$s^{-1}$; all fits to theoretical predictions were good except at the highest value of $v_g$, the data from which appear in a later figure. The low temperature branching ratio $I_{SHG}:I_{TPE}$, determined by $\gamma_o$, L, and $v_g$, ranges for the data shown from 6:1 for the exciton clothed with the most photon character to 1:35 for the least clothed. Data are plotted normalized to the strongest signal observed, so that $I_{TPE} + I_{SHG} = 1$; the branching ratio is obtained from the plots as $(1-I_{TPE})/I_{TPE}$. The change in branching behavior with $v_g$ is a consequence of the fact that the more exciton-like polaritons scatter more strongly then do the more photon-like polaritons created at lower $|\theta_{EXT}|$. The more photon-like polaritons are also observed to reach the "plateau region" of constant integrated TPE intensity at a higher temperature than those with less photon character; that is, to exhibit a stronger polariton effect in their behavior.

The effect of varying $\gamma_o$ may be seen by examining data from a crystal made imperfect by doping with anthracene, $1.4 \times 10^{-4}$ m/m. The

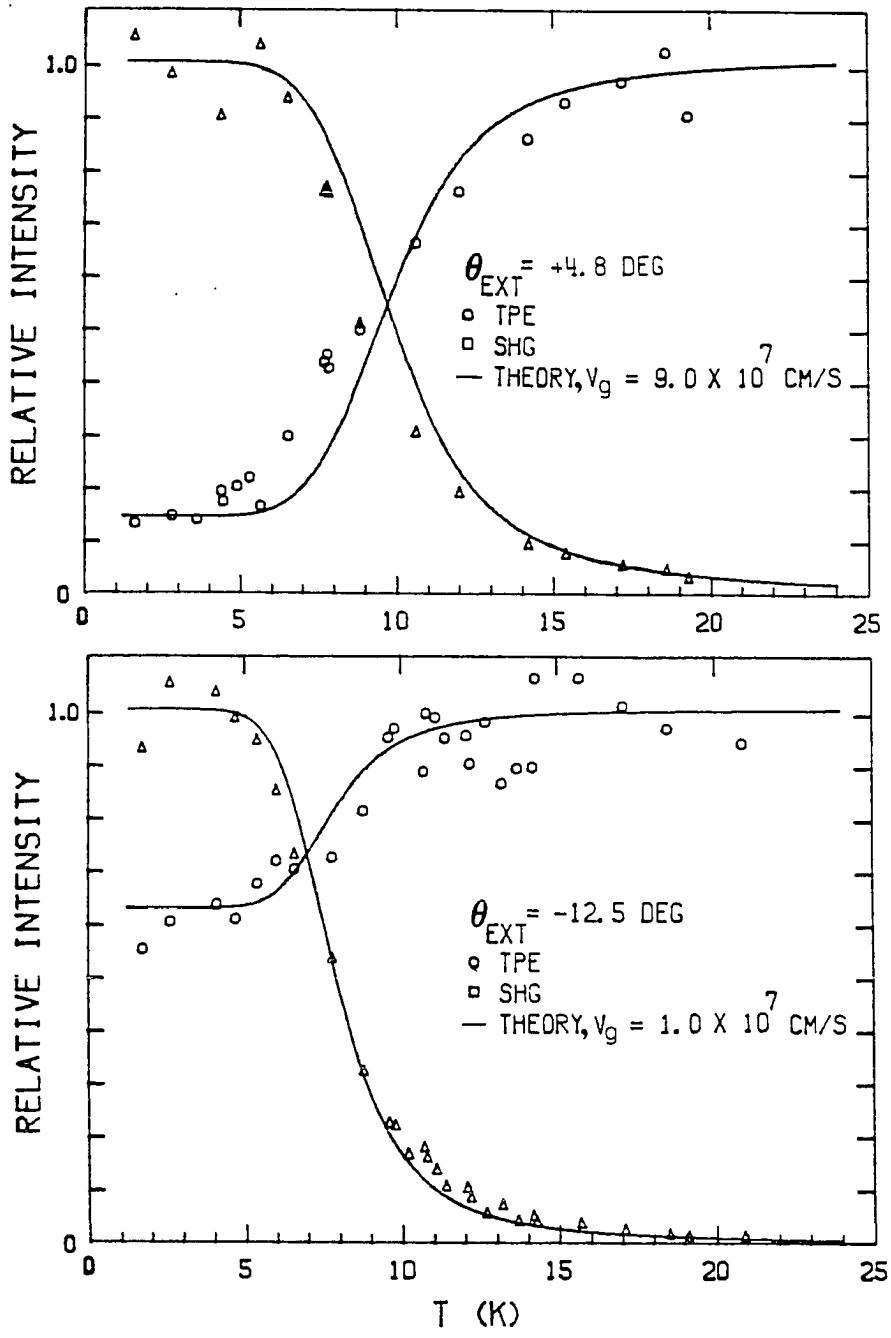


Figure 18. Integrated intensites of TPE and SHG profiles as a function of temperature at four orientations for a 55 μm PSF naphthalene crystal. The solid lines are computed from the fusion rate expressions [96] using the experimentally determined temperature-dependent damping (see text) with $\gamma_0 = 4 \times 10^9\ s^{-1}$

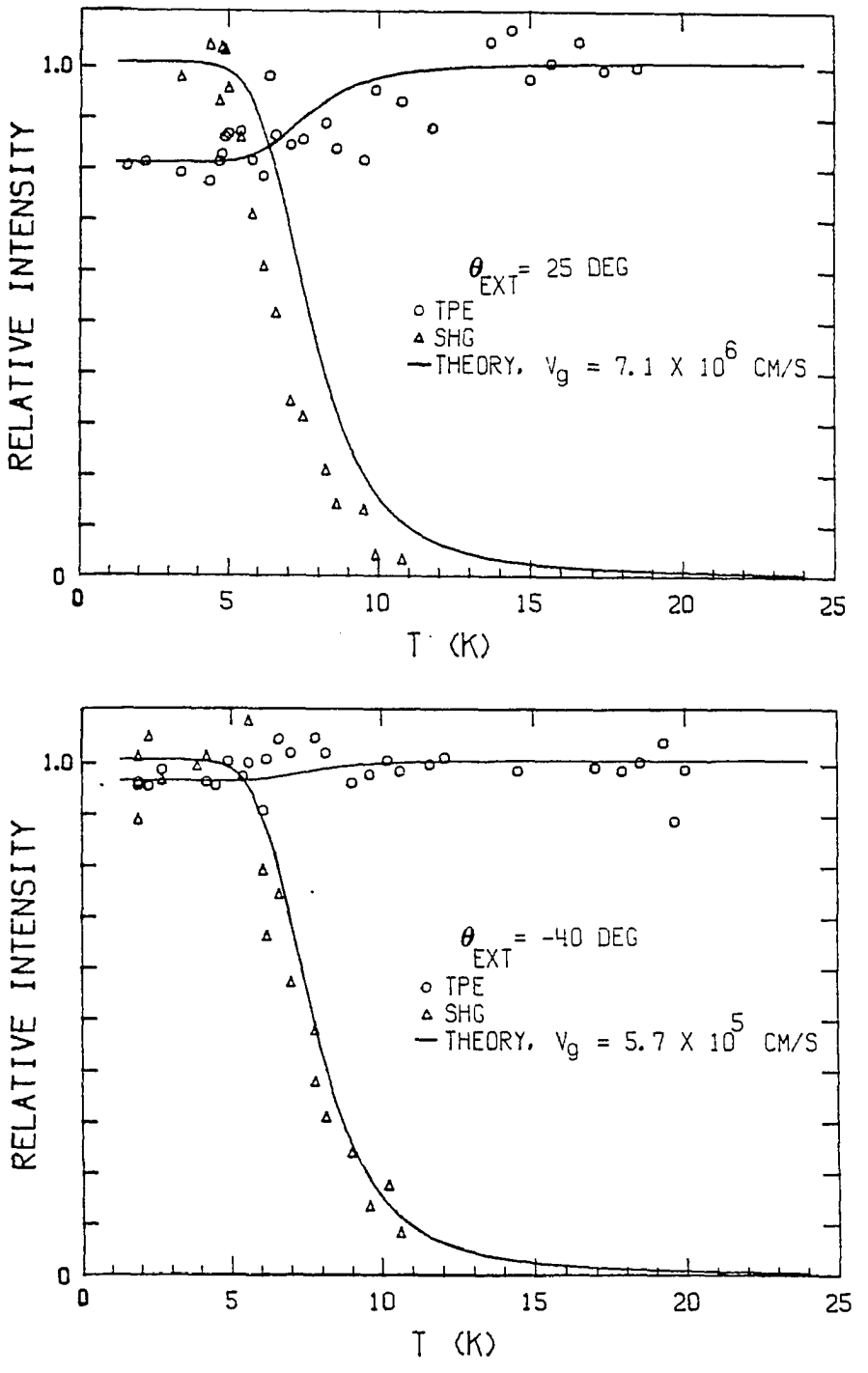


Figure 18. (continued)

resulting inhomogeneous broadening may be seen in Figure 19. The low temperature FWHM's of the two higher-$\Theta$ data sets shown are both 1.1 $cm^{-1}$. The "residual width" contribution at $\Theta_{EXT} = 4.5°$ is appreciable; the low temperature width of this profile is 1.9 $cm^{-1}$. Because the homogeneous contribution to each profile is convoluted with rather than added to the inhomogeneous contribution, the broadening curve does not exactly parallel that of the pure crystals, shown as a solid line. The intensity behavior of the doped crystal at two incident angles is compared to data obtained at the same values of $\Theta_{EXT}$ from pure crystals of comparable thickness (about 30 μm) in Figure 20. The curves differ mainly at low temperatures, owing to the difference in $\gamma_o$ ($\gamma_o$ for the doped crystal is about $3 \times 10^{10}$ $s^{-1}$), and merge at high temperatures, where the damping is dominated by exciton-phonon scattering and the contribution by $\gamma_o$ is minimal.

The effect on the branching behavior of varying crystal thickness at a few given values of $v_g$ and $\gamma_o$ is shown in Figure 21. For a group velocity of $9 \times 10^6$ $cm\text{-}s^{-1}$, for example, the low temperature branching ratio is 2:1 for a 12.5 μm crystal and 4:5 for a 27 μm crystal; these ratios are successfully predicted by the polariton model (solid lines).

Figure 22 compares theoretical calculations to data for four values of $\Theta_{EXT}$ for a 27 μm crystal. The fit is reasonably good except at $\Theta_{EXT} = 5°$; in contrast to the success of the fit at the same angle for the 55 μm sample (see Figure 18), the data for the TPE intensity lie above the predicted curve for most of the temperature range. This illustrates the general observation that for a given crystal the models are successful in

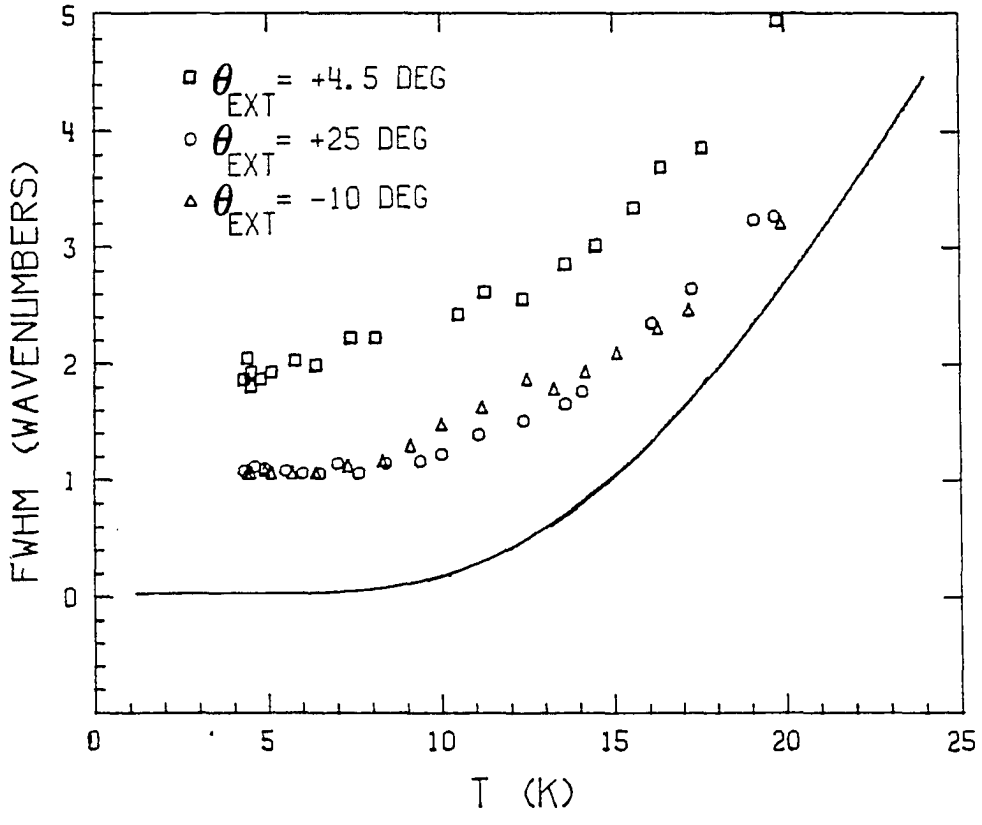


Figure 19. Temperature-broadening data for a 30 μm $1.4 \times 10^{-4}$ m/m anthracene-doped naphthalene crystal at three angles of beam incidence with respect to $\underline{c}'$. The solid curve is a theoretical fit to $\langle n \rangle$ for a 39 $cm^{-1}$ phonon, expression [82]

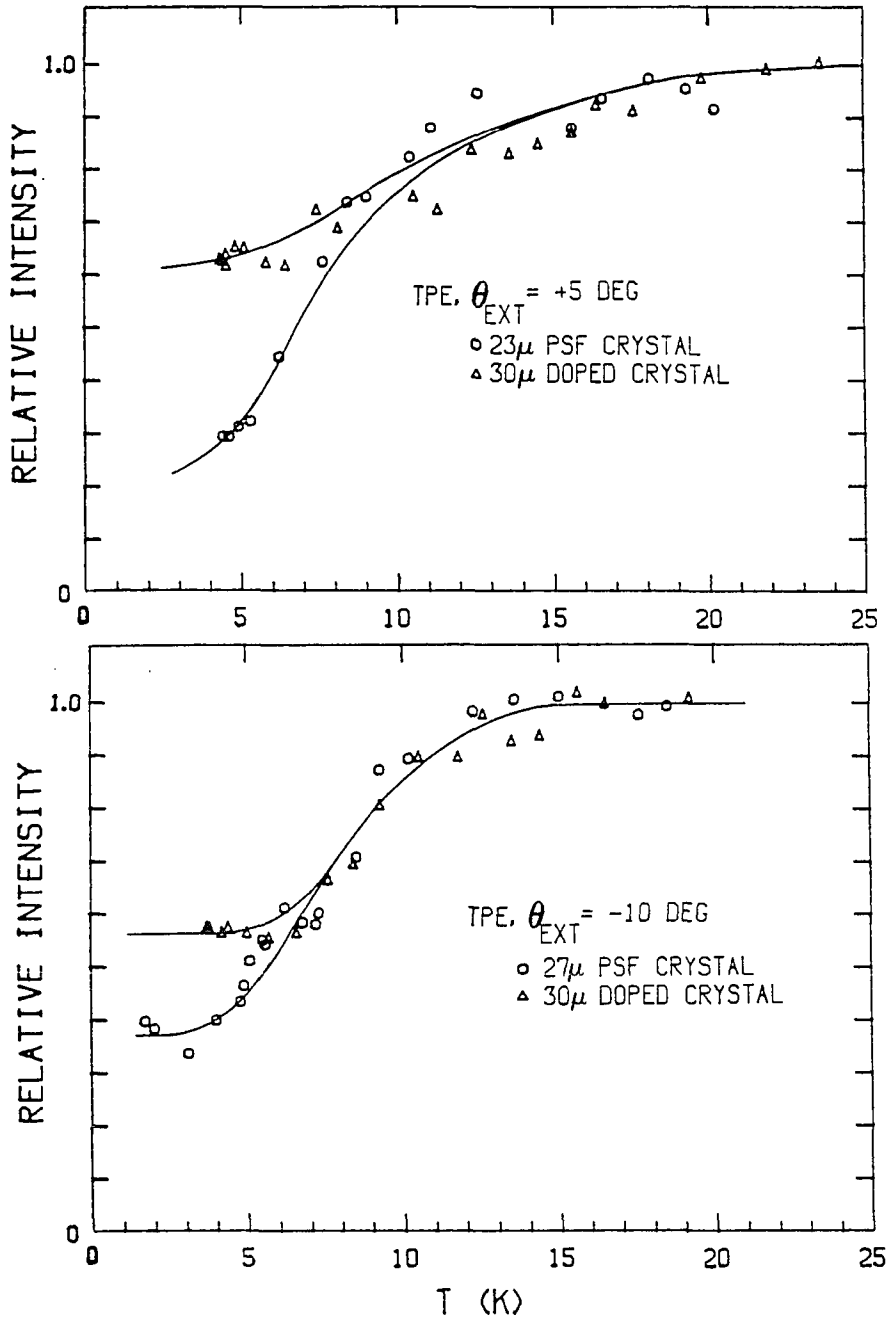


Figure 20. Integrated intensities of TPE profiles as a function of temperature for a 30 μm $1.4 \times 10^{-4}$ m/m anthracene-doped naphthalene crystal and PSF naphthalene crystals of similar thickness. The solid lines are intended as visual guides

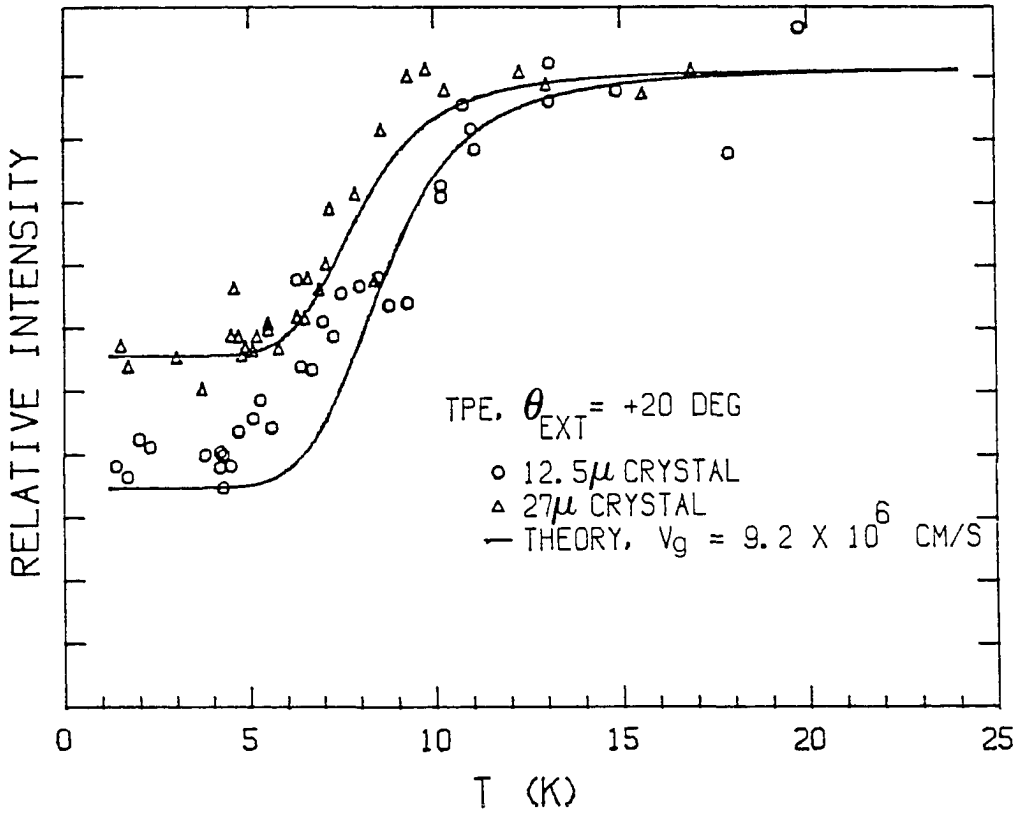


Figure 21. Comparisons of integrated TPE profile intensity behavior for crystals of different thicknesses at the same orientations with respect to the incoming laser beam. The solid lines are computed from the fusion rate expressions [96] using the experimentally determined temperature-dependent damping (see text) with $\gamma_0 = 4 \times 10^9\ s^{-1}$

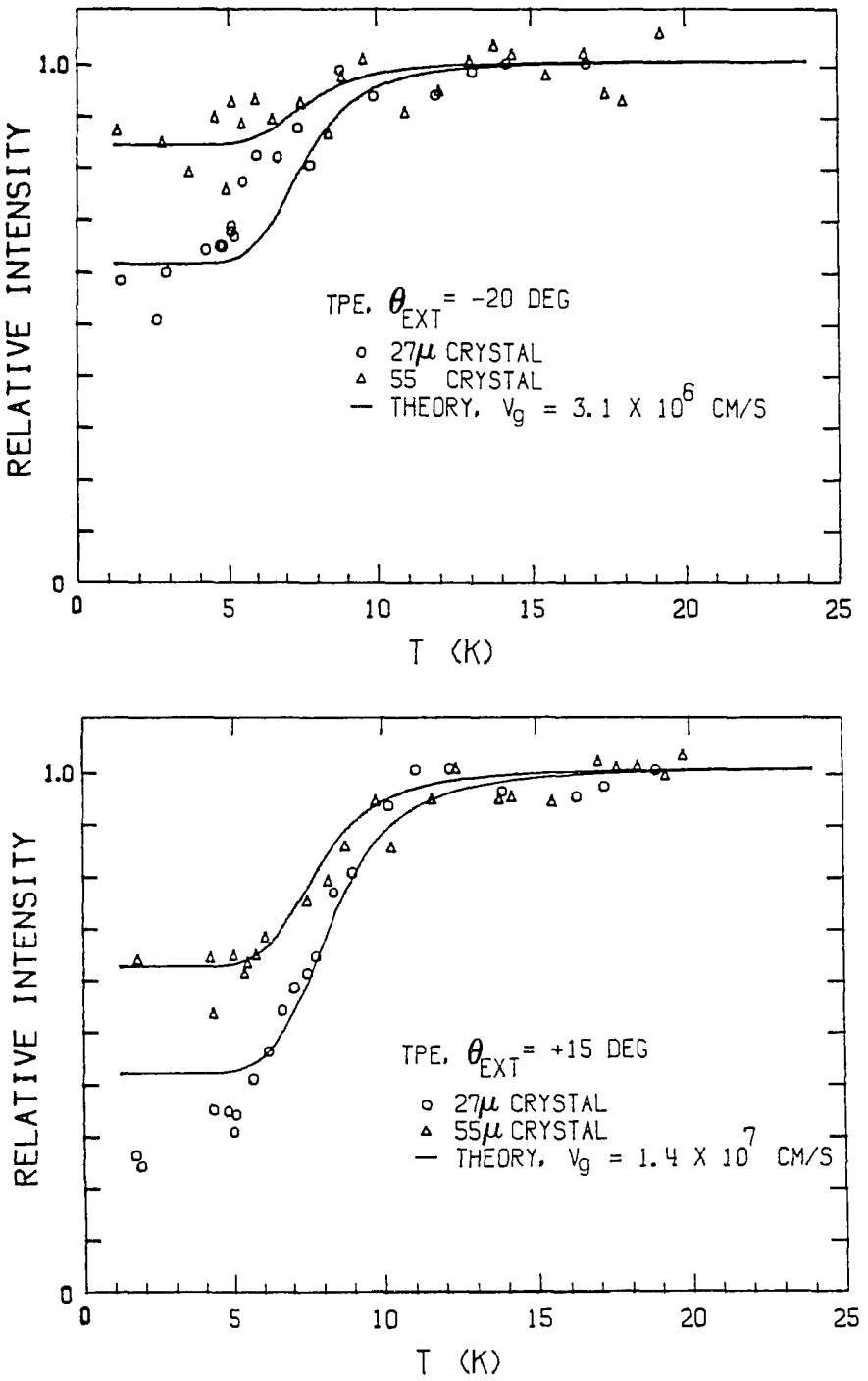


Figure 21. (continued)

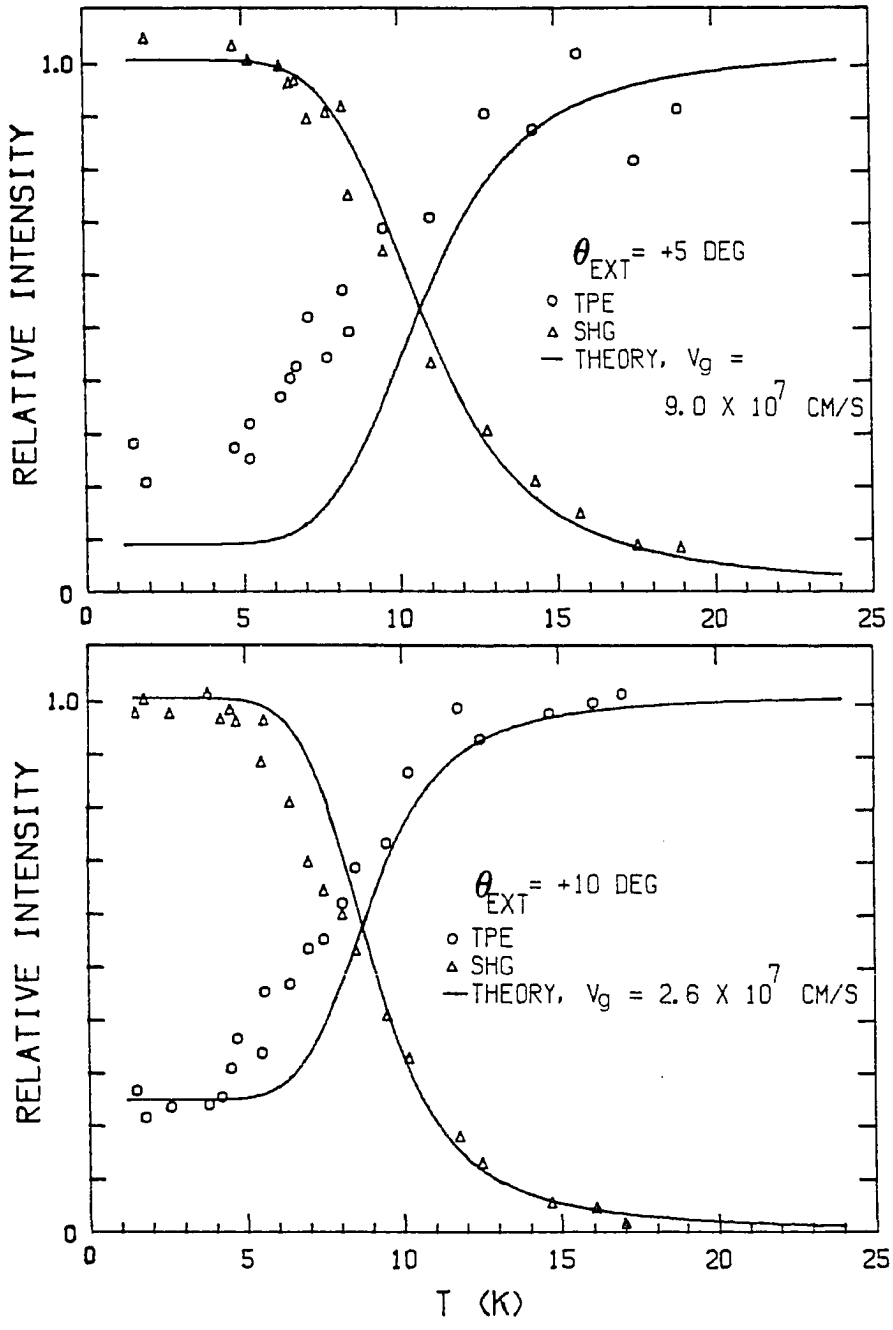


Figure 22. Integrated intensities of TPE and SHG profiles as a function of temperature at four orientations of a 27 μm PSF naphthalene crystal. The solid lines are computed from the fusion rate expressions [96] using the experimentally determined temperature-dependent damping (see text) with $\gamma_0 = 4 \times 10^9\ s^{-1}$

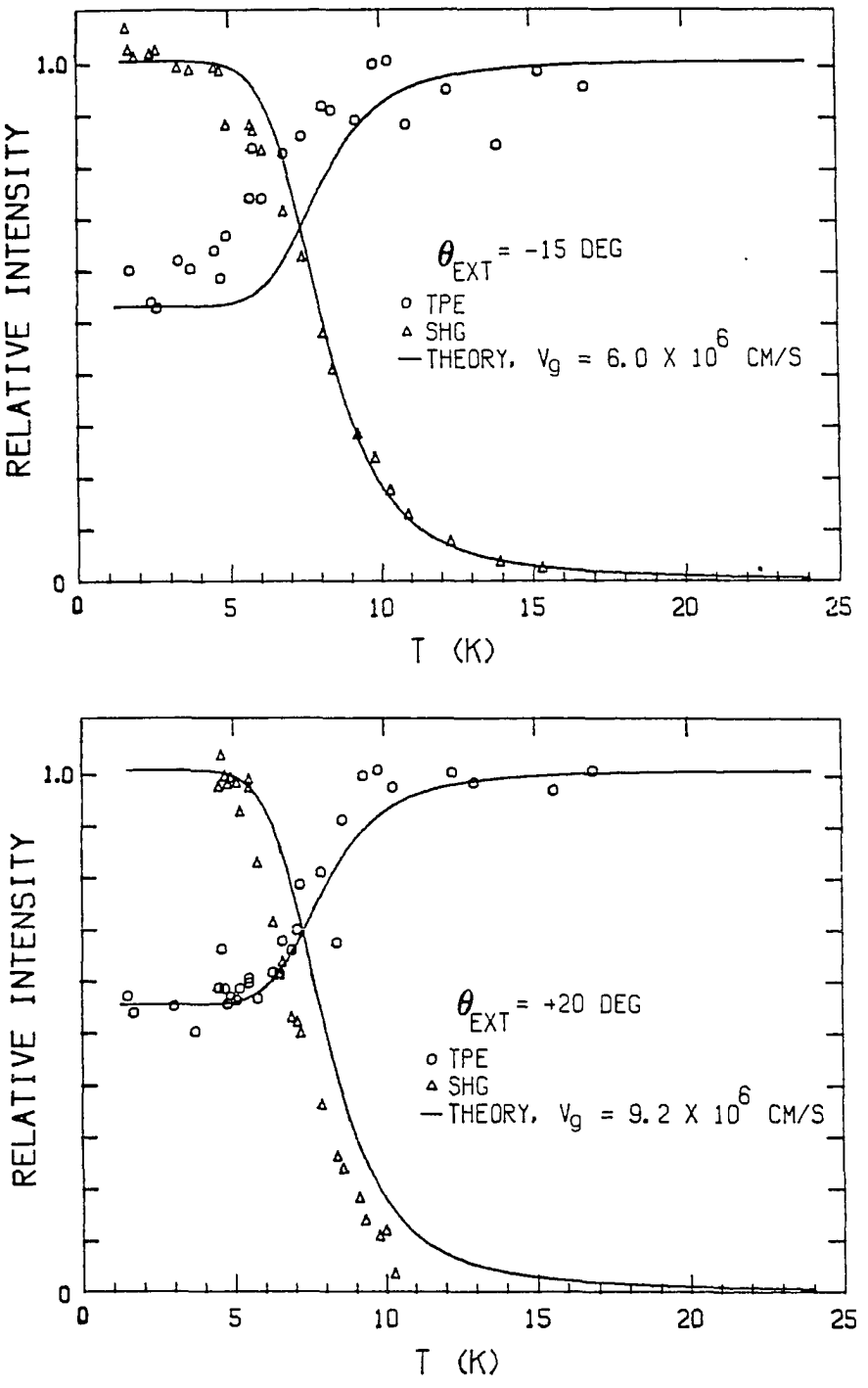


Figure 22. (continued)

accounting for temperature-dependent intensity data for all group velocities below some value, but fail at higher values of $v_g$. It is appropriate at this point to compute the scattering-dominated coherence lengths of the excitations. Using the relation $l_c = \pi v_g/\gamma$, for a typical intermediate temperature of 10 K, coherence lengths of 2, 40, and 350 μm result at incident beam angles of 20, 5, and 2°, respectively. At an incident angle of 5°, a 55 μm crystal is more than one coherence length thick for most of the temperature range of interest, while a 27 μm crystal is less than one coherence length thick up to about 15 K, the temperature at which the data in Figure 22 begin to approach the values predicted by the model. In general, data are observed to fit the predictions of equations [96] when T and $v_g$ are such that the crystal is more than one coherence length thick. Had the forms of [96] been dependent on the simplifying assumptions made in their derivations (equivalent to assuming small coherence lengths) these deviations would be understood as interference phenomena. In view of the fact that the same branching predictions are derived from full consideration of the phase matching term in the polariton fusion rate expression, however, it is evident that this behavior is not simply related to that term. Further illustration of this observation is given in Figure 23, where temperature-dependent intensity data are plotted for crystals of different thicknesses at the same low angle of incidence. Although the predicted behavior for the two crystals is quite different, the data fall together and on neither of the predicted curves. The large-$l_c$ behavior which does not fit the predictions for a given $v_g$ appears to be independent of sample thickness; the signals evidently arise from sources other than the bulk phase matching

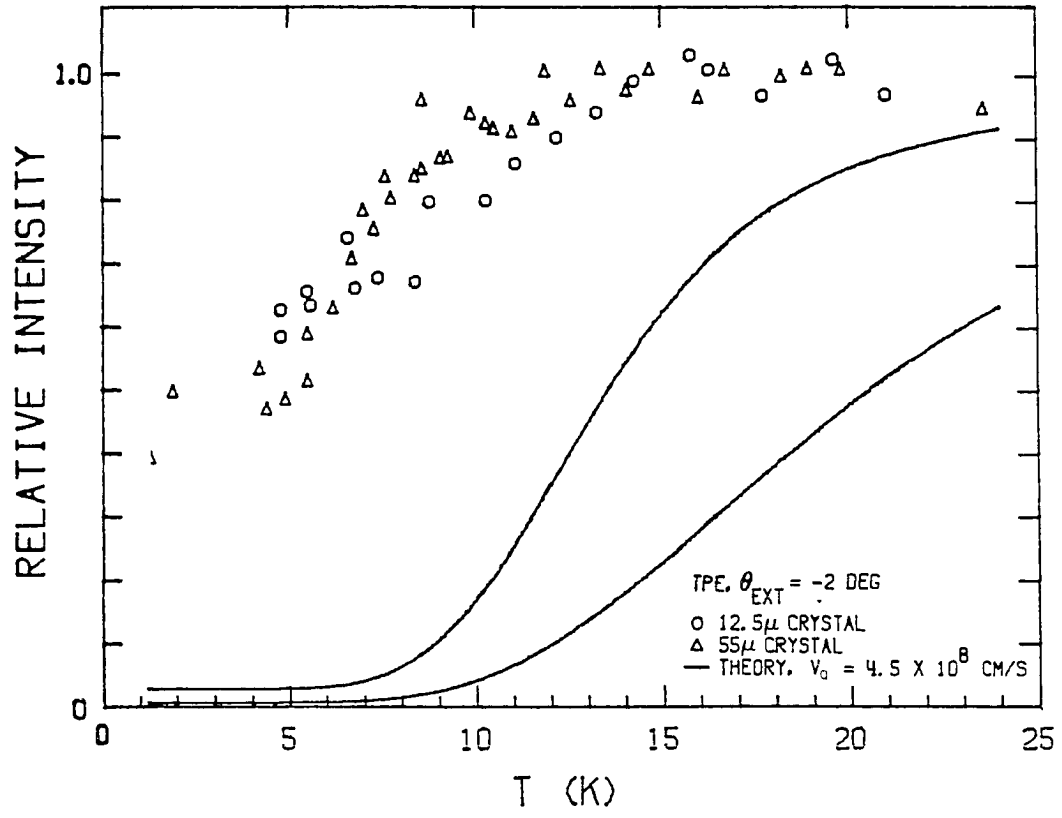


Figure 23. Integrated intensity behavior for TPE and SHG profiles from crystals of different thicknesses at near-normal angles of beam incidence. The solid lines are computed from the fusion rate expressions [96] using the experimentally determined temperature-dependent damping (see text) with $\gamma_0 = 4 \times 10^9\ s^{-1}$

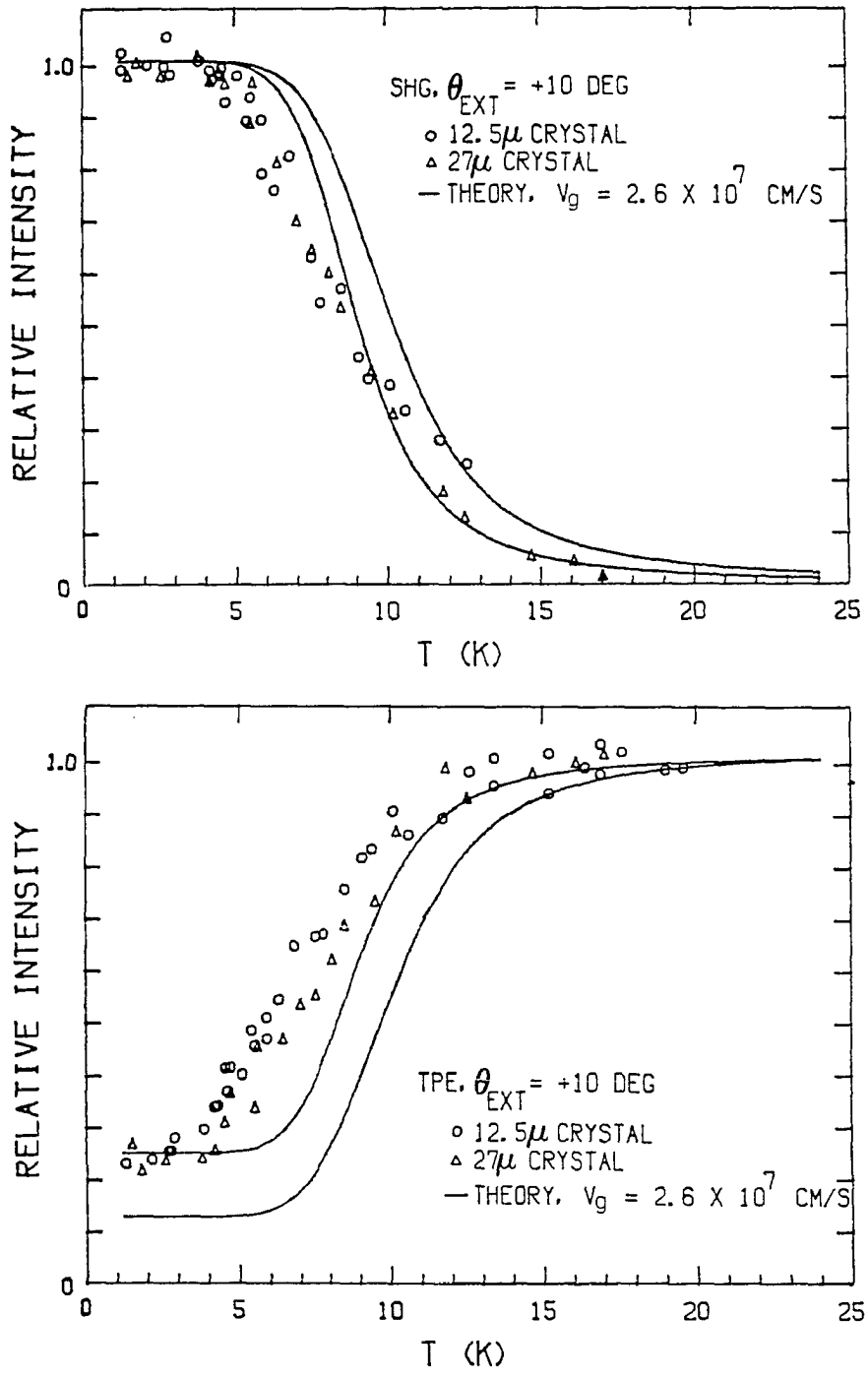


Figure 23. (continued)

term $\Delta kL$. The data in Figure 23 also argue convincingly against fitting intensity behavior by allowing $\gamma_o$ to vary with incident angle. This approach could be justified by assuming that the change in path length with incident angle will manifest itself as an effective change in "residual scatterer" concentration. However, data from crystals of different thicknesses would then be expected to exhibit different values of $\gamma_o$ as well, and that is not the case.

The anomalous intensity behavior displayed by crystals less than one coherence length in thickness may arise from a coherent component of the signal originating at the surfaces of the crystal and not completely attenuated in thin crystals. In centrosymmetric crystals one could reasonably expect to see an enhancement of nonlinear intensity at the surface, where the crystal symmetry breaks down and dipole contributions are allowed; these contributions would be important for thin crystals. Enhancement of this kind has been reported in reflected SHG from silicon by Tom et al. (48) and by Bloembergen and coworkers (11b, 206). However, a simple model including a high fusion rate term for the first few unit cells of the excitation path cannot account for the data. Because the signal is enhanced at all temperatures, there is a limit to the amount by which the normalized low-temperature predictions can be improved in this way. A thorough treatment of surface effects necessitates consideration of the breakdown of the phase matching requirement at the crystal surface in addition to the breakdown of inversion symmetry. This additional non-phase matched second harmonic generated at the two surfaces interferes to enhance the phase matched SHG signal in thin crystals, and contributes to the non

phase matched SHG intensity from all crystals, mainly affecting the signal baselines. The TPE signal would be augmented by a non-phase matched resonance-enhanced component. Such a signal was observed from one crystal in this study, vide infra; however, that crystal was the thickest sample used, while this effect should be the most prominent for the thinnest samples. Another possible effect which might alter the rate of generation of nonlinear signals is alteration of the exciton spatial dispersion at the crystal surface.

## Appearances of Nonlinear Profiles

The appearances of the one-photon absorption and nonlinear profiles for the 31475 $cm^{-1}$ a-exciton of naphthalene are distinguished by the signal lineshapes as well as by broadening. The OPA profile is fairly symmetric at low temperatures; at higher temperatures (above about 7 K) the high-frequency side of the peak becomes Lorentzian, while the low-frequency side tails more slowly. This behavior is illustrated in Figure 24. In contrast, the nonlinear profiles generally progress from asymmetry at low temperatures to symmetric Lorentzian lineshapes at high temperatures.

Several one-photon absorption exciton lineshape theories, attempting to explain profile asymmetries, have invoked contributions from scattering processes other than the exciton-phonon interaction, e.g., disorder scattering or scattering from isotopic impurities (207). However, these treatments have not proven useful in predicting the shapes of the naphthalene OPA profiles (50b, 117c). A recent explanation by Stevenson and

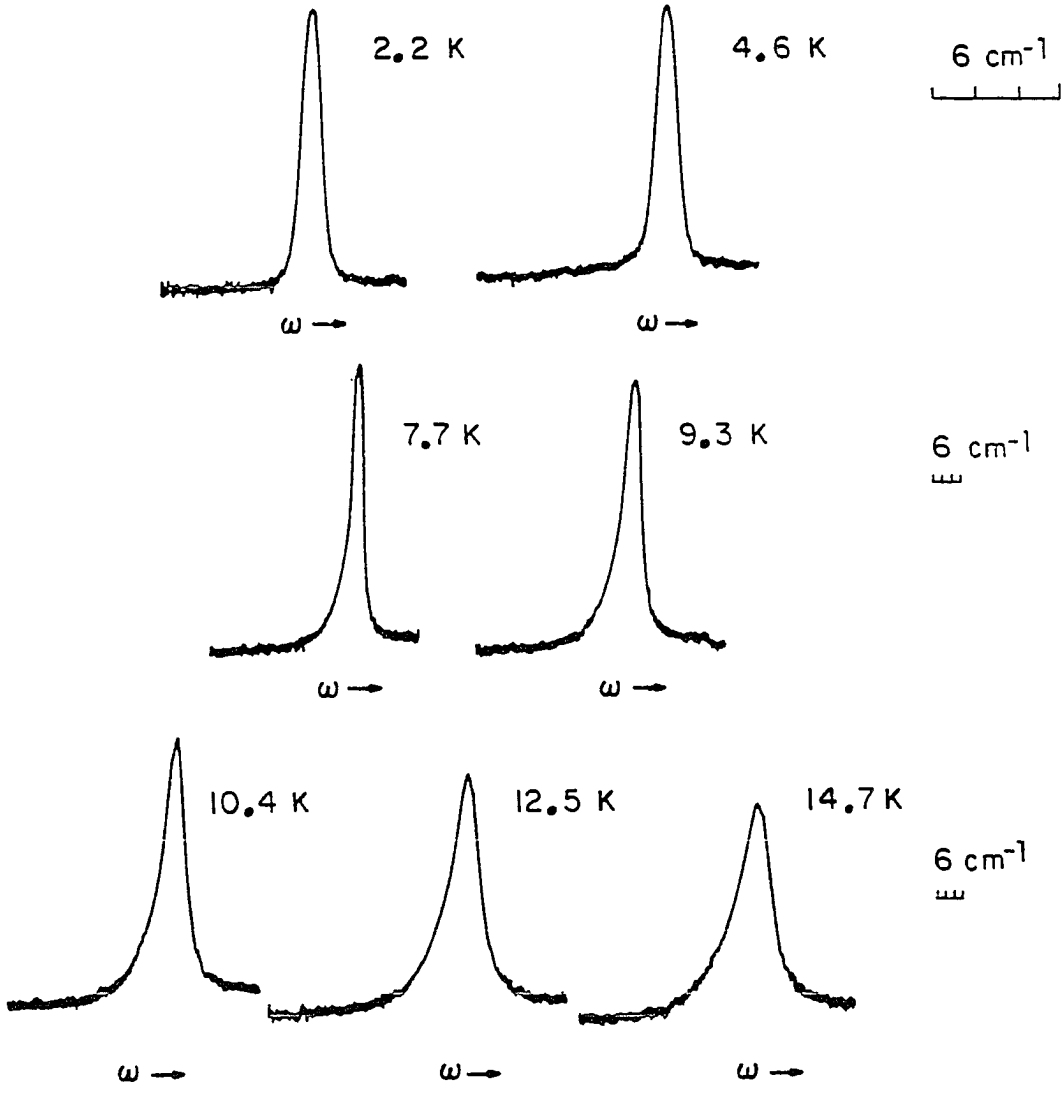


Figure 24. One-photon transmission profiles of the a-exciton of naphthalene (from ref. 117a)

Small (50b) invoking "hot phonon" sideband activity has been more successful. Because the lattice may be distorted in the OPA process by acoustic phonons in the time it takes the excitation (exciton) to traverse a unit cell, the two excitations are strongly coupled, leading to "one-particle" exciton-phonon optical transitions (132). The momentum conservation rule for such transitions is $k_{ex} + k_{ph} \approx 0$. Since naphthalene's exciton spatial dispersion is strong enough to cross the acoustical phonon branch dispersion (Figure 25), transitions involving simultaneous exciton creation and one-phonon annihilation are expected to "bunch up" at a frequency lower than that of the (0,0) exciton transition by an amount $\Delta\omega = -c_s^2 m_{ex} \pi/h$ (50b), where $c_s$ is the speed of sound in the crystal and $m_{ex}$ is the effective exciton mass. For naphthalene the value of $m_{ex}$ may be deduced from the implication of the thermal broadening data that the exciton dispersion, $\omega_{ex} = hk_{ex}^2/4\pi m_{ex}$, crosses the acoustical phonon branch dispersion, $\omega_{ph} = k_{ph}c_s$, at $\omega_{ph} \approx 12\ cm^{-1}$. This results in a predicted clustering of hot one-phonon transitions at $\Delta\omega \approx -3\ cm^{-1}$, which is the frequency at which the low-energy asymmetric tails of the OPA profiles are the most prominent (50b, 117c). Thus, similar asymmetries are predicted for any excitonic (0,0) transition of sufficiently high positive effective exciton mass.

The polaritons created in the polariton fusion process propagate fast on the time scale of unit cell distortion and may be said to be coupled weakly to the lattice phonons. Exciton creation - phonon annihilation transitions must be of the "two-particle" kind, with optical selection rule $k_{ph} \approx 0$; consequently, there is no predicted asymmetric contribution to the nonlinear lineshape from hot acoustic exciton-phonon transitions. At low

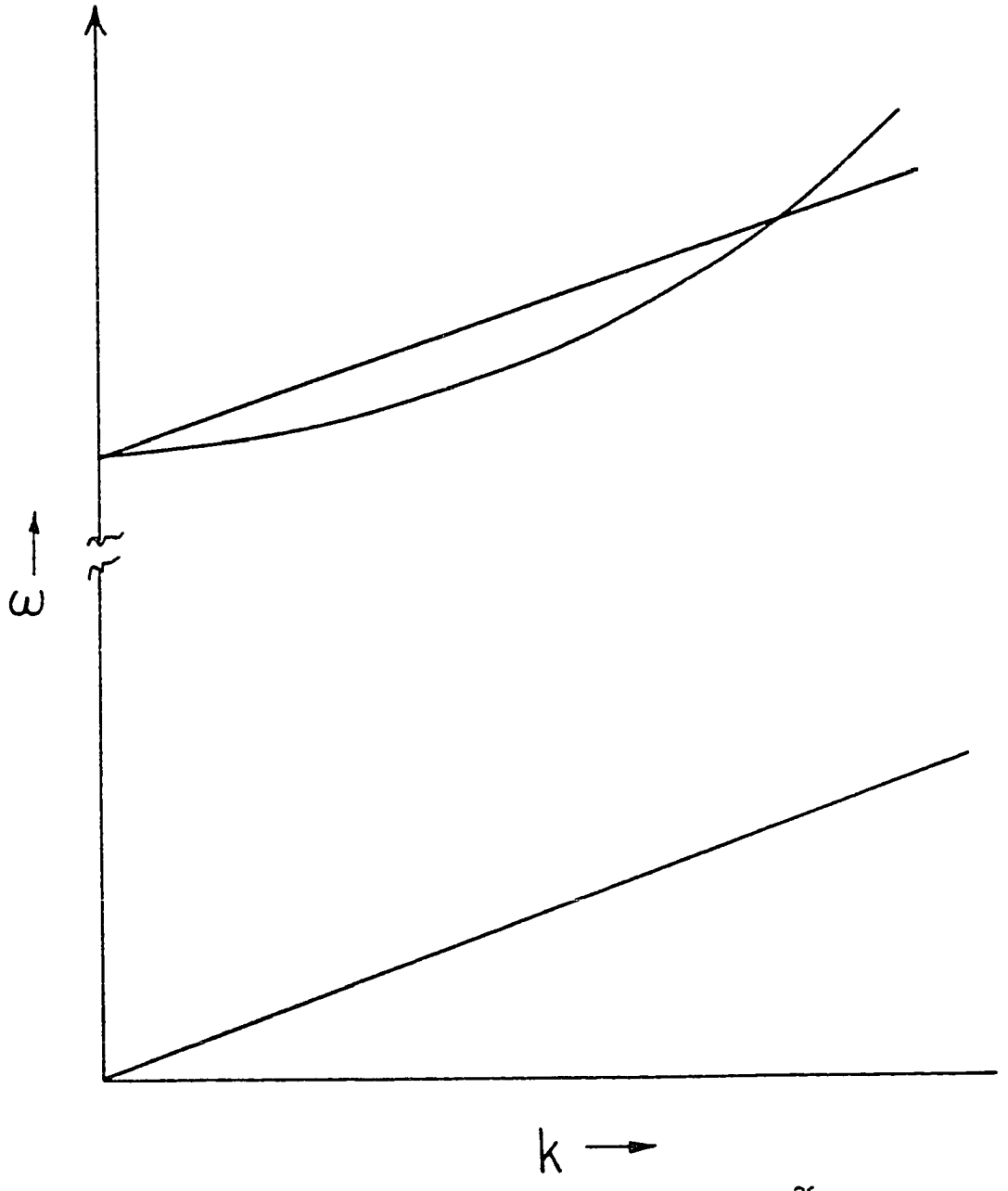


Figure 25. Spatial dispersion of the exciton ($m_{ex} \approx 3.2 \times 10^{-26}$ g, ref. 50b) and acoustic phonon branch dispersion ($c_s \approx 2 \times 10^5$ cm-s$^{-1}$, ref. 50b). Note that "hot" one-particle (vertical) exciton-phonon transitions may occur at frequencies lower than that of the (0,0) transition, by an amount determined by the crossing of the two curves and the curvature of the exciton dispersion curve

temperatures the shapes of the nonlinear signals are dictated by the function $\Delta k(\omega)$. In the limit of zero damping, the phase matching expression [88] reduces to:

$$R \approx \frac{\sin(\Delta kL/2)}{(\Delta kL/2)^2} \equiv \mathrm{sinc}^2(\Delta kL/2) \qquad [98]$$

The principal zeroes of this function are at $\Delta kL = \pm\pi$; the half-maximum occurs at $\Delta kL = \pm 0.886\pi$. For a given value of $\Theta_{EXT}$ (a given $\Delta k(\omega)$), then, the low-temperature residual width should vary approximately in inverse proportion to crystal thickness. An example of this behavior is given in Figure 26, which shows broadening data at $\Theta_{EXT} = -10°$ for three different crystal thicknesses. The residual widths are roughly proportional to the reciprocals of the measured crystal thicknesses. Measurement of the low-temperature value of $\omega$ at half maximum for crystals of known thickness may be used as another way to fit values for $\omega_p^2 F$, $n_o(\Theta)$, and $\omega_o$, using expression [97] and the above half-maximum relation.

The temperature-dependent broadening of the data in Figure 26 is the same for all thicknesses. FWHM data for different values of $\Theta_{EXT}$ and constant sample thickness (see Figures 10-14) also broaden alike, vide supra, differing only in the residual frequency widths determined by the relationship between $\Delta k$ and $\omega$ for different senses of k; that is, by the group velocity of the polariton. At some low values of $\Theta_{EXT}$, for a few samples the residual width of the TPE signals observed in this experiment were slightly greater (typically 0.05 $cm^{-1}$) than those observed for the SHG profiles. This may be a result of the "difference function" nature of

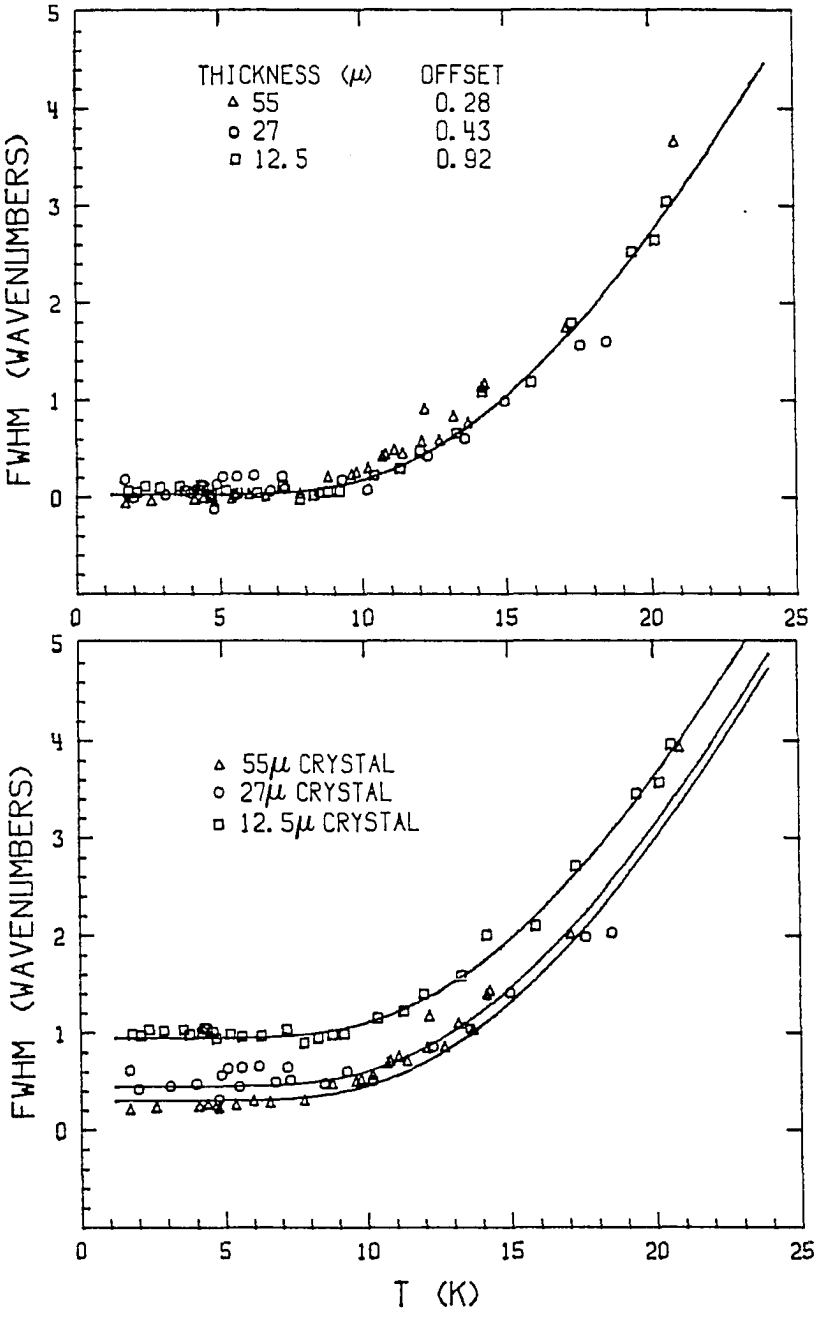


Figure 26. Broadening behavior at an incident angle of -10° with respect to the crystal $\underline{c}'$ axis for three PSF naphthalene crystals of different thicknesses. The solid curves are obtained from expression [82], using an effective phonon frequency of $\Omega = 39\ cm^{-1}$ and preexponential value $C = 43\ cm^{-1}$

the TPE signal, discussed below.

Theoretical prediction of the SHG lineshape from the damped fusion rate expression [91] and from the semiclassical model, using $\chi_{nr}^{(2)} = 0$ and polariton damping, give similar results as it is mainly the interference (phase matching) term which determines the profile shape in both models. However, the theory of the lineshape in the polariton fusion model is not well-developed. The theoretical profiles which follow were computed using the semiclassical expressions [75] and [76]. At most angles of incidence (values of $\chi^{(1)}$) the intensity of the TPE signal is largely due to the $\chi^{(2)}\chi^{(2)}$ term in equation [76]; this term contains the phase matching condition. The TPE peak shape at these orientations therefore depends primarily on $\Delta kL$, as in the case of the SHG signal, and may be expected to be similar to the SHG profile shape. Close to normal incidence, however, where $\chi_{2\omega}^{(1)}(ac)$ approaches $\chi_{\omega}^{(1)}(b)$, the $\chi^{(2)}\chi^{(2)}$ and $|\chi^{(2)}|^2$ terms of equation [76] become comparable and the nonphase matched $\mathrm{Im}(\chi^{(3)})$ term becomes important. The effect of this is to shift the TPE maximum toward the exciton resonance, a phenomenon observed experimentally in this study. Furthermore, the TPE profile develops a peculiar appearance owing to the interference of the three terms of equation [76].

The next few figures show calculated and observed TPE and SHG profiles for several crystals and several values of $\theta_{EXT}$. The calculated profiles were obtained from the semiclassical expressions, [75] and [76], using the experimentally determined 39 $cm^{-1}$ damping constant. Profiles at 5 K and $\theta_{EXT} = 15°$ for a 27 μm PSF naphthalene crystal are shown in Figure 27. Also shown are the computed profiles, for zero and nonzero

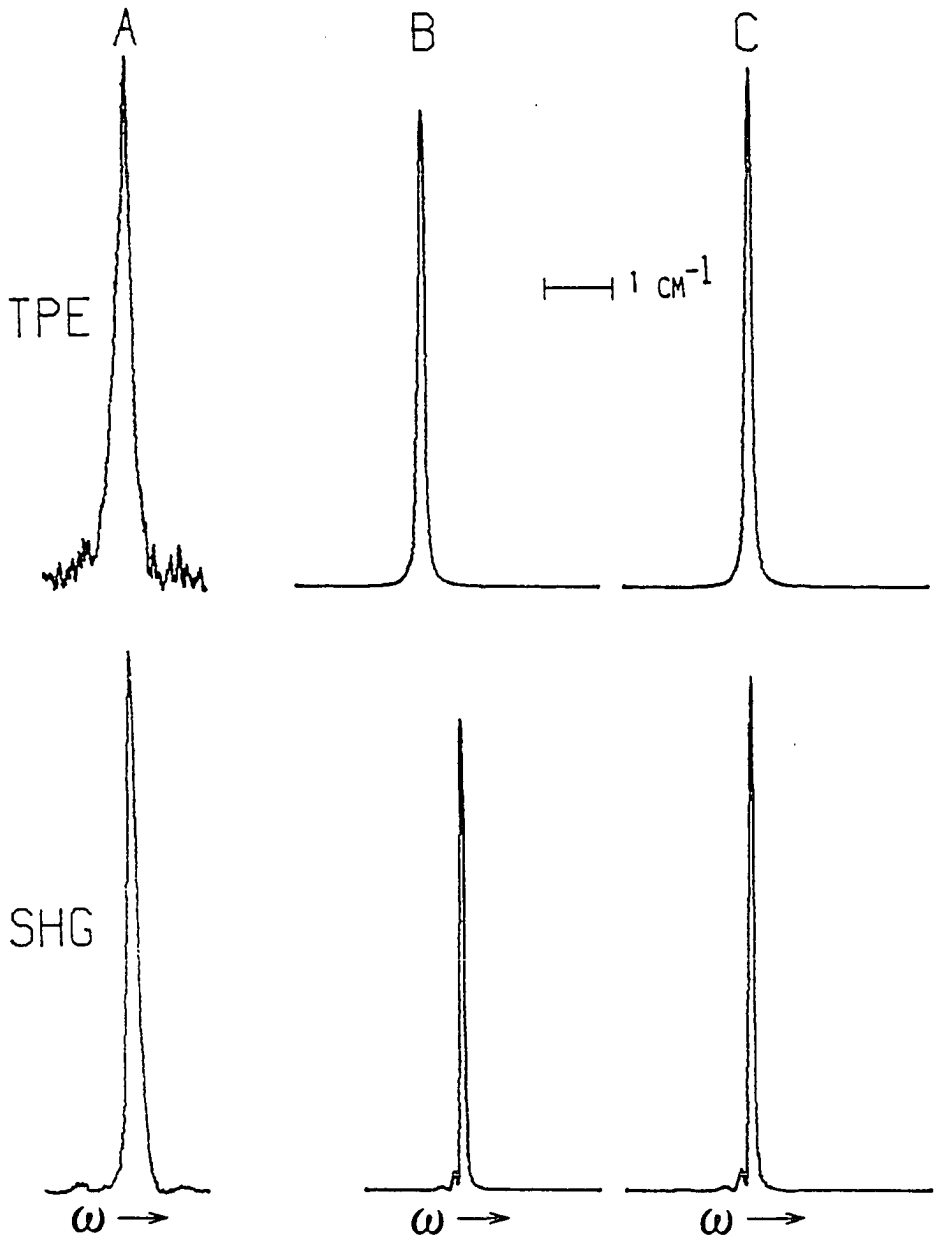


Figure 27. TPE (top) and SHG (bottom) profiles from a 27 μm PSF naphthalene crystal at T = 5 K and an external incident angle of 15° with respect to $\underline{c}'$: A) experimental, B) calculated from eqs. [75] and [76] ($X_{nr}^{(2)} = 0$, $\Omega_{eff} = 39\ cm^{-1}$, all other parameters as in Figure 17), and C) calculated ($X_{nr}^{(2)} = 10^{-9}$ e.s.u.)

($10^{-9}$ e.s.u.) nonresonant $X^{(2)}$. The value of $X_{nr}^{(2)}$ has little effect at this orientation and temperature except to enhance both signals somewhat. The predicted oscillatory behavior near the baseline of the SHG profile is an example of the fringing behavior discussed in Chapter II which results from changing the value of $\Delta kL$. In the experiments reported here, any appreciable bumps in the SHG signal near the baseline at other than near-normal incidence were generally mirrored in the TPE signal, as is the case in part A of Figure 27. This is not a predicted fringing phenomenon. Such features were therefore usually ascribed to irregularities in the frequency profile of the laser. Fringing behavior was not observed in this study at high values of $\Theta_{EXT}$; from Figure 27 it is evident that limited signal resolution or a small amount of baseline noise could prevent their observation.

The effect of nonzero nonresonant $X^{(2)}$ on SHG profiles is more evident in Figure 28, which shows data and calculations for the same crystal and the same orientation as those in Figure 27, but at a temperature of 12 K. Again both signals are slightly enhanced by $X_{nr}^{(2)}$, but this time it is clear that the fringes in the calculated SHG profile are enhanced relative to the parent peak as well. Thus, the absence of significant fringing in the experimental SHG profile can provide an upper limit for the value of $X_{nr}^{(2)}$.

The effect of $X_{nr}^{(2)}$ on predicted profile appearance at angles of incidence nearer normal is more pronounced and is shown in Figure 29 for a 55 μm crystal at $\Theta_{EXT} = 5°$ and T = 19 K. Again the oscillatory asymmetry in the SHG signal is enhanced by $X_{nr}^{(2)}$. Within the limits of the resolution of this experiment, it can be said that the value of $X_{nr}^{(2)}$ for naphthalene at

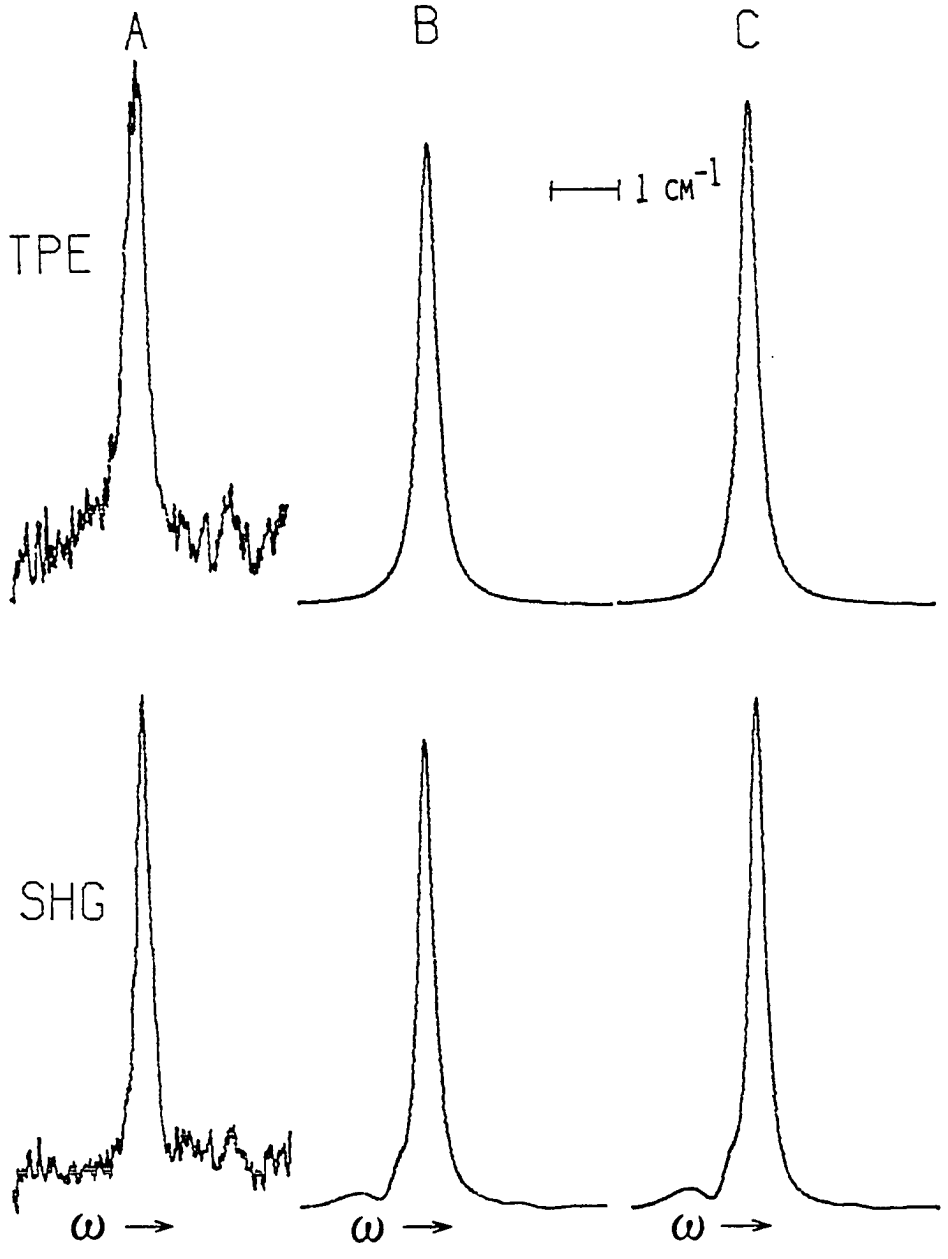


Figure 28. TPE (top) and SHG (bottom) profiles from a 27 μm PSF naphthalene crystal at T = 12 K and an external incident angle of 15° with respect to $\underline{c}'$: A) experimental, B) calculated from eqs. [75] and [76] ($X_{nr}^{(2)} = 0$, $\Omega_{eff} = 39$ cm$^{-1}$, all other parameters as in Figure 17), and C) calculated ($X_{nr}^{(2)} = 10^{-9}$ e.s.u.)

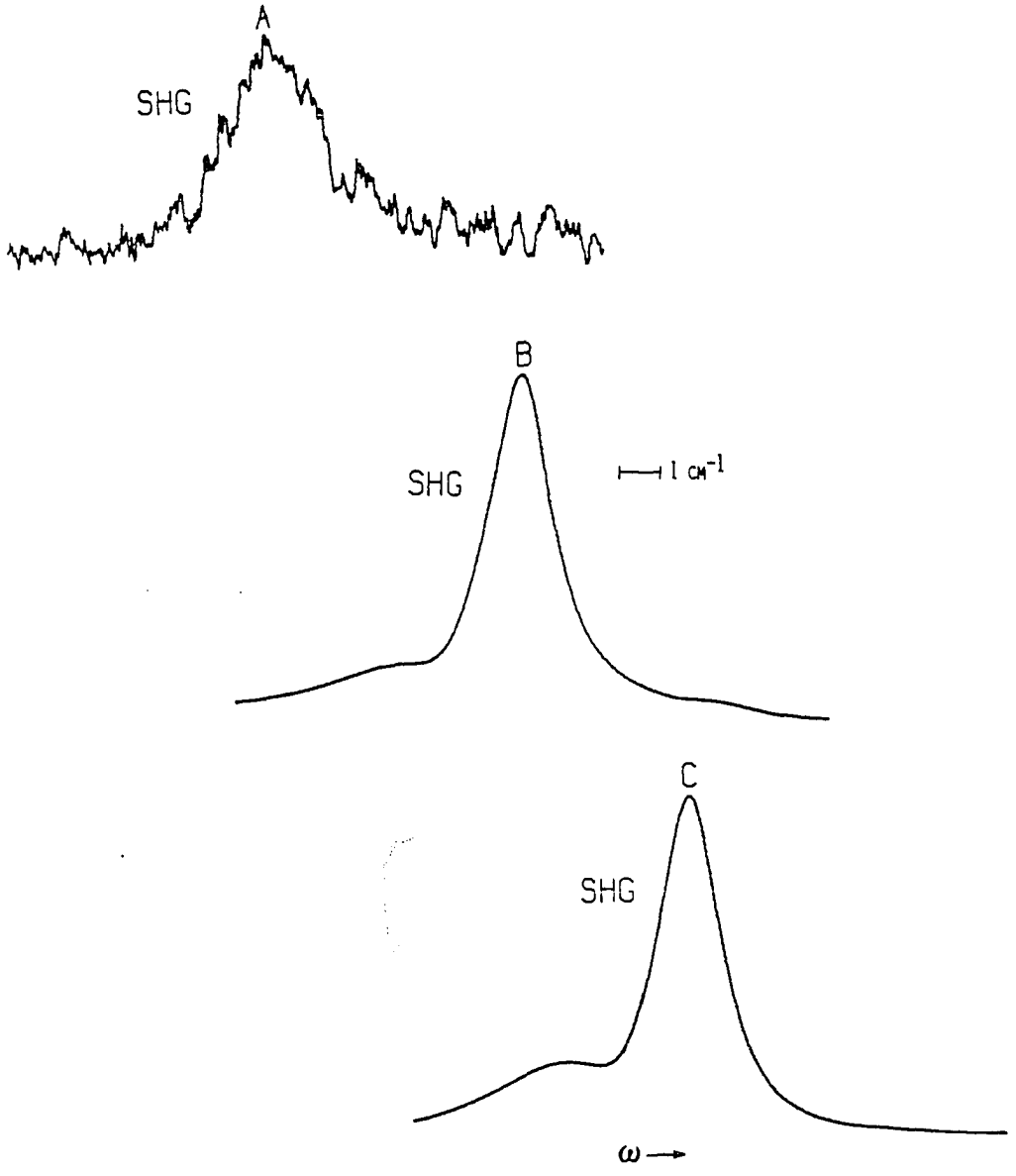


Figure 29. SHG (this page) and TPE (next page) profiles from a 55 μm PSF naphthalene crystal at T = 19 K and an external incident angle of 5° with respect to c': A) experimental, B) calculated from eqs. [75] and [76] ($X_{nr}^{(2)} = 0$, $\Omega_{eff} = 39\ cm^{-1}$, all other parameters as in Figure 17), and C) calculated ($X_{nr}^{(2)} = 10^{-9}$ e.s.u.)

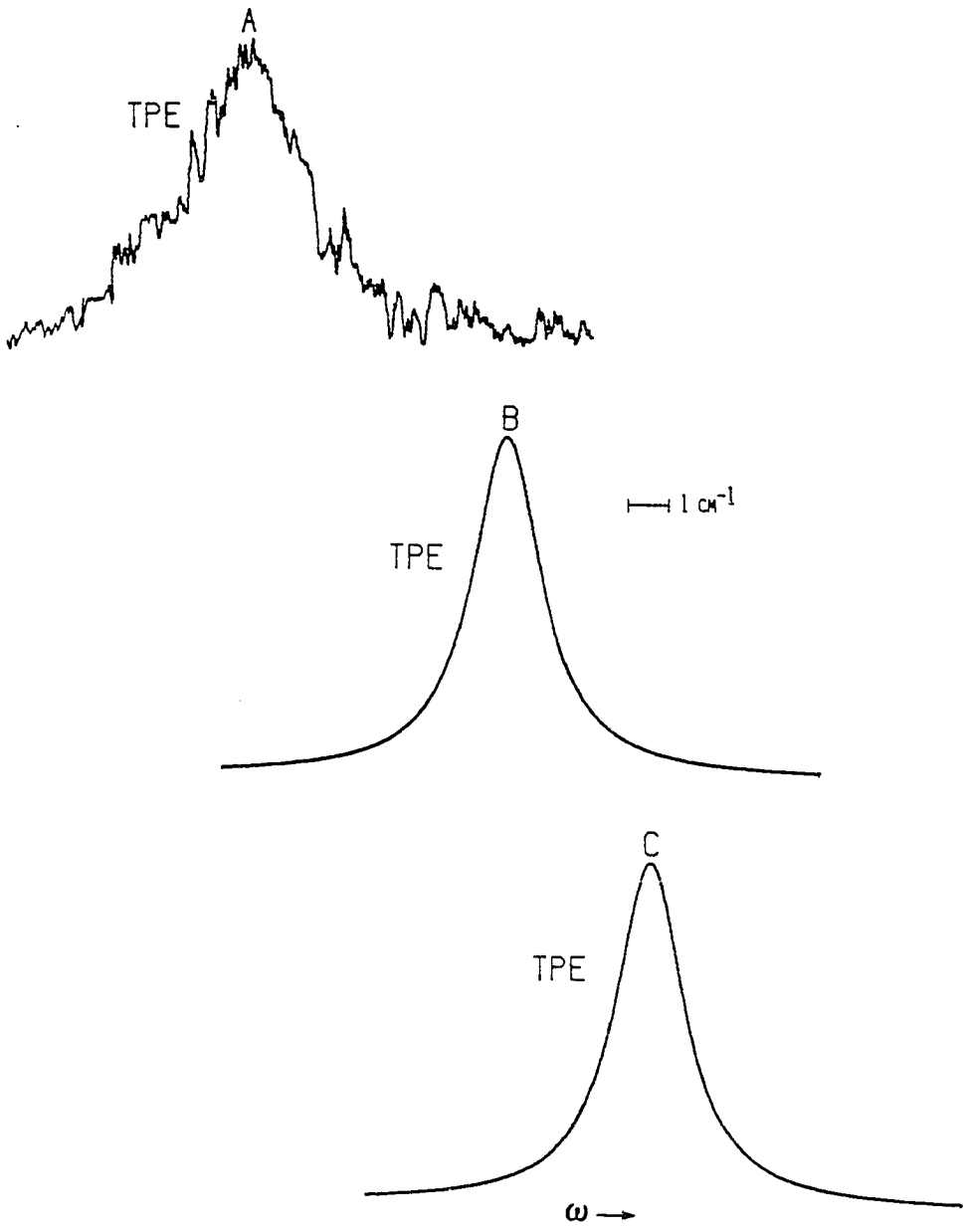


Figure 29. (continued)

31475 $cm^{-1}$ is substantially less than 1 x $10^{-9}$ e.s.u.. This conclusion is borne out by the intensity dispersion data, vide infra.

Phase matching oscillations in the SHG profile occur most dramatically at near-normal incidence. Figure 30 shows the theoretical SHG profile for a 15.5 μm crystal at $\theta_{EXT}$ = 0.2°. The profile consists of two broad, asymmetric lobes resulting from phase matching onto each branch of the polariton dispersion curve and separated by several sharp oscillations. (For large L, the peaks of the two broad signals occur at Re($\Delta k$) = 0 and map out the polariton dispersion curve exactly. For thin crystals, the position of the maximum of each peak is closer to the exciton resonance.) The asymmetry and width of the broad signals results from the fact that a small $\Delta k$, which determines signal intensity, is equivalent to a large $\Delta\omega$ in the direction away from the exciton resonance on a polariton dispersion curve and to a small $\Delta\omega$ in the direction toward the exciton resonance. What is a symmetric $sinc^2x$ function where k is the independent variable accordingly becomes an asymmetric function when $\omega$ is scanned as the independent variable.

The inflection at $\omega_o$ in Figure 30 is a result of the resonant parts of the first and second order susceptibilities becoming pure imaginary. This feature was observed in several profiles obtained experimentally for incident angles near 0°. Figure 31 is an experimental $\theta_{EXT}$ = 0° profile from a 27 μm crystal. Both the fringes and the resonant inflection behavior are clearly visible, providing a novel demonstration of phase matching behavior near a resonance. This kind of observation has not been reported by other workers.

The values chosen for several of the parameters in equation [75] have

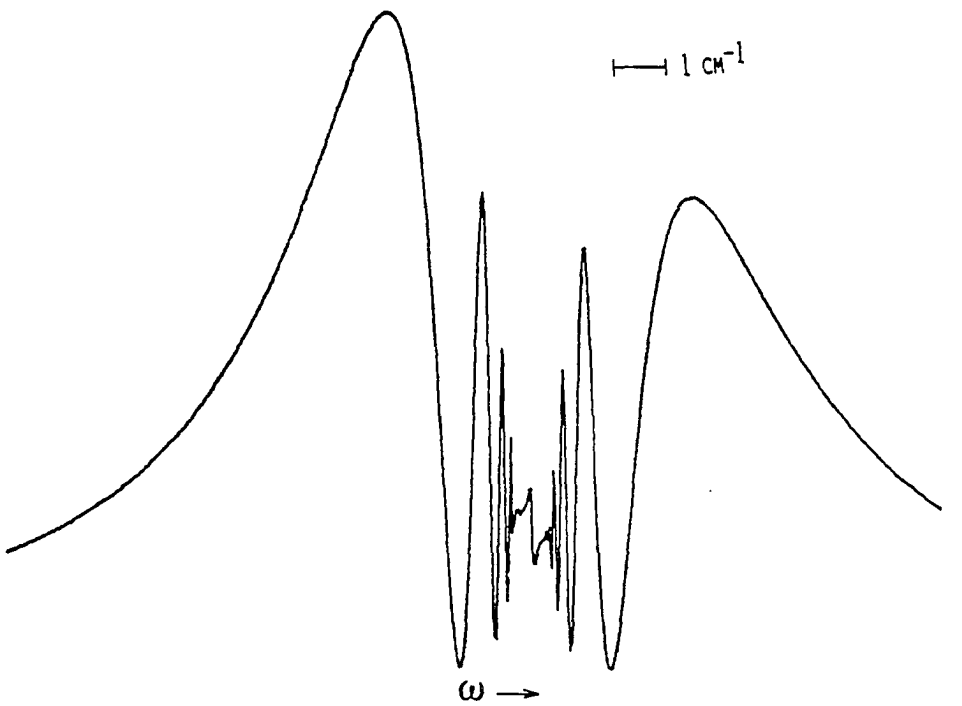


Figure 30. SHG profile calculated from equation [75] for a 15.5 μm naphthalene crystal at T = 7 K and near-normal beam incidence ($X^{(1)}(2\omega)$ = .1533, $\Omega_{eff}$ = 39 $cm^{-1}$, all other parameter values as in Figure 17). The inflection point at the center of the pattern occurs at frequency $\omega_o$

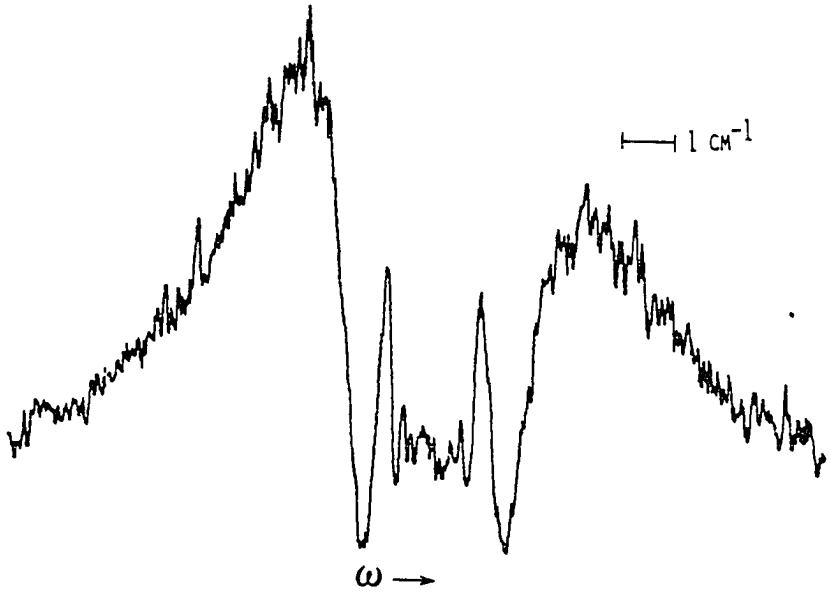


Figure 31. Experimental SHG profile for a 27 μm naphthalene crystal at T = 7K and normal beam incidence (compare to Figure 30)

an effect on the predicted relative intensities and spacing of the fringes. Fixing the parameter values listed earlier (see Figure 17), the only variable affecting the calculated fringe spacing is the crystal thickness. It was always found necessary in this work to use an effective value for L in the theoretical calculations that was about 35% less than the experimental sample thickness in order to reproduce the observed fringe spacing. (Very slight adjustments to the value of F, for example, or to the crystal density, can produce the same effect.)

The predicted T = 7 K profiles for a 12.5 μm crystal (a value of 7 μm was used in the calculation) at normal incidence are shown in Figure 32; data for comparison appear in Figure 33. The intensity ratio of the two most intense narrow fringes in the experimental SHG profile is different from what is usually observed; generally the fringe intensities are ordered like those of the parent peaks. It is likely that the behavior of the SHG data in Figure 33 is a consequence of limited digital resolution in data collection and very sharp peaks. In other respects, the calculated SHG profile fits the data fairly well. On the other hand, the calculated TPE profile is distinctly peculiar looking; the flattened peak top does not appear in the data profile. At this crystal orientation, however, it was very unusual in this study to observe any TPE signal at all. The profile in Figure 33 was the only one collected at normal incidence with any reasonable signal-to-noise value. It is consequently difficult to make any assertions about the TPE peak shape at normal incidence beyond noting that the intensity maximum occurs, as predicted, between the two SHG maxima and close to the exciton resonance.

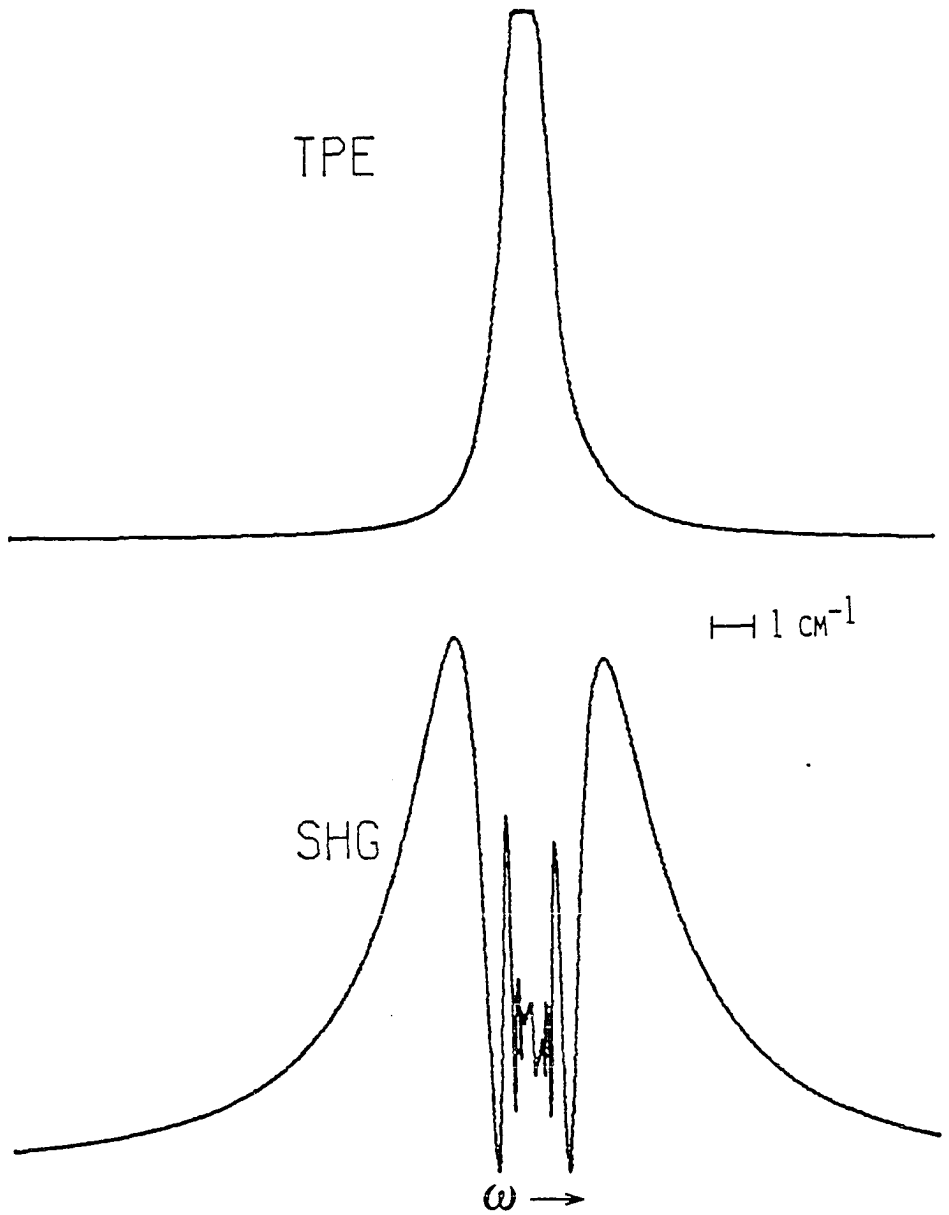


Figure 32. Profiles calculated from eqs. [75] and [76] for a 7 μm naphthalene crystal at T = 7 K and normal beam incidence ($X^{(1)}(2\omega) = .1535$, $\Omega_{eff} = 39$ cm$^{-1}$, all other parameter values as in Figure 17). The inflection point at the center of the SHG pattern occurs at $\omega_o$

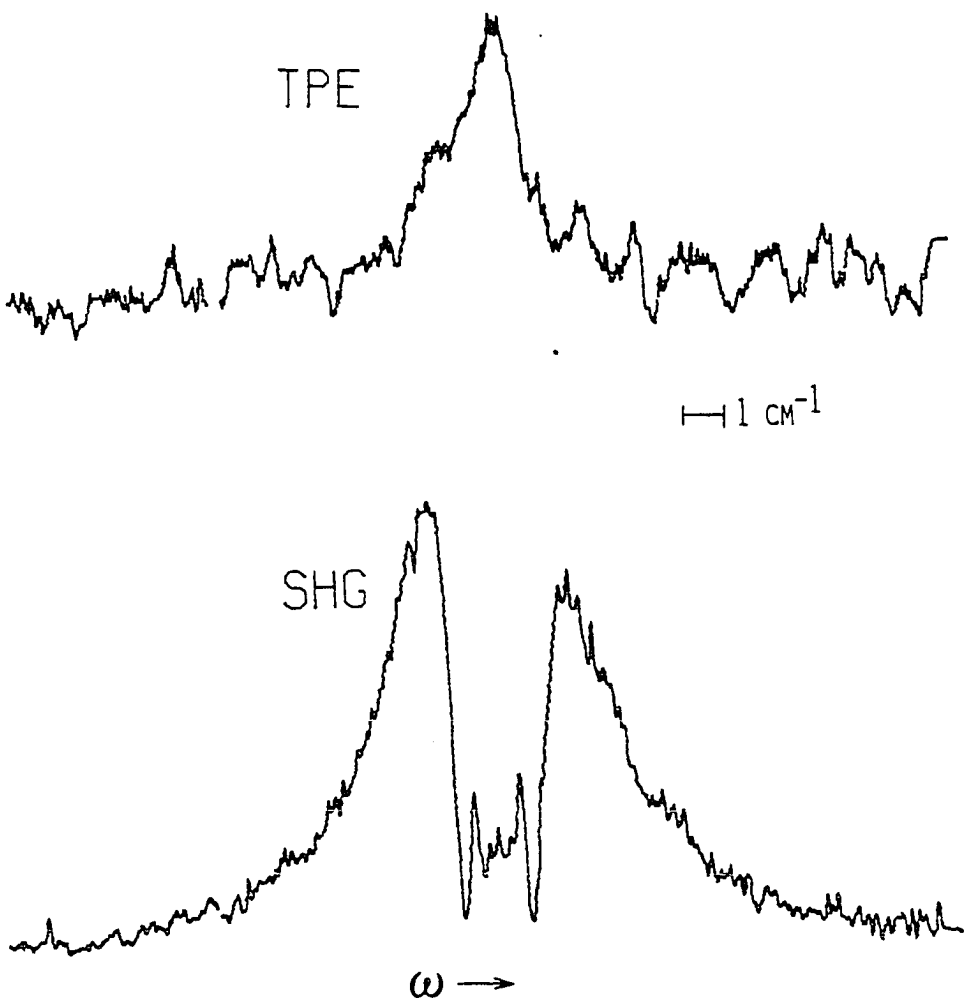


Figure 33. Experimental profiles for a 12.5 μm naphthalene crystal at T = 7 K and normal beam incidence (compare to Figure 32)

Calculated and measured profiles for the same 12.5 μm crystal at $\Theta_{EXT} = -2°$ are given in Figures 34 and 35, respectively, at a temperature of 5 K, and in Figures 36 and 37 at a temperature of 13.8 K. All theoretical profiles appear to match the data quite well; note especially the accuracy of the theoretical TPE profile at 5 K, which has an unusual appearance but reproduces the data faithfully. The higher temperature profiles illustrate the effect of damping on fringing, which is a coherent phenomenon; as expected, they are "washed out" when damping is high.

In general, the predictions of the semiclassical model, using polariton damping and setting $X_{nr}^{(2)}$ equal to zero, appear to fit both TPE and SHG profile shape data very well. The polariton fusion model predicts essentially the same SHG profiles and may also be considered successful in this respect.

## Directional Dispersion Behavior

### Dispersion of intensities; axial dispersion

The possibility of axial dispersion in the naphthalene optical indicatrix was a major concern in this study, as the dispersion curve fitting procedure described earlier presumes knowledge of $\partial$, the angle between the crystal $\underline{c}'$ axis and the optical $\underline{c}^*$ axis. Results of the fit are then employed as known values for the physical parameters used in the theoretical calculations of $v_g$, $\Delta k$, integrated signal intensities, and peak profiles. The effects of minor variations in the values of some of the quantities used on these results have already been discussed; the critical nature of the initial fitting step is evident. It is consequently desirable to devise a

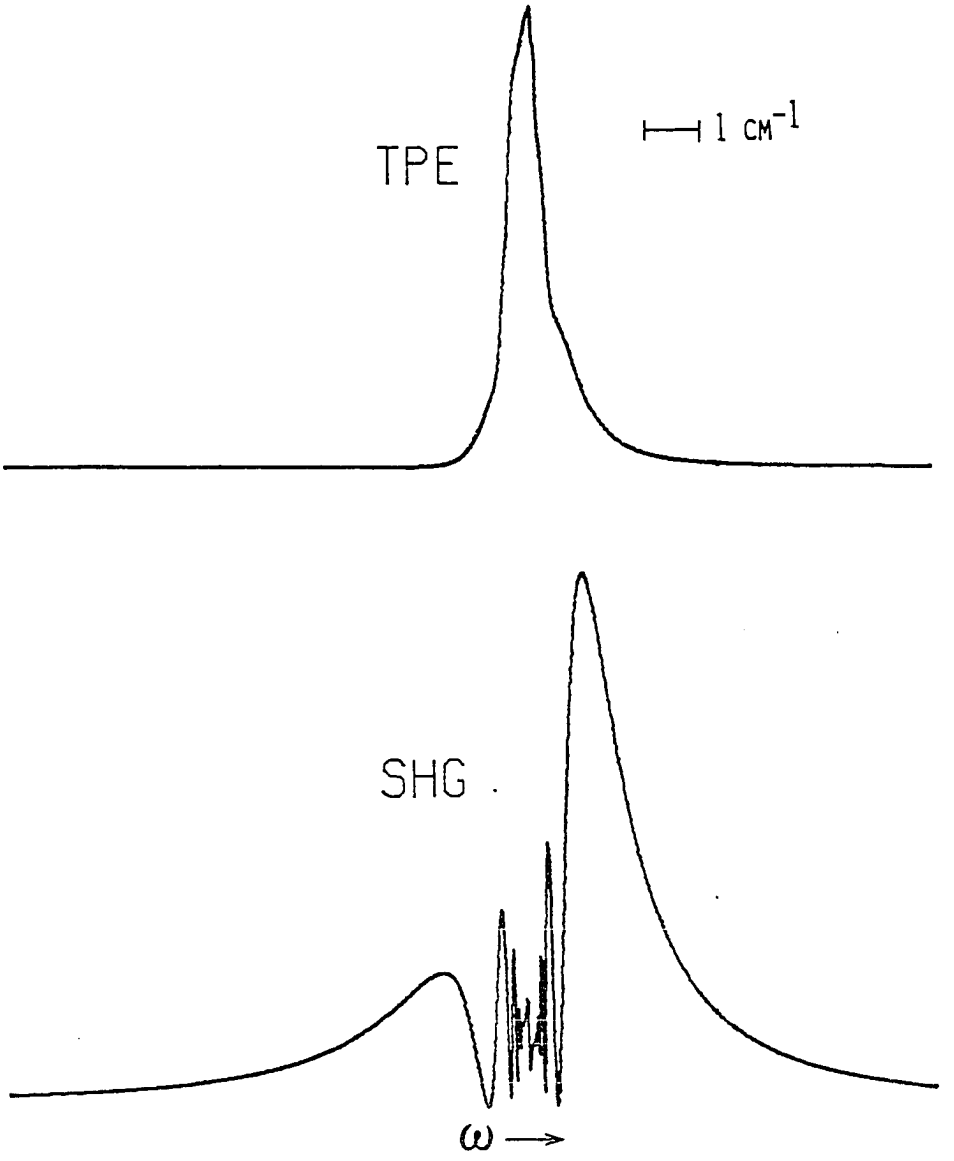


Figure 34. Profiles calculated from Eqs. [75] and [76] for a 7 μm naphthalene crystal at T = 5 K and an incident beam angle with respect to $\xi'$ of -2° ($\chi^{(1)}(2\omega) = .1557$, $\Omega_{eff} = 39\ cm^{-1}$, all other parameter values as in Figure 17). The inflection point at the center of the SHG pattern occurs at frequency $\omega_o$

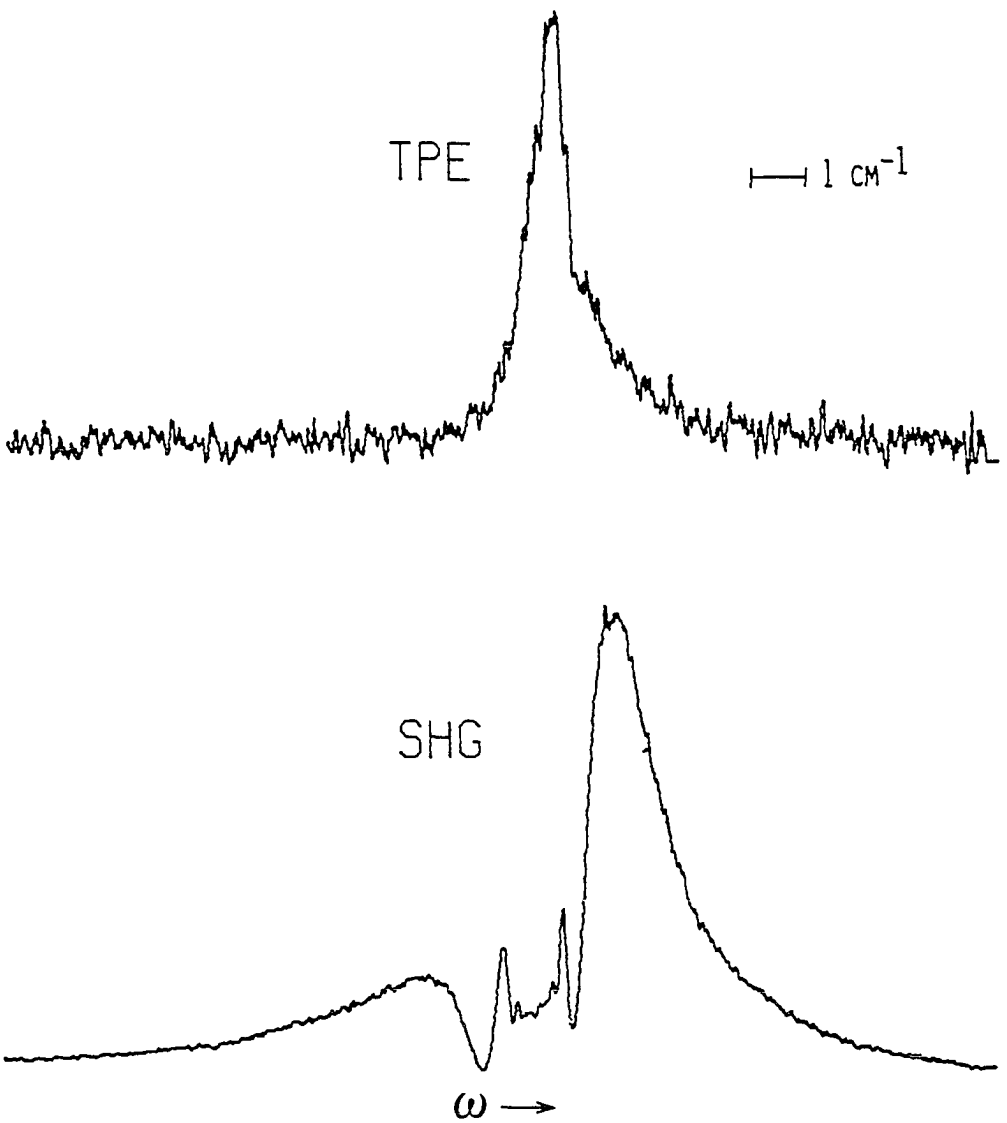


Figure 35. Experimental profiles for a 12.5 μm naphthalene crystal at T = 5 K and -2° external beam incidence (compare to Figure 34)

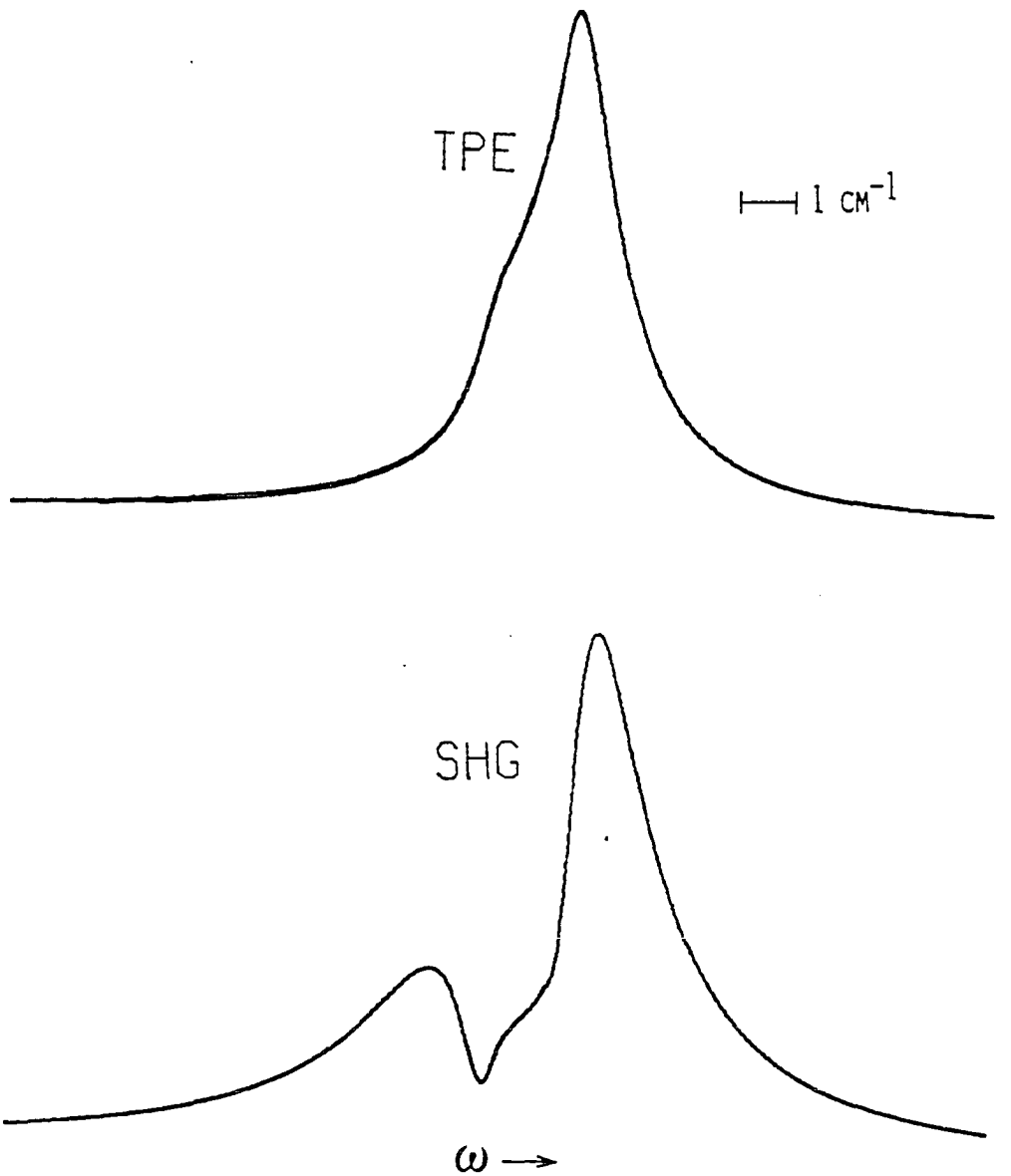


Figure 36. Profiles calculated from eqs. [75] and [76] for a 7 μm naphthalene crystal at T = 13.3 K and an incident beam angle with respect to $\underline{c}'$ of -2° ($X^{(1)}(2\omega)$ = .1557, $\Omega_{eff}$ = 39 cm$^{-1}$, all other parameter values as in Figure 17). The inflection point at the center of the pattern occurs at frequency $\omega_o$

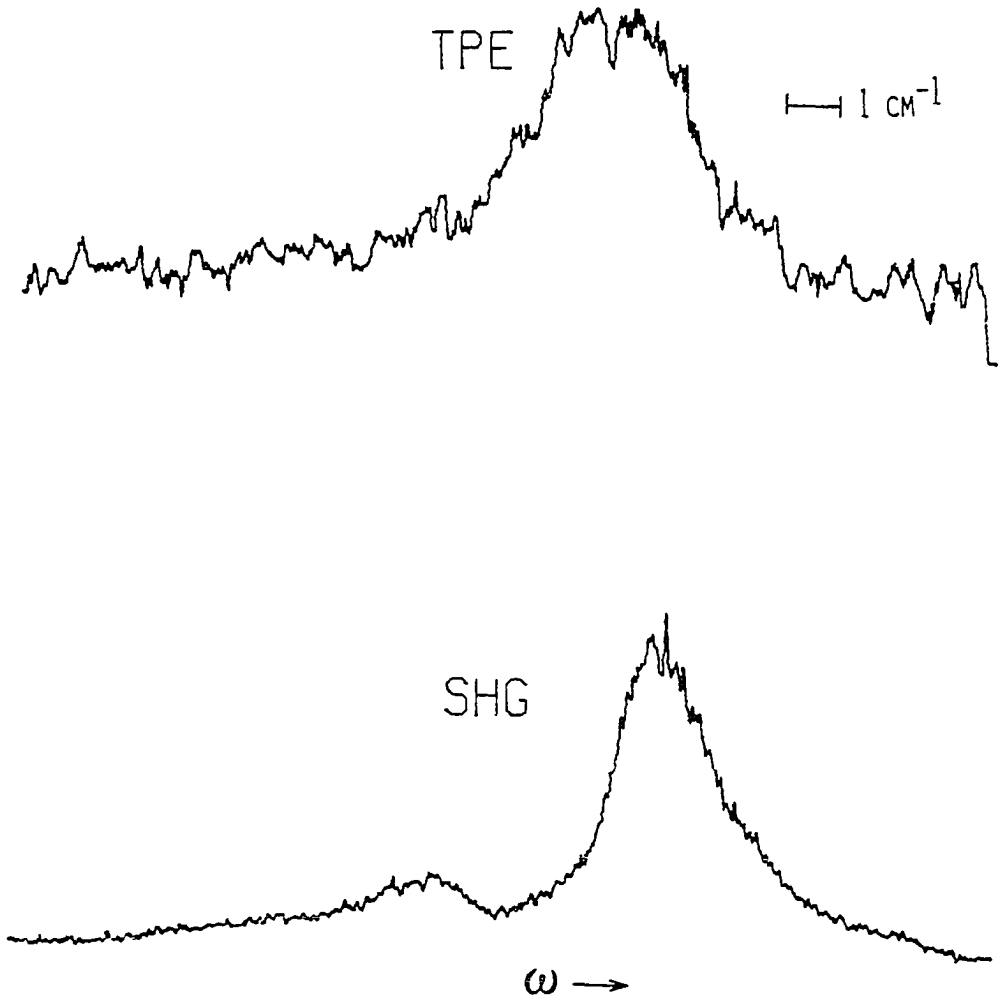


Figure 37. Experimental profiles for a 12.5 μm naphthalene crystal at T = 13.3 K and -2° external beam incidence (compare to Figure 36)

method for deducing the axial orientation at frequencies near the exciton resonance.

The possible orientations for $\underline{k}$ in this experiment may be obtained from consideration of Snell's Law and the values of $n_o$ determined from the angles $\underline{k}$ may make with $\underline{c}^*$ (more exactly, the angles $\underline{D}$ may make with $\underline{a}^*$). If $\partial = 23°25'$, the value at 5461 Å, it turns out that $\underline{D}$ should cross the optical $\underline{a}^*$ axis at an external angle of 42°51'. Experimentally, this means that data for angles greater than 42°51' should mirror that for angles less than 42°51'. In this manner, directional dispersion data for a large range of $\theta_{EXT}$ should provide a check on the assumed value for $\partial$. Unfortunately, this approach is impractical; the phase matching frequency varies so slowly with incident angle at large values of $\theta_{EXT}$ that any symmetry in the data near 42°51' would be lost in the scatter. Theoretically, tuning the sample to still larger angles would eventually result in phase matching onto a steeper part of the polariton dispersion curve; practically, however, the sample forms a limiting aperture for the beam, and in general it is angles of orientation not much greater than 40° that are the maximum possible.

Owing to the nature of the problem, experimentally obtained directional dispersion data must still be used to derive information about axial dispersion of the indicatrix. It is not practical to depend on the frequency dispersion for this information for the reasons discussed above; however, dispersion of the signal intensities with angle tuning is another possibility. Significant phase matched polariton fusion is possible for a broad range of frequencies at near-normal incidences. The integrated SHG signal

intensity is therefore expected to grow as the crystal is tuned toward low $|\Theta|$ and dip again at $\Theta_{EXT} = 0°$, the "crossover point" where phase-matching is not possible. Because the phase-matched polaritons increase in photon character as $\Theta_{EXT}$ approaches 0°, the polaritons created at these orientations scatter less strongly than those created at higher values of $|\Theta_{EXT}|$; the TPE signal intensity is accordingly predicted to go through a minimum at normal incidence. Theoretical values of integrated signal intensities are plotted as a function of incident angle in Figure 38. Also shown in Figure 38 is the effect of nonzero $\chi_{nr}^{(2)}$ on directional intensity dispersion. While the behavior of the TPE signal intensity is not much affected, the SHG distribution becomes asymmetric, the positive angle (lower branch) profiles far more intense than the corresponding signals at negative angles (upper branch) for positive $\chi_{nr}^{(2)}$.

In an experiment to measure the directional dispersion of the TPE signal intensity, the variation in intensity detected by the photomultiplier tube as a result of crystal and sample holder geometry must also be taken into account. At near normal orientations, the crystal is situated edgewise to the detector, weakening the signal, and at high angles of orientation the sample holder may block the sample emission somewhat. Hochstrasser and Sung have reported a two-photon vibronic absorption in naphthalene lying at 31684 $cm^{-1}$ (31b). Anisotropy studies in that work demonstrated that the signal exhibits no directional dispersion independent of polarization changes. Thus, excitation of this mode with $\underline{b}$-polarized red light at various angles of incidence provides a direct calibration of experimental geometry effects. In this experiment, the signal from the

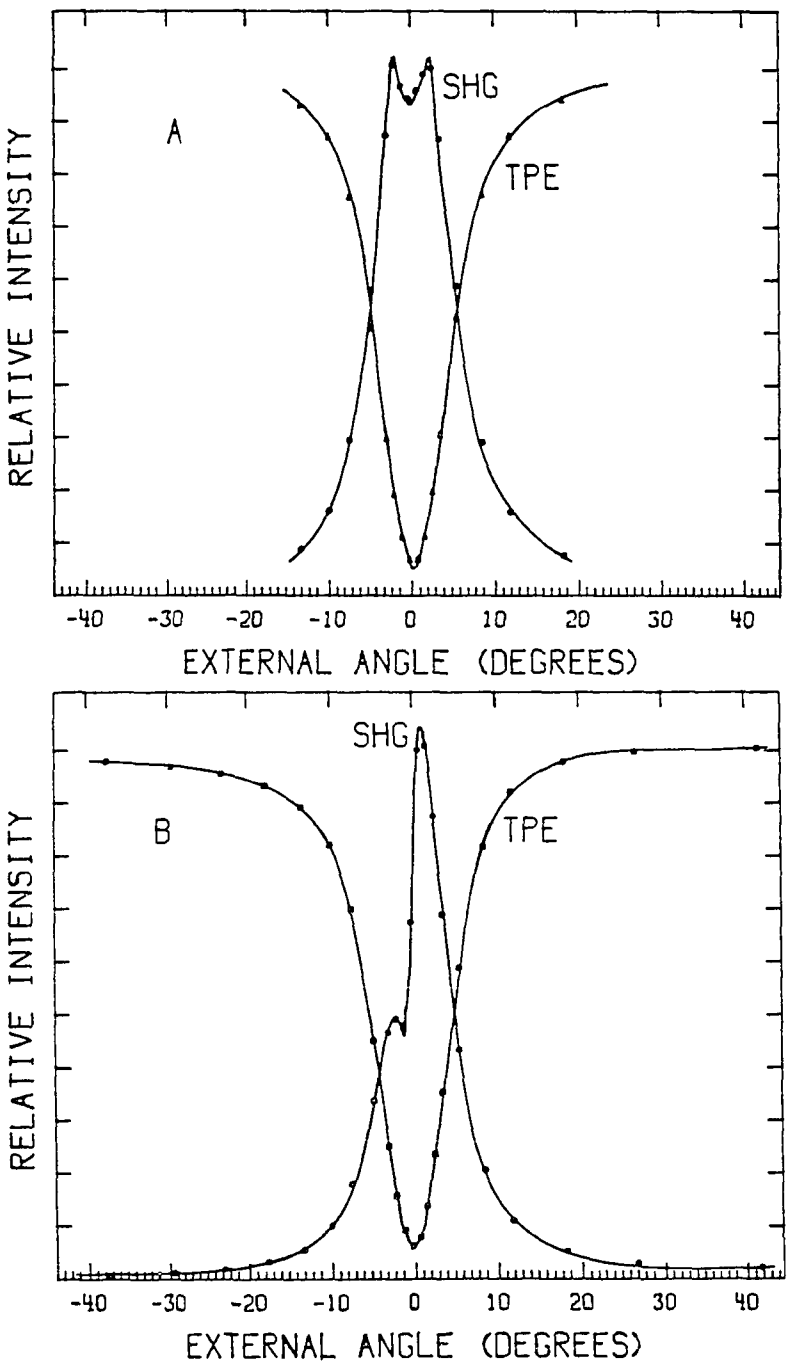


Figure 38. Integrated intensities, calculated from eqs. [75] and [76], of TPE and SHG profiles as a function of incident beam angle with respect to the $\underline{c}'$ axis of a 30μm naphthalene crystal at 7 K, for: A) $X_{nr}^{(2)} = 0$ and B) $X_{nr}^{(2)} = 1 \times 10^{-9}$ e.s.u.

31684 $cm^{-1}$ absorption was weak but observable for pure crystals; in doped crystals the inhomogeneous broadening apparently washed the signal out so that it was no longer detectable (in addition, the lasing was extremely weak at this frequency; however, it was not possible to optimize the incident intensity without throwing the validity of the geometry calibration into doubt). Results from intensity dispersion measurements made on two crystals are shown in Figure 39. The TPE signal is normalized to the measured 31684 $cm^{-1}$ signal. In both cases the TPE intensity distribution is asymmetric, but the nature of the asymmetry reverses from one crystal to the other. The intensity dispersion in the SHG signal fits in appearance the theoretical prediction for $X_{nr}^{(2)} = 0$ in Figure 38. The asymmetric tailing on the positive-$\Theta$ side is a result of different values for $dn_0/d\Theta$; that is, a result of the fact that the ac-polariton is an extraordinary polariton. (It should be noted that the curves in Figure 38 were computed using the results of a preliminary dispersion curve fit; use of the final values for $n_{a*}$ and $n_{c*}$ would produce a more pronounced tail in the predicted curves, matching the observed behavior very well.)

In the neighborhood of $\Theta_{EXT} = 42°51'$, where mirror symmetry should be observed if the assumed value for $\partial$ is correct, the SHG signal is very weak. The TPE signal intensity measurements display considerable scatter owing to signal attenuation by the sample holder; that is, because the normalized emission intensity is a result of dividing one weak signal (the TPE) by another (the geometry calibration). Looking for patterns in either signal at high values of $|\Theta_{EXT}|$ is not a practical way to seek information about axial dispersion. However, the asymmetry in the SHG intensity dis-

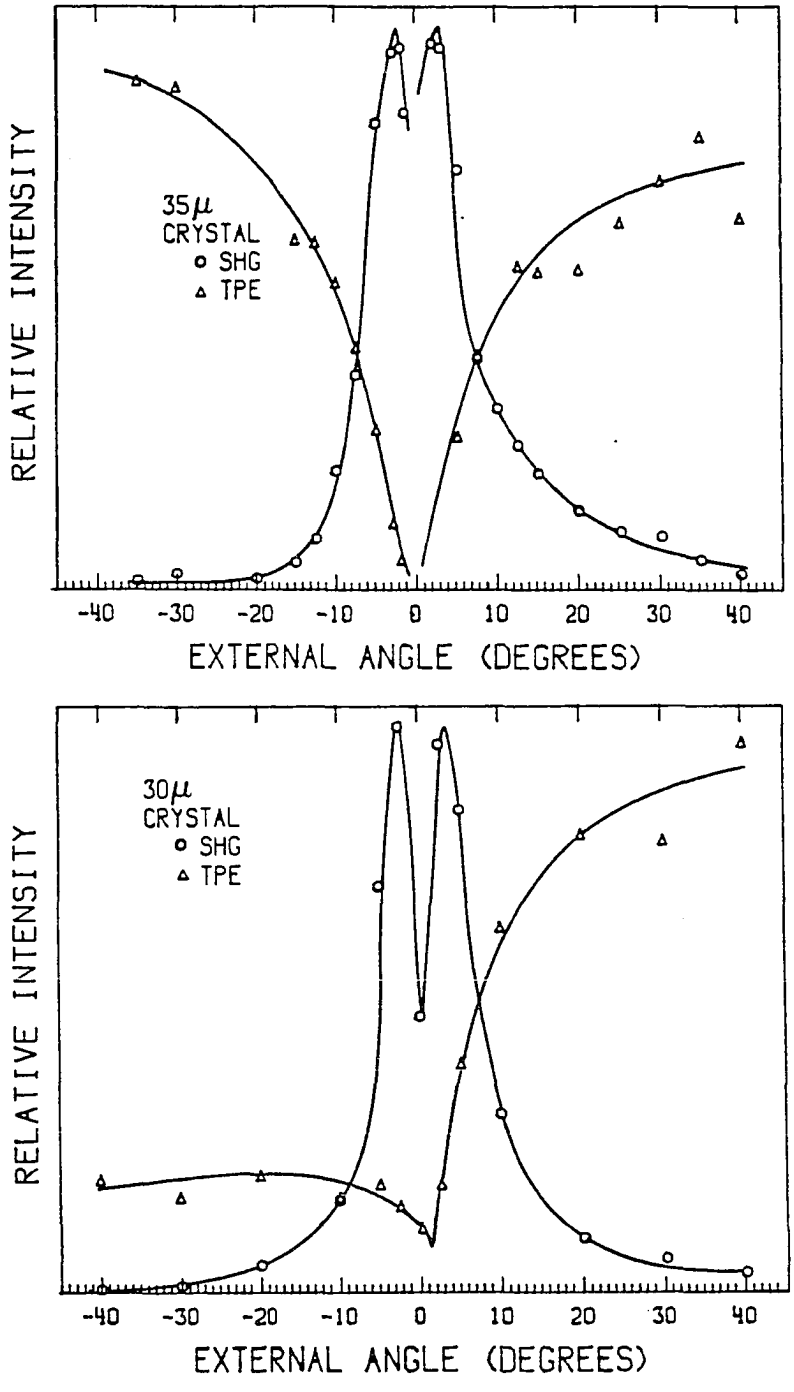


Figure 39. Integrated experimental TPE and SHG profile intensities as a function of incident beam angle for two PSF naphthalene crystals. TPE intensities are corrected for experimental geometry (see text)

persion curve may be used to extract the desired information about the orientation of the indicatrix.

Points of equal intensity on the SHG curve represent polaritons of equal group velocity (see equations [96]); using the expression for group velocity given in equation [83] and approximating $\omega = \omega_{pm}$, it can be shown that to a good approximation this is equivalent to the statement that points of equal intensity are points of equal $|n_o^2 - n_b^2|$. Using this relationship and paired values of $\Theta_{EXT}$ for points of equal intensity read from the SHG data in Figure 39, the value of $\partial$ may be derived from each pair and an average value obtained. When this was done for a total of ten points from the two sets of data, a value of $\partial = 23.64 \pm 0.48°$ was obtained with no significant differences in the results from the two plots. The assumed value of 23.42° is well within the limits of uncertainty on the measurement. It can therefore be reported that the axial dispersion of the optical indicatrix for naphthalene at 3176 Å with respect to the orientation at 5461 Å is negligible.

Frequency dispersion

For nonzero damping, when $\Delta k$ is small the terms not containing $\Delta k$ in the damped fusion rate expression [91] become important. For thin crystals, the signal profile over an appreciable frequency range near the phase matching frequency $\omega_{pm}$ is determined by these terms; consequently, the peak maximum may not appear at exactly $\omega_{pm}$. Calculated dispersion of the peak maximum, using equations [75] and [76] to compute profiles, shows that for thin crystals the resulting dispersion curve slopes much less steeply than that predicted from simple phase matching consid-

erations. Figure 40 shows the calculated directional dispersion of $\omega_{max}$ for a thin crystal and a thick crystal. The inflection behavior predicted for the peak maximum of the TPE signal is a result of the destructive interference (discussed earlier) between the two phase-matched terms in equation [76]. The theoretical dispersion may be compared to data presented in Figures 8 and 41-43 for PSF naphthalene crystals 30, 12.5, 27, and 55 μm in thickness, respectively. The two thinner crystals display the predicted inflection behavior. All the data match the theoretical predictions well, with the exception of the thinnest crystal, which displays dispersion behavior appropriate to a still thinner crystal. The thickness used in the computation would only have to be adjusted to about 10 μm to improve the match.

An interesting feature observed in the TPE signal from the 55 μm sample and shown in Figure 43 is the appearance of a second peak in the signal, near the transverse exciton resonance. This peak did not display orientational frequency dispersion, and at crystal orientations at which the dispersive signal had shifted enough to resolve the two, no angular intensity dispersion was observed. The signal was weak compared to the TPE signal at high $|\theta_{EXT}|$, but strong compared to the TPE signal near normal incidence. It is tempting to ascribe the appearance of this signal in the thickest sample studied to the fact that SHG comes mainly from the back of the crystal, while the TPE signal is generated throughout the crystal, so that "true" TPE behavior might only be expected in thick crystals. A nondispersive TPE signal is predicted from the semiclassical theory for crystals <u>thin</u> enough so that the contributions of the front surface are

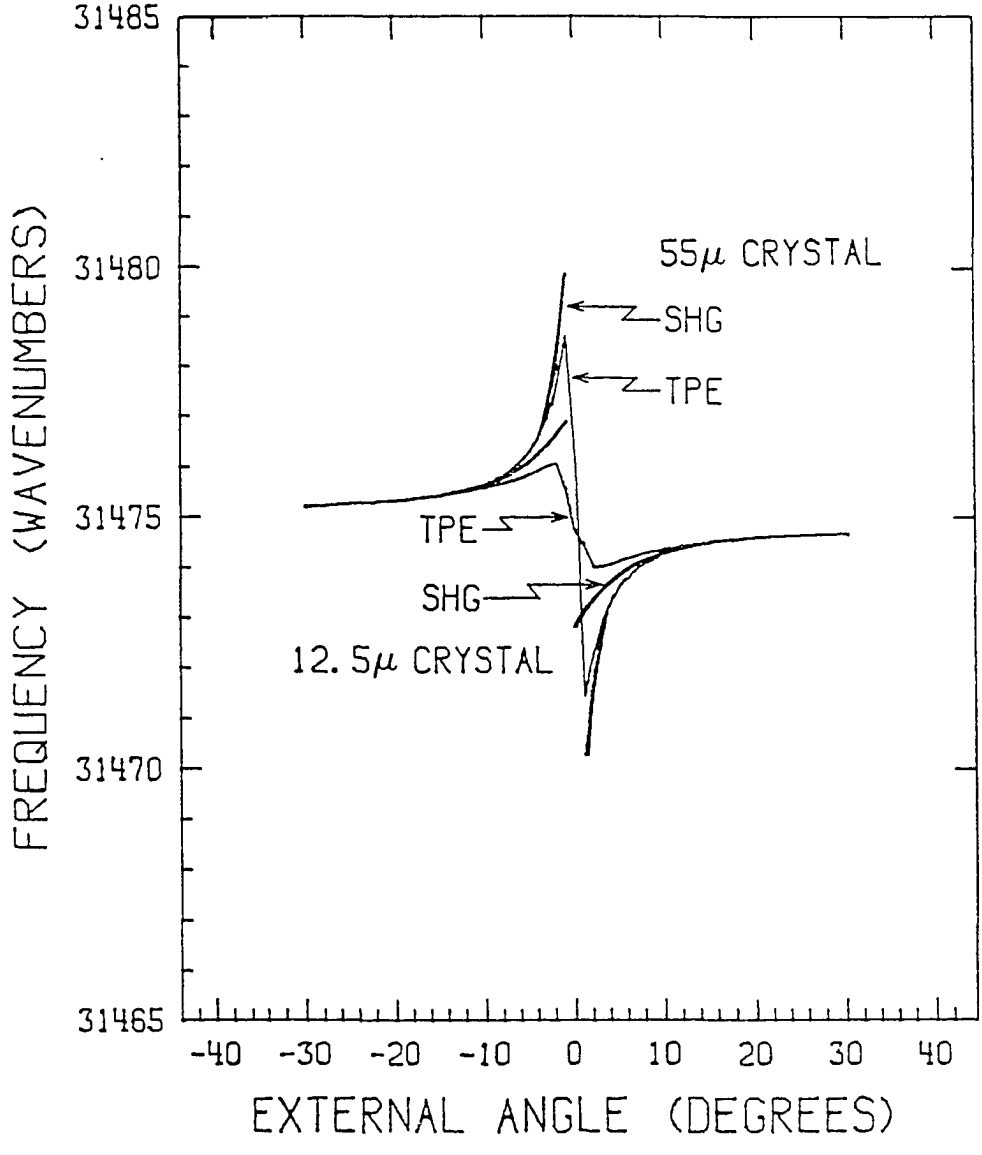


Figure 40. Directional dispersion for naphthalene crystals of two different thicknesses at T = 5 K, calculated from the semiclassical rate expressions [75] and [76]

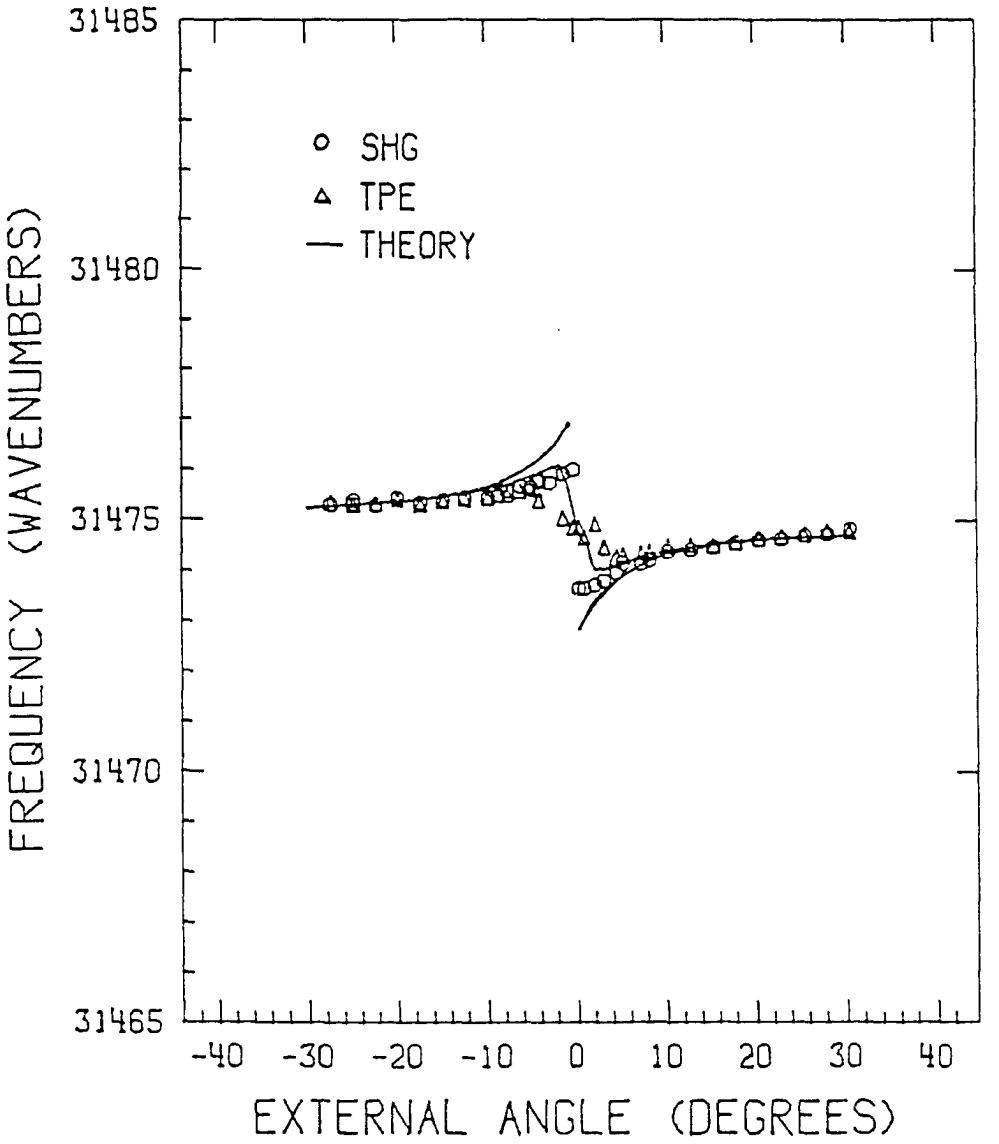


Figure 41. Experimentally determined directional dispersion of the extraordinary polariton in a 12.5 μm PSF naphthalene crystal. The theoretical curves are computed from equations [75] and [76]

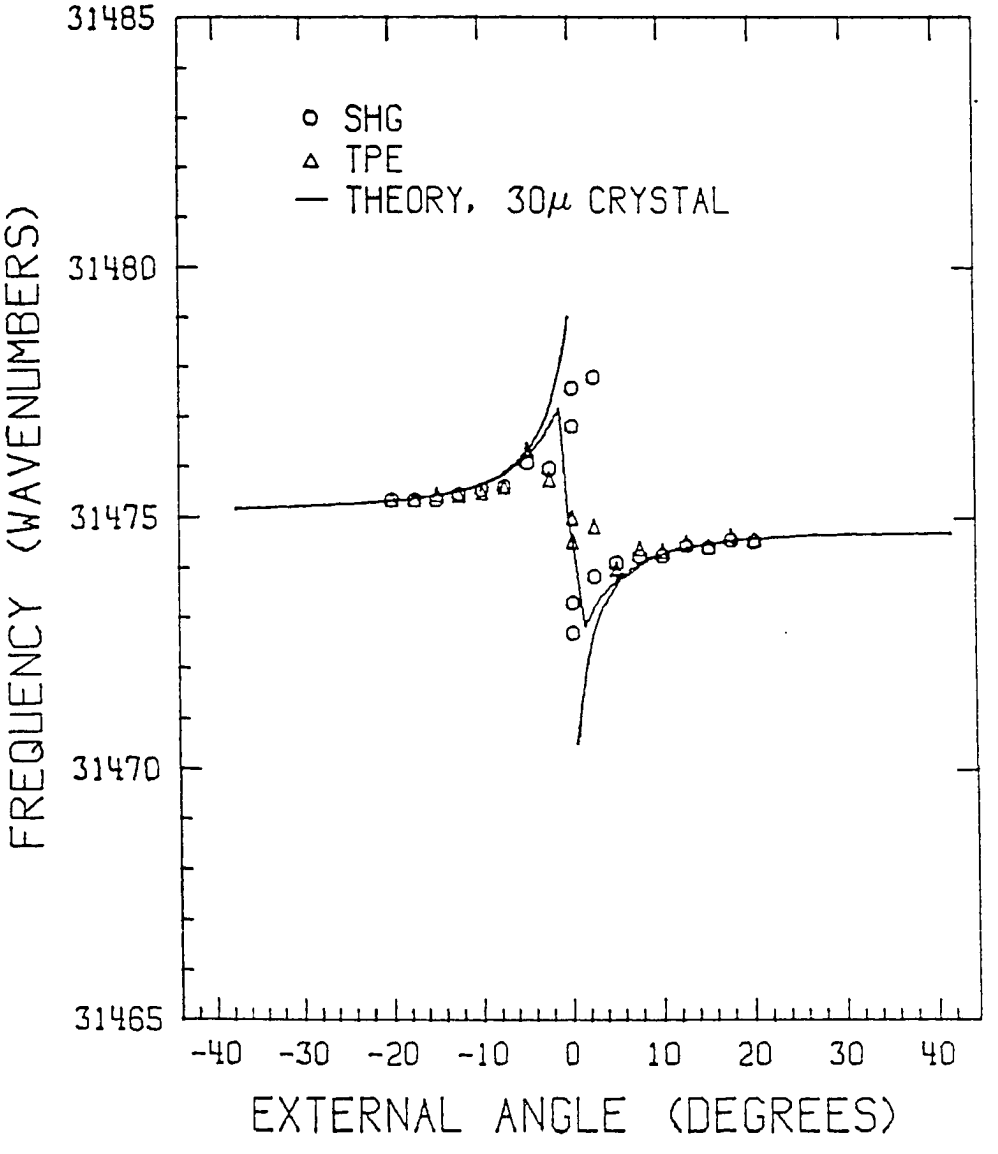


Figure 42. Experimentally determined directional dispersion of the extraordinary polariton in a 27 μm PSF naphthalene crystal. The theoretical curves are computed from equations [75] and [76]

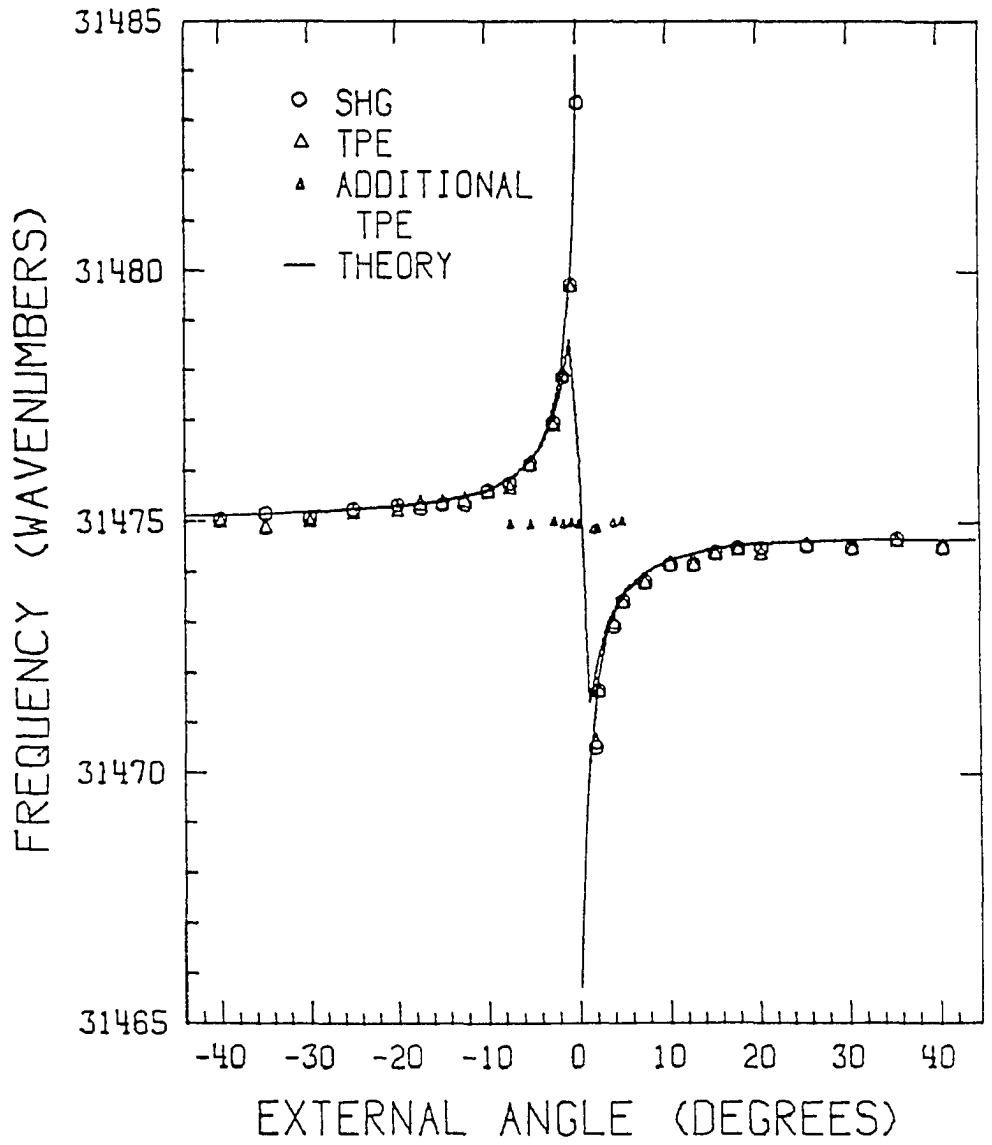


Figure 43. Experimentally determined directional dispersion of the extraordinary polariton in a 55 μm PSF naphthalene crystal. The theoretical curves are computed from equations [75] and [76]

significant. The angular frequency behavior of the bulk signal calculated from the semiclassical rate equation [76] includes contributions from the non-phase matched $\chi^{(3)}$ term as well as from the phase matched $\chi^{(2)}$ terms; however, deviation from the phase matched SHG dispersion behavior is predicted only for thinner crystals for this part of the signal also (see Figures 40-43). The angular behavior of the second TPE signal, coupled with the fact that no corresponding signal was observed in SHG, lead to the speculation that the additional signal is produced from excitation of a longitudinal exciton (208). Johnson (37) has recently reported the observation of a longitudinal exciton in phenanthrene with TPE.

The appropriateness of the fitting procedure described at the beginning of this chapter may now be evaluated. It is apparent that the use of dispersion data obtained from a very thin crystal in fitting to undamped polariton dispersion curves would be a mistake (see Figures 40-43). However, naphthalene crystals 30 μm or more in thickness should give accurate results, particularly in light of the fact that it is the high-$|\theta_{EXT}|$ data which have the most impact on the results of the fit. The assumption that axial dispersion is unimportant has already been discussed and justified. The other important assumption made at the outset was that the range of orientations of $\underline{D}$ inside the crystal does not affect the value of the effective oscillator strength significantly. Breakdown of this assumption would manifest itself as a progressively worse fit along the $\theta$ coordinate in the dispersion figures. Since this does not appear to be the case, the range of angles studied is probably not a range over which the value of $\cos^2\alpha$ changes rapidly. This implies that the transition dipole lies

somewhat close to the crystal c' axis. (The long axis of the naphthalene molecule makes an angle of 26.6° with the c' axis; however, the failure of the "oriented gas" approach for naphthalene has already been discussed). It is not possible to deduce the exact orientation of the transition dipole from the data collected in this study.

# V. SUMMARY AND CONCLUSIONS

The second-order nonlinear response of naphthalene at 31475 $cm^{-1}$ has been demonstrated in this study to suggest aspects of exciton-photon behavior in the strong coupling regime which are not observable by more conventional linear methods. Second harmonic generation (SHG) and two-photon excited emission (TPE) signals produced by light at a nonresonant fundamental frequency near 15737 $cm^{-1}$ have been observed simultaneously, and the frequency dispersion and temperature-dependent lineshape and intensity behavior have been shown to be consistent with models of strong exciton-photon coupling.

The two models for exciton-photon interaction developed in Chapter II are the semiclassical model and the (second-quantization) polariton model. In the semiclassical model, strong coupling between an electromagnetic field and material resonances is expressed by the use of Maxwell's equations in their complete form, including the material relations. The parameters of the material relations are then derived quantum mechanically, using a perturbation treatment, and the final expressions are written for molecular crystals in terms of the exciton frequencies, transition moments, and damping constants. The semiclassical model may therefore be said to assume both strong and weak (perturbative) coupling of the material to the applied field. In the fully quantized polariton model, the linear exciton-photon interaction Hamiltonian is included in the unperturbed crystal Hamiltonian (strong coupling is assumed) and basis states which are combinations of the photon and exciton basis states of the

uncoupled problem are found using second quantization techniques.

Both the semiclassical and fully quantized models successfully predict polariton (coupled oscillator) behavior in one-photon experiments. The integrated intensity of the transition in the strong coupling approach is dependent both on the transition moment (oscillator strength) and on the damping of the exciton. In other words, without damping of its excitonic component, the polariton is free to exit the crystal as a photon of the same frequency as that which entered the crystal and absorption has not occurred. A weak coupling interaction, for which the interaction between excitons and photons may be viewed as a perturbation of the crystal Hamiltonian, predicts intensity dependence mainly on the magnitude of the transition moment. Temperature studies of one-photon processes in naphthalene (117) have shown the strong coupling approach to be the correct one and it is appropriate to approach the nonlinear response of the same resonance from a similar viewpoint.

In the semiclassical model, SHG arises from the second-order susceptibility ($X^{(2)}$) of the medium. In the limit of zero damping, the intensity of the SHG is determined by how closely the phase velocities of the fundamental and second harmonic waves are matched, and the fundamental wave must donate this intensity. If the doubled wave is damped, the fundamental wave loses further energy through maintaining the intensity of the second harmonic wave. In addition, when $2\omega$ is near a material resonance the fundamental beam may excite the resonance through the third-order susceptibility ($X^{(3)}$). Two-photon absorption (emission) is a combination of a phase matched ($X^{(2)}$) and a non- phase matched ($X^{(3)}$) part.

The fully quantized strong coupling approach predicts phase matched SHG as a consequence of the first order perturbation of the polariton Hamiltonian, which results in terms representing the creation of a polariton at $2\omega$ from two polaritons at $\omega$, a process called polariton fusion. In analogy to the polariton picture of one-photon absorption, the phase matched two-photon emission signal is viewed as arising from the scattering of the fused polaritons. The non-phase matched part of the signal which arises from $X^{(3)}$ in the semiclassical approach will find its counterpart in terms resulting from a second order perturbation treatment of the polariton Hamiltonian, representing the creation and annihilation of two polaritons at frequency $\omega$. To date, the fully quantized polariton treatment has not been extended to second order perturbation, and may be considered incomplete in its description of two-photon absorption.

The orientational frequency dispersion of the SHG and TPE signals, predicted by both the semiclassical and quantum mechanical models, has been observed and the values of the background major and minor refractive indices have been extracted by fitting the experimental dispersion to the theoretical polariton dispersion curves. The value of the oscillator strength obtained from one-photon experiments was used and within the limits of the experiment appeared to behave as a constant, indicating that the transition dipole lies approximately parallel to the crystal $\underline{c}'$ axis in naphthalene. The orientation of the optical indicatrix was assumed to be the same as that reported for visible light; this assumption has been justified by comparing the orientations of the crystal at points of equal integrated intensity. The use of these parameter values has produced good fits

to the SHG frequency dispersion for crystals of several different thicknesses, approaching thickness-independence for crystals thicker than about 25 μm. The TPE dispersive behavior, predicted by the semiclassical model to deviate from that of the SHG signal for thin crystals, has also been successfully fit, using the derived two-photon excited emission intensity expression, [76].

The temperature-broadening of both the SHG and TPE signals at all angles of orientation used have been fit to an effective phonon frequency of 39 $cm^{-1}$, indicating that it is low-frequency optical phonons which dominate the line broadening for the nonlinearly generated polaritons. This contrasts with the results of one-photon work which indicate an active acoustic (12 $cm^{-1}$) phonon. The explanation lies in the character of the polaritons which are created in the two different types of experiments: those formed from an incident beam near the resonant frequency are predominantly exciton-like, with very little photon character, while those produced in the nonlinear experiments are subject to a phase matching condition and may have considerably more photon character. This difference means that the group velocities of the coherently generated polaritons are far greater than those of one-photon generated polaritons, and the altered polariton-phonon spatial correlation results in a modification in coupling strength which leads to the observed motional narrowing. Calculation of the Tyablikov coefficient of exciton creation has demonstrated that in spite of this difference the polaritons of the nonlinear experiment are still principally exciton-like in character. Thus, the speed of energy transfer may be controlled by nonlinear generation of the excitation under

selected phase matching conditions. Direct testing of this hypothesis requires ultrafast time-of-flight measurements which may prove impractical owing to the spectral breadth of picosecond laser pulses, since second-order nonlinear signal intensity varies as the square of the input field intensity, and to complications arising from the group velocities (wavepacket behavior) of the input laser pulses themselves. However, investigation of energy transfer rates in naphthalene crystals through controlled doping with trap molecules and nonlinear generation of excitations is currently underway in this laboratory (209). Vidmont and coworkers (151) have recently demonstrated qualitatively the frequency dispersion of polariton group velocities in anthracene by looking at the temporal delay of the transmission of light at frequencies near resonance at low temperatures.

The temperature dependences of the SHG and TPE signals have been successfully predicted from the polariton fusion model by inclusion of temporal damping in the fusion rate expression. The simple expressions which result describe the two signals as competing for intensity, with the branching ratio evolving from a low-temperature limit, determined by the value of the temperature-independent part of the damping constant, to the high-temperature limit where TPE dominates. The same behavior is predicted using the semiclassical theory only if the damping of the strongly coupled (polariton) state is substituted for that of the exciton in the expressions for the susceptibilities (derived from weak coupling theory). In addition, the value of the nonresonant part of $X^{(2)}$ must be set to zero, the value which is also required in order to explain the distribution of

signal intensities as a function of crystal orientation. The value of the resonant part of $\chi^{(2)}$ is obtained by assuming an effective value for the two-photon polarizability which is zero in the dipole approximation but nonzero when magnetic dipole and electric quadrupole effects are included. Nonresonant background contributions must come from multipole mechanisms as well, and are expected to be weak. The role of the background nonlinear susceptibility deserves investigation, since there are no corresponding terms in the polariton fusion expression; this will best be accomplished in systems where two-photon processes are dipole-allowed.

The temperature-dependent intensity behavior predicted by both models fails in the limit of thin crystals, when the coherence length of the excitation (including the effects of scattering) may be longer than the crystal thickness for photon-like polaritons at low temperatures. This may be a result of enhancement of the nonlinear signal at the surface of the sample through disruption of inversion symmetry or of the exciton band, or of an enhanced path length effect owing to multiple internal reflections which are not damped in thin crystals. The observation that the resultant intensity behavior is independent of crystal thickness is a strong argument for surface effects.

The shapes of the SHG and TPE profiles have been compared to shapes predicted from the semiclassical theory (the explicit intensity profile expression has not been developed in the polariton fusion formalism). The theoretical peak shapes appear to match those of the observed signals well, again provided that the polariton damping (39 $cm^{-1}$ optical phonon) and zero-valued $\chi_{nr}^{(2)}$ are used. At low temperatures, the profile appear-

ances are dominated by the phase matching function, which produces an asymmetric shape when frequency is scanned. At near-normal angles of incidence, the experimental SHG profile displayed multiple fringing maxima as a result of the behavior of $\Delta k$ near resonance, including a pronounced inflection point at the frequency of the transverse exciton resonance. These features are described accurately by the semiclassical expressions. At higher temperatures, the overall coherence length of the excitation becomes dominated by scattering and the effect of phase matching on profile shapes is washed out; this has also been demonstrated experimentally.

The strong coupling of the 31475 $cm^{-1}$ exciton to the photon field has been demonstrated to dictate the second-order nonlinear behavior of naphthalene crystals at frequencies near half-resonance. The dynamics of polaritons produced coherently via nonlinear interactions which are dependent on phase matching has been shown to deviate in a controllable way from the dominant exciton dynamics of the one-photon polaritons produced in a linear experiment. The necessity of using a strong coupling model to explain dispersion, intensity, and lineshape behavior has been established. It is also evident that a completely satisfactory theoretical treatment of resonance-enhanced nonlinear effects in solids does not as yet exist. The success of the semiclassical model with phenomenological changes to allow for nonperturbative interactions promises that further development of the polariton fusion model will produce expressions which successfully describe resonant nonlinear behavior in molecular crystals.

REFERENCES

1. Basu, S.: Ind. Eng. Chem. Prod. Res. Dev. 23, 183 (1984).

2. Garito, A.F.; Singer, K.D.: Laser Focus 1982, 59 (1982).

3. Williams, D.J., ed.; Nonlinear Optical Properties of Organic and Polymeric Materials, American Chemical Society series 233, American Chemical Society, Washington, D.C. (1983).

4. Garito, A.F.; Teng, C.C.; Wong, K.Y.; Zammani'Khamiri, O.: Mol. Cryst. Liq. Cryst. 106, 219 (1984).

5. Williams, D.J.: Angew. Chem. Int. Ed. Engl. 23, 690 (1984).

6. McClure, D.S.: Sol. St. Phys. 8, 1 (1960).

7. McClure, D.S.: in Optical Properties of Solids, ed. S. Nudelman and S.S. Mitra, Plenum Press, New York (1969), p.555.

8. Wolf, H.C.: Sol. St. Phys. 9, 1 (1961).

9. Franken, P.A.; Hill, A.E.; Peters, C.W.; Weinrich, G.: Phys. Rev Lett. 7, 118 (1961).

10. Kaiser, W.; Garrett, C.G.B.: Phys. Rev. Lett. 7, 229 (1961).

11. a. Armstrong, J.A.; Bloembergen, N.; Ducuing, J.; Pershan, P.S.: Phys. Rev. 127, 1918 (1962).
    b. Bloembergen, N.; Pershan, P.S.: Phys. Rev. 128, 606 (1962).

12. Ducuing, J.: in Quantum Optics, Proc. Int. School of Physics, "Enrico Fermi" course XLII, ed. R.J.Glauber, Academic Press, New York (1969), p.421.

13. Kurtz; Jerphagnon; Choy: in Numerical Data and Functional Relationships in Science and Technology, v. 11, ed. K.-H. Hellewege, Springer-Verlag, New York (1979), p. 671.

14. a. Shen, Y.R.: Rev. Mod. Phys. 48, 1 (1976).
b. Shen, Y.R.: in Proc. Int'l. School Phys. "Enrico Fermi" Course LXIV, ed. N. Bloembergen, North-Holland Co., New York (1977), p.170.

15. De Witt, R.N.; Harvey, A.B.; Tolles, W.M.: Naval Research Laboratory Memorandum Report 3260, Office of Naval Research, Arlington, Virginia (1976).

16. Chemla, D.S.: Rep. Prog. Phys. 43, 76 (1980).

17. Butcher, P.N.: Nonliear Optical Phenomena, Bulletin 200, Engineering Experimental Station, Ohio State University (1965).

18. Baldwin, G.C.: An Introduction to Nonlinear Optics, Plenum Press, New York (1969).

19. Bloembergen, N.: Nonlinear Optics, corrected edition, W.A.Benjamin, Inc., Reading, Mass. (1977).

20. Hanna, D.C.; Yuratich, M.A.; Cotter, D.: Nonlinear Optics of Free Atoms and Molecules, Springer-Verlag, New York (1979).

21. Shen, Y.R.: The Principles of Nonlinear Optics, Wiley-Interscience, New York (1984).

22. Göppert-Mayer, M.: Ann. Physik 9, 273 (1931).

23. Honig, B.; Jortner, J.; Szöke, A.: J. Chem. Phys. 46, 2714 (1967).

24. Peticolas, W.L.: Ann. Rev. Phys. Chem. 18, 233 (1967).

25. Mahan, G.D.: Phys. Rev. 170, 825 (1968).

26. Denisov, M.M.; Makarov, V.P.: J. Phys. C 5, 2651 (1972).

27. a. Hopfield, J.J.; Worlock, J.M.; Park, K.J.: Phys. Rev. Lett. 11, 414 (1963).
b. Hopfield, J.J.; Worlock, J.M.: Phys. Rev. 137, A1455 (1965).

28. a. Peticolas, W.L.; Goldsborough, J.P.; Rieckhoff, K.E.: Phys. Rev. Lett. 10, 43 (1963).
b. Peticolas, W.L.; Rieckhoff, K.E.: J. Chem. Phys. 39, 1347 (1963).

29. Singh, S.; Stoicheff, B.P.: J. Chem. Phys. 38, 2032 (1963).

30. Hochstrasser, R.M.; Sung, H.N.; Wessel, J.E.: J. Chem. Phys. 58, 4694 (1973).

31. a. Hochstrasser, R.M.; Sung, H.N.; Wessel, J.E.: Chem. Phys. Lett. 24, 168 (1974).
b. Hochstrasser, R.M.; Sung, H.N.: J. Chem. Phys. 66, 3276 (1977).

32. Mikami, N.; Ito, M.: Chem. Phys. 23, 141 (1977).

33. Dick, B.; Hohlneicher, G.: Chem. Phys. Lett. 84, 471 (1981).

34. Mikami, N.; Hong, H.-K.: Bull. Chem. Soc. Japan 52, 3484 (1979).

35. Hochstrasser, R.M.; Klimcak, C.M.; Meredith, G.R.: J. Chem. Phys. 70, 870 (1979).

36. Sethuraman, V.; Edelson, M.C.; Johnson, C.K.; Sethuraman, C.; Small, G.J.: Mol. Cryst. Liq. Cryst. 57, 89 (1980).

37. Johnson, C.K.: Ph.D. dissertation, Iowa State University (1981).

38. Bergman, A.; Jortner, J.: Chem. Phys. Lett. 15, 309 (1972).

39. Giordmaine, J.A.; Phys. Rev. Lett. 8, 19 (1962).

40. Maker, P.D.; Terhune, R.W.; Nisenoff, M.; Savage, C.M.: Phys. Rev. Lett. 8, 21 (1962).

41. Terhune, R.W.; Maker, P.D.; Savage, C.W.: Phys. Rev. Lett. 8, 404 (1962).

42. Franken, P.A.; Ward, J.F.: Rev. Mod. Phys. 35, 23 (1963).

43. Akhmanov, S.A.; Kovrigin, A.I.; Khokhlov, R.V.; Chunaev, O.N.: Sov. Phys.

JETP 18, 919 (1964).

44. Hobden, M.V.: J. Appl. Phys. 38, 4365 (1967).

45. Bass, M.; Franken, P.A.; Hill, A.E.; Peters, C.W.; Weinrich, G.: Phys. Rev. Lett. 8, 18 (1962).

46. Rustagi, K.C.; Mehendale, S.C.; Gupta, P.K.: Appl. Phys. Lett. 43, 811 (1983).

47. Driscoll, T.A.; Giudotti, D.: Phys. Rev. B 28, 1171 (1983).

48. Tom, H.W.K.; Heinz, T.F.; Shen, Y.R.: Phys. Rev. Lett. 51, 1983 (1983).

49. a. Hochstrasser, R.M.; Meredith, G.R.: J.Chem. Phys. 67, 1273 (1977).
    b. Hochstrasser, R.M.; Meredith, G.R.: J. Lum. 18/19, 32 (1979).

50. a. Stevenson, S.H.; Johnson, C.K.; Small, G.J.: J. Phys. Chem. 85, 2709 (1981).
    b. Stevenson, S.H.; Small, G.J.: Chem. Phys. Lett. 95, 18 (1983).
    c. Stevenson, S,H,; Small, G.J.: Chem. Phys. Lett. 100, 334 (1983).

51. Johnson, C.K.; Small, G.J.: J. Chem. Phys. 76, 3837 (1982).

52. Zyss, J.; Chemla, D.S.; Nicoud, J.F.: J. Chem. Phys. 74, 4800 (1981).

53. Carenco, A.; Jerphagnon, J.; Perigaud, A.: J. Chem. Phys. 66, 3806 (1976).

54. Teng, C.C.; Garito, A.F.: Phys. Rev. B 28, 6766 (1983).

55. Baden, J.; Hierle, R.; Perigaud, A.; Zyss, J: in Nonlinear Optical Properties of Organic and Polymeric Materials, American Chemical Society Symposium Series 233, ed. David J. Williams, American Chemical Society, Washington, D.C. (1983), p.81.

56. Hermann, J.P.: Opt. Commun. 9, 74 (1973).

57. a. Meredith, G.R.; Buchalter, B.; Hanzlik, C.: J.Chem. Phys. 78, 1533 (1983).
b. Meredith, G.R.; Buchalter, B.; Hanzlik, C.: J.Chem. Phys. 78, 1543 (1983).

58. Thalhammer, M.; Penzkofer, A.: Appl. Phys. B 32, 137 (1983).

59. Ward, J.F.; Elliott, D.S.: J. Chem. Phys. 80, 1003 (1984).

60. Singer, K.D.; Garito, A.F.: J. Chem. Phys. 75, 3572 (1981).

61. Ahluwalia, H.S.; May, E.J.P.; Vandamme, L.K.J.: J. Appl. Phys. 53, 6482 (1982).

62. Meredith, G.R.; Williams, D.J.; Fishman, S.N.; Goldburt, E.S.; Krongauz, V.A.: J. Phys. Chem. 87, 1697 (1983).

63. Enns, R.H.; Rangnekar, S.S.: Phys. Status Solidi B 94, 9 (1979).

64. Dick, B.; Hochstrasser, R.M.: Phys. Rev. Lett. 51, 2221 (1983).

65. Morrell, J.A.; Albrecht, A.C.; Levin, K.H.; Tang, C.L.: J. Chem. Phys. 71, 5063 (1979).

66. Lipscomb, G.F.; Garito, A.F.; Narang, R.S.: J. Chem. Phys. 75, 1509 (1981).

67. Gadomski, W.: J. Appl. Phys. 54, 1029 (1983).

68. Aroney, M.J.; Pratten, S.J.: J. Chem. Soc. Faraday Trans. 1, 80, 1201 (1984).

69. Midwinter, J.E.: Proc. R. Soc. Lond. A 392, 247 (1984).

70. Stegeman, G.I.; Seaton, C.T.; Chilwell, J.; Smith, S.D.: Appl. Phys. Lett. 44, 830 (1984).

71. Goldstone, J.A.; Garmire, E.: Phys. Rev. Lett. 53, 910 (1984).

72. Heisel, F.; Miehe, J.A.; Schott, M.; Sipp, B.: Hennberger, F.; Rossmann, H.: Phys. Status Solidi B 121, 685 (1984).

73. a. Chen, C.K.; de Castro, A.R.B.; Shen, Y.R.: Phys. Rev. Lett. 46, 145 (1981).
b. Chen, C.K.; Heinz, T.F.; Ricard, D.; Shen. Y.R.: Phys. Rev. B 27, 1965 (1983).
c. Heinz, T.F.; Chen. C.K.; Ricard, D.; Shen, Y.R.: Chem. Phys. Lett. 83, 180 (1981).
d. Chen, C.K.; Heinz, T.F.; Ricard, D.F.; Shen, Y.R.: Phys. Rev. B 27, 1965 (1983).

74. Richmond, G.L.: Chem. Phys. Lett. 106, 26 (1984).

75. Deck, R.T.; Grygler, R.K.: Appl. Optics 23, 3202 (1984).

76. Reinisch, R.; Nevière, M.: Phys. Rev. B 28, 1870 (1983).

77. Ricard, D.: Ann. Phys. Fr. 8, 273 (1983).

78. Keilmann, F.; Bai, Y.H.: Appl. Phys. A 29, 9 (1982).

79. Guosheng, Z.; Fauchet, P.M.; Siegman, A.E.: Phys. Rev. B 26, 5366 (1982).

80. Ehrlich, D.J.; Brueck, S.R.J.; Tsao, J.Y.: Appl. Phys. Lett. 41, 630 (1982).

81. Sipe, J.E.; Young, J.F.; Preston, J.S.; van Driel, H.M.: Phys. Rev. B 27, 1141 (1983).

82. a. Frenkel, J.: Phys. Rev. 37, 17 (1931).
b. Frenkel, J.: Phys. Rev. 37, 1276 (1931).

83. a. Davydov, A.S.; Lubchenko, A.F.: Sov. Phys. JETP 35, 1048 (1959).
b. Davydov, A.S.: Sov. Phys. JETP 18, 496 (1964).
c. Davydov, A.S.; Sov. Phys. Usp. 82, 145 (1964).
d. Davydov, A.S.; Myasnikov, E.N.: Phys. Status Solidi 20, 153 (1967).

84. Davydov, A.S.: Theory of Molecular Excitons, trans. by S.B. Dresner, Plenum Press, New York (1971).

85. Knox, R.S.: Theory of Excitons, Academic Press, New York (1963).

86. Dexter, D.L.; Knox, R.S.: Excitons, Wiley-Interscience, New York (1965).

87. Philpott, M.R.: Adv. Chem. Phys. 23, 227 (1973).

88. Craig, D.P.; Walmsley, S.H.: Excitons in Molecular Crystals, Benjamin, New York (1968).

89. Fox, D.; Schnepp, O.: J. Chem. Phys. 23, 767 (1955).

90. Craig, D.P.; Walmsley, S.H.: Mol. Phys. 4, 97 (1961).

91. a. Broude, V.L.: Sov. Phys. Usp. 4, 584 (1962).
b. Broude, V.L.: Opt. Spectry. Suppl. 2, 25 (1967).

92. Colson, S.D.; Hanson, D.M.; Kopelman, R.; Robinson, G.W.: J. Chem. Phys. 48, 2215 (1968).

93. Mc Clure, D.S.; Schnepp, O.: J. Chem. Phys. 23, 1575 (1955).

94. Craig, D.P.; Lyons, L.E.; Walsh, J.R.: Mol. Phys 4, 97 (1961)

95. Sidman, J.W.: J. Chem. Phys. 25, 115 (1956).

96. Matsui, A.; Ishi, Y.: J. Phys. Soc. Japan 23, 581 (1967).

97. Morris, G.C.; Rice, S.A.; Sceats, M.G.; Martin, A.E.: J. Chem. Phys. 55, 5610 (1971).

98. Craig, D.P.; Gordon, R.D.: Proc. R. Soc. London 288, 69 (1965).

99. a. Philpott, M.R.: J. Chem. Phys. 50, 5117 (1969).
b. Philpott, M.R.; Lee, J.W.: J. Chem. Phys. 58, 595 (1973).

c. Philpott, M.R.: J. Chem. Phys. 58, 588 (1973).
d. Philpott, M.R.: J. Chem. Phys. 58, 639 (1973).

100. Silbey, R.; Jortner, J.; Vala, M.T.; Rice, S.A.: J. Chem. Phys. 42, 2948 (1965).

101. Greer, W.L.; Rice, S.A.; Jortner, J.: J. Chem. Phys. 48, 5667 (1968).

102. Craig, D.P.; Walmsley, S.H.: Mol. Phys. 4, 113 (1961).

103. Schlosser, D.W.; Philpott, M.R.: J. Chem. Phys. 77, 1969 (1982).

104. Huang, K.: Proc. R. Soc. London A208, 352 (1951).

105. Fano, U.: Phys. Rev. 103, 1202 (1956).

106. Hopfield, J.J.: Phys. Rev. 112, 1555 (1958).

107. a. Hopfield, J.J.: J. Phys. Soc. Japan 21 (suppl.), 77 (1966).
b. Hopfield, J.J.: in Proc. Intl. Sch. Phys. "Enrico Fermi" course XLII, ed. R.J. Glauber, Academic Press, New York (1969), p.340.
c. Hopfield, J.J.: Phys. Rev. 182, 945 (1969).
d. Hopfield, J.J.: in Elementary Excitations, ed. A. Maradudin and G.F. Nordelli, Plenum Press, New York (1969), p.413.

108. a. Pekar, S.I.: Sov. Phys. JETP 9 (36), 314 (1959).
b. Pekar, S.I.: Sov. Phys. JETP 11 (38), 1286 (1960).

109. a. Agranovich, V.M.: Sov. Phys. JETP 37, 307 (1960).
b. Agranovich, V.M.: Sov. Phys. - Solid State 3, 592 (1961).

110. Fishman, G.: Ann. Phys. Fr. 5, 5 (1980).

111. Johnson, C.K.; Small, G.J.: in Excited States, v.6, ed. E.C. Lim, Academic Press, New York (1982), p.97.

112. a. Davydov, A.S.; Serikov, A.A.: Phys. Status Solidi B56, 351 (1973).
b. Davydov, A.S.: Preprint ITP-75-51E, Institute for Theoretical

Physics, Kiev (1975).
c. Davydov, A.S.: Preprint ITP-75-96E, Institute for Theoretical Physics, Kiev (1975).

113. Voigt, J.: Phys. Status Solidi B64, 549 (1974).

114. Kreingol'd, F.I.; Makarov, V.L.: Sov. Phys. Solid State 17, 297 (1975).

115. Ferguson, J.: Chem. Phys. Lett. 36, 316 (1975).

116. Bosacchi, A.; Bosacchi, B.; Franchi, S.: Phys. Rev. Lett. 36, 1086 (1976).

117. a. Robinette, S.L. : Ph.D. dissertation, Iowa State University (1977).
b. Robinette, S.L.; Small, G.J.: J. Chem. Phys. 65, 837 (1976).
c. Robinette, S.L.; Small, G.J.; Stevenson, S.H.: J.Chem.Phys. 68, 4790 (1978).
d. Robinette, S.L.; Stevenson, S.H.; Small, G.J.: J.Chem.Phys. 69, 5231 (1978).

118. a. Weiser, G.; Fuhs, W.; Hesse, H.J.: Chem. Phys. 52, 183 (1980)
b. Hayne, T.; Weiser, G.: Phys. Status Solidi B 123, 271 (1984).

119. Schultheis, L.; Ploog, K.: Phys. Rev. B 29, 7058 (1984).

120. Philpott, M.R.: Ann. Rev. Phys. Chem. 31, 97 (1980).

121. a. Lagois, J.; Fischer, B.: Phys. Rev. Lett. 36, 680 (1976).
b. Lagois, J.; Fischer, B.: Phys. Rev. B 17, 3814 (1978).

122. Borstel, G.; Falge, H.J.: Appl. Phys. 16, 211 (1978).

123. Hopfield, J.J.; Thomas, D.G.: Phys. Rev. 132, 563 (1963).

124. Philpott, M.R.: Phys. Rev. B 14, 3471 (1976).

125. Akhmediev, N.N.: Sov. Phys. JETP 52, 773 (1980).

126. Agranovich, V.M.; Ginzburg, V.L.: Crystal Optics with Spatial Dispersion, and Excitons, 2nd edition, Springer-Verlag, New York (1984).

127. Craig, D.P.; Dissado, L.A.: Chem. Phys. Lett. 44, 419 (1976).

128. Davydov, A.S.: Phys. Status Solidi 20, 143 (1967).

129. a. Cho, K.; Toyozawa, Y.: J. Phys. Soc. Japan 30, 1555 (1971).
b. Nakajima, S.; Toyozawa, Y.; Abe, R.: The Physics of Elementary Excitations, Springer-Verlag, New York (1980).

130. a. Dissado, L.A.: Chem. Phys. 8, 289 (1975).
b. Dissado, L.A.: Chem. Phys. Lett. 33, 57 (1975).
c. Craig, D.P.; Dissado, L.A.: Chem. Phys. 14, 89 (1976).

131. Sumi, H.: J. Chem. Phys. 67, 2943 (1977).

132. Port, H.; Rund, D.; Small, G.J.; Yakhot, V.: Chem. Phys. 39, 175 (1979).

133. Clarke, M.D.; Craig, D.P.; Dissado, L.A.: Mol. Cryst. Liq. Cryst. 44, 309 (1978).

134. Munn, R.W.: Chem. Phys. 84, 413 (1984).

135. Benson,H.J.; Mills, D.L.: Phys. Rev. B 1, 4835 (1970).

136. Tait, W.C.: Phys. Rev. B 5, 648 (1972).

137. Merten, L.; Borstel, G.: Z. Naturforsch. A 27, 1792 (1972)

138. Egler, W.; Haken, H.: Z. Physik B 28, 51 (1977).

139. a. Kopelman, R.; Argyrakis, P.: J. Chem. Phys. 72, 3053 (1980).
b. Kopelman, R.: in Spectroscopy and Excitation Dynamics of Condensed Molecular Systems, ed. V.M. Agranovich and R.M. Hochstrasser, North-Holland, New York (1983).
c. Gentry, S.T.; Kopelman, R.: J. Phys. Chem. 88, 3170 (1984).

140. Chow, H.C.; Powell, R.C.: Phys. Rev. B 21, 3785 (1980).

141. Munn, R.W.; Silbey, R.: Mol. Cryst. Liq. Cryst. 57, 131 (1980).

142. Powell, R.C.; Soos, Z.G.: J. Lum. 11, 1 (1975).

143. Silbey, R.: in Spectroscopy and Excitation Dynamics of Condensed Molecular Systems, ed. V.M. Agranovich and R.M. Hochstrasser, North-Holland, New York (1983).

144. Kenkre, V.M.; Reineker, P.: Exciton Dynamics in Molecular Crystals and Aggregates, Springer-Verlag, New York (1982).

145. Kazzaz, A.A.; Zahlan, A.B.: Phys. Rev. 124, 90 (1961).

146. Agranovich, V.M.; Konobeev, Yu.V.: Sov. Phys. - Solid State 5, 999 (1963).

147. Powell, R.C.: Phys. Rev. B 4, 628 (1971).

148. Auweter, H.; Mayer, U.; Schmid, D.: Z. Naturforsch. 33a, 651 (1978).

149. Stevenson, S.H.; Connolly, M.A.; Small, G.J.: J. Lum., to be published.

150. Duong, P.H.; Itoh, T.; Lavallard, P.: Sol. St. Commun. 43, 879 (1982).

151. Vidmont, N.A.; Maksimov, A.A.; Tartakovskii, I.I.: JETP Lett. 37, 689 (1983).

152. a. Ovander, L.N.: Sov. Phys.- Solid State 5, 641 (1963).
b. Ovander, L.N.: Sov. Phys. Usp. 86, 337 (1965).

153. Lang, M.: Phys. Rev. B 2, 4022 (1970).

154. Loudon, R.: in Proc. Int'l. Sch. Phys. "Enrico Fermi" course LXIV, ed. N. Bloembergen, North-Holland, New York (1977), p.296.

155. Loudon, R.: Proc. Phys. Soc. 80, 952 (1962).

156. Uihlein, C.;Fröhlich, D.; Mohler, E.: in Polaritons, ed. E. Burstein and F. De Martini, Pergamon Press, New York (1974), p.303.

157. De Martini, F.: in Polaritons, ed. E. Burstein and F. De Martini, Pergamon Press, New York (1974), p.335.

158. a. Boggett, D.; Loudon, R.: Phys. Rev. Lett. 28, 1051 (1972).
b. Boggett, D.; Loudon, R.: J. Phys. C: Solid State Phys. 6, 1763 (1973).

159. Fröhlich, D.; Mohler, E.; Uihlein, C.: Phys. Status Solidi B55, 175 (1973).

160. De Martini, F.: in Proc. Int'l. Sch. Phys. "Enrico Fermi" course LXIV, ed. N. Bloembergen, North-Holland Co., New York (1977), p.319.

161. De Martini, F.; Giuliani, G.; Mataloni, P.; Palange, E.; Shen, Y.R.: Phys. Rev. Lett. 37, 440 (1976).

162. Agranovich, V.M.; Babichenko, V.S.; Chernyak, V.Ya.: JETP Lett. 32, 512 (1981).

163. Arya, K.: Phys. Rev. B. 29, (1984).

164. Schultheis, L.; Lagois, J.: Phys. Rev. B 29, 6784 (1984).

165. Hopfield, J.J.; Thomas, D.G.: Phys. Rev. Lett. 15, 22 (1965).

166. Porto, S.P.S.; Tell, B.; Damen, T.C.: Phys. Rev. Lett. 16, 450 (1966).

167. Henry, C.H.; Hopfield, J.J.: Phys. Rev. Lett. 15, 964 (1965).

168. Coffinet, J.P.; De Martini, F.: Phys. Rev. Lett. 22, 60 (1969).

169. a. Haueisen, D.C.; Mahr, H.: Phys. Rev. Lett. 26, 838 (1971).
b. Mahr, H.; Haueisen, D.C.: in Polaritons, ed. E. Burstein and F. DeMartini, Pergamon Press, New York (1972), p.313.
c. Haueisen, D.C.; Mahr, H.: Phys. Rev. B 8, 2969 (1973).

170. Fröhlich, D.; Mohler, E.; Weisner, P.: Phys. Rev. Lett. 26, 554 (1971).

171. Itoh, T.; Suzuki, T.: J. Phys. Soc. Japan 45, 1939 (1978).

172. Koteles, E.S.; Winterling, G.: Phys. Rev. Lett. 44, 948 (1980).

173. Lyssenko, V.G.; Kemf, K.; Bohnert, K.; Schmeider, G.; Klingshirn, C.; Schmitt-Rink, S.: Sol. St. Commun. 42, 401 (1982).

174. Boiko, S.A.; Terekhova, S.F.: Opt. Spectrosc. USSR 49, 630 (1980)

175. Pao, Y.-H.; Rentzepis, P.M.: J. Chem. Phys. 43, 1281 (1965).

176. Johnson, C.K.; Small, G.J.: Chem. Phys. 64, 83 (1982).

177. Glownia, J.H.; Sander, R.K.: Phys. Rev. Lett. 49, 21 (1982).

178. a. Jackson, D.J.; Wynne, J.J.: Phys. Rev. Lett. 49, 543 (1982).
b. Wynne, J.J.: Phys. Rev. Lett. 52, 751 (1984).

179. Feynman, R.P.; Vernon, F.L.; Hellwarth, R.W.: J. Appl. Phys. 28, 49 (1957).

180. Kleinman, D.A.: Phys. Rev. 126, 1977 (1962).

181. Yariv, A.: Quantum Electronics, 2nd edition, John Wiley & Sons, New York (1975).

182. Meredith, G.R.: in Nonlinear Optical Properties of Organic and Polymeric Materials, American Chemical Society Symposium Series 233, ed. David J. Williams, American Chemical Society, Washington, D.C. (1983), p.27.

183. Levine, B.F.; Bethea, C.G.: J. Chem. Phys. 63, 266 (1975).

184. Mahr, H.: in Quantum Electronics: A Treatise, vol. IA, ed. by H. Rabin and C.L. Tang, Academic Press, New York (1975), p.285.

185. Meredith, G.R.: J. Chem. Phys. 75, 4317 (1981).

186. Meredith, G.R.: J. Chem. Phys. 77, 5863 (1982).

187. Ward, J.F.; New, G.H.C.: Phys. Rev. 185, 57 (1968).

188. Adler, E.: Phys. Rev. 134 P, A728 (1964)

189. Applequist, J.: Chem. Phys. 85, 279 (1984).

190. Flytzanis, C.: in Quantum Electronics: A Treatise, vol.IA, ed. H. Rabin and C.L. Tang, Academic Press, New York (1975), p.9.

191. Hanson; Robinson: J. Chem. Phys. 43, 4174 (1965).

192. Gia, H.-B.; Jerome, R.; Teyssie, Ph.: J. Organomet. Chem. 190, 107 (1980).

193. Winchell, A.N.: The Optical Properties of Organic Compounds, second edition, Academic Press, New York (1954).

194. Wallenstein, R.; Hänsch, T.W.: Appl. Opt. 13, 1625 (1974).

195. Lawler, J.E.; Fitzsimmons, W.A.; Anderson, L.W.: Appl. Opt. 15, 1083 (1976).

196. Fitzsimmons, W.A.; Anderson, L.W.; Riedhauser, C.E.; Vrtilek, J.M.: IEEE J. Quantum Elect. QE-12, 624 (1976).

197. a. Kaiser, J.F.; Reed, W.A.: Rev. Sci. Inst. 48, 1447 (1977).
b. Kaiser, J.F.; Reed, W.A.: Rev. Sci. Inst. 49, 1103 (1978).

198. Maureen A. Connolly, Iowa State University, data analysis (1983).

199. a. McClure, D.S.: J. Chem. Phys. 22, 1668 (1954).
b. McClure, D.S.: J. Chem. Phys. 24, 1 (1956).

200. Abrahams, S.C.; Robertson, J.M.; White, J.G.: Acta Cryst. 2, 233 (1949).

201. Hochstrasser, R.M.; McAlpine, R.D.; Whiteman, J.D.: J. Chem. Phys. 68, 5078 (1973).

202. Hendricks; Jefferson: J. Opt. Soc. Am. 23, 299 (1933).

203. Cruickshank, D.W.J.; Robertson, A.P.: Acta Cryst. 6, 698 (1953).

204. Anderson, P.W.: J. Phys. Soc. Japan 9, 316 (1954).

205. Personal communication, Dr. Gerald Meredith, Xerox Corporation, Rochester, New York (1983).

206. Bloembergen, N.; Chang, R.K.; Jha, S.S.; Lee, C.H.: Phys. Rev. 174, 813 (1968).

207. Burland, D.M.; Konzelmannn, V.; McFarlane, R.M.: J. Chem. Phys. 67, 1926 (1977).

208. Hopfield, J.J.; Thomas, D.G.: J. Phys. Chem. Solids 12, 276 (1960).

209. Connolly, M.A.: Ph.D. dissertation, Iowa State University (in preparation).

210. Born, Max; Wolf, Emil: Principles of Optics, 6th edition, Pergamon Press, New York 1980.

211. Hartshorne, N.N.; Stuart, A.: Crystals and the Polarizing Microscope, 4th ed., Edward Arnold Ltd., London 1970.

212. Wahlstrom, E.E.: Optical Crystallography, 3rd ed., John Wiley & Sons, New York (1960).

213. Wood, Elizabeth A.: Crystals and Light: An Introduction to Optical Crystallography, 2nd edition, Dover Publications, New York (1977).

214. Jerrard, H.G.: J. Opt. Soc. Am. 38, 35 (1948).

215. Leitz corporation, Kippkompensator M data sheet (1972).

# ACKNOWLEDGMENTS

I would like to thank some of the people whose help during the various phases of this project was greatly appreciated. I am especially grateful to my research advisor, Professor Gerald J. Small. It was his enthusiasm that first sparked my interest in polariton problems, and his availability and willingness to discuss data and theories at any hour was a terrific advantage throughout this study. I am fortunate to have enjoyed the benefits of his insights into the physics of molecular crystals for many years, and I thank him for his guidance and patience during the course of my graduate career.

Thanks are also due to Professor Harry Svec for several years of counsel and support.

Dr. John Hayes and Dr. Martin Edelson are thanked for their valuable advice and help with experimental techniques. Martin's encouragement and help in the laboratory during a difficult phase of this project were especially appreciated.

I owe thanks to Dr. Johnie Brown and Mike McGlade, who were invaluable as electronics consultants. Thanks also go to Johnie for teaching me everything I know about small computers and interfacing techniques.

I would like to thank Dr. Gerald Meredith for many helpful insights into nonlinear optical problems, and Dr. Carey Johnson for discussions about polaritons which helped solidify many ideas.

I am grateful to Maureen Connolly for her assistance in cutting and weighing innumerable peak profiles, and for her help in the laboratory. The

company late at night was appreciated, as was the reinforcement in the continuous counteroffensive against nocturnal cockroach onslaughts.

To the rest of the group members go my thanks for hours of entertainment in the form of styrofoam snowstorms, minty-fresh detergents (thanks Matt), and bad jokes. The creative atmosphere of the Small group made research a pleasure.

Finally, I would like to express my appreciation to my parents, Dr. and Mrs. Peter Stevenson, and to my husband, Douglas Adelman, for their constant encouragement, understanding, and support. I am grateful for Doug's patience with an eccentric schedule dictated by the caprices of laser and cryostat, for his availability over the years as an on-demand laboratory assistant and take-out chef, and for his invaluable help with the typing and assembly of this dissertation.

# APPENDIX A

## Thickness Determination and Alignment of Birefringent Samples

The fundamental theory and techniques of optical crystallography pertinent to the experiments described in this dissertation and to similar studies on materials other than naphthalene are discussed in this Appendix. Crystallographic data and technical information specific to materials and equipment used in this study are also included.

The subject of crystal optics and the use of the polarizing microscope has been treated by numerous authors (210-213). Optical data for many organic crystals have been compiled by Winchell (193). The fundamental equation relating the displacement vector $\underline{D}$ to the electric field vector $\underline{E}$ of an electromagnetic wave is the material relation

$$D_j = \epsilon_{jk} E_k \qquad (j, k = x, y, z) \qquad , \qquad [A.1]$$

where $\epsilon$ is the dielectric tensor for the material and summation over repeated indices is understood. It is straightforward to show that the tensor $\epsilon$ must be symmetric (210); that is, that there are six independent components (which may be related by the symmetry properties of the material). Thus, in any (x,y,z) space a surface may be defined by:

$$\epsilon_{xx}x^2 + \epsilon_{yy}y^2 + \epsilon_{zz}z^2 + 2\epsilon_{xy}xy + 2\epsilon_{xz}xz + 2\epsilon_{yz}yz = C, \quad [A.2]$$

where C is some constant. If the space is defined by the electric field components $E_x$, $E_y$, and $E_z$, C is proportional to the electric energy density $\omega_e$; this implies that each side of equation [A.2] must be positive definite. The surface defined is therefore an ellipsoid. For monochromatic light at a frequency far from a material resonance, the terms in the dielectric tensor are real constants and it is possible to transform the ellipsoid to a set of principal axis coordinates so that equation [A.2] becomes

$$\epsilon_{xx}x^2 + \epsilon_{yy}y^2 + \epsilon_{zz}z^2 = C' \quad , \qquad [A.3]$$

and the electric energy density may be written simply as

$$\epsilon_{xx}E_x^2 + \epsilon_{yy}E_y^2 + \epsilon_{zz}E_z^2 = \frac{D_x^2}{\epsilon_{xx}} + \frac{D_y^2}{\epsilon_{yy}} + \frac{D_z^2}{\epsilon_{zz}} = 8\pi\omega_e \quad . \qquad [A.4]$$

Maxwell's equations for an electromagnetic wave in a nonmagnetic medium with no current may be combined to yield the expression

$$\underline{D} = n^2[\underline{E} - \underline{s}(\underline{s}\cdot\underline{E})] \quad , \qquad [A.5]$$

where $\underline{s}$ is a unit vector in the direction of propagation. In the principal axis coordinate system of the dielectric tensor, equation [A.1] may be used to rewrite this expression as three independent equations of the form

$$\epsilon_{jj}E_j = n^2[E_j - s_j(s\cdot E)] \qquad (j = x, y, z) \quad . \qquad [A.6]$$

Combination of these three equations leads to Fresnel's equation, the fundamental relation of crystal optics:

$$\frac{s_x^2}{n^2 - \epsilon_{xx}} + \frac{s_y^2}{n^2 - \epsilon_{yy}} + \frac{s_z^2}{n^2 - \epsilon_{zz}} = \frac{1}{n^2} \quad . \qquad [A.7]$$

Fresnel's equation is quadratic in n. The implication is that for a given propagation direction (a given $\underline{s}$), there are two possible indices of refraction and hence two possible phase velocities for a wavefront moving in that direction. This birefringence is a phenomenon which is a property of optically anisotropic materials. Equations [A.6] and [A.7] may be used to show that both possible waves traveling along $\underline{s}$ are linearly polarized (the ratios of the field components are real).

The dielectric displacement vectors $\underline{D}$ for the two waves lie in the plane perpendicular to $\underline{s}$. The indicial ellipsoid described in equation [A.4] (and also called the optical indicatrix) intersects this plane to form an ellipse given by:

$$\frac{x^2}{\epsilon_{xx}} + \frac{y^2}{\epsilon_{yy}} + \frac{z^2}{\epsilon_{zz}} = 1 \quad ; \quad \underline{r} \cdot \underline{s} = 0 \quad (\underline{r} = \{x, y, z\}) \quad . \qquad [A.8]$$

By solving equations [A.8] for the major and minor axes of the ellipse normal to $\underline{s}$, an expression is obtained which is identical in form to equation [A.5], substituting $\underline{r}$ for $\underline{D}$. There are two important conclusions to be drawn: (1) that the two independent waves which may propagate in a given direction in an anisotropic medium are polarized in mutually perpendicular directions; and (2) that these directions and their associated refractive indices may be determined simply from geometric considerations. The lengths of the major and minor axes of the cross-sectional indicial ellipse

perpendicular to the propagation direction $\underline{s}$ give the values of the indices of refraction for waves propagating along $\underline{s}$, and the orientation of the axes gives the polarization directions for the two kinds of waves. It is also useful to consider the cross-section of the indicatrix containing both $\underline{s}$ and one of the displacement vectors, vide infra.

In anisotropic materials, where $\epsilon$ is a tensor rather than a constant, equation [A.1] implies that in general $\underline{D}$ is not parallel to $\underline{E}$. The electric field vector is perpendicular to the direction of propagation of energy (the ray direction), while the displacement vector is normal to the wave front. It is therefore necessary to be careful to define what is meant by refraction of a wave upon entering an anisotropic medium. Snell's law of refraction,

$$\frac{n_2}{n_1} = \frac{\sin \theta_1}{\sin \theta_2} \quad , \qquad [A.9]$$

holds where $\theta_2$ is defined to be the angle of refraction of $\underline{s}$, the wave normal. However, $n_2$ will be a function of $\theta_2$ if the displacement vector for the wave lies in the plane of refraction. The direction of refraction for a wave normal in an anisotropic medium, as well as that of the associated ray, may be determined geometrically from the optical indicatrix. (This is unnecessary for determination of the internal propagation direction of the fundamental wave in the naphthalene crystal for the experiments described in this dissertation. Because the incident beam is refracted only in the $\underline{ac}$ plane and is polarized along $\underline{b}$, the index of refraction is independent of the refraction angle and Snell's Law [A.9] may be used directly, as

for ordinary rays.)

The orientation of the optical indicatrix with respect to the crystalline axis system is dictated in part by the symmetry of the crystal. Monoclinic crystals are all of symmetry class $C_2$, $C_s$, or $C_{2h}$; the crystalline b-axis is parallel to a two-fold symmetry axis or perpendicular to a mirror plane or both. Since symmetry operations which leave the crystal unchanged must also leave the indicial ellipsoid unchanged, the b-axis must lie parallel to one of the principal axes of the indicatrix. The indicatrix for a monoclinic crystal has principal axes of three different lengths. As a result, there are two directions of propagation along which there is only one value for n (geometrically, there are two ways to cut circular cross-sections of a general ellipsoid). These two directions are the optic axes, and crystals with two optic axes are called biaxial crystals. It is easy to shôw from geometric arguments or using equation [A.7] that the two optic axes must lie in the plane of the major and minor principal axes of the indicatrix, located symmetrically with respect to the indicatrix axes. The angle between the two optic axes is 2V, the optic angle; for naphthalene, that angle is (-)2V = 83°, the minus sign indicating that the minor axis of the ellipsoid is the acute bisectrix. The optic plane of naphthalene has been determined to be the ac plane (193); the axis with which the crystalline b-axis coincides must therefore be the optic normal, the principal axis of intermediate length. The major and minor axes, Z and X by convention, must lie in the ac plane, but are unrestricted in orientation with respect to rotation about the b-axis. The orientation of the indicatrix for a monoclinic crystal such as naphthalene may therefore

change with frequency, a phenomenon known as inclined axial dispersion for a crystal with fixed optic normal. Winchell (193) reports that naphthalene displays "strong inclined dispersion," but the axial dispersion over a large transparent frequency range has been measured by McClure and Schnepp (93) and found to be less than 2°. Axial dispersion at frequencies near the lower electronic resonances in naphthalene is discussed in the text of this dissertation.

The orientation of the a- and c-axes of naphthalene with respect to the indicatrix cross-section in the ac plane at visible wavelengths is shown in Figure 44. The Z- and X-axes have been given the names $c^*$ and $a^*$, respectively, to indicate their proximities to the crystalline c- and a-axes. (Note: the $c^*$ and $a^*$ axes are unrelated to the $c^*$ and $a^*$ reciprocal axes of the Bravais lattice!)

Special mention should be made of the location of the Z-axis ($c^*$). It makes an angle of 9.5° with the crystalline c-axis in the obtuse ß (31b, 193, 202, 213). Winchell's book (193), a common source of optical data for researchers, gives an unclear description of the sign convention used to indicate whether this angle lies in the acute or the obtuse ß. A negative sign in reference (193) should always be taken to mean "in the obtuse ß."

Another kind of dispersion exhibited by optical media is indicial dispersion. In the transparent region of a crystal, the refractive index in any direction generally increases with frequency. An empirical equation that works well in predicting the value of $n_j$ as a function of wavelength

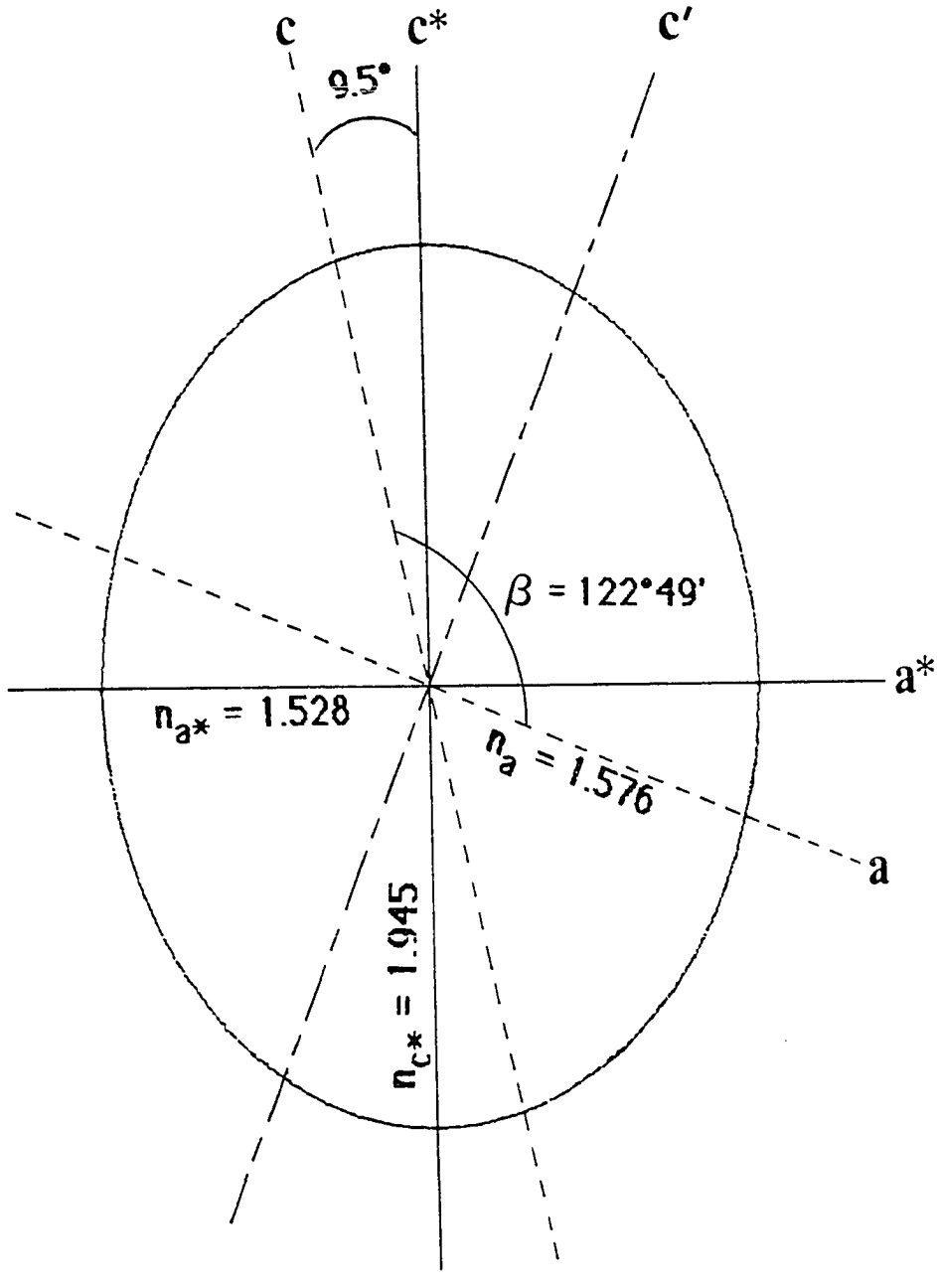


Figure 44. ac cross-section of the optical indicatrix for naphthalene at 5461 Å

is Cauchy's equation:

$$n = A + B\omega^2 + C\omega^4 + \ldots , \qquad [A.10]$$

where A, B, C, etc., are all constants. The value of $n_{a^*}$ shown in Figure 44 for naphthalene at 5461 Å (the wavelength used for measurement of crystal thicknesses) and that of $n_b$ at 6352 Å (the fundamental wavelength used in this study) were obtained using this expression and the data given in Table 1. The value of $n_{c^*}$ was obtained from reference (193).

Figure 44 may be used to determine the index of refraction of 5460 Å light polarized in the ac plane by computing the length of that axis of the ellipse which lies parallel to the displacement vector:

$$n = \frac{n_{a^*} n_{c^*}}{n_{a^*}^2 \sin^2\theta + n_{c^*}^2 \cos^2\theta} , \qquad [A.11]$$

where $\theta$ is the angle D makes with a* (s makes with c*). Light passing through an ab flake of naphthalene in a direction normal to the plane of the flake propagates along c', the crystallographic direction normal to both a and b. The two allowed vibration directions normal to c' are parallel to b and parallel to a. Using Table 1 and equation [A.10], the refractive index $n_b$ for a b-polarized wave at 5460 Å is found to be 1.7254. From equation [A.11] and Figure 44, the value of $n_a$ at the same wavelength is 1.5761. The difference, .1493, is the "partial birefringence" of naphthalene for a 5461 Å wave traveling along c'. Viewed through a polarizing microscope (crossed polarizers), a naphthalene sublimation flake will pass the a- and b-polarized components of the linearly polarized light passed by the

Table 1. Optical data for naphthalene, from reference (202)

| Frequency ($cm^{-1}$) | $n_{a^*}$ | $n_b$ |
|---|---|---|
| 19931 | 1.5333 | |
| 18307 | 1.5291 | 1.7255 |
| 17296 | 1.5249 | 1.7196 |
| 16965 | 1.5238 | 1.7182 |
| 14973 | 1.5188 | 1.7077 |

Polarizer (the first polarizer); the Analyzer (the second polarizer) will then pass the components of the two rays parallel to its polarization direction (normal to that of the Polarizer). Since the two rays propagate through the crystal at different phase velocities c/n, they emerge out of phase with one another by an amount determined by the partial birefringence and the crystal thickness. If they are exactly out of phase, the light passed through the Analyzer interferes destructively and the crystal appears dark.

When the crystal is illuminated with white light between crossed polarizers, the phase difference of the emergent rays varies with wavelength. For a very thin crystal, only a small range of wavelengths of the white light interferes destructively, and the crystal appears colored with the color which is complementary to the missing part of the spectrum. A thicker crystal satisfies the interference condition for a larger subset of the wavelengths present in the white light, and the interference colors observed are not the dark primary colors produced by thin crystals. Very

thick crystals will not exhibit interference colors at all. Generally, it is possible to measure the thickness of any crystal thin enough to appear colored under a polarizing microscpe by using a compensator.

A compensator is a birefringent substance placed in the light path after the crystal with its vibration directions oriented so that the retardation induced by the compensator counteracts that induced by the crystal. That is, the vibration direction of higher refractive index in the compensator is placed parallel to that of lower refractive index in the sample. The theory and use of several kinds of compensators has been discussed by Jerrard (214). The compensator used in these experiments was a tilting compensator, a small plate of magnesium fluoride cut normal to its optic axis, so that tilting the compensator is equivalent to passing successively through the "cones" of equal retardation about its optic axis. The angle of tilt, i, required to compensate an amount of retardation $\partial$ is related to $\partial$ by the expression

$$\partial = dn_2 \left\{ \left[ \frac{1 - \sin^2 i}{n_1^2} \right]^{1/2} - \left[ \frac{1 - \sin^2 i}{n_2^2} \right]^{1/2} \right\} , \quad [A.12]$$

where d is the thickness of the $MgF_2$ and for 5460 Å (roughly the maximum of the "white light" used by the microscope) the two refractive indices for $MgF_2$ are 1.39043 and 1.37859 (215). The retardation is in units of length and must be divided by the wavelength of the light used to get the phase difference r in number of wavelengths in air. This is related to the two different indices of refraction in the sample by:

$$r = \frac{L}{\lambda_{slow}} - \frac{L}{\lambda_{fast}} \; ; \quad \lambda_i = \frac{n_{air}}{n_i} \lambda_{air} \quad (i = slow, fast) \quad [A.13]$$

where L is the thickness of the crystal. Equation [A.13] may be rearranged to yield a simple formula for calculating the thickness of a crystal from the measured retardation and known partial birefringence:

$$L = \partial \left\{ \frac{n_{air}}{n_{slow} - n_{fast}} \right\} \approx \frac{\partial}{n_{slow} - n_{fast}} \; . \quad [A.14]$$

The retardation measured in white light for a naphthalene sublimation flake should be divided by .1493 to obtain the crystal thickness.

The polarizing microscope is also used to determine crystal orientation for optical experiments. Viewed in parallel light, the sample appears dark whenever its polarization directions are aligned with those of the Polarizer and Analyzer in the microscope. When the crystal is in one of these extinction positions but illuminated instead with convergent light, extinction occurs only in specific directions and a dark pattern emerges, its appearance determined by the location of the optic axes in the crystal. In the case of naphthalene, the ab flake is oriented obliquely to one optic axis, vide supra. The pattern viewed is therefore a dark brush (isogyre), which traces the ac plane in the crystal and thus the a-axis in the flake. Mounting the naphthalene crystal so that the isogyre is parallel to the slot in the sample holder (see Chapter III) is equivalent to mounting the crystalline b-axis vertically in the laboratory frame.

The brush observed for a naphthalene flake is asymmetric. One end

of it is thicker than the other, as a result of the fact that the optic axis is not normal to the crystal ab plane. The field of view contains more "cones of equal retardation" along one direction away from the optic axis than along the other; the splaying of the isogyre is due to the more gradual curvature of the cones further from the optic axis. This gives a convenient way to locate the c* axis; it is on the side of c' (the normal to the ab plane) away from the optic axis and toward the thicker end of the isogyre.

# APPENDIX B: SOFTWARE

## Pressure-Tuned Data Acquisition: PTUNE

```
1          .TITLE  PTUNE, PRESSURE-TUNING OF NRG LASER
2  ;;
3  ;;   PTUNE IS A PROGRAM TO USE WHEN PRESSURE-TUNING THE NRG
4  ;;   PTL-2000 LASER AND DESIRING TO SAVE DATA ON FLOPPY DISK.
5  ;;   HOOKUP INSTRUCTIONS MAY BE REQUESTED, AND THE PRESSURE
6  ;;   TRANSDUCER MAY BE CALIBRATED AGAINST THE WALLACE-TIERMAN GAUGE
7  ;;   (THIS MUST BE DONE AT LEAST ONCE OR YOU WILL NOT BE ABLE TO
8  ;;   PROCESS THE DATA FILES).  YOU CONTROL THE SCAN RATE AND
9  ;;   DURATION VIA THE TOGGLE SWITCHES AND NEEDLE VALVES ON THE
10 ;;   WALLACE-TIERMAN GAUGE MANIFOLD.  YOU ALSO READ THE BALANCING
11 ;;   VOLTAGE ON THE TEMPERATURE SENSOR.  THE COMPUTER ACCUMULATES
12 ;;   TWO CHANNELS OF INTENSITY VERSUS TEMPERATURE
13 ;;   AND PRESSURE TRANSDUCER VOLTAGE AND SAVES THE INFORMATION IN
14 ;;   MEMORY.  YOU HAVE THE OPTION OF IMPLEMENTING A DIGITAL
15 ;;   BUTTERWORTH FILTER.  THIS WILL NOT AFFECT THE DATA IN MEMORY,
16 ;;   BUT WILL FILTER THE DAC OUTPUT TO THE CHART RECORDER THAT
17 ;;   YOU ARE SEEING DURING THE EXPERIMENT.  THE FILTER WILL NOT
18 ;;   HURT ANYTHING, BUT IT IS NOT REALLY USEFUL.  IT IS A GOOD IDEA
19 ;;   TO LEAVE IT "OFF."  WHEN YOU STOP THE SCAN, YOU MAY CHOOSE TO
20 ;;   SAVE THE DATA ON DISK.  YOU MAY THEN START ANOTHER SCAN OR OPT
21 ;;   OUT OF THE PROGRAM.  WHEN YOU END THE PROGRAM, A DIRECTORY OF
22 ;;   YOUR DATA DISK WILL BE PRINTED.
23 ;;
24
25         .MCALL  .PRINT,.TTYIN,GETDEC,.TTINR
26         .MCALL  ADC,FILRAD,CREATE,.EXIT
27         .MCALL  PROCT
28         .GLOBL  PARKAY,BUTTER,BUSTAT,SCALE,DATA
29         .GLOBL  ALPHAH,ALPHAL,BETAH,BETAL,GETDEC
30         .GLOBL  HP,LP
31
32         JSW = 44
33
34 PTUNE:  BIS     #100,@#JSW      ;ENABLE CARRY BIT FOR TTINR
35         CLR     ALPHAH          ;INITIALIZE FILTER AT NO FILTER
36         CLR     ALPHAL
37         CLR     BETAL
38         MOV     #040200,@#BETAH
39 FINDOU: .PRINT  #INTRO
40         JSR     R4,YORN         ;INSTRUCTIONS REQUIRED?
41         BR      TELALL          ;YES, GIVE INSTRUCTIONS
42         BR      PRESCN          ;NO, SKIP INSTRUCTIONS
43         BR      FINDOU          ;BAD CHARACTER,ASK AGAIN
44 TELALL: .PRINT  #INSTRC         ;GIVE HOOKUP INSTRUCTIONS
45 PRESCN: MOV     LIMIT+2,R3      ;POINT TO DATA BUFFER BEGINNING
46         CLR     DUMCNT          ;COUNTER FOR FALSE CALIBRATION DATA
47 ASKCAL: .PRINT  #CALASK         ;CALIBRATION REQUIRED?
48         JSR     R4,YORN
49         BR      DOCAL           ;Y, GET CALIBRATION
50         BR      DONTCL          ;N, SKIP CALIBRATION
51         BR      ASKCAL          ;BAD CHR, ASK AGAIN
52 DONTCL: JSR     PC,DUMMY        ;FILL DATA BUFFER WITH 2000'S
53         INC     DUMCNT          ;IN CALIBRATION POSITIONS
54         CMP     DUMCNT,#3
55         BLT     DONTCL
```

```
56          BR      LPASK
57 DUMMY:   MOV     #42772,(R3)+    ;ROUTINE TO PUT FP 2000
58          CLR     (R3)+           ;IN NEXT BUFFER SPOT
59          RTS     PC
60 DOCAL:   .PRINT  #PAMBG          ;ASK FOR AMBIENT P
61          JSR     PC,GGTDEC       ;OBTAIN AND STORE
62          .PRINT  #PAMBU
63          JSR     PC,GGTDEC
64          .PRINT  #TAMB           ;ASK FOR AMBIENT T
65          JSR     PC,GGTDEC
66 LPASK:   .PRINT  #VOLTS          ;ASK FOR LP INPUT FULL-SCALE INFO
67          .PRINT  #A
68          JSR     PC,GGTDEC
69          .PRINT  #VOLTS
70          .PRINT  #B
71          JSR     PC,GGTDEC
72          .PRINT  #VOLTS
73          .PRINT  #R
74          JSR     PC,GGTDEC
75          .PRINT  #PULSE          ;ASK FOR PULSE-AVGE. NUMBER
76          JSR     PC,GGTDEC
77          .PRINT  #REPS           ;GET REP RATE
78          JSR     PC,GGTDEC
79          MOV     #3,CHAN         ;SPECIFY PRESSURE ADC
80          TST     DUMCNT
81          BEQ     GETP
82 BLANK:   JSR     PC,DUMMY        ;PUT 2000'S IN P CALB SPOTS
83          TST     (R3)+           ;SKIP ADC READING SPOTS
84          INC     DUMCNT
85          CMP     DUMCNT,#11
86          BLT     BLANK
87          BR      READY
88 GETP:    .PRINT  #CALMSG
89          CLR     CNTR            ;CLEAR CALIBRATION COUNTER
90 GETCAL:  .PRINT  #PASK           ;ASK FOR PRESSURE READING
91          JSR     PC,GGTDEC       ;GET PRESSURE READING
92          JSR     PC,ADC          ;GET VOLTAGE READING
93          MOV     DEST,(R3)+      ;STORE VOLTAGE
94          INC     CNTR            ;COUNT POINTS TAKEN
95          CMP     CNTR,#6         ;IS IT 6 YET?
96          BLT     GETCAL          ;NO, GET ANOTHER
97 READY:   CLR     PSTD            ;YES, SET 'P TO LOOK FOR' AT ZERO
98 QUES:    .PRINT  #ASKBUT         ;ASK WHETHER TO CHANGE FILTER
99          JSR     R4,YORN
100         BR      NEWCO           ;YES, CALCULATE NEW COEFFICIENTS
101         BR      NOCO            ;NO, RETAIN COEFFICIENTS
102         BR      QUES            ;BAD CHARACTER, REPEAT
103 NEWCO:  JSR     PC,PARKAY       ;NEW COEFFICIENTS ROUTINE
104 NOCO:   .PRINT  #TASK           ;GET SAMPLE TEMPERATURE
105         JSR     PC,GETTMP
106         .PRINT  #WAITPR         ;WAIT TO START SCAN
107 WAIT:   .TTYIN                  ;LOOK FOR CONSOLE INPUT
108         CMP     R0,#107         ;IS IT A G?
109         BNE     WAIT            ;NO, KEEP LOOKING
110         JMP     START           ;YES, START SCAN
111
112 GGTDEC: JSR     PC,GETDEC       ;ROUTINE TO GET FP # AND STORE IN
113                                 ;DATA BUFFER
114         MOV     HP,(R3)+
115         MOV     LP,(R3)+
116         RTS     PC
117
118 GETDEC: GETDEC   HP,LP           ;ROUTINE TO GET DECIMAL NUMBER FROM
119                                 ;CONSOLE
120         RTS     PC
```

```
121
122 MP:      .WORD   0
123 LP:      .WORD   0
124 CNTR:    .WORD   0
125 DUMCNT:  .WORD   0
126 INTRO:   .ASCII  //<14>/PROGRAM TO COLLECT DATA WHILE PRESSURE-/
127          .ASCII  /TUNING THE NRG LASER./<15><12><12>/HOOKUP /
128          .ASCII  /INSTRUCTIONS REQUIRED, Y OR N?/<11><11><200>//
129 INSTRC:  .ASCII  //<15><12><12><12>//
130          .ASCII  /MAKE CONNECTIONS:/<15><12><11>/ADC 3 TO P /
131          .ASCII  /(PRESSURE)/<15><12><11>/ADC 4 TO A /<15><12><11>//
132          .ASCII  /ADC 2 TO B/<15><12><11>/DAC 1 TO UPPER PEN/
133          .ASCII  //<15><12><11>/DAC 2 TO LOWER PEN/<15><12>/SET /
134          .ASCII  /RECORDER AT 10 VOLTS FULL SCALE./<15><12>/SET /
135          .ASCII  /LAMBDA-PHYSIK TO TRIGGER INTERNALLY OFF R./
136          .ASCII  //<15><12>/WHEN PROMPTED TO 'ENTER,' TYPE /
137          .ASCII  /INFORMATION AND HIT RETURN OR LINEFEED./<15><12>//
138          .ASCII  /PROGRAM STARTS AT 1000./<15><12>/DATA ARE /
139          .ASCII  /INITIALLY UNFILTERED./<12><12>//
140
141 CALASK:  .ASCII  /DO YOU WISH TO CALIBRATE, Y OR N?/<11><11><200>//
142 PAMBW:   .ASCII  /AMBIENT P, MBARS, FROM WALL?/<11><11><11><200>//
143 PAMBG:   .ASCII  /AMBIENT P, TORR X 10, FROM W-T GAUGE?/
144          .ASCII  //<11><11><200>//
145 TAMB:    .ASCII  /AMBIENT T, FAHRENHEIT?/<11><11><11><11><200>//
146 VOLTS:   .ASCII  /LAMBDA-PHYSIK INPUT VOLTAGE FULL SCALE, /<200>//
147 A:       .ASCII  /A?/<11><200>//
148 B:       .ASCII  /B?/<11><200>//
149 R:       .ASCII  /R?/<11><200>//
150 REPS:    .ASCII  /REP RATE OF LASER, HZ?/<11><11><11><11><200>//
151 PULSE:   .ASCII  /NUMBER OF PULSES AVERAGED BY L-P?/<11><11><200>//
152 CALMSG:  .ASCII  //<12><12>/CALIBRATE PRESSURE TRANSDUCER:  AT /
153          .ASCII  /PROMPT, ENTER PRESSURE READING FROM WALLACE-/
154          .ASCII  //<15><12>/TIERNAN GAUGE.  AIM FOR PRESSURES OF /
155          .ASCII  /ABOUT 0, 30, 60, 90, 120, AND 150 X 10 TORR./
156          .ASCII  //<12><200>//
157 PASK:    .ASCII  /P?/<11><200>//
158 ASKBUT:  .ASCII  //<12><12>/CHANGE BUTTERWORTH FILTER, Y OR N?/
159          .ASCII  //<11><11><200>//
160 TASK:    .ASCII  //<12>/ENTER SAMPLE TEMPERATURE SIGNAL IN VOLTS:/
161          .ASCII  //<11><200>//
162 WAITPR:  .ASCIZ  //<12><12>/ENTER G TO START SCAN/
163          .EVEN
164
165 ADC:     CMP     CHAN,#5         ;DOES IT ASK FOR ADC 5?
166          BNE     NOTBAD          ;NO,GO ON.
167          MOV     #2,CHAN         ;YES, SUBSTITUTE ADC 2.
168 NOTBAD:  ADC     CHAN,DEST       ;ROUTINE TO READ ADC'S
169          RTS     PC
170
171 CHAN:    .WORD   0
172 DEST:    .WORD   0
173 PSTD:    .WORD   0
174 HTBUFF:  .WORD   0
175 LTBUFF:  .WORD   0
176
177 GMSGE:   .ASCII  /ENTER S TO STOP SCAN; TO ENTER NEW SAMPLE /
178          .ASCIZ  /TEMPERATURE, TYPE T AND ENTER VOLTAGE./
179          .EVEN
180
181 START:   .PRINT  #GMSGE
182          CLR     BUSTAT
183          MOV     #3,CHAN
184          JSR     PC,ADC          ;NOTE INITIAL PRESSURE.
185          MOV     DEST,PSTD
```

```
186 SCAN:   .TTINR                  ;CHECK CONSOLE FOR INPUT
187         BCS     NOINPT
188         JMP     INPUT
189 NOINPT: MOV     #3,CHAN         ;NO CONSOLE INPUT-- LOOK AT SIGNALS
190         JSR     PC,ADC          ;LOOK AT PRESSURE (ADC #3)
191         CMP     DEST,PSTD       ;IS IT HIGH ENOUGH TO TAKE DATA?
192         BLT     SCAN            ;NO, GO BACK
193         ADD     #3,PSTD         ;YES, SET NEXT P TO LOOK FOR
194         JSR     PC,ADC          ;READ   PRESSURE
195         MOV     DEST,(R3)+      ;STORE PRESSURE DATA
196         INC     CHAN
197         JSR     PC,ADC          ;READ A/R ADC (#4)
198         MOV     DEST,(R3)+      ;STORE A/R DATA
199         INC     CHAN
200         JSR     PC,ADC          ;READ B/R ADC (#5)
201         MOV     DEST,(R3)+      ;STORE B/R DATA
202         MOV     HTBUFF,(R3)+    ;STORE TEMPERATURE DATA
203         MOV     LTBUFF,(R3)+
204         MOV     -10(R3),DATA
205         JSR     PC,BUTTER       ;FILTER AND SCALE ADC READING
206                                 ;FOR A/R
207         MOV     R0,@#176760     ;PUT OUT A/R ON DAC 1
208         BIS     #200,@#BUSTAT
209         MOV     -6(R3),DATA
210         JSR     PC,BUTTER       ;FILTER AND SCALE B/R ADC READING
211         MOV     R0,@#176762     ;PUT OUT B/R ON DAC 2
212         BIC     #200,@#BUSTAT
213         BIS     #100000,@#BUSTAT
214         BR      SCAN            ;CONTINUE SCAN
215
216 SCALE:  TST     R1
217         BGE     NOMIN           ;RETURN FROM FILTER CAN BE LESS
218                                 ;THAN ZERO.
219         CLR     R1              ;IF SO, SET TO ZERO.
220 NOMIN:  CMP     #2314,R1        ;ROUTINE TO SCALE ADC READING
221         BGE     NOSPYK          ;FOR OUTPUT ON DAC
222         MOV     #2314,R1
223 NOSPYK: MUL     #5,R1
224         CLR     R0
225         DIV     #3,R0
226         RTS     PC
227
228 LIMIT:  .LIMIT                  ;PROGRAM STATS WILL GO HERE
229
230 GETTMP: JSR     PC,GETDEC       ;ROUTINE TO GET SAMPLE TEMP
231         MOV     HP,HTBUFF
232         MOV     LP,LTBUFF
233         RTS     PC
234
235 INPUT:  BIC     #177600,R0      ;MASK ASCII PARITY BIT
236         CMP     R0,#15          ;IS IT A CR?
237         BEQ     GOBAK           ;YES, IGNORE
238         CMP     R0,#12          ;NO, IS IT A LF?
239         BEQ     GOBAK           ;YES, IGNORE
240         CMP     R0,#124         ;NO, IS IT A T?
241         BNE     SEEK            ;NO, KEEP TESTING
242         JSR     PC,GETTMP       ;YES, UPDATE TEMP BUFFER
243         BR      GOBAK
244 SEEK:   CMP     R0,#123         ;IS IT AN S?
245         BEQ     STOP            ;YES, STOP SCAN
246         .PRINT  #HUH            ;NO, BAD CHARACTER
247 GOBAK:  JMP     SCAN            ;CONTINUE SCAN
248 STOP:   .PRINT  #GORB           ;ASK WHETHER TO SAVE SCAN
249         JSR     R4,YORN         ;LOOK FOR Y OR N
250         BR      SAVIT           ;Y, SAVE SCAN
```

```
251          BR      THREW           ;NO, DON'T SAVE SCAN
252          BR      STOP            ;BAD CHARACTER, ASK AGAIN
253 THREW:   JMP     THRU
254 SAVIT:   SUB     LIMIT+2,R3      ;GET SIZE OF DATA BUFFER IN BYTES
255          ASR     R3              ;CHANGE TO SIZE IN WORDS
256          MOV     R3,LENGTH
257 SAVE:    FILRAD  DSBLK           ;ASK FOR FILNAME
258          CREATE  LIMIT+2,LENGTH,DSBLK,ERRWRD     ;SAVE DATA ON DY1
259          BCC     THRU            ;SUCCESSFUL CREATION, GO ON
260          JMP     ERANAL          ;UNSUCCESSFUL CREATION, ANALYZE
261 THRU:    .PRINT  #GORS           ;ASK WHETHER ALL DONE
262          JSR     R4,YORN         ;LOOK FOR Y OR N
263          BR      OUT             ;Y, END RUN
264          BR      RESTRT          ;N, START ANOTHER SCAN
265          BR      THRU            ;BAD CHARACTER, ASK AGAIN
266 RESTRT:  .PRINT  #NUPAGE
267          JMP     PRESCN
268
269 YORN:    .TTYIN                  ;ROUTINE TO LOOK FOR Y OR N
270          BIC     #177600,R0      ;MASK ASCII PARITY BIT
271          CMP     R0,#15          ;IS IT A CR?
272          BEQ     YORN            ;YES, IGNORE
273          CMP     R0,#12          ;NO, IS IT A LF?
274          BEQ     YORN            ;YES, IGNORE
275          CMP     R0,#131         ;IS IT A Y?
276          BEQ     CLRBUF          ;YES, RETURN FOR INSTRUCTION
277          TST     (R4)+           ;NO, INCREMENT MPROG PC
278          CMP     R0,#116         ;IS IT A N?
279          BEQ     CLRBUF          ;YES, RETURN FOR INSTRUCTION
280          .PRINT  #HUH            ;CHASTIZE USER FOR BAD CHARACTER
281          TST     (R4)+           ;INCREMENT MPROG PC
282 CLRBUF:  .TTINR
283          BCC     CLRBUF
284          RTS     R4              ;RETURN FOR INSTRUCTIONS
285
286 LENGTH:  .WORD   0
287 DSBLK:   .BLKW   4
288 ERRWRD:  .WORD   0
289 NUPAGE:  .ASCIZ  //<14>//
290 HUH:     .ASCIZ  /?/
291 GORB:    .ASCIZ  /SAVE SCAN, Y OR N?/
292 GORS:    .ASCIZ  /ALL DONE, Y OR N?/
293          .EVEN
294
295 ERANAL:  CMP     #10,ERRWRD      ;IS ERROR WORD VALUE 10?
296          BNE     OTHERR          ;NO, SOFT OR HARD ERROR
297          .PRINT  #ERR10          ;YES, USER ERROR-- INFORM
298          JMP     SAVE            ;RETURN FOR NEW FILSPECS
299 OTHERR:  .PRINT  #ERRVAL         ;TELL USER ERROR WORD VALUE
300          MOV     ERRWRD, NUM
301          JSR     PC,PROCT
302          .PRINT  #BEGVAL         ;TELL USER WHERE DATA BUFFER BEGINS
303          MOV     LIMIT+2,NUM
304          JSR     PC,PROCT
305          .PRINT  #LGTVAL         ;TELL USER LENGTH OF DATA BUFFER
306          MOV     R3,NUM
307          JSR     PC,PROCT
308
309 OUT:     MOV     #510,R0         ;STARTING ADDRESS FOR KEYBOARD
310                                  ;COMMAND BUFFER
311          MOV     #OUTCMD,R1      ;STARTING WORD FOR COMMAND
312 COMAND:  MOV     (R1)+,(R0)+     ;FILL COMMAND BUFFER WITH COMMAND
313          CMP     R1,#CMDDUN      ;COMMAND ALL TRANSFERRED?
314          BLO     COMAND          ;NO, KEEP FILLING
315          BIS     #4000,@#JSW     ;TELL COMPUTER IT'S GOT A KEYBOARD
```

```
316                                     ;COMMAND
317             CLR     R0              ;THIS HAS TO BE CLEARED
318             .EXIT
319
320 PROCT:  PROCT   NUM                 ;ROUTINE TO PRINT AN OCTAL NUMBER
321                                     ;FROM MEMORY
322             RTS     PC
323
324 NUM:      .WORD   0
325 OUTCMD: .WORD   CMDDUN-CMDSAY
326 CMDSAY: .ASCIZ  "DIRECTORY/COLUMNS:3/BLOCKS/VOL DY1:"
327 CMDDUN: .BYTE   0
328 ERR10:  .ASCIZ  /FILE ALREADY EXISTS ON DY1/
329 ERRVAL: .ASCII  /ERROR ENCOUNTERED; ERROR WORD VALUE = /<200>//
330 BEGVAL: .ASCII  //<15><12>/DATA BEGINS AT ADDRESS /<200>//
331 LGTVAL: .ASCII  //<15><12>/DATA LENGTH IN WORDS IS /<200>//
332             .EVEN
333
334
335
336             .END    PTUNE
```

## Grating-Tuned Data Acquisition: GTUNE

```
 1              .TITLE  GTUNE, GRATING-TUNING OF NRG LASER
 2 ;;
 3 ;;   GTUNE IS INTENDED FOR USE WHEN TUNING THE NRG PTL-2000 DYE
 4 ;;   LASER BY USING THE STEPPING MOTOR ON THE GRATING.  YOU MAY
 5 ;;   CHOOSE TO SEE THE HOOKUP INSTRUCTIONS.  YOU SELECT THE SCAN
 6 ;;   SPEED, DURATION AND DIRECTION; THE COMPUTER STEPS THE GRATING
 7 ;;   ACCORDINGLY.  THE NUMBER LABELLED "REF:" IS THE NUMBER OF
 8 ;;   TIMES THE GRATING WILL BE STEPPED PER DATA POINT COLLECTED.
 9 ;;   INTENSITIES OF TWO SIGNALS WILL BE STORED ALONG WITH
10 ;;   TEMPERATURE INFORMATION (YOU ENTER THE BALANCING VOLTAGE
11 ;;   ACROSS THE TEMPERATURE SENSOR THROUGH THE TELETYPE) AND
12 ;;   GRATING POSITION.  THE GRATING POSITION STORED WILL BE
13 ;;   RELATIVE TO WHERE IT WAS WHEN YOU STARTED THE PROGRAM.  WHEN A
14 ;;   SCAN IS OVER OR WHEN YOU STOP IT YOURSELF, YOU WILL BE GIVEN
15 ;;   THE OPTION OF SAVING THE DATA ON FLOPPY DISK.  (DATA FILES
16 ;;   SAVED WILL  EMULATE THOSE SAVED BY PROGRAM PTUNE, SO THERE
17 ;;   WILL BE SOME MEANINGLESS CALIBRATION INFORMATION IN THEM.)
18 ;;   YOU MAY THEN CONTINUE SCANNING OR END THE PROGRAM; WHEN YOU DO
19 ;;   THAT, A DIRECTORY OF YOUR DATA DISK WILL PRINT OUT.
20 ;;
21              .MCALL  .PRINT,.TTYIN,GETDEC,.TTINR
22              .MCALL  ADC,FILRAD,CREATE,.EXIT
23              .MCALL  PROCT,TTCLR,GETINT
24              .GLOBL  GETDEC
25              .GLOBL  HP,LP
26
27 KWPB=172542
28 KWCSR=172540
29 DRCSR=167770
30 DRINBUF=167774
31              JSW = 44
32
33 GTUNE:   BIS     #100,@#JSW      ;ENABLE CARRY BIT FOR TTINR
34              CLR     @STRAK          ;COUNTER FOR GRATING STEPS
35 FINDOU: .PRINT  #INTRO
```

```
36          JSR     R4,TORN         ;INSTRUCTIONS REQUIRED?
37          BR      TELALL          ;YES, GIVE INSTRUCTIONS
38          BR      PRESCN          ;NO, SKIP INSTRUCTIONS
39          BR      FINDOU          ;BAD CHARACTER,ASK AGAIN
40 TELALL:  .PRINT  #INSTRC         ;GIVE HOOKUP INSTRUCTIONS
41 PRESCN:  MOV     LIMIT+2,R3      ;POINT TO DATA BUFFER BEGINNING
42          CLR     DUMCNT          ;COUNTER FOR FALSE CALIBRATION DATA
43 CALFAK:  CLR     (R3)+           ;EMULATE AMBIENT CALIBRATION DATA
44          INC     DUMCNT          ;IN PTUNE
45          CMP     DUMCNT,#6
46          BLT     CALFAK
47 LPASK:   .PRINT  #VOLTS          ;ASK FOR LP INPUT FULL-SCALE INFO
48          .PRINT  #A
49          JSR     PC,GGTDEC
50          .PRINT  #VOLTS
51          .PRINT  #B
52          JSR     PC,GGTDEC
53          .PRINT  #VOLTS
54          .PRINT  #R
55          JSR     PC,GGTDEC
56          .PRINT  #PULSE          ;ASK FOR PULSE-AVGE. NUMBER
57          JSR     PC,GGTDEC
58          .PRINT  #REPS           ;GET REP RATE
59          JSR     PC,GGTDEC
60          MOV     #40400,DUMCNT   ;EMULATE TRANSDUCER CALIBRATION
61          MOV     #2,CNTR         ;IN PTUNE
62 FAKCAL:  MOV     DUMCNT,(R3)+
63          CLR     (R3)+
64          MOV     CNTR,(R3)+
65          ADD     #100,DUMCNT
66 INCRES:  INC     CNTR
67          CMP     CNTR,#4
68          BLE     FAKCAL
69          MOV     #141220,DUMCNT
70          INC     CNTR
71          CMP     CNTR,#6
72          BLE     FAKCAL
73          MOV     #041460,DUMCNT
74          CMP     CNTR,#10
75          BLE     FAKCAL
76          CLR     DUMCNT
77          ADD     #2,CNTR
78          CMP     CNTR,#14
79          BLE     FAKCAL
80 MRGMOV:  CLR     FLAG
81          .PRINT  #UPDOWN         ;ASK FOR SCAN DIRECTION
82          .TTYIN
83          CMP     R0,#104         ;IS IT DOWN?
84          BNE     NOTDWN          ;NO, GO ON.
85          BIS     #200,@#FLAG     ;YES, SET FLAG.
86          BIS     #1,@#DRCSR      ;ENABLE DOWN SCAN
87          BR      MOVON
88 NOTDWN:  CMP     R0,#125         ;IS IT UP?
89          BNE     MRGMOV          ;NO, ERROR OCCURRED.
90          BIC     #200,@#FLAG     ;YES, CLEAR FLAG.
91          BIC     #1,@#DRCSR      ;ENABLE UP SCAN
92 MOVON:   TTCLR
93          .PRINT  #VFEEL          ;ASK FOR # OF STEPS TO SCAN.
94          JSR     PC,GETGET
95          MOV     INTGR,STEPS
96          BIS     #100,@#JSW
97          TTCLR
98          .PRINT  #SPEED          ;ASK FOR SCAN SPEED.
99          JSR     PC,GETGET
100         CLR     R0
```

```
101          MOV     #10000.,R1
102          DIV     INTGR,R0        ;CALCULATE CLOCK PULSES PER STEP.
103          MOV     R0,@#KWPB
104          MOV     #0,@#106        ;PS VALUE FOR CLOCK INTERRUPTS.
105          MOV     #RUTEEN,@#104   ;INTERRUPT HANDLER
106 NOCO:    .PRINT  #TASK           ;GET SAMPLE TEMPERATURE
107          JSR     PC,GETTMP
108          .PRINT  #WAITPR         ;WAIT TO START SCAN
109 WAIT:    .TTYIN                  ;LOOK FOR CONSOLE INPUT
110          CMP     R0,#107         ;IS IT A G?
111          BNE     WAIT            ;NO, KEEP LOOKING
112          JMP     START           ;YES, START SCAN
113
114 GGTDEC:  JSR     PC,GETDEC       ;ROUTINE TO GET FP # AND STORE
115          MOV     HP,(R3)+        ;IN DATA BUFFER
116          MOV     LP,(R3)+
117          RTS     PC
118
119 GETDEC:  GETDEC  HP,LP           ;ROUTINE TO GET DECIMAL NUMBER
120          RTS     PC              ;FROM CONSOLE
121
122 HP:      .WORD   0
123 LP:      .WORD   0
124 CNTR:    .WORD   0
125 DUMCNT:  .WORD   0
126 RESCNT:  .WORD 0
127 RES:     .WORD 4
128 GSTRAK:  .WORD 0
129 INTRO:   .ASCII  //<14>/PROGRAM TO COLLECT DATA WHILE GRATING-TUNING/
130          .ASCII  / THE NRG LASER./<15><12><12>/HOOKUP INSTRUCTIONS /
131          .ASCII  /REQUIRED, Y OR N?/<11><11><200>//
132 INSTRC:  .ASCII  //<15><12><12><12>/MAKE CONNECTIONS:/<15><12><11>//
133          .ASCII  /ADC 4 TO A/<15><12><11>/ADC 2 TO B/<15><12><11>//
134          .ASCII  /DAC 1 TO UPPER PEN/<15><12><11>/DAC 2 TO LOWER /
135          .ASCII  /PEN/<15><12>/SET RECORDER AT 10 VOLTS FULL SCALE./
136          .ASCII  //<15><12>/SET LAMBDA-PHYSIK TO TRIGGER OFF LASER /
137          .ASCII  /"TRIG OUT."/<15><12>/WHEN PROMPTED TO 'ENTER,'/
138          .ASCII  / TYPE INFORMATION AND HIT RETURN OR LINEFEED./
139          .ASCIZ  //<15><12>/DATA ARE UNFILTERED./<12><12>//
140 VOLTS:   .ASCII  /LAMBDA-PHYSIK INPUT VOLTAGE FULL SCALE, /<200>//
141 A:       .ASCII  /A?/<11><200>//
142 B:       .ASCII  /B?/<11><200>//
143 R:       .ASCII  /R?/<11><200>//
144 REPS:    .ASCII  /REP RATE OF LASER, HZ?/<11><11><11><11><200>//
145 PULSE:   .ASCII  /NUMBER OF PULSES AVERAGED BY L-P?/<11><11><200>//
146 TASK:    .ASCII  //<12>/ENTER SAMPLE TEMPERATURE SIGNAL IN VOLTS:/
147          .ASCII  //<11><200>//
148 WAITPR:  .ASCIZ  //<12><12>/ENTER G TO START SCAN/
149          .EVEN
150
151 ADC:     ADC     CHAN,DEST       ;ROUTINE TO READ ADC'S
152          RTS     PC
153
154 CHAN:    .WORD   0
155 DEST:    .WORD   0
156 PSTD:    .WORD   0
157 HTBUFF:  .WORD   0
158 LTBUFF:  .WORD   0
159
160 GMSGE:   .ASCII  /ENTER S TO ABORT SCAN; TO ENTER NEW SAMPLE /
161          .ASCIZ  /TEMPERATURE, TYPE T AND ENTER VOLTAGE./
162          .EVEN
163
164 START:   CLR     DUMCNT
165          CLR     RESCNT
```

```
166          TSTB    @#FLAG          ;DETERMINE WHETHER TO INCREMENT OR
167          BPL     PLUSTP          ;DECREMENT GSTRAK
168          DEC     DUMCNT
169          BR      STAR
170 PLUSTP:  INC     DUMCNT
171 STAR:    .PRINT  #GMSGE
172          MOV     #113,@#KWCSR    ;START 10 KHZ CLOCK.
173 SCAN:    .TTINR                  ;CHECK CONSOLE FOR INPUT
174          BCS     NOINPT
175          JMP     INPUT
176 NOINPT:  WAIT
177          INC     RESCNT
178          CMP     RESCNT,RES
179          BLT     SCAN
180          CLR     RESCNT
181          MOV     GSTRAK,(R3)+    ;SAVE STEP #
182          MOV     #4,CHAN
183          JSR     PC,ADC          ;READ A/R ADC (#4)
184          MOV     DEST,(R3)+      ;STORE A/R DATA
185          MOV     #2,CHAN
186          JSR     PC,ADC          ;READ B/R ADC (#2)
187          MOV     DEST,(R3)+      ;STORE B/R DATA
188          MOV     HTBUFF,(R3)+    ;STORE TEMPERATURE DATA
189          MOV     LTBUFF,(R3)+
190          MOV     -10(R3),R1
191          JSR     PC,SCALE        ;SCALE ADC READING FOR A/R
192          MOV     R0,@#176760     ;PUT OUT A/R ON DAC 1
193          MOV     -6(R3),R1
194          JSR     PC,SCALE        ;SCALE B/R ADC READING
195          MOV     R0,@#176762     ;PUT OUT B/R ON DAC 2
196          TST     @#FLAG          ;DONE BIT SET?
197          BPL     SCAN            ;NO, KEEP STEPPING.
198          CLR     @#KWCSR         ;STOP CLOCK.
199          .PRINT  #DONE
200          JMP     STOP
201
202 GETGET: GETINT  INTGR
203          RTS     PC
204
205 RUTEEN: TST     @#DRINBUF       ;STEP GRATING.
206          ADD     DUMCNT,GSTRAK   ;KEEP TRACK
207          DEC     STEPS
208          TST     STEPS           ;ALL DONE?
209          BNE     BACK            ;NO, GO BACK.
210          BIS     #100000,@#FLAG  ;YES, SET DONE FLAG.
211 BACK:   RTI
212
213 FLAG:   .WORD   0
214 INTGR:  .WORD   0
215 STEPS:  .WORD   0
216
217 UPDOWN: .ASCII  /ENTER U FOR UPWARD SCAN, D FOR DOWNWARD SCAN:/
218          .ASCII  //<11><200>//
219 VFEEL:  .ASCII  /ENTER NUMBER OF STEPS TO MOVE (32000 MAXIMUM):/
220          .ASCII  //<11><200>//
221 SPEED:  .ASCII  /ENTER DESIRED SPEED (STEPS PER SECOND):/
222          .ASCII  //<11><200>//
223 DONE:   .ASCII  /READY FOR NEXT SCAN. (TYPE CONTROL-C TO ESCAPE /
224          .ASCII  /PROGRAM.)/<15><14><200>//
225          .EVEN
```

(lines 226-342 are the same as PTUNE lines 216-242.)

```
1         .TITLE  FPPROG, FILE-PROCESSING PROGRAM
2 ;;
3 ;;  THIS PROGRAM MUST BE USED TO PROCESS DATA COLLECTED BY PTUNE OR
4 ;   GTUNE TO GET IT INTO THE INTENSITY-VS-WAVELENGTH FORM EXPECTED
5 ;;  BY FPFIG AND MAN10.  CREATES NEW FILES BUT DOESN'T DESTROY THE
6 ;;  OLD.  ALLOWS YOU TO CORRECT ANY VALUES YOU MIS-ENTERED AT THE
7 ;;  START OF A SCAN.  FPPROG WAS ORIGINALLY WRITTEN TO PROCESS
8 ;;  PTUNE FILES, SO THE DOCUMENTATION IS SLANTED THAT WAY.  WHEN
9 ;;  PROCESSING A GTUNE FILE, SOME OF THE INFORMATION PRINTED OUT
10 ;;  WILL BE DUMMY DATA (AMBIENT CONDITIONS AT TIME OF RUN, E.G.)
11 ;;  FOR THE SAME REASON.  THE CALIBRATION INFORMATION REQUESTED
12 ;;  (PRESSURE-VS-WAVELENGTH) SHOULD HAVE BEEN DETERMINED WITH A
13 ;;  MONOCHROMATOR.  GENERALLY IT IS A GOOD IDEA TO SUBTRACT SOME
14 ;;  LARGE OFFSET FROM THE INTERCEPT WAVELENGTH SO THAT THE LEAST-
15 ;;  SQUARES FIT WON'T LOSE PRECISION UNNECESSARILY.  YOU WILL NEED
16 ;;  TO REMEMBER WHAT THAT OFFSET IS, HOWEVER, IF YOU EVER NEED TO
17 ;;  KNOW THE ABSOLUTE WAVELENGTH-- THE COMPUTER WON'T SAVE IT.  FOR
18 ;;  SCANS FROM GTUNE, THE SLOPE SHOULD BE ANGSTROMS PER STEP (IT'S
19 ;;  ABOUT .0017) AND THE INTERCEPT WHATEVER THE WAVELENGTH WAS
20 ;;  WHEN YOU STARTED GTUNE RUNNING (AGAIN, SUBJECT TO AN OFFSET).
21 ;;
22        .MCALL  .TTYOUT,.PRINT,.EXIT,TTCLR
23        .MCALL  PROCT,.TTYIN,CREATE
24        .GLOBL  PROCTF,GETFIL,LIMIT,GETDEC
25        .GLOBL  FILRAD,FLOAT,LSTFIT
26
27 FPPROG: .PRINT  #REQUES          ;ASK FOR FILE TO PROCESS.
28        MOV     #GFLIST,R5
29        MOV     #DSBLK,2(R5)
30        MOV     #BEGIN,4(R5)
31        MOV     #LENGTH,6(R5)
32        JSR     PC,GETFIL         ;CALL FILE INTO MEMORY.
33        MOV     LENGTH,R3
34        ASL     R3                ;COMPUTE LENGTH OF FILE
35        ADD     BEGIN,R3          ;COMPUTE EOF ADDRESS
36        MOV     R3,NEWBEG         ;SAVE AS STARTING ADDRESS FOR
37                                  ;NEW FILE.
38 CHECKS: CLR     CNTR
39        CLR     ERRFLG
40        CLR     FLAG
41        MOV     BEGIN,R2          ;POINT TO TOP OF FILE WITH R2
42        MOV     #BUF,R4           ;POINT R4 TO TOP OF '2000' LIST.
43 BLANKS: INC     CNTR
44        CMP     (R2)+,#042772
45        BEQ     DBLCHK
46        TST     (R2)+
47        BR      FULL
48 DBLCHK: TST     (R2)+             ;IS FILE ENTRY 2000?
49        BNE     FULL              ;NO, GO ON
50        MOV     #100000,(R4)+     ;YES, SET FLAG IN LIST
51        BR      SHIFT
52 FULL:  CLR     (R4)+             ;NO, CLEAR FLAG IN LIST.
53 SHIFT: CMP     CNTR,#11          ;WAS THAT P1?
54        BLT     ENDTST            ;NO, KEEP GOING.
55        TST     (R2)+             ;YES, SKIP V.
56 ENDTST: CMP     CNTR,#16          ;WAS IT P6?
57        BLT     BLANKS            ;NO, CONTINUE EXAMINING.
58        CLR     CNTR
59        MOV     #BUF,R4           ;INFORM USER OF '2000' LOCATIONS:
60        MOV     #MSG1,WRITE       ;POINT TO FIRST VARIABLE NAME.
```

```
61 TRANSF: INC     CNTR
62         TST     (R4)+          ;IS FLAG SET IN LIST?
63         BEQ     NEXMES         ;NO, GO ON.
64         TSTB    @#FLAG         ;WAS THIS THE FIRST 2000?
65         BMI     LISTIT         ;NO, GO ON.
66         BIS     #200,@#FLAG    ;YES, MAKE A NOTE.
67         .PRINT  #EXPLAN        ;INFORM USER THERE ARE MISSING
68                                ;QUANTITIES.
69 LISTIT: .PRINT  WRITE          ;SAY WHICH VALUE IS MISSING.
70         .PRINT  #CRLF
71 NEXMES: ADD     #7,WRITE       ;POINT TO NEXT VARIABLE NAME.
72         CMP     CNTR,#16       ;WAS THAT THE LAST VALUE?
73         BLT     TRANSF         ;NO, KEEP GOING.
74         MOV     #DSBLK,R4
75         MOV     (R4)+,(R3)+    ;PUT OLD FILE NAME AT TOP OF
76         MOV     (R4)+,(R3)+    ;NEW FILE.
77         MOV     (R4)+,(R3)+
78         MOV     (R4)+,(R3)+
79         TSTB    @#FLAG         ;WERE THERE 2000 VALUES?
80         BMI     SUBST          ;YES, GO TO SUBSTITUTION ROUTINE.
81         MOV     #200,(R3)+     ;NO, MARK POSITION IN NEW FILE
82         JMP     SCALE          ;AND SKIP ROUTINE.
83 SUBST:  SUB     #10,R3         ;MARK POSITION IN FILE.
84         MOV     R3,2(R5)
85         ADD     #10,R3
86         CLR     (R3)+
87         MOV     R3,R1          ;POINT R1 TO TOP OF LIST.
88         ADD     #34,R3         ;POINT R3 TO TOP OF FILE
89         MOV     R3,LIMIT+2
90         MOV     #START,4(R5)
91         MOV     #WORDS,6(R5)
92         .PRINT  #GETNEW        ;ASK FOR SUBSTITUTION-FILE
93         JSR     PC,GETFIL      ;STORE NAME AND FILE AT END OF
94                                ;EVERYTHING.
95         MOV     BEGIN,R2       ;POINT R2 TO TOP OF OLD FILE
96         MOV     #BUF,R4        ;POINT R4 TO TOP OF OLD LIST
97         CLR     CNTR
98 MAKSUB: INC     CNTR
99         TST     (R4)+          ;WAS LOCATION A 2000?
100        BEQ     NOSUB          ;NO, GO ON.
101        MOV     #100000,(R1)+  ;YES, NOTE IN NEW LIST
102        MOV     (R3)+,(R2)+    ;AND MAKE SUBSTITUTION.
103        MOV     (R3)+,(R2)+
104        BR      CONT
105 NOSUB: CLR     (R1)+          ;NO, NOTE IN NEW LIST
106        ADD     #4,R3          ;AND POINT TO NEXT LOCATION.
107        ADD     #4,R2
108        CMP     CNTR,#11
109        BLT     MAKSUB
110        TST     (R3)+
111        TST     (R2)+
112        BR      NOTHER
113 CONT:  CMP     CNTR,#11       ;WAS THAT P1 OR MORE?
114        BLT     MAKSUB         ;NOT YET, GO BACK.
115        MOV     (R3)+,(R2)+
116 NOTHER: CMP    CNTR,#16       ;WAS THAT THE LAST ONE?
117        BLT     MAKSUB         ;NO, GO BACK.
118        SUB     #104,R3        ;YES, RESTORE R3 TO TOP
119                               ;OF DATA FILE.
120        JMP     CHECKS         ; CHECK FOR 2000'S AGAIN.
121 SCALE: MOV     BEGIN,R2       ;POINT R2 TO TOP OF ORIGINAL FILE.
122        MOV     #037231,(R3)   ;PUT .075012 IN STACK.
123        MOV     #117744,2(R3)
124        MOV     4(R2),4(R3)    ;PUT PAMBUALL IN STACK.
125        MOV     6(R2),6(R3)
```

```
126             FMUL    R3              ;COMPUTE PAMBWALL IN CM HG
127             SUB     #4,R3
128             MOV     (R2)+,(R3)      ;PUT PAMBGAUGE IN STACK.
129             MOV     (R2)+,2(R3)
130             FSUB    R3              ;COMPUTE OFFSET.
131             .PRINT  #PIS            ;INFORM USERS OF PAMBS.
132             SUB     #4,R3
133             MOV     (R3)+,HNUM
134             MOV     (R3)+,LNUM
135             MOV     #PRBUF,R5
136             JSR     PC,PROCTF
137             .PRINT  #DELTIS
138             MOV     (R3)+,HNUM
139             MOV     (R3)+,LNUM
140             JSR     PC,PROCTF
141             .PRINT  #ENDSEN
142             CLR     CNTR
143             ADD     #4,R2
144             MOV     #MSG3,WRITE
145 TELL:       MOV     (R2)+,(R3)
146             MOV     (R3)+,HNUM
147             MOV     (R2)+,(R3)
148             MOV     (R3)+,LNUM
149             .PRINT  WRITE
150             JSR     PC,PROCTF       ;PRINT & TRANSFER VARIABLE VALUE.
151             .PRINT  #CRLF
152             ADD     #7,WRITE        ;POINT TO NEXT NAME.
153             INC     CNTR
154             CMP     CNTR,#6         ;HAS REPS BEEN DONE YET?
155             BLT     TELL            ;NO, CONTINUE PRINTING.
156             .PRINT  #ANYCH          ;YES, ASK USER FOR CHANGES.
157             .TTYIN
158             CMP     R0,#45          ;ARE THERE CHANGES?
159             BNE     NXTPHS          ;NO, GO ON.
160             TTCLR                   ;YES, ASK USER TO SPECIFY.
161             MOV     #MSG1,WRITE     ;POINT TO PAMBG.
162             MOV     BEGIN,R2
163             CLR     CNTR
164             .PRINT  #INST           ;INSTRUCT USER.
165 CHANGE:    .PRINT  WRITE           ;ASK FOR VARIABLE CHANGE.
166             INC     CNTR
167             .TTYIN
168             CMP     R0,#45          ;CHANGE THIS VARIABLE?
169             BNE     SKIP            ;NO, GO ON.
170             JSR     PC,GETDEC       ;YES, GET VALUE
171             MOV     HNUM,(R2)+      ;TRANSFER VALUES TO POSITION
172             MOV     LNUM,(R2)+      ;IN OLD FILE.
173             BR      MOVON
174 SKIP:      TTCLR
175             TST     (R2)+           ;POINT TO NEXT VARIABLE.
176             TST     (R2)+
177 MOVON:     ADD     #7,WRITE
178             CMP     CNTR,#10        ;HAVE WE DONE REPS?
179             BLT     CHANGE          ;NO, GO BACK.
180             SUB     #40,R3          ;YES, POINT TO TOP OF LIST
181                                     ;IN NEW FILE.
182             JMP     SCALE           ;AND FILL WITH NEW INFO.
183 NXTPHS:    TTCLR
184             CLR     CNTR
185             TST     -(R2)
186             MOV     #GFLIST,R5
187 FLVOLT:    ADD     #6,R2           ;POINT TO V IN OLD FILE.
188             MOV     R2,2(R5)
```

```
189         MOV     R3,4(R5)
190         TST     (R3)+
191         MOV     R3,6(R5)
192         TST     (R3)+
193         JSR     PC,FLOAT        ;FLOAT V AND STORE IN NEW FILE.
194         INC     CNTR
195         CMP     CNTR,#6         ;WAS THAT V6?
196         BLT     FLVOLT          ;NO,KEEP GOING.
197         CLR     CNTR
198         SUB     #42,R2          ;POINT TO TOPS OF P AND V LISTS.
199         SUB     #30,R3
200         MOV     #LSTBUF,R5
201         TST     (R5)+
202 FILBUF: MOV     R3,(R5)+        ;TRANSFER P AND V ADDRESSES
203         TST     (R3)+           ;TO LSTBUF.
204         MOV     R3,(R5)+
205         TST     (R3)+
206         MOV     R2,(R5)+
207         TST     (R2)+
208         MOV     R2,(R5)+
209         TST     (R2)+
210         TST     (R2)+
211         INC     CNTR
212         CMP     CNTR,#6         ;WAS THAT THE SIXTH POINT?
213         BLT     FILBUF          ;NO, RETURN.
214 LINE:   MOV     #LSTBUF,R5
215         JSR     PC,LSTFIT       ;YES, RUN REGRESSION ON P/V'S.
216         .PRINT  #SLOPE          ;PRINT EQUATION OF LINE.
217         MOV     #HB,R4
218         MOV     #PRBUF,R5
219         JSR     PC,SPILL
220         .PRINT  #INTCPT
221         JSR     PC,SPILL
222         .PRINT  #ENDEQ
223         JSR     PC,SPILL        ;PRINT CORRELATION COEFFICIENT.
224         .PRINT  #HEDLIN
225         MOV     #60,R1
226         SUB     #44,R2
227         MOV     R2,PTOP         ;SAVE LOCATIONS OF P'S AND V'S.
228         SUB     #30,R3
229         MOV     R3,VTOP
230         TSTB    ERRFLG
231         BPL     SPEAK
232         JMP     NOCHNG
233 SPEAK:  MOV     (R3)+,HV        ;PUT P AND V IN STACK
234         MOV     (R3)+,LV
235         MOV     (R2)+,HPR
236         MOV     (R2)+,LPR
237         TST     (R2)+
238         MOV     HA,HINT
239         MOV     LA,LINT
240         INC     R1
241         MOV     R1,R0
242         .TTYOUT                 ;PRINT I.
243         MOV     #HV,R4
244         JSR     PC,SPILHT       ;PRINT V.
245         MOV     #HPR,R4
246         JSR     PC,SPILHT       ;PRINT P.
247         MOV     #HB,R4          ;COMPUTE DELTA-P
248         FMUL    R4
249         FADD    R4
250         FSUB    R4
251         SUB     #4,R4
252         MOV     HSIGMA,(R4)
253         MOV     LSIGMA,2(R4)
```

```
254          FDIV    R4              ;COMPUTE DELTA-P:SIGMA RATIO
255          JSR     PC,SPILHT       ;PRINT RATIO.
256          .PRINT  #CRLF
257          CMP     R1,N            ;WAS THAT ALL POINTS?
258          BLT     SPEAK           ;NO, RETURN.
259          .PRINT  #OKCHEK         ;ASK FOR DELETIONS.
260          .TTYIN
261          CMP     R0,#45          ;ARE THERE CHANGES TO MAKE?
262          BNE     NOCHNG          ;NO, SKIP ROUTINE.
263          TTCLR
264 WHATI:   .PRINT  #WHICH          ;ASK WHICH I TO DELETE.
265          .TTYIN
266          CMP     R0,N            ;IS REQUESTED I ILLEGAL?
267          BGT     ERR
268          SUB     #60,R0          ;NO,CALCULATE NUMBER.
269          BGT     FINE
270 ERR:     TTCLR
271          .PRINT  #MISTAK
272          BR      WHATI
273 FINE:    MOV     R0,N
274          TTCLR
275          DEC     N               ;RE-CALCULATE N.
276          MOV     PTOP,R2         ;POINT TO P, V, AND LSTBUF LISTS.
277          MOV     VTOP,R3
278          MOV     #LSTBUF,R5
279          CLR     CNTR
280          SUB     #4,(R5)         ;RE-CALCULATE # OF PTS. IN LSTBUF.
281          MOV     (R5)+,COMPAR
282          SUB     #12,COMPAR
283 MAYBE:   INC     CNTR            ;POINT TO ENTRY.
284          CMP     CNTR,N          ;IS IT THE ONE TO DELETE?
285          BGE     ERASE           ;YES, DELETE IT.
286          ADD     #4,R3           ;NO, SKIP IT.
287          ADD     #6,R2
288          ADD     #10,R5
289          BR      MAYBE           ;LOOK AT NEXT ONE.
290 ERASE:   MOV     N,CNTR
291          ADD     N,CNTR          ;GET 2N IN CNTR.
292          MOV     CNTR,NMULT
293 MOVEV:   MOV     4(R3),(R3)+     ;COLLAPSE V LIST.
294          INC     CNTR
295          CMP     CNTR,#14
296          BLT     MOVEV
297          MOV     NMULT,CNTR
298          ADD     N,CNTR          ;GET 3N IN CNTR.
299          MOV     CNTR,NMULT
300 MOVEP:   MOV     6(R2),(R2)+     ;COLLAPSE P LIST.
301          INC     CNTR
302          CMP     CNTR,#22
303          BLT     MOVEP
304          MOV     NMULT,CNTR
305          ADD     N,CNTR          ;GET 4N IN CNTR.
306 MOVLOC:  TST     (R5)+
307          INC     CNTR
308          CMP     CNTR,COMPAR
309          BLT     MOVLOC
310 COLAPS:  MOV     10(R5),(R5)+    ;COLLAPSE LSTBUF.
311          INC     CNTR
312          CMP     CNTR,#46
313          BLT     COLAPS
314          MOV     VTOP,R3
315          MOV     PTOP,R2
316          ADD     #44,R2
317          ADD     #30,R3
318          JMP     LINE            ;RETURN TO CALCULATE LINE AGAIN.
```

```
319 NOCHNG: MOV     PTOP,R2
320         ADD     #44,R2
321         ADD     #2,VTOP         ;SAVE LOCATION FOR NEW FILE'S
322                                 ;LENGTH
323         MOV     VTOP,R3         ;POINT TO FIRST LOCATION AFTER
324                                 ;LENGTH IN NEW FILE.
325         MOV     HA,4(R3)        ;PUT P VS. V INTERCEPT IN STACK.
326         MOV     LA,6(R3)
327         TTCLR
328         .PRINT  #GETSLP         ;GET WAVELENGTH-VS.-P SLOPE.
329         MOV     #PRBUF,R5
330         JSR     PC,GETDEC
331         MOV     HNUM,(R3)       ;STORE IN STACK.
332         MOV     LNUM,2(R3)
333         .PRINT  #GTINT          ;GET WAVELENGTH-VS-P INTERCEPT.
334         JSR     PC,GETDEC
335         MOV     HNUM,10(R3)     ;STORE IN STACK.
336         MOV     LNUM,12(R3)
337         FMUL    R3
338         FADD    R3              ;CALCULATE WAVELENGTH-VS-V
339         MOV     (R3),HA         ;INTERCEPT.
340         MOV     2(R3),LA
341         MOV     VTOP,R3
342         MOV     HB,4(R3)        ;PUT P-VS-V SLOPE IN STACK.
343         MOV     LB,6(R3)
344         FMUL    R3
345         MOV     (R3),HB
346         MOV     2(R3),LB        ;CALCULATE WAVELENGTH-VS-V SLOPE.
347         ADD     #10,R3          ;POINT TO TOP OF DATA BUFFER.
348         MOV     BEGIN,R4
349         ADD     #10,R4
350         MOV     14(R4),(R4)
351         MOV     16(R4),2(R4)
352         FDIV    R4
353         MOV     (R4),HASCL
354         MOV     2(R4),LASCL
355         MOV     10(R4),(R4)
356         MOV     12(R4),2(R4)
357         FDIV    R4
358         MOV     (R4),HBSCL
359         MOV     2(R4),LBSCL
360         MOV     #42,CNTR
361         MOV     #GFLIST,R5
362 ATLAST: MOV     R2,2(R5)
363         TST     (R2)+
364         MOV     R3,4(R5)
365         MOV     R3,6(R5)
366         ADD     #2,6(R5)
367         JSR     PC,FLOAT
368         MOV     HB,4(R3)
369         MOV     LB,6(R3)
370         MOV     HA,10(R3)
371         MOV     LA,12(R3)
372         FMUL    R3
373         FADD    R3
374         MOV     (R3),-10(R3)
375         MOV     2(R3),-6(R3)
376         MOV     R2,2(R5)
377         TST     (R2)+
378         MOV     R3,4(R5)
379         MOV     R3,6(R5)
380         ADD     #4,4(R5)
381         ADD     #6,6(R5)
382         JSR     PC,FLOAT
383         MOV     HASCL,(R3)
```

```
384             MOV     LASCL,2(R3)
385             FMUL    R3
386             SUB     #10,R3
387             MOV     HBSCL,(R3)
388             MOV     LBSCL,2(R3)
389             MOV     R2,2(R5)
390             TST     (R2)+
391             MOV     R3,4(R5)
392             MOV     R3,6(R5)
393             ADD     #4,4(R5)
394             ADD     #6,6(R5)
395             JSR     PC,FLOAT
396             FMUL    R3
397             MOV     (R2)+,-4(R3)
398             MOV     (R2)+,-2(R3)
399             ADD     #10,R3
400             ADD     #5,CNTR
401             CMP     CNTR,LENGTH
402             BLT     ATLAST
403             SUB     NEWBEG,R3
404             ASR     R3
405             MOV     R3,NULONG
406             MOV     VTOP,R4
407             TST     -(R4)
408             MOV     R3,(R4)
409             .PRINT  #GETNAM
410 NAME:       MOV     #NAMBUF,R5
411             JSR     PC,FILRAD
412             CREATE  NEWBEG,NULONG,DSBLK,ERRWRD
413             BCS     NOKAY
414             JMP     OKAY
415 NOKAY:      CMP     ERRWRD,#10
416             BNE     OTHERR
417             .PRINT  #BADNAM
418             JMP     NAME
419 OTHERR:     .PRINT  #CRERR
420             ADD     #60,ERRWRD
421             MOV     ERRWRD,R0
422             .TTYOUT
423             .PRINT  #ALL
424             MOV     #NAME,RESTRT
425             PROCT   RESTRT
426 OKAY:       .PRINT  #OVRMES
427
428             .EXIT
429 SPILL:      MOV     (R4)+,HNUM
430             MOV     (R4),LNUM
431             SUB     #6,R4
432             JSR     PC,PROCTF
433             RTS     PC
434
435
436 SPILHT:     .PRINT  #HT
437             JSR     PC,SPILL
438             RTS     PC
439 DSBLK:      .BLKW   4
440 BEGIN:      .WORD   0
441 LENGTH:     .WORD   0
442 CNTR:       .WORD   0
443 FLAG:       .WORD   0
444 BUF:        .BLKW   16
445 WRITE:      .WORD   0
446 NEWBEG:     .WORD   0
447 PRBUF:      .WORD   2
448             .WORD   HNUM
449             .WORD   LNUM
450 HNUM:       .WORD   0
451 LNUM:       .WORD   0
452 GFLIST:     .WORD   3
453             .BLKW   3
454 START:      .WORD   0
455 WORDS:      .WORD   0
456 N:          .WORD   66
457 LSTBUF:     .WORD   46
458             .BLKW   30
459             .WORD   15
460             .WORD   HB
461             .WORD   LB
462             .WORD   HA
463             .WORD   LA
464             .WORD   HR
465             .WORD   LR
466             .WORD   HSIGMA
467             .WORD   LSIGMA
468             .WORD   HSIGB
469             .WORD   LSIGB
470             .WORD   HSIGAY
471             .WORD   LSIGAY
472             .WORD   ERRFLG
473 HSIGB:      .WORD   0
474 LSIGB:      .WORD   0
475 HSIGAY:     .WORD   0
476 LSIGAY:     .WORD   0
477 HSIGMA:     .WORD   0
478 LSIGMA:     .WORD   0
479 HR:         .WORD   0
480 LR:         .WORD   0
481 HA:         .WORD   0
482 LA:         .WORD   0
483 HB:         .WORD   0
484 LB:         .WORD   0
485 HV:         .WORD   0
486 LV:         .WORD   0
487 HINT:       .WORD   0
488 LINT:       .WORD   0
489 HPR:        .WORD   0
490 LPR:        .WORD   0
491 M:          .WORD   0
492 PTOP:       .WORD   0
493 VTOP:       .WORD   0
494 HASCL:      .WORD   0
495 LASCL:      .WORD   0
496 HBSCL:      .WORD   0
497 LBSCL:      .WORD   0
498 NULONG:     .WORD   0
499 NAMBUF:     .WORD   1
500             .WORD   DSBLK
501 ERRWRD:     .WORD   0
502 RESTRT:     .WORD   0
503 MMULT:      .WORD   0
504 COMPAR:     .WORD   0
505 ERRFLG:     .WORD   0
```

```
506 ALL:    .ASCII  /./<15><12>/FILE CREATION BEGINS AT /<200>//
507 ANYCH:  .ASCII  //<12>/ENTER Z TO MAKE CHANGES IN THE FIRST 8 /
508         .ASCII  /VARIABLES./<11><200>//
509 BADNAM: .ASCIZ  /FILE ALREADY EXISTS--CHOOSE ANOTHER NAME./
510 CRERR:  .ASCII  /FILE CREATION ERROR; VALUE OF ERROR WORD IS /
511         .ASCII  //<200>//
512 CRLF:   .ASCIZ  //
513 DELTIS: .ASCII  / TORR X 10, WHICH IS /<200>//
514 ENDEQ:  .ASCII  /)/<15><12>/R = /<200>//
515 ENDSEN: .ASCII  / TORR X 10 LESS THAN THE HG BAROMETER READING./
516         .ASCIZ  //<12>//
517 EXPLAN: .ASCII  /THE FOLLOWING QUANTITIES REQUIRE SUBSTITUTION /
518         .ASCIZ  /FROM ANOTHER FILE:/
519 GETNAM: .ASCII  /FILE IS PROCESSED.  CHOOSE A NAME FOR THE NEW /
520         .ASCIZ  /FILE (ENABLE DRIVES!)./
521 GETNEW: .ASCIZ  /CHOOSE A FILE FROM WHICH TO SUBSTITUTE./
522 GETSLP: .ASCII  /SLOPE OF WAVELENGTH (Y) VS. P (X) CALIBRATION:/
523         .ASCII  //<11><200>//
524 GTINT:  .ASCII  /INTERCEPT:/<11><200>//
525 HEDLIN: .ASCII  //<12><12><15>/I/<11>/V/<11><11>/P/<11><11>//
526         .ASCIZ  /# OF DEVS P(I) IS OFF/<12>//
527 HT:     .ASCII  //<11><200>//
528 INTCPT: .ASCII  /)V + (/<200>//
529 INST:   .ASCII  /TO MAKE CHANGE WHEN PROMPTED, STRIKE Z AND THEN /
530         .ASCIZ  /ENTER NUMBER./
531 MISTAK: .ASCIZ  /YOU CAN'T CHOOSE THAT VALUE FOR I./
532 MSG1:   .ASCII  /PAMBG /<200>//
533 MSG2:   .ASCII  /PAMBW /<200>//
534 MSG3:   .ASCII  /TAMB  /<200>//
535 MSG4:   .ASCII  /V(A)  /<200>//
536 MSG5:   .ASCII  /V(B)  /<200>//
537 MSG6:   .ASCII  /V(R)  /<200>//
538 MSG7:   .ASCII  /PULSE /<200>//
539 MSG8:   .ASCII  /REPS  /<200>//
540 MSG9:   .ASCII  /P#1   /<200>//
541 MSG10:  .ASCII  /P#2   /<200>//
542 MSG11:  .ASCII  /P#3   /<200>//
543 MSG12:  .ASCII  /P#4   /<200>//
544 MSG13:  .ASCII  /P#5   /<200>//
545 MSG14:  .ASCII  /P#6   /<200>//
546 OKCHEK: .ASCII  //<15><12><12>/ENTER Z TO DELETE A POINT /
547         .ASCII  /(YOU MUST LEAVE AT LEAST THREE POINTS):/
548         .ASCII  //<11><200>//
549 OVRMES: .ASCIZ  /THAT'S ALL, FOLKS!/
550 PIS:    .ASCII  //<12>/AMBIENT P FROM GAUGE:/<11><200>//
551 REQUES: .ASCII  //<12><12>/FILE-PROCESSING PROGRAM FOR DATA/
552         .ASCII  /FROM PTUNE:/<15><12><12><12>/CHOOSE FILE TO BE /
553         .ASCIZ  /PROCESSED./
554 SLOPE:  .ASCII  //<12>/P = (/<200>//
555 WHICH:  .ASCII  /DELETE WHICH POINT?  ENTER I:/<11><200>//
556         .EVEN
557         .END    FPPROG
```

## Other Software

Following are descriptions of routines used by PTUNE, GTUNE, and FPPROG and not provided by Digital Equipment Corporation (listings are available on request):

```
;;   HNDLER IS A PROGRAM WRITTEN TO DRAW A DATA FILE CREATED BY
;;   PROGRAM FPPROG ON THE HEATH TWO-PEN RECORDER. THE USER IS
;;   INFORMED OF ALL THE DIFFERENT TEMPERATURE ENTRIES DURING THE
;;   SCAN AND AT WHAT WAVELENGTH THEY WERE ENTERED.  THE FIRST
;;   TEMPERATURE IN THE LIST GIVES THE STARTING WAVELENGTH FOR THE
;;   SCAN.  IF AN OFFSET WAS SUBTRACTED BY PROGRAM FPPROG, THE
;;   WAVELENGTHS WILL ALL BE OFFSET.  THE USER MAY THEN CHOOSE
;;   WHETHER TO DRAW THE SCAN AND, IF SO, HOW COARSELY THE DATA
;;   SHOULD BE READ.  THE USER SELECTS CHART EXPANSION AND MARKER
;;   SPACING.  THIS PROGRAM ALSO GIVES THE OPTION OF ENSEMBLE-
;;    AVERAGING TWO OR MORE FILES.
;;
;;
;;  BUTTER IS A SUBROUTINE TO PERFORM DIGITAL BUTTERWORTH FILTER ON
;;   INPUT DATA.  USES FILTER COEFFICIENTS COMPUTED IN SUBROUTINE
;;   PARKAY.
;;
;;
;;  FILRAD IS A SUBROUTINE TO ALLOW USER TO ENTER A FILE NAME WHILE
;;   PROGRAM IS RUNNING.  USES MACRO FILRAD FROM LIBRARY MYMACS.
;;
;;
;;  FIX IS A SUBROUTINE IN SYLLIB WHICH CONVERTS A FLOATING-POINT
;;   NUMBER X, IN MEMORY, TO A FIXED-POINT X, AND RETURNS THE
;;   RESULT TO A SINGLE MEMORY LOCATION.
;;
;;
;;  FLOAT IS A SUBROUTINE TO USE MACRO FLOAT.  FLOATS AN INTEGER N,
;;   RETURNING THE VALUE IN HP AND LP.
;;
;;
;;  GETDEC IS A SUBROUTINE WHICH USES MACRO GETDEC.  TAKES DECIMAL
;;   INPUT FROM THE CONSOLE KEYBOARD, CONVERTS IT TO OCTAL FLOATING
;;   POINT IN MEMORY.
;;
;;
;;  GETFIL IS A SUBROUTINE WHICH ALLOWS USER TO NAME FILE
;;   INTERACTIVELY AND THEN READS IT INTO MEMORY.  RETURNS VALUES
;;   FOR FILE LENGTH AND AN ERROR WORD DEFINED BY RECALL.
;;
;;
;;  LSTFIT IS A SUBROUTINE WHICH COMPUTES THE BEST LINE THROUGH A
;;   SET OF N POINTS (X,Y) BY LINEAR REGRESSION.
;;
;;
;;  PARKAY IS A SUBROUTINE TO COMPUTE COEFFICIENTS FOR USE BY THE
;;   BUTTERWORTH FILTER ROUTINE BUTTER.
```

```
;;  PROCTF IS A SUBROUTINE WHICH PRINTS AN OCTAL NUMBER, IN MEMORY,
;;   ON THE TELETYPE AS A FLOATING-POINT DECIMAL NUMBER.
;;
;;
;;  ROOTF IS A SUBROUTINE WHICH COMPUTES THE N-TH ROOT OF X, WHERE
;;   X IS A FLOATING-POINT NUMBER IN MEMORY, AND RETURNS A
;;   FLOATING-PONT ANSWER TO MPROG.
;;
;;
;;  ADC IS A MACRO WHICH READS A SIGNAL FROM AN ANALOG-TO-DIGITAL
;;   CONVERTER CHANNEL.  THE CALL IS OF THE FORM:
;;                       ADC  ARG1,ARG2
;;   WHERE ARG1 CONTAINS THE CHANNEL NUMBER (#0-7) AND ARG2 IS THE
;;   LOCATION  OF THE RESULT.
;;
;;
;;  CREATE IS A MACRO WHICH WRITES DATA FROM MEMORY ONTO DY1.
;;   THE CALL IS OF THE FORM:
;;                       CREATE  ARG1,ARG2,ARG3,ARG4
;;   WHERE ARG1 IS AN ADDRESS CONTAINING THE LOW ADDRESS OF THE
;;   DATA BUFFER IN MEMORY, ARG2 IS AN ADDRESS CONTAINING THE
;;   (OCTAL) LENGTH IN WORDS OF THE DATA BUFFER, ARG3 IS THE LOW
;;   ADDRESS OF A FOUR-WORD BLOCK OF MEMORY CONTAINING DY1, AND
;;   ARG4 IS THE ADDRESS OF A WORD TO BE USED AS AN 'ERROR WORD.'
;;
;;
;;  FILRAD IS A MACRO WHICH ALLOWS THE USER TO SPECIFY A NAME AND
;;   TYPE FOR A FILE WHILE A PROGRAM IS IN PROGRESS.  THE CALL IS
;;   OF THE FORM:
;;                       FILRAD ARG
;;   WHERE ARG IS THE LOW ADDRESS OF A FOUR-WORD DEVICE-NAME BLOCK.
;;
;;
;;  FLOAT IS A MACRO TO FLOAT A SINGLE-PRECISION OCTAL INTEGER.
;;   THE CALL IS OF THE FORM:
;;                       FLOAT   ARG1,ARG2,ARG3
;;   WHERE ARG1 CONTAINS THE INTEGER TO BE FLOATED AND THE HIGH AND
;;   LOW PARTS OF THE FLOATED NUMBER ARE RETURNED IN ARG2 AND ARG3,
;;   RESPECTIVELY.
;;
;;
;;  GETDEC IS A MACRO TO TAKE A REAL DECIMAL FIXED-POINT NUMBER
;;   FROM THE KEYBOARD AND STORE IT AS A FLOATING-POINT OCTAL
;;   NUMBER.  THE CALL IS OF THE FORM:
;;                       GETDEC   ARG1,ARG2
;;   WHERE THE HIGH AND LOW PARTS OF THE FLOATED NUMBER ARE
;;   RETURNED IN ARG1 AND ARG2, RESPECTIVELY.
;;
;;
;;  GETINT IS A MACRO TO GET A DECIMAL INTEGER FROM THE KEYBOARD
;;   AND STORE IT AS AN OCTAL INTEGER.  THE CALL IS OF THE FORM:
;;                       PROCT ARG
;;   WHERE ARG IS THE LOCATION OF THE STORED INTEGER.
;;
;;
;;  PROCT IS A MACRO WHICH PUTS AN OCTAL NUMBER OUT ON THE
;;   KEYBOARD.  THE CALL IS OF THE FORM:
;;                       PROCT  ARG
;;   WHERE ARG IS AN ADDRESS CONTAINING THE NUMBER.
;;
;;
;;  PULL IS A MACRO FOR USE IN SUBROUTINES WHICH ARE WRITTEN TO
;;   BE FORTRAN-COMPATIBLE.  THE CALL IS OF THE FORM:
;;                       PULL    ARG
```

```
;;   WHERE ARG IS AN ADDRESS AT THE TOP OF THE COMMON VARIABLE
;;   LIST IN THE ROUTINE.  PULL TRANSFERS THE COMMON VARIABLES FROM
;;   THE MAIN PROGRAM TO THE SUBROUTINE.
;;
;;
;;  PUSH IS A MACRO FOR USE IN SUBROUTINES WHICH ARE WRITTEN TO BE
;;   FORTRAN-COMPATIBLE.  THE CALL IS OF THE FORM:
;;              PUSH    ARG
;;   WHERE ARG IS AN ADDRESS AT THE TOP OF THE COMMON VARIABLE
;;   LIST IN THE ROUTINE.  PUSH TRANSFERS THE COMMON VARIABLES FROM
;;   THE SUBROUTINE BACK TO THE MAIN PROGRAM.
;;
;;  RECALL IS A MACRO WHICH READS DATA, FROM A FILE ON DY1, INTO
;;   MEMORY.  THE CALL IS OF THE FORM:
;;                       RECALL  ARG1,ARG2,ARG3,ARG4
;;   WHERE ARG1 IS AN ADDRESS WHERE THE LOW ADDRESS OF THE DATA
;;   BUFFER WILL BE WRITTEN, ARG2 IS AN ADDRESS WHERE THE LENGTH
;;   (OCTAL) IN WORDS WILL GO, ARG3 IS THE LOW ADDRESS OF A FOUR-
;;   WORD DEVICE-NAME BLOCK OF MEMORY, AND ARG4 IS THE ADDRESS OF
;;   AN 'ERROR WORD.'
;;
;;
;;  TTCLR IS A MACRO WHICH CLEARS THE TELETYPE RING BUFFER OF
;;   EXTRANEOUS CHARACTERS.
;;
```